JOURNAL OF FLUID MECHANICS

VOLUME 6 PART 2

AUGUST 1959

THE UNIVERSITY OF MICHIGAN
OCT 9 1959
ENGINEERING LIBRARY

PUBLISHED BY

CAMBRIDGE UNIVERSITY PRESS

BENTLEY HOUSE, 200 EUSTON ROAD, LONDON, N.W.1

AMERICAN BRANCH: 32 EAST 57TH STREET, NEW YORK 22, N.Y.

Price 30*s.* (*U.S.A.* $5.00)

The JOURNAL OF FLUID MECHANICS exists for the publication of theoretical and experimental investigations of all aspects of the mechanics of fluids, and is issued in four parts per volume.

EDITOR

DR G. K. BATCHELOR

Cavendish Laboratory, University of Cambridge, Cambridge, England

ASSISTANT EDITORS

DR T. B. BENJAMIN, DR I. PROUDMAN, DR P. G. SAFFMAN

Cavendish Laboratory, University of Cambridge, Cambridge, England

ASSOCIATE EDITORS

PROF. G. F. CARRIER

Pierce Hall, Harvard University, Cambridge 38, *Massachusetts, U.S.A.*

DR W. C. GRIFFITH

Research and Development Laboratory, Missile Systems Division, Lockheed Aircraft Corporation, Palo Alto, California, U.S.A.

PROF. M. J. LIGHTHILL

Department of Mathematics, The University, Manchester, England

PROF. R. R. LONG

School of Engineering, The Johns Hopkins University, Baltimore 18, *Maryland, U.S.A.*

Authors wishing to have papers published in the JOURNAL should communicate them to any one of the persons named above, choosing one in their own country where possible.

Authors are urged to ensure that their papers are written clearly and attractively, in order that their work will be readily accessible to readers.

Manuscripts should be typed in double spacing on one side of the paper only, with references listed at the end in alphabetical order of authors. Drawings should be done on a large scale in Indian ink on tracing cloth or drawing paper, the lettering being shown clearly in pencil for reproduction by the printer; the list of captions should be typed at the end of the manuscript. Proofs of papers from overseas will usually be despatched to authors by airmail. There is no charge for publication. Authors are entitled to receive 50 offprints of a paper in the JOURNAL free of charge, and additional offprints can be purchased if ordered in advance.

SUBSCRIPTIONS

The subscription price for a volume of four parts is £5. 10*s*. net, post free, payable in advance; separate parts 30*s*. net, plus postage. Subscriptions may be sent to any bookseller, or to the Cambridge University Press, Bentley House, 200 Euston Road, London, N.W. 1.

Subscribers in the United States should send their orders to the Cambridge University Press, American Branch, 32 East 57th Street, New York 22. The subscription price per volume is $18.50, post free, payable in advance; separate parts $5.00, plus postage.

Shearing flow over a wavy boundary

By T. BROOKE BENJAMIN
Department of Engineering, University of Cambridge

(Received 10 December 1958)

A theoretical study is made of shearing flows bounded by a simple-harmonic wavy surface, the main object being to calculate the normal and tangential stresses on the boundary. The type of flow considered is approximately parallel in the absence of the waves, being exemplified by two-dimensional boundary layers over a plane. Account is taken of viscosity; but, as the Reynolds number is assumed to be large, its effects are seen to be confined within narrow 'friction layers', one of which adjoins the wave and another surrounds the 'critical point' where the velocity of flow equals the wave velocity. The boundary conditions are made as general as possible by including the three cases where respectively the boundary is rigid, flexible yet still solid, or completely mobile as if it were the interface with a second fluid.

The theory is developed on the model of stable laminar flow, although it is proposed that the same theory may usefully be applied also to examples of turbulent flow considered as 'pseudo-laminar' with velocity profiles corresponding to the mean-velocity distribution. Use is made of curvilinear co-ordinates which follow the contour of the wave-train. This admits a linearized form of the problem whose validity requires only that the wave amplitude be small in comparison with the wavelength, even when large velocity gradients exist close to the boundary. The analysis is made largely without restriction to particular forms of the velocity profile; but eventually consideration is given to the example of a linear profile and the example of a boundary-layer profile approximated by a quarter-period sinusoid. In § 7 some general methods are set out for the treatment of disturbed boundary-layer profiles: these apply with greatest precision to thin boundary layers, but are also useful for the initially very steep but on the whole fairly diffuse profiles which occur in most practical instances of turbulent flow over waves.

The phase relationships found between the stresses and the wave elevation are discussed for several examples, and their interest in connexion with problems of wave generation by wind is pointed out. It is shown that in most circumstances the stresses are distributed in much the same way as if the leeward slopes of the waves were sheltered. For instance, the pressure distribution often has a substantial component in phase with the wave slope, just as if a wake were formed behind each wave crest—although of course actual separation effects are outside the scope of the present theory. In this aspect, the analysis amplifies the work of Miles (1957).

1. Introduction

The main purpose of this work is to estimate the stresses on wavy surfaces bounding several kinds of shearing flow at high yet finite Reynolds number, including uniform shearing flow and flows characterized by a boundary layer. To make a tractable theoretical model, the primary motion is taken to be parallel and in the direction of the waves, so the disturbance due to the waves is two-dimensional and strictly periodic in the x co-ordinate. We neglect the spontaneous fluctuations with respect to time which would usually occur in the real case (i.e. due to instability of a laminar flow or to fully developed turbulence); but while the theory applies rigorously only to stable laminar flows, we consider there is sufficient justification to take the bold step of applying it also to examples of turbulent flow, assuming that the mean-velocity distribution is disturbed by the waves in approximately the same way as the velocity distribution in an equivalent laminar flow. This course seems to bring the work into much closer relation to practical problems than if only laminar flows were considered, even though admittedly the neglect of interactions between the turbulence and the wave motion constitutes a very severe simplification for which *a priori* theoretical justification is difficult to find. However, some justification for this, together with a clear statement of what it implies mathematically, was given by Miles (1957, see particularly the Appendix) whose work bears closely on the present problem and will be frequently cited in what follows.

Expressions will be found for the surface stresses rather more readily in the case of a rigid boundary than in the case where flexure of the boundary allows the wave-train to travel in the direction of flow. In the latter case the wave velocity may equal the fluid velocity at a certain distance from the boundary; and this 'critical point' becomes a vital factor in the analysis in much the same way as it does in the stability theory of parallel flows (see Lin 1955, chapters 3, 8). However, the results for the latter case have special interest in that they might be applied to problems of wave generation by flow over a mobile boundary, for instance wind over a water surface. Such problems are commonly approached by considering a simple wave-train of arbitrary wavelength and speed superposed on the equilibrium state and then finding conditions under which the reaction of the disturbed flow is just sufficient to maintain the waves. Knowledge of the forces exerted on the wave surface therefore comprises an intermediate step towards the solution of the problem; and the remaining steps need be concerned only with the matter (e.g. the water) under the action of these forces. Although the subject of wave generation is incidental to the main contents of this paper, some features of the results will be discussed which are particularly interesting from this aspect.

Most previous work relevant to this investigation has in fact been directly concerned with questions of how the action of wind may give rise to waves of one sort and another. Particularly in the vast literature concerning wave generation on deep water,† several distinct theoretical models have been used to account for

† Two other practical problems of wave generation by wind have become important in recent times: the first relates to the flutter of membranes and thin panels, and the second to the instability of liquid films dragged over a solid boundary by a gas stream, the latter

flow over a prescribed wavy boundary; and it is desirable to note what relation some of these have to the present contribution.

The classical Kelvin–Helmholtz theory is based on the simplest model (Lamb 1932, §§ 234, 268). This assumes uniform flow initially in the air and the water, the velocities being discontinuous at the interface. Viscosity is neglected, so that the disturbed motion arising when the interface is perturbed by a simple wave-train can be described by a velocity potential. Apart from the obvious gravity force, the only effect of the air stream upon the water surface is a periodic pressure which, if the wave amplitude does not vary with time, is in opposite phase to the wave elevation and thus acts exactly contrary to the total effect of gravity and surface tension. The pressure is proportional to the square of the air velocity relative to the waves, and is just the same for a rigid wave-train if a uniform primary velocity is assumed for this case also. Such a rudimentary model has obvious physical limitations; but we shall see in § 7 that the pressure component given by the Kelvin–Helmholtz theory is consistent with the results of a more realistic theory valid for thin boundary layers: it will be shown that this pressure component is the only stress remaining in the limit as the Reynolds number is taken uniformly to infinity.

An approach to the problem of water-wave generation similar in principle to the Kelvin–Helmholtz theory, but taking account of viscosity, was used by Wuest (1949) and Lock (1954); and the model on which their analyses were based is of the type considered in this paper. Laminar flow is assumed in the air and the water; and the stability of the motion with respect to wavy disturbances is investigated in the way usual for problems of boundary-layer stability (i.e. the velocity profile is assumed to have negligible variation over distances comparable with the wavelength, so that linearized equations of motion of the Orr–Sommerfeld type are obtained—see Lin (1955, chapter 5)). The velocity profiles considered by Wuest were arbitrarily chosen as rough approximations to actual boundary-layer profiles; but Lock considered an exact profile which he had previously calculated for a boundary layer starting from a certain point upstream. Now, as both the air and water motions can be separately unstable even in the absence of the additional factor presented by the mobility of the interface, stability analyses of this sort are extremely complicated. Thus, although Lock's results are undoubtedly valuable, they are of such complexity that it would seem unlikely they could ever be checked by experimental observation. In this paper we shall study disturbed laminar flows of the kind treated by Lock; but we shall ignore possible instability of the flow and accordingly take the disturbance to be stationary relative to the waves on the boundary, thus enabling us to study much more clearly the interesting effects due specifically to the presence of the waves.

Another model which is to be taken as an example in this paper has previously been used by Feldman (1957), who considered a stability problem akin to Wuest's and Lock's but for a horizontal liquid film in contact with a semi-infinite air

problem having importance in chemical engineering and in connexion with the cooling of rocket motors (Knuth 1954). As in the water-wave problem, the main difficulty in these two also is to account for the disturbed air flow; and so the present work may be said to have equal bearing on all three.

stream. He also assumed parallel laminar flow, but introduced the simplification that both fluids are initially in uniform shearing motion (i.e. plane Couette flow). This rules out the occurrence of 'self-instability' of the air stream as encountered in Lock's work, since semi-infinite Couette flow is completely stable (this was proved by Zondek & Thomas (1953)). But, as Feldman was careful to point out, this model of the air flow is an extreme idealization. One might expect that for results calculated on this basis to apply in practice, the actual velocity profile would have to admit a linear approximation to a distance of at least the order of a wavelength from the interface; and this requirement is certainly not met in experiments such as those of Knuth (1954), in which the air flow is turbulent and the slope of the profile varies very rapidly near the interface—whereas the waves observed are much longer than, say, the thickness of the viscous sublayer. Nevertheless, the linear-profile model has the unique merit that, while it is a physically *possible* example of viscous shearing flow, the respective form of the Orr–Sommerfeld equation (which determines the structure of a periodic disturbance) can be solved exactly. And so there is generally much to be said in favour of using this fairly manageable model as a first step towards clarifying physical problems concerned with shearing flows.

In § 5 we shall consider uniform shearing flow as a first example on which to try our general theory. The equations obtained in this example for the stresses on fixed or very slowly moving waves reduce to attractively simple approximate forms, whose compactness invites a generalization by Fourier's theorem. This is done in § 8, mainly to illustrate an interesting 'quasi-sheltering' effect (see three paragraphs below) depending on the phase relations between the stresses and the boundary displacement, an example being provided by a single-humped perturbation of the boundary shaped like the graph of $f(x) = (x^2+b^2)^{-1}$.

We next recall what has been done in the past to account for *turbulent* flow over waves. In attempts to explain water-wave formation several theories have been put forward which recognize in some way the turbulent character of the wind; but there are in general only two courses open towards workable theories, each of these having to start from a bold simplification of the physical problem. One of these is based on considerations quite different from the material of this paper: the effects of the waves on the air flow are neglected entirely, and attention is fixed on the response of the water surface to random fluctuations of normal pressure, which are taken to be the same as on a plane surface.†

The alternative course which has been followed by a number of authors interested in water-wave formation is to deal with the turbulent flow in much the same way as we shall. The turbulence is neglected except inasmuch as it may determine relevant properties of the mean shear flow, and attention is fixed on effects arising from the wavy disturbance of the air stream. The best-known example of this approach is the sheltering theory of Jeffreys (1924, 1925), which makes use of the principle that an already existing wave-train will grow if the wind supplies energy to it at a rate greater than that of viscous dissipation in the water. Inertial effects and tangential stresses due to the wind are neglected; and the only

† Phillips (1957) has published a new theory on these lines, giving an illuminating account of water-wave generation by a random pressure distribution.

property of the normal pressure distribution needed for the calculation of the average energy supply is the Fourier component in phase with the wave slope. This component is supposed to arise as the flow separates from the leeward side of each wave, causing the pressure there to be lower than on the windward side; and, to express its magnitude, a sheltering coefficient s is introduced. Jeffreys's theory provides no estimate of s, and was for a long time held in doubt since experimental estimates of s by use of fixed wave models (e.g. Motzfeld 1937) give values much too small to explain observed rates of wave growth.

However, this objection has been removed by the recent work of Miles (1957), who showed theoretically that even when there is no separation of the flow (i.e. no sheltering in the sense in which this term is usually understood) sufficiently large values of s can occur when there is a critical point away from the wave surface in a region of the velocity profile where the curvature is large negatively. The development of a substantial pressure component in phase with the wave slope is related to the phase discontinuity in the longitudinal velocity which is well known to occur across the friction layer surrounding the critical point (Tollmien 1929). Thus, the value of s for a moving wave may greatly differ from that for a similar fixed model, which has the critical point right at the boundary. It is remarkable that the 'quasi-sheltering' effect discovered by Miles is indicated by linearized perturbation theory, and is therefore quite distinct from the essentially non-linear effect (i.e. the formation of a wake) implied by the term sheltering. For the velocity profile, Miles took the 'universal' logarithmic law applicable to turbulent boundary layers at very large Reynolds numbers.

Miles's paper appears to have greatly invigorated the 'stability theory' of wave generation by turbulent wind† (the description 'sheltering theory' now seems inappropriate); and the present investigation owes largely to the stimulus of his work. In part, the following analysis will amplify Miles's treatment of disturbed turbulent profiles: for instance, all the surface stresses will be estimated, and the significant effect of viscosity at the wave surface will be examined. We shall see that both the normal and tangential stress distributions may in some circumstances be such as to do work on a moving wave, and their effectiveness in this respect will be compared: this property will be disclosed for a linear profile as well

† It seems evident that the two types of theory of which respectively the contributions of Phillips and Miles are the most advanced examples are both relevant to natural cases of wave generation by wind, despite the greatly different character of the two. They can be regarded as alternatives for *ad hoc* application according to the nature of the observed waves. For instance, if waves are seen to develop which are fairly regular and long-crested and which travel much slower than the wind, then clearly a stability theory is the more likely to be useful (and the present work a possible help). To mention just one instance where observation suggests that effects of the disturbed mean flow predominate over effects of the turbulence, the author has noticed that when a turbulent air-stream blows over a thin layer of highly viscous liquid like syrup the free surface may not be visibly agitated by the turbulent pressure fluctuations acting upon it; but when the wind speed is increased beyond a certain limit, regular long-crested waves of the order of 1 cm in length suddenly appear. When a film of water is observed in the same circumstances, some apparently random agitation is always discernible. Nevertheless, long-crested and fairly slow-moving waves arise at a wind speed rather less than before; and in all respects except the smoothness of the surface, their character seems much the same as of the waves on the more viscous liquid.

as for boundary-layer profiles, although the former case is special in that viscous effects at the boundary are primarily responsible for 'quasi-sheltering'. In each case, these viscous effects cause 'quasi-sheltering' when the boundary is rigid (i.e. when there is no critical point away from the boundary, so that the mechanism considered by Miles is absent).

To conclude this introduction, we must refer again to the matter of flow separation from the wave surface, which is probably the most vital consideration of all regarding the practical usefulness of the present linearized theory. It is to be expected that any actual flow at fairly high Reynolds number will separate if the waves are made steep enough or the wave-train long enough; but the value of our analysis rests on the supposition that the flow will remain attached to a fairly short wave-train of reasonably small steepness. In this respect applications to turbulent flows are more secure than to laminar flows, which tend rather readily to separate when given a wavy disturbance (Quick & Schröder (1944) showed this theoretically by use of numerical methods). The experiments of Motzfeld (1937) are a source of encouragement here. He in turn fixed four different rigid wave models in a wind tunnel, and measured pressure and velocity distributions throughout the whole flow—which was fully turbulent. The results obtained with the first model, which was a sinusoidal wave-train of 0·75 cm amplitude and 30 cm wavelength, are of particular interest at present. The pressure distribution over the wave surface was found to be very approximately sinusoidal, as it should be according to our theory; and no evidence of separation was found. The next two models were steeper waves, the ratio of wavelength to amplitude being for both about 20; and the pressure distribution was found to be slightly skew in the windward direction. However, there was still no evidence of separation, as may be seen from Motzfeld's diagrams of the streamlines following the contour of the waves. The fourth wave model was sharp-crested; and the flow was observed to separate from the wave crests and re-attach close to the troughs. A comparison between some of Motzfeld's measurements on his first wave model and results from the present theory will be made in § 7, a reasonable agreement being found.

It must be noted that Stanton, Marshall & Houghton (1932) also measured pressure distributions over wave models in a wind tunnel and found results markedly different in character from those of Motzfeld: the discrepancy has been commented upon by Ursell (1956). For their first series of measurements, the model was a train of twenty-seven sine waves, whose amplitude and wavelength increased linearly with distance but kept a constant ratio of about 0·1: the length of the first wave was 5·1 cm, and that of the last was 21·6 cm. The pressure distributions were measured over the tenth and twenty-seventh waves for various wind speeds. For their second series of measurements, two models were used on which the waves were of constant wavelength, the ratio of amplitude to wavelength being about 0·2. Pressure distributions were measured at 40 and 80 wavelengths from inlet, and were found to be much the same in the two places. These various observations differed from Motzfeld's in that the pressure distributions were very irregular, being not even roughly sinusoidal: for instance, Fourier analysis of a typical distribution shows the amplitude of the second harmonic to be of the same order of magnitude as the fundamental amplitude. Thus, it seems

evident that in these experiments there was turbulent boundary-layer separation from the wave profiles. That this should have occurred here and not in Motzfeld's experiments with a sinusoidal profile is readily accountable to the fact that the waves were considerably steeper (particularly in the second series of measurements), and also to the fact that the wave-train was much longer (Motzfeld's results considered in § 7 were obtained from a model only three wavelengths long). These considerations suggest that the present theory should preferably be restricted to waves with an amplitude to length ratio less than, say, about 0·03 or 0·02 and with fairly short fetch.

2. Formulation of the problem

We shall express all variables in non-dimensional form, implying that the units of length and of velocity are to be taken as a certain length l and velocity U_0 characteristic of the physical problem: thus, for instance, any symbol representing a velocity is to be interpreted finally as a multiple of U_0. Time is made dimensionless on the understanding that l/U_0 is the unit; and stresses are considered as multiples of ρU_0^2, ρ being the density of the fluid in question. The Reynolds number $R = U_0 l/\nu$, where ν is the kinematic viscosity, becomes an important parameter in this problem since the effects of viscosity will not be ignored.

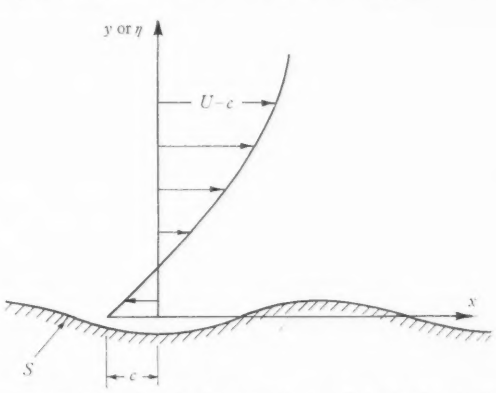

FIGURE 1. Definition sketch showing the undisturbed velocity profile as it would appear to an observer moving with the wave.

It is convenient to use a frame of reference in which the wave upon the bounding surface S is stationary. Thus, with respect to Cartesian axes (x, y) taken as in figure 1 and moving at speed c with the wave, the velocity parallel to x in the primary flow above the surface S is $U(y) - c$, where $U(y)$ is the velocity relative to the material surface (which in this frame of reference slips to the left with speed c). The equation of S is taken to be

$$y = a\, e^{ikx} \tag{2.1}$$

with the understanding that the real part represents the physical boundary. The amplitude a is assumed to be small compared with the wavelength $2\pi/k$, so that $(ka)^2$ is negligibly small; and this is intended to be our only restriction on the size

of the wave. However, a difficulty now appears on consideration of the boundary conditions which apply at S. Large velocity gradients are to be expected right at this boundary (i.e. $U'(0)$ will be large), so that the trace of equation (2.1) upon the primary velocity profile may represent large velocity variations notwithstanding the present assumption about the smallness of a. But two boundary conditions relating respectively to the normal and tangential velocity components must be satisfied at S. It would seem therefore that a linearized theory along the lines so far suggested would require for accuracy a further restriction on the wave amplitude, namely, that a be small enough for the curve (2.1) to be confined to a region over which the variation of U is small. For instance, a would need to be considerably less than the width of the viscous sublayer in a turbulent boundary layer. This restriction would be too severe for a realistic theory; but fortunately it can be avoided by a slight change in approach to the problem.

A way out of the difficulty is suggested by a well-known property of boundary layers along curved walls (see, for example, Goldstein 1938, p. 119; or Schlichting 1955, p. 98). In a region where the wall curvature is fairly small and there is no large adverse pressure gradient, the changes in the boundary-layer profile at different positions along the wall are not large if measured relatively to the wall, being in fact of the first order in the curvature. In other words, the flow tends to follow the contour of the wall in such a way that the main features of the boundary layer, which may include a sharp velocity gradient right at the wall, are largely preserved—or at least undergo no more than first-order changes in a reasonable distance. Now, if for the present problem use is made of a curvilinear orthogonal system of co-ordinates in which the wave S is a co-ordinate line, the disturbed flow can be described by a perturbation representing only the *difference* between the actual flow pattern and the pattern formed by 'bending' the primary profile to follow the wave (i.e. the latter is simply $U(\eta)$, where η is the curvilinear co-ordinate perpendicular to S). This perturbation will be of the order of ka at most; and since the boundary conditions on it will not entail an 'overlapping' of the primary flow pattern as before, there need be no additional restriction on the magnitude of a in order to satisfy these boundary conditions with sufficient accuracy. The reasoning outlined here will perhaps be made a good deal clearer by what follows.

We take orthogonal co-ordinates (ξ, η) defined by

$$\left.\begin{aligned} \xi &= x - ia\, e^{-k(y-ix)}, \\ \eta &= y - a\, e^{-k(y-ix)}, \end{aligned}\right\} \tag{2.2}$$

in terms of which the equation of S is, to the first order in ka, simply $\eta = 0$. The Jacobian of this transformation is

$$J = \frac{\partial(\xi, \eta)}{\partial(x, y)} = 1 + 2ka\, e^{-k(\eta - i\xi)} \tag{2.3}$$

to the first order. Note that incidentally ξ and η are the same as the velocity potential and stream function for irrotational wave motion in an inviscid fluid (cf. Lamb 1932, § 233).

Let ψ denote the stream function for the present case, its form in the absence of waves (i.e. $a = 0$, $\eta = y$) being

$$\psi_0 = \int_0^\eta \{U(\eta) - c\}\, d\eta.$$

For the disturbed flow, ψ may be expressed in the form ψ_0 plus a periodic perturbation proportional to a: thus we write

$$\psi(\xi, \eta) = \psi_0(\eta) + a\{F(\eta) + [U(\eta) - c]\, e^{-k\eta}\}\, e^{ik\xi}, \tag{2.4}$$

where the function $F(\eta)$ has yet to be determined. (The inclusion in (2.4) of the term with $(U - c)$ as a factor simplifies the ensuing work to some extent; it can be included arbitrarily since $F(\eta)$ is unspecified.) Following from (2.4), the velocity components parallel to ξ and η are given respectively by

$$\left.\begin{aligned} u &= J^{\frac{1}{2}}\psi_\eta = U - c + a\{F' + U'\, e^{-k\eta}\}\, e^{ik\xi}, \\ v &= -J^{\frac{1}{2}}\psi_\xi = -ika\{F + (U - c)\, e^{-k\eta}\}\, e^{ik\xi}, \end{aligned}\right\} \tag{2.5}$$

where the subscripts denote partial differentiations, and the vorticity is

$$\zeta = J\{\psi_{\xi\xi} + \psi_{\eta\eta}\} = U' + a\{F'' - k^2 F + U''\, e^{-k\eta}\}\, e^{ik\xi}. \tag{2.6}$$

Consider now the boundary conditions to be satisfied by the velocity components at S, that is, at $\eta = 0$. If S is a solid boundary (which need, of course, be flexible if c is not to be zero), a requirement for the primary flow is that $U(0) = 0$. Two boundary conditions then apply to the disturbed velocity components expressed by (2.5). First, the normal velocity v at S must be zero since the wave is stationary; and hence (2.5) shows that

$$F(0) = c. \tag{2.7}$$

Secondly, the tangential velocity u must satisfy a condition of non-slipping relative to solid particles fixed in S; and this requires that

$$F'(0) = -U'(0), \tag{2.8}$$

which follows from (2.5) on consideration that, at the wave surface, $u = -c$ to the first order of approximation in ka.

These boundary conditions can easily be modified to include the case where S is the boundary of another fluid, so that the tangential velocity along S may vary. Clearly, by adjusting the frame of reference the velocity of the undisturbed interface can be put equal to $-c$, i.e. $U(0) = 0$ as before: the velocities in the second fluid must then take negative values in order that the shearing stress due to the primary flow should be continuous across the interface. It may also be supposed that the variable component of the tangential velocity can always be expressed in the form $\beta a\, e^{ik\xi}$. Accordingly, the boundary condition (2.7) remains unchanged; but (2.8) is replaced by

$$F'(0) = -U'(0) - \beta. \tag{2.9}$$

The cases now covered may be summarized as follows:

(i) The boundary is solid and rigid; thus $c = 0$ and $\beta = 0$.

(ii) It is solid but flexible (e.g. an inextensible membrane); thus a wave can be propagated along it with finite c, but $\beta = 0$.

(iii) It is an interface between fluids; thus both c and β may be non-zero, and are likely to depend on the properties of the second fluid.†

The validity of these boundary conditions depends only on ka being small: that is, they are consistent with the linearized approximation to ψ expressed in (2.4). The difficulty mentioned earlier has therefore been avoided, which is due essentially to the fact that the expressions (2.5) for the velocities involve $U(\eta)$ rather than $U(y)$ as they would if developed in Cartesian co-ordinates: in the latter case the boundary conditions would be applied on $y = a\,e^{ikx}$ instead of $\eta = 0$. For a boundary-layer flow, $U'(0)$ will become infinite in the limit as the Reynolds number $R \to \infty$; but we can expect the present method of linearization to remain valid at indefinitely high Reynolds numbers, since $R \to \infty$ is precisely the condition for vorticity to be constant along streamlines, e.g. the streamline $\eta = 0$.

Expressions will now be found for the stresses acting upon S. Their derivation is slightly more complicated in curvilinear rather than Cartesian co-ordinates; but there is no need to go into details of the derivation here, since the calculations require merely a straightforward application of the theory of general orthogonal co-ordinates as is explained in many text-books (e.g. Goldstein 1938, § 39). It will be convenient to express the stresses in terms of ψ rather than of the velocity components.

Consider first the shearing stress τ, which according to a well-known result is the same as $R^{-1}(\psi_{yy} - \psi_{xx})$, where R is the Reynolds number. (This is, of course, the dimensionless form of τ implied by the remarks at the beginning of this section.) An alternative expression involving derivatives of ψ with respect to ξ and η is found to be

$$\tau = R^{-1}\{(\xi_x^2 - \xi_y^2)\,(\psi_{\eta\eta} - \psi_{\xi\xi}) + 4\xi_x\xi_y\psi_{\xi\eta} - 2\eta_{xy}\psi_\xi + 2\xi_{xy}\psi_\eta\}. \tag{2.10}$$

Substituting (2.2) and (2.4) into (2.10) and omitting second-order terms, we get

$$\tau = R^{-1}[U' + a\{F'' + k^2F + U''\,e^{-k\eta}\}\,e^{ik\xi}]. \tag{2.11}$$

This is evaluated at $\eta = 0$ to give the surface shearing stress, say τ_s. The first term in the expression for τ_s is $R^{-1}U'(0)$, which is the stress exerted by the

† Case (iii) needs special qualification when we apply the theory to turbulent flows. Turbulent fluctuations in the first fluid will always in some degree be transmitted to the second; and if the densities and viscosities of the two fluids were not much different, Reynolds stresses would have a predominant effect on the interface, and there would be no viscous sublayer as in the case of a solid boundary. But in the following analysis we need to assume a viscous layer at the boundary; and so in case (iii) we imply that the second fluid is comparatively very viscous and dense (e.g. water if the first fluid is air). It is then reasonable to assume that the flow has a structure similar to one over a solid boundary, including a definite sublayer. In fact, for the case of air–water, the main effect of turbulence in the water would appear to be only the resulting roughness of the surface, whose equivalent 'roughness length' affects the air profile in the well-known way (e.g. see Miles 1957). Therefore, provided the surface agitation is mild enough for the air flow to remain 'aerodynamically smooth' (i.e. the sublayer thickness exceeds the height of the random surface disturbances), the mobility of the boundary remains a factor of secondary importance in relation to the structure of the air flow.

undisturbed primary flow. If the variable part of τ_s is denoted by $T_s a\, e^{ik\xi}$ and the boundary condition (2.7) is introduced, then the factor T_s is given by

$$T_s = R^{-1}\{F''(0) + k^2 c + U''(0)\}. \tag{2.12}$$

The component of direct stress in the η-direction is expressible in the form

$$-p + 2R^{-1}J^{-1}(\xi_y^2 - \xi_x^2)\{(\xi_x^2 - \xi_y^2)\psi_{\xi\eta} + \xi_x\xi_y\psi_{\xi\xi} + \eta_x\eta_y\psi_{\eta\eta} + \xi_{xy}\psi_\xi + \eta_{xy}\psi_\eta\},$$

where p denotes the pressure. For convenience gravity forces are neglected, being independent of the hydrodynamic forces of present interest; but it is obvious that if the y-direction is upward, the (dimensional) pressure variation on S due to gravity is simply $-\rho g a\, e^{ik\xi}$. On substituting (2.2) and (2.4) and evaluating this expression at $\eta = 0$, we find that the normal stress σ_s acting *downward* on S is given by

$$\begin{aligned}\sigma_s &= p_s + 2ikaR^{-1}F'(0)\, e^{ik\xi} \\ &= p_s - 2ikaR^{-1}\{U'(0) + \beta\}\, e^{ik\xi},\end{aligned} \tag{2.13}$$

where p_s is the pressure at S, and where the second equality follows from the boundary condition (2.9). Here the term in R^{-1} is completely known; but this term will appear later to be negligible within the overall scheme of approximation to be adopted.

To find p_s, we consider the Navier–Stokes dynamical equations expressed in terms of the co-ordinates (ξ, η) and with ψ and p as dependent variables. The two equations of motion respective to the ξ and η-directions are found to be

$$J(\psi_\eta\psi_{\eta\xi} - \psi_\xi\psi_{\eta\eta}) + \tfrac{1}{2}J_\xi(\psi_\xi^2 + \psi_\eta^2) = -p_\xi + R^{-1}\zeta_\eta, \tag{2.14}$$

$$J(-\psi_\eta\psi_{\xi\xi} + \psi_\xi\psi_{\xi\eta}) + \tfrac{1}{2}J_\eta(\psi_\xi^2 + \psi_\eta^2) = -p_\eta - R^{-1}\zeta_\xi, \tag{2.15}$$

in which ζ is to be related to ψ by equation (2.6). The substitution of (2.3), (2.4) and (2.6) into (2.14) and (2.15) leads to two alternative equations for p in terms of F and its derivatives. The pressure variations due to the wave disturbance may be considered distinctly from those in the primary flow, so that we may put $p = P(\eta)\, a\, e^{ik\xi}$ and therefore $p_\xi = ikp$. Hence, the first equation for p (obtained from (2.14)) gives

$$P = U'F - (U - c)F' - i(kR)^{-1}\{F''' - k^2F' + (U''' - kU'')\, e^{-k\eta}\}. \tag{2.16}$$

Alternatively, P can be found by an integration of (2.15) with respect to η, using the fact that the disturbance of the flow vanishes for $\eta \to \infty$. The result then is

$$P = k^2\int_\eta^\infty (U - c)F\, d\eta - i(kR)^{-1}\left\{k^2F' + \int_\eta^\infty (k^4F - k^2U''\, e^{-k\eta})\, d\eta\right\}. \tag{2.17}$$

Either of these results, which obviously must be equivalent, may be evaluated at $\eta = 0$ to give $P(0) = P_s$, say, the amplitude of the surface pressure p_s. However, this step is postponed until § 3 where the alternative expressions for P_s will be shown to have an interesting physical interpretation.

Since T_s and P_s may have real and imaginary parts, they express both the magnitudes of the respective stresses and their phases in relation to the wave on the boundary. As $F(0)$ and $F'(0)$ are determined by the boundary conditions,

it is seen from (2.12) and (2.16) that the problem is reduced essentially to finding $F''(0)$ and $F'''(0)$. This is by far the most difficult part of the task.

At this point it is suitable to list some assumptions which can be made on physical grounds regarding the magnitudes of certain quantities arising parametrically in these calculations. The assumptions form the basis for various approximations which will be introduced later on; and there is some advantage in setting them out beforehand for reference. They can be expressed symbolically as follows:

$$\left.\begin{array}{ll} \text{(i)}\ \ kR \gg 1; & \text{(ii)}\ \ [kRU'(0)]^{\frac{1}{3}} \gg k; \\ \text{(iii)}\ \ U'(0) \gg \beta; & \text{(iv)}\ \ (kRc^3)^{\frac{1}{2}} \gg U'(0). \end{array}\right\} \tag{2.18}$$

The first three of these rest essentially on the single assumption of large Reynolds number; but (iv) is rather special, and will be assumed only when the critical point is considered to lie well away from the boundary. Condition (iii) is totally satisfied if S is a rigid or flexible solid boundary, and is quite amply satisfied if S is an interface with a comparatively viscous second fluid (e.g. water if the main fluid is air). The basis for these various assumptions will be fully examined in later parts of the discussion.

3. The function F

The elimination of P between (2.16) and (2.17) leads to the fourth-order equation for $F(\eta)$

$$(U-c)(F''-k^2F)-U''F = (ikR)^{-1}\{F^{\mathrm{iv}}-2k^2F''+k^4F+(U^{\mathrm{iv}}-2kU''')\,e^{-k\eta}\}, \tag{3.1}$$

which is seen to be reducible to the Orr–Sommerfeld equation by the omission of the terms in U on the right-hand side. It will now be shown that this omission is in fact justified. We note first that the assumption of a parallel primary flow implies, strictly speaking, that $U^{\mathrm{iv}} = U''' = 0$ everywhere, since U must itself be a solution of the Navier–Stokes equations. However, we do not intend to confine the argument to velocity profiles of the strictly parallel sort (i.e. linear or parabolic ones), and we therefore assume that $U \equiv U(y)$ is an adequate approximation for many distributions, particularly of boundary-layer type, whose variation with x is small over several wavelengths. This assumption has commonly been introduced in theories of boundary-layer stability, and its validity amply confirmed (see, for instance, Lin 1955, § 5.1).

A more cogent reason for simplifying (3.1) is forthcoming when another familiar point from stability theory is recalled. Suppose that the primary distribution is characterized by a boundary layer whose thickness is selected as the reference length on which the Reynolds number R is based (cf. Schlichting 1955, p. 316). We note that U''' and U^{iv} are then not of a greater order of magnitude than U or U'', and also that by the boundary conditions F is of the same order as U or c. Hence, as the parameter $(kR)^{-1}$ multiplying the right-hand side of (3.1) is taken to be very small (assumption (i) in (2.18)), it is seen that this side of the equation plays an insignificant part in determining F, except in regions where F^{iv} becomes exceptionally large—certainly much larger than U^{iv} and U'''. One such region may occur very close to the boundary, where viscosity becomes important by

virtue of the non-slipping condition; and the only other possibility is a region around a so-called 'critical point' at which $U = c$ and the 'inviscid' equation (i.e. (3.1) with the right-hand side zero) therefore has a singular point. Accordingly, the equation for F can be taken to be the Orr–Sommerfeld equation

$$(U-c)(F''-k^2F)-U''F = (ikR)^{-1}\{F^{\mathrm{iv}}-2k^2F''+k^4F\} \tag{3.2}$$

with the understanding that the right-hand side is strictly accurate only for linear or parabolic velocity profiles, but is negligible anyway except at 'friction layers'—where the most important viscous term $(ikR)^{-1}F^{\mathrm{iv}}$ is alone an adequate approximation to the right-hand side of (3.1).

Equation (3.2) has been studied extensively as part of stability theory, some details of which are immediately useful for the present problem. Note, however, that the present F is rather different from the dependent variable in the Orr–Sommerfeld equation as it occurs in stability theory: there y is usually the independent variable, here it is η.

We first recall some well-known properties associated with critical points. Let $\phi(\eta)$ be the solution of

$$(U-c)(\phi''-k^2\phi)-U''\phi = 0 \tag{3.3}$$

(i.e. the inviscid form of (3.2)). At a position $\eta = \eta_c$, where $U = c$, this equation has a singular point, and consequently ϕ ceases to be an approximate solution of the complete Orr–Sommerfeld equation, even with $(kR)^{-1}$ very small. Since $U''/(U-c)$ has a simple pole at $\eta = \eta_c$, the formal expansion of ϕ about $\eta = \eta_c$ involves a term in $(\eta-\eta_c)\log(\eta-\eta_c)$; and therefore the correct form of ϕ as an approximate solution away from the critical point is in doubt until the appropriate branch of the logarithm is decided. This ambiguity can only be resolved by consideration of the complete equation (3.2); in other words, account must necessarily be taken of the effects of viscosity in the vicinity of the critical point. Tollmien (1929) first demonstrated that if the logarithm is expressed as $\log(\eta-\eta_c)$ for $\eta > \eta_c$, it is to be replaced by $\log(\eta_c-\eta)-i\pi$ for $\eta < \eta_c$. (This matter is one of the most vital and frequently discussed topics in stability theory; and it can be said that the lucid account given originally by Tollmien is one of the major contributions to modern fluid mechanics.) When this adjustment is made, ϕ can confidently be taken as an approximate solution of (3.2) applying either side of the critical region, the error being known to be $O(1/kR)$. We shall adopt this approximation for cases where c is substantially greater than zero: that is, the critical point occurs well within the fluid. Attention is confined to velocity profiles in which U increases monotonically with η (i.e. profiles of boundary-layer type), so that there cannot be more than one critical point. For the case $c \doteqdot 0$ where the critical point occurs at or very close to the boundary, special treatment will be needed.

The inviscid solution ϕ may not be a valid approximation close to the boundary S, since viscosity has a significant effect there as a result of the boundary condition on the tangential velocity. Mathematically speaking, this also follows clearly from the fact that the solution of a second-order equation (2.3) cannot in general satisfy the condition that $\phi \to 0$ far from S and also two boundary condi-

tions at S. Accordingly, we express an approximation to the complete solution F in the form

$$F(\eta) = \phi(\eta) + f(\eta), \tag{3.4}$$

where $f(\eta)$ is the appropriate rapidly varying solution of the full Orr–Sommerfeld equation: this must be the solution which diminishes rapidly with increasing η, since the other rapidly varying solution (which may be shown to increase in exponential fashion with η) is inadmissible physically (see Tollmien 1929; or Lin 1955, § 3.4 or § 8.5; or Schlichting 1955, p. 327). The region where $f(\eta)$ is significant may suitably be called the 'wall friction layer'.

The boundary conditions (2.7) and (2.9) can now be rewritten as

$$\phi(0) + f(0) = c, \tag{3.5}$$

$$\phi'(0) + f'(0) = -U'(0) - \beta; \tag{3.6}$$

and these expressions can be combined to give

$$\phi'(0) - [f'(0)/f(0)]\,\phi(0) = -U'(0) - \beta - c[f'(0)/f(0)], \tag{3.7}$$

which may be regarded as the boundary condition on ϕ. This will be examined in § 4. Note that if $f'(0)/f(0) \gg U'(0)/\phi(0)$, this condition is approximately $\phi(0) = c$, which is the form of the kinematical boundary condition which would arise if viscosity were neglected entirely. Note also that β may be neglected in (3.7) according to assumption (iii) of (2.18).

Let us now reconsider the expressions (2.16) and (2.17) for the pressure amplitude P. When evaluated at $\eta = 0$, (2.16) gives

$$P_s = k^2 \int_0^\infty (U - c)\, F\, d\eta + O(kR)^{-1}. \tag{3.8}$$

The terms which are $O(kR)^{-1}$ may be neglected according to assumption (i) of (2.18); and, as a further approximation (which in fact can be shown to be well within the limits of the previous one), F will be replaced by ϕ in the integral. The latter step can be taken because the integral is insensitive to the contribution from the wall friction layer—which is the only place where $F = \phi$ is not a good approximation (note that it is good through the friction layer about the critical point, even though the derivatives of ϕ cease to be valid approximations there). Thus we get

$$P_s = k^2 \int_0^\infty (U - c)\, \phi\, d\eta. \tag{3.9}$$

A result of this form might be obtained by neglecting viscosity from the start; but now viscosity can affect P_s through the boundary condition (3.7) on ϕ. The form of (3.9) suggests the attractive physical interpretation that the variable pressure at the boundary is, so to speak, generated by the cumulative action of the disturbance over the whole flow field, and is not particularly sensitive to the state of affairs near S. This is a familiar idea in boundary-layer theory. On the other hand, the form of (2.11) and (2.12) indicates that the surface shearing stress depends chiefly on circumstances close to the boundary (note F'' becomes much larger in the wall layer than elsewhere, due to the component f'').

An alternative expression for P_s follows from (2.17). When evaluated at $\eta = 0$, the first two terms on the right-hand side reduce to $-\beta c$ because of the boundary conditions; and we get

$$P_s = -\beta c + (ikR)^{-1}[F'''(0) + U'''(0) - kU''(0) + k^2\{U'(0) + \beta\}], \tag{3.10}$$

$$= (ikR)^{-1} F'''(0), \tag{3.11}$$

where (3.11) follows from the exact expression (3.10) because of assumptions (i) and (iv). A comparison of (3.11) with (3.9) shows $F'''(0)$ to be a large quantity, at least $O(kR)$; and clearly it is large due to the f component of F arising in the wall layer (in fact $F'''(0)$ can be replaced by $f'''(0)$ within the order of approximation implied in proceeding from (3.10) to (3.11)).

Let us consider equation (2.17) a stage further. We know from (2.16), and also as a familiar result from boundary-layer theory, that the pressure varies quite gradually with η; in particular, it does not change significantly over the thin wall layer. A good approximation to P_s will therefore be given by evaluating (2.17) just outside the wall layer, say at $\eta = \epsilon$: this takes the form

$$P_s = U'(\epsilon)\,\phi(\epsilon) - [U(\epsilon) - c]\,\phi'(\epsilon), \tag{3.12}$$

the terms in $(kR)^{-1}$ on the right-hand side of (2.17) being negligible outside the wall layer. But we have seen when deriving (3.11) that the terms independent of R in (2.16) (i.e. the terms like (3.12)) reduce at $\eta = 0$ to the small quantity $-\beta c$, and that a term negligible at $\eta = \epsilon$ becomes dominant at $\eta = 0$. In other words, the two groups of terms rapidly exchange role in keeping P approximately constant across the wall layer. This behaviour is perhaps obvious physically; but it is interesting to see mathematically how, when proper account is taken of viscosity, the pressure variation—an effect generated essentially by inviscid behaviour in the main flow—is transmitted to the boundary through the 'region of influence' of the non-slipping boundary condition, which would have to be ignored on the basis of at best some tentative physical argument if viscosity were neglected entirely. (Note, by the way, that (3.12) is exactly equivalent to (3.9) with the lower limit of integration replaced by ϵ: this relationship is proved by an integration of (3.3).)

Of the three approximate expressions which have been given for P_s, the first (3.9) would seem likely to be most generally useful, being of a form comparatively insensitive to errors in ϕ. Its intuitive appeal has already been remarked; and it indicates clearly the important fact, to be discussed fully later, that conditions at the critical point largely determine the *phase* of P_s. This was first demonstrated by Miles (1957), whose work will be recalled in some detail just below. As was mentioned in the discussion following equation (3.3), the inviscid solution undergoes a phase change across the critical point. The magnitude and sign of this change depend on the values of U' and U'' at $\eta = \eta_c$ (Tollmien 1929); and hence these values obviously must affect the phase of P_s as calculated from (3.9).

The imaginary part of P_s has an important physical significance, as it can be shown that in the absence of viscosity the rate of energy transfer from the fluid to unit area of the wave surface is $ka^2c\mathscr{I}\{P_s\}$. An estimation of this quantity is the vital step in 'sheltering' theories of wave generation by wind, in which the

growth of water waves is supposed to occur when the energy supply exceeds the rate of dissipation by viscosity in the water (see Ursell (1956) for a review of this subject). Miles (1957) has published an interesting calculation of $\mathscr{I}\{P_s\}$ for velocity profiles characteristic of turbulent boundary layers, the calculation being based essentially on the evaluation of an expression similar to (3.12). His theory was developed in Cartesian co-ordinates; but the restriction implied by the presence of large velocity gradients—as explained in § 2—was recognized, and a way of avoiding it was suggested (p. 191 of his paper). The most important difference between the present model and that considered by Miles is the neglect of viscosity in his, so that the boundary condition on the inviscid solution ϕ needs to be a purely kinematic one applied at some distance from the wave surface—in contrast to the exact condition (3.7) which clearly depends on viscosity. In our notation the boundary condition assumed by Miles is equivalent to $\phi = -U+c$ at a surface approximately parallel to S but a little way from it, say $\eta = \epsilon$. This implies that $\eta = \epsilon$ is a streamline, which is not an obviously justifiable assumption *a priori*, particularly in view of the large velocity gradient near S. However, there is little cause to doubt the validity of Miles's theory in the particular examples treated by him. It will appear in § 4 that the inviscid boundary condition can be established rigorously as an approximation to the exact condition in some cases.

(It may be noted, incidentally, that if the behaviour of $\phi(\eta)$ implied by the assumption of an inviscid boundary condition (i.e. $\phi = c - U$ for η small) were to persist right to $\eta = 0$, the full viscous condition (3.7) would be satisfied—at least when β is neglected in comparison with $U'(0)$. At first sight this fact might seem to justify the inviscid condition as an approximation to the full viscous condition; but in fact this does not follow. Since $\phi = c - U$ is not an exact solution of (3.3), there is no assurance that this approximation satisfies (3.7) adequately because of the large parameter $f'(0)/f(0)$ in (3.7) which multiplies the error in ϕ.)

An important result due to Miles (1957) deserves to be recalled here. The opportunity will be taken to outline a derivation rather different from his. If the inviscid boundary condition noted above is accepted, equation (3.12) leads immediately to

$$\mathscr{I}\{P_s\} = [c - U(\epsilon)]\,\mathscr{I}\{\phi'(\epsilon)\}. \tag{3.13}$$

Now a property deducible from (3.3) (see Lin 1955, § 8.2) is that, for c real as at present, the quantity

$$W = \tfrac{1}{2}i(\phi\phi^{*\prime} - \phi^*\phi'),$$

where ϕ^* denotes the complex conjugate of ϕ, is constant everywhere except at the critical point ($U = c$) where it has a discontinuity. The exact form of the discontinuity can only be decided by a study of the complete Orr–Sommerfeld equation, which shows it to be

$$[W] = W(\eta_c^+) - W(\eta_c^-) = \pi(U_c''/U_c')\,|\phi_c|^2, \tag{3.14}$$

where the subscript c refers to values at the critical point. But $W = 0$ for $\eta > \eta_c$ since $\phi \to 0$ for large η; therefore $W(\epsilon) = -[W]$ if $\eta_c > \epsilon$. Also, owing to the boundary condition $\phi(\epsilon) = c - U(\epsilon)$ (i.e. $\phi = \phi^*$ at $\eta = \epsilon$), we have

$$W(\epsilon) = \tfrac{1}{2}i[c - U(\epsilon)]\,[\phi^{*\prime}(\epsilon) - \phi'(\epsilon)] = [c - U(\epsilon)]\,\mathscr{I}\{\phi'(\epsilon)\}, \tag{3.15}$$

which is the same as the right-hand side of (3.13). Hence

$$\mathscr{I}\{P_s\} = -\pi(U_c''/U_c')\,|\phi_c|^2. \tag{3.16}$$

This is the result found in a somewhat different way by Miles. It shows the energy supply from the fluid to be proportional to the curvature of the velocity profile at the elevation where $U = c$, the supply being positive (i.e. such as to promote the growth of waves) when the curvature is negative. However, it is clear that $\mathscr{I}\{P_s\}$ will not be given as simply as this when the exact boundary condition (3.7) has to be applied.

4. The wall friction-layer

We now consider the function $f(\eta)$, which can be regarded as an adjustment to the inviscid solution required near the boundary in order to satisfy the viscous boundary conditions. This idea is familiar from stability theory; but perhaps the clearest account of what it implies physically is that given by Lighthill (1953), who introduced it in another context. The wall friction-layer (i.e. the region where $f(\eta)$ is appreciable) should not, of course, be confused with the boundary layer by which the velocity profile U may be characterized: the wall layer is likely to be only a very small fraction of the whole boundary layer (see Lighthill 1953, p. 480).

If it is assumed that the effective thickness of the wall layer is very small compared with the wavelength $2\pi/k$, the equation (3.2) satisfied by $f(\eta)$ may be simplified by neglecting the terms in k^2. If it is further assumed that f varies much more rapidly than U, then the term $U''f$ can be neglected in comparison with $(U-c)f''$. Also, $\eta U'(0)$ can be taken as an approximation to $U(\eta)$ over the wall layer. (The fact that $U''(0) = 0$ if the primary flow has no pressure gradient provides further justification for these approximations; but clearly this is not essential.) Thus, the equation for f becomes

$$f^{\mathrm{iv}} = ikR\{\eta U'(0) - c\}\,f''. \tag{4.1}$$

The various approximations which have been introduced can best be justified *a posteriori* by considering the properties of the solution of (4.1) (see § 8). The assumption which probably has greatest need of being tested in particular applications is the linear approximation for U over the wall layer. It will be shown in § 8 that this assumption is well justified in the case of laminar boundary-layer profiles. It is less secure, however, for turbulent boundary layers; because, although the wall layer is much thinner than in corresponding laminar cases, U varies very much more rapidly near the boundary. In effect, applications to turbulent boundary-layer profiles require that the wall layer should lie within the viscous sublayer, over which U is well known to vary linearly.

The 'inviscid' solution $a + b\eta$ of (4.1) is irrelevant here, being in fact equivalent to a linear approximation for $\phi(\eta)$ near $\eta = 0$. The solution of (4.1) which approaches zero rapidly for large η is expressible in the form

$$f(\eta) = A\int_C \exp\left[\tfrac{1}{3}t^3 + im\{\eta - c/U'(0)\}\,t\right]t^{-2}\,dt, \tag{4.2}$$

in which $m = [kRU'(0)]^{\frac{1}{3}}$, A is an arbitrary constant, and the path of integration in the complex t-plane is terminated at $-\infty$ and $\infty e^{\frac{1}{3}\pi i}$. The form of C in finite parts of the plane is immaterial except that C must pass above the origin; but it is most convenient to trace C along the two radii C_1 and C_2 indicated in figure 2, the singularity at $t = 0$ being skirted by a small arc as shown in the figure. In discussing this integral, the notation $z = m\{\eta - c/U'(0)\}$ will be useful.

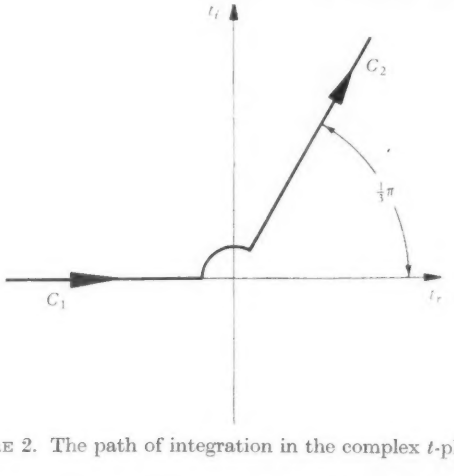

FIGURE 2. The path of integration in the complex t-plane.

Numerical values of this function have been calculated by several authors interested in stability theory, the usual course being to consider $-z$ as the independent variable. (This is the function usually denoted by ϕ_3 in papers on stability.) The values given by Holstein (1950) appear to be the most accurate, and a useful graph of the function appears as figure 4 in his paper (the abscissa there is equivalent to our $-z$). This figure shows both the real and imaginary parts of f to oscillate for increasing values of the argument z, but to decrease at an enormous rate over all ranges of z; for instance, their magnitudes decrease by factors which are $O(10^{-3})$ as z goes from 0 to about 4. Thus, we may consider the length m^{-1} as a measure of the effective thickness of the wall layer; and the assumption that this thickness is small compared with wavelength can therefore be expressed $m \gg k$ (i.e. assumption (ii) of (2.18)). It may be noted also that this solution is expressible in terms of Bessel functions (e.g. see Lin 1955, § 3.6; or Schlichting 1955, p. 327).

Let us consider how the quantity z will vary over the wall layer in some particular physical examples. First, for a rigid solid boundary we have $c = 0$; and so $z = m\eta$ is zero at the boundary and becomes positive away from it. The value of $f(\eta)$ will become negligibly small compared with its value on the boundary as $m\eta$ increases beyond, say, 1 or 2. Values of $f(0)$, $f'(0)$ and $f''(0)$ as required in the present analysis can be obtained very easily from (4.2) in this case.

Now suppose that c has a positive value small enough for the critical point $\eta = \eta_c$ to lie within the region next to the boundary over which the linear approximation $U = \eta U'(0)$ applies. Then $\eta_c = c/U'(0)$, and so $z = -m\eta_c$ at the boundary.

In fact, z increases from this negative value to zero at the critical point, and becomes positive for $\eta > \eta_c$. The viscous solution $f(\eta)$ diminishes rapidly as before, and will reach a quite insignificant magnitude at $z = 0$ if the ratio $mc/U'(0)$ $(= m\eta_c)$ is much larger than unity: i.e. the critical point lies well outside the wall layer. On the other hand, the critical point will occur in the wall layer if this ratio is of the order of unity. Now, even if the critical point lies outside the region where $U = \eta U'(0)$, the approximation for $f(\eta)$ is still valid provided that $mc/U'(0)$ is large; for, though $\eta = c/U'(0)$ is no longer the critical point, the wall layer is covered effectively while z still has large negative values, i.e. $f(\eta)$ has practically vanished well before z increases to zero. We remark that in this respect our use of the function $f(\eta)$ differs from the usual course in stability theory: there it is generally assumed that a linear approximation holds between the critical point and the (plane) wall, and in fact $U'(\eta_c)$ rather than $U'(0)$ is commonly written in the definitions of parameters corresponding to our m (cf. Lin 1955, p. 40).

A possible limitation of the present analysis must now be mentioned. The difficulty might be expected to arise in applications to turbulent boundary-layer profiles which have exceedingly high values of $U'(0)$. It appears feasible that the parameter $mc/U'(0) = (kR)^{\frac{1}{3}} c[U'(0)]^{-\frac{2}{3}}$ could be quite small even when the critical point occurred well away from the boundary. According to the line of argument considered above, the approximation (4.2) would not apply in this case. To meet an objection of this sort, it is necessary to examine the relation between $U'(0)$ and R for actual boundary layers. This step is deferred until § 8; and we meanwhile introduce the special assumption—to be justified there—that the parameter in question is reasonably large for all applications where the critical point is outside the region where $U = U'(0)\,\eta$, e.g. outside the viscous sublayer of a turbulent boundary layer. This assumption is listed as item (iv) in (2.18).

The quantity $f'(0)/f(0)$ appearing in (3.7) has special interest at present since it determines how, through the boundary conditions, viscosity affects the 'inviscid' solution $\phi(\eta)$ representing the disturbance in the main body of the fluid. In the literature on stability theory, this quantity is commonly expressed in terms of a certain function often named after Tietjens, who first introduced it: thus, in our notation

$$\frac{f'(0)}{f(0)} = -\frac{m}{D(-mc/U'(0))}, \tag{4.3}$$

where $D(\ )$ is the Tietjens function according to the usual definition. (Apparently many writers on stability have kept the notation D originally used by Tietjens, although F is used for $D \div z_0$ by Lin (1945, Part I; 1955, § 3.6).) At least six authors have given numerical tables of the real part D_r and imaginary part D_i of this function. The values given by Holstein (1950) cover the widest range of the argument; and a useful feature of his table is that the values calculated by five previous authors are included.

Graphs of $D_r(-z_0)$ and $D_i(-z_0)$ are shown in figure 3. It is seen that for z_0 greater than about 8 both functions cease to oscillate and rapidly approach the asymptote $1/\sqrt{(2z_0)}$ (see equation (4.13) below). The range of positive z_0 for which D_i is negative has special interest in a later part of our discussion. This is

$0 < z_0 < 2{\cdot}3$, the upper limit having been estimated from values of D_i tabulated by Holstein (1950) and Lin (1945). (Holstein includes values for $z_0 = 1{\cdot}5, 2{\cdot}0, 2{\cdot}5$; and Lin gives values (actually of his $F \equiv D/z_0$) at intervals of $0{\cdot}2$ for z_0. The latter are consistent with Holstein's, except that Lin's values for $z_0 = 2{\cdot}4$ and $2{\cdot}6$ seem to be incorrect.)

Figure 3 indicates that, for a given m, $f'(0)/f(0)$ becomes progressively larger as c gets fairly large. And so, recalling the remarks made below (3.7), we see that the exact boundary condition on ϕ tends to assume the simple form $\phi(0) = c$ which might be proposed as the (kinematical) boundary condition if viscosity were

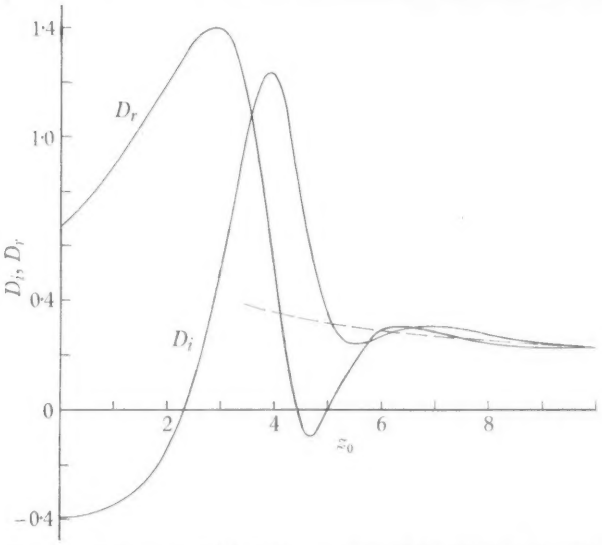

FIGURE 3. Graphs of the real and imaginary parts of the Tietjens function $D(-z_0)$. The dashed line is part of the curve $(2z_0)^{-\frac{1}{2}}$, which is the asymptote of D_r and D_i.

neglected from the start. The fact that for large wave velocities the effects of friction at the wave surface cease to be significant is, of course, to be expected on physical grounds (cf. Miles 1957, bottom of p. 187). However, it should be noted that as a criterion for neglecting viscosity a Reynolds number based on wave velocity and wavelength is not really adequate: the parameter $mc/U'(0)$ seems to provide a more reliable test, particularly in view of the fact that $U'(0)$ increases with Reynolds number in any self-consistent model for the flow.

We shall next consider the specific form taken by the boundary condition (3.7) in some special cases. To evaluate $f'(0)/f(0)$ explicitly, we might justifiably resort to existing tabulations of the Tietjens function; but it seems worth while to proceed directly from (4.2) for a few illustrations.

The case $c = 0$

Here the critical point coincides with the boundary. It will be assumed that there is no pressure gradient in the primary flow, so that $U''(0) = 0$: hence, as (3.3) now does not have a singular point at $U = c$, ϕ and ϕ' remain valid approxima-

tions over the whole flow. We also take $\beta = 0$ as the boundary is implied to be solid in this case. To find $f(0)$ explicitly from (4.2), the component integrals along the two radii shown in figure 2 are reduced to the same real integral by the substitutions $t = -s$ along C_1 and $t = e^{\frac{1}{3}\pi i}s$ along C_2. Thus we get

$$f(0) = A(e^{-\frac{1}{3}\pi i}+1)\left\{\int_{s^+}^{\infty} e^{-\frac{1}{3}s^3}\frac{ds}{s^2} - \frac{1}{s^+}\right\},$$

in which $s^+ \to 0$. An integration by parts now leads easily to

$$f(0) = -A3^{\frac{1}{3}}\Gamma(\tfrac{2}{3})\,e^{-\frac{1}{6}\pi i}. \tag{4.4}$$

The integral expression for $f'(0)$ obtained from (4.2) has a rather different character, as the contributions from C_1 and C_2 cancel, leaving as sole contribution the residue from the 120° circuit of the simple pole of the integrand at $t = 0$. It is found without difficulty that

$$f'(0) = A\tfrac{2}{3}\pi m, \tag{4.5}$$

and hence

$$f'(0)/f(0) = -1{\cdot}288\,e^{\frac{1}{6}\pi i}\,m. \tag{4.6}$$

The fractional error in this result (due to our neglecting terms in k^2 when deriving (4.1)) can be shown to be $O(k/m)^2$, which is very small according to assumption (ii) of (2.18).

Incidentally, a result which will be needed later can be found in the same way from (4.2): this is

$$f''(0)/f(0) = 1{\cdot}372\,e^{\frac{1}{3}\pi i}\,m^2. \tag{4.7}$$

The substitution of (4.6) into (3.7) now shows that the boundary condition to be satisfied by the inviscid condition is

$$\phi'(0) + 1{\cdot}288\,e^{\frac{1}{6}\pi i}\,m\phi(0) = -U'(0). \tag{4.8}$$

This covers both the kinematical and viscous conditions at the wave surface, and appears at first sight quite unlike any boundary condition that might be applied if viscosity were to be neglected from the start. The implications of this boundary condition will be examined later when $\phi(\eta)$ has been established explicitly; but this is a suitable place to note an interesting interpretation given by Lighthill (1953), who investigated the wall friction-layer in the course of his work on the upstream influence of boundary layers in supersonic flow.

To bring (4.8) into line with Lighthill's argument, the equation is multiplied by $(1{\cdot}288\,e^{\frac{1}{6}\pi i}\,m)^{-1}$, which may be denoted by $0{\cdot}776L$, say, where L has the same meaning as in Lighthill's notation. Thus, (4.8) becomes

$$\phi(0) + 0{\cdot}776L\phi'(0) = -0{\cdot}776LU'(0). \tag{4.9}$$

Now L is a complex parameter whose magnitude is a length comparable with the thickness of the wall layer; and over such a length from the wall the linear approximation $\phi(\eta) = \phi(0) + \eta\phi'(0)$ is certainly adequate. Hence, (4.9) has the interpretation that $\phi(\eta) = -U(\eta)$ approximately for $\eta = 0{\cdot}776L$, which could be taken to mean that the flow satisfies a kinematical condition on a certain surface $\eta = 0{\cdot}776L$ a small distance from the boundary $\eta = 0$. In other words, the effect of the wall layer appears to be as if the surface $\eta = 0{\cdot}776L$ were replaced by a solid wall, outside which viscosity had no effect.

It must be emphasized, however, that the equation $\eta = 0{\cdot}776L$ does *not* represent any surface in the physical plane. For, like the other complex parameters in this analysis, L is merely an operator carrying phase as well as magnitude significance, and obviously has no physical meaning divorced from the connotation of operating on periodic functions of ξ. This hypothetical wall has therefore to remain an abstract concept.

The case $mc/U'(0) = O(1)$ or less

The critical point now occurs away from the boundary yet still within the friction layer. This case is exemplified by waves upon a film of highly viscous liquid dragged along a plane wall by an air stream: the wave speed would be of the order of the mean velocity of the film, which would be only a very small fraction of the velocity in the main air stream. However, this case may still apply when c is a significant fraction of the free-stream velocity, if the initial velocity gradient is large as in turbulent flows with a boundary layer.

It would be appropriate here to use the expression (4.3) in terms of the Tietjens function. But, to bring out the effects of small yet finite values of $mc/U'(0)$, a useful alternative might be to approximate the integrals for $f(0), \ldots, f^n(0)$ by the leading terms of Taylor series in powers of this parameter. Accordingly, (4.2) gives

$$f^n(0) = A[I_n - \{imc/U'(0)\} I_{n+1} + \tfrac{1}{2}\{imc/U'(0)\}^2 I_{n+2} + \ldots], \tag{4.10}$$

where $$I_N = \int_C e^{\frac{1}{3}t^3} t^{N-2}\, dt \quad \text{with} \quad N = 0, 1, 2, \ldots.$$

This scheme of approximation leads to

$$f'(0)/f(0) = -1{\cdot}288\, e^{\frac{1}{6}\pi i}\, m[1 - 0{\cdot}223\, e^{\frac{1}{6}\pi i}\{mc/U'(0)\} + \ldots]. \tag{4.11}$$

Obviously, the results for $c = 0$ apply approximately to this also if $mc/U'(0)$ is small enough.

The case $mc/U'(0) \gg 1$

The critical point now occurs well outside the wall layer. We first remark that, as $f'(0)/f(0)$ gets very large in this case, the term $U'(0)$ in the boundary condition (3.7) takes on secondary importance. Hence, according to assumption (iii) of (2.18), the term β may be neglected entirely. This boundary condition may therefore be rewritten

$$\phi(0) - c = \{f(0)/f'(0)\}\{\phi'(0) + U'(0)\}. \tag{4.12}$$

Near the boundary the exponent z in (4.2) is large negatively; and so it is suitable to use an asymptotic approximation to the integral—and to similar integrals for f' and f''. These may be obtained by the method of steepest descents. In this way we obtain (cf. Lin 1945, p. 136; 1955, § 8.5)

$$f'(0)/f(0) \sim -e^{-\frac{1}{4}\pi i}\,(kRc)^{\frac{1}{2}}, \tag{4.13}$$

and

$$f''(0)/f(0) \sim -ikRc. \tag{4.14}$$

These two formulae are reliable for $mc/U'(0)$ greater than about 8. We note that (4.13) is equivalent to $D(-z_0) \sim e^{\frac{1}{4}\pi i} z_0^{-\frac{1}{2}}$.

5. The solution for a linear velocity profile†

This model for the primary flow is exceptional in that the equation for $F(\eta)$ is exactly the Orr–Sommerfeld equation, which moreover can be solved completely in this case: consequently, it is worth brief consideration as an example on which to test some of the foregoing theory. The model obviously suffers from lack of realism, its practical applications being essentially restricted to cases where the disturbance of the flow is confined to a region over which a linear approximation can be made to the actual velocity profile. Since the disturbance penetrates to distances of the order of a wavelength from the boundary, the model would generally be reliable only for very short waves.

When $U(\eta) = G\eta$, where G is a constant (see figure 4(*a*)), the exact equation (3.1) for $F(\eta)$ becomes

$$im^3(\eta - c/G)(F'' - k^2F) = F^{\mathrm{iv}} - 2k^2F'' + k^4F, \tag{5.1}$$

with $m^3 = kRG$. The complete solution of (5.1) which tends to zero for large η is $F = \phi + f$, where

$$\phi = A\,e^{-k\eta}, \tag{5.2}$$

and

$$f = B\int_C \exp\left[\tfrac{1}{3}t^3 + \{im(\eta - c/G) + \alpha^2\}t\right]\frac{dt}{t^2+\alpha^2}, \tag{5.3}$$

in which $\alpha = k/m$, and the path of integration is the same as in (4.2). Again C must pass over the origin and be terminated at $-\infty$ and $\infty\, e^{\frac{1}{3}\pi i}$, but is otherwise arbitrary. Although it appears that the integral (5.3) takes different values accordingly as C passes above or below the singularity at $t = i\alpha$, this choice of path is in fact immaterial, since the residue from $t = i\alpha$ simply reproduces the solution (5.2). The mathematical steps leading to (5.3) are not difficult, and an account of them may reasonably be omitted: it is easily verified by differentiation that (5.3) is a solution of (5.1). The present ϕ and f have precisely the meanings associated with these symbols in § 3, but are exceptional in that both are exact solutions.

It is not possible to express the required quantities $f(0)$, $f'(0)$, etc., exactly in forms any simpler than the integrals given directly by (5.3). To obtain compact results, therefore, approximate expressions will have to be introduced. This step nullifies to an extent the advantage of having exact solutions, which is the outstanding merit of the present model; but there remains the advantage that the scheme of approximation can be extended without difficulty to successively higher degrees of accuracy.

As α may be assumed to be small, which corresponds to assumption (ii) of (2.18), f may suitably be approximated in terms of ascending powers of α. The factor $\exp(\alpha^2 t)$ in the integrand of (5.3) can be expanded as a power series and

† I have recently learnt that this example was also treated by Dr M. S. Longuet-Higgins in unpublished work done in 1952 while he was at the Scripps Institute of Oceanography, La Jolla. By means of a theory developed in Cartesian co-ordinates, he calculated the pressure distribution over a solid corrugated surface bounding a uniform shearing flow. His results agree with the present ones for a solid boundary.

integrated term by term, since this expansion is convergent for all t and the series of integrals is also convergent. Now, the binomial expansion

$$\frac{1}{t^2+\alpha^2} = \frac{1}{t^2} - \frac{\alpha^2}{t^4} + \frac{\alpha^4}{t^6} - + \dots$$

is convergent for $|t| > \alpha$, and so this expansion can clearly be used in the integrand and integrated term by term if the path C passes outside the circle of non-convergence $|t| = \alpha$. But the integrand of each integral in this expansion has no finite singularity other than at $t = 0$, so that by Cauchy's theorem each integral along C outside $|t| = \alpha$ is the same as that along the path used in § 4, i.e. along the two radii and small arc shown in figure 2. Thus (5.3) can be evaluated by expanding the integrand as suggested and integrated term by term along the path in figure 2. For example, we would obtain in this way, with $c = 0$,

$$f(0) = B\{I_0 + \alpha^2(I_1 - I_{-2}) + \alpha^4(I_2 + I_{-4}) + \dots\},$$

where I_N is the function of $N\,(= 0, \pm 1, \pm 2, \dots)$ defined below (4.10). Hence, the problem can in principle be completed to any order of approximation in terms of α. However, it seems enough for present purposes to take only the leading term in the expansion of (5.3), which is the function defined by (4.2). That is, we neglect $O(\alpha^2)$. Terms which are $O(\alpha)$ will arise through the boundary conditions; and these seem sufficient to illustrate the effect of the parameter α.

Owing to the fact that the critical point $\eta_c = c/G$ is not a singular point in this example, the various cases considered separately in § 4 can conveniently be covered at once by taking the form (4.12) of the boundary condition and allowing c to have any value including zero. If $f'(0)/f(0)$ is expressed in terms of the Tietjens function according to (4.3), and (5.2) is used for $\phi(0)$ and $\phi'(0)$, this boundary condition gives

$$A - c = -m^{-1}D(-z_0)\{-kA + G\}$$

with $z_0 = mc/G$, and hence

$$A = -Gm^{-1}\{D(-z_0) - z_0\}\{1 + \alpha D(-z_0)\} \tag{5.4}$$

to the first order in α.

We now find the normal stress σ_s on the boundary, which (2.13) shows to be the same as the pressure $p_s = \mathscr{R}\{P_s e^{ik\xi}\}$ to the present order of approximation. Equation (3.9) gives with the same accuracy simply $P_s = (G - kc)A$; and so, using (5.4), we have

$$P_s = -k^{-\frac{1}{3}}R^{-\frac{1}{3}}G^{\frac{5}{3}}(1 - \alpha z_0)\{D(-z_0) - z_0\}\{1 - \alpha D(-z_0)\}. \tag{5.5}$$

This relation shows both the real and imaginary parts of P_s to vary in a very complicated way with the parameter z_0. Consider first the real part $(P_s)_r$, which measures the amplitude of the pressure component in phase with the wave elevation. If we ignore the quantity $\alpha D(-z_0)$, which is always small since $D(-z_0)$ is never large, (5.5) shows $(P_s)_r$ to be negative—as it is for a potential flow over waves with U constant—when $(1 - \alpha z_0)\{D_r - z_0\} > 0$. This condition is satisfied only with $z_0 < 0{\cdot}9$ and $z_0 > \alpha^{-1}$: that is, with $c < 0{\cdot}9G/m$ and $c > G/k$. The

imaginary part $(P_s)_i$ is positive, which implies a positive 'sheltering coefficient'—whose significance is to be explained later, when $(1-\alpha z_0)\,D_i < 0$. This occurs with $z_0 < 2{\cdot}3$ and $z_0 > \alpha^{-1}$. The occurrence of positive values of $(P_s)_i$ for a range of small values of c and then only for fairly large values will also be observed in § 7, where velocity profiles more realistic than the present one will be treated. This will be pointed out to have considerable physical interest.

An explicit expression for p_s will now be written down with $c = 0$, this case being sufficient for purpose of illustration. According to (4.6), we have $D(0) = 0{\cdot}776\,e^{-\frac{1}{6}\pi i}$. Hence, (5.5) leads immediately to†

$$p_s = -0{\cdot}776ak^{-\frac{1}{3}}R^{-\frac{1}{3}}G^{\frac{4}{3}}\{\cos(k\xi - \tfrac{1}{6}\pi) + 0{\cdot}776\alpha\cos(k\xi - \tfrac{1}{3}\pi)\}. \tag{5.6}$$

The shearing stress τ_s on the wave surface can also be calculated easily for this case. Equation (2.12) gives

$$\begin{aligned} T_s &= R^{-1}\{f''(0) + k^2 A\} \\ &= R^{-1}A\{-f''(0)/f(0) + k^2\}. \end{aligned} \tag{5.7}$$

Using (5.4) together with the expression (4.7) for $f''(0)/f(0)$, and neglecting terms which are $O(\alpha^2)$, we obtain directly

$$T_s = 1{\cdot}065\,e^{\frac{1}{6}\pi i}\,R^{-1}mG(1 + 0{\cdot}776\,e^{-\frac{1}{6}\pi i}\,\alpha). \tag{5.8}$$

The stress τ_s is the real part of $T_s a\,e^{ik\xi}$: thus, when we put $m = (kRG)^{\frac{1}{3}}$, (5.8) shows that

$$\tau_s = 1{\cdot}065aR^{-\frac{2}{3}}k^{\frac{1}{3}}G^{\frac{4}{3}}\{\cos(k\xi + \tfrac{1}{6}\pi) + 0{\cdot}776\alpha\cos k\xi\}. \tag{5.9}$$

Note that the amplitude of the first cosine term may be written $1{\cdot}065\tau_0 ma$, where $\tau_0 = G/R$ is the uniform shearing stress exerted by the primary flow.

In these formulae x may be written instead of ξ if preferred. For comparison with them it is appropriate to recall from (2.1) that the wave surface is expressed in terms of (x, y) by the equation $y = a\cos kx$. Note that both τ_s and σ_s vanish for $R \to \infty$.

An interesting feature of (5.6) and (5.9) is the phase relation between the stresses and the wave on the boundary. It is seen that at high Reynolds numbers ($\alpha \to 0$) the shearing stress is approximately $\frac{1}{6}\pi$ in advance of the wave: that is, the maxima occur at points one-twelfth of a wavelength in the rear of the wave crests (x being regarded as the forward direction on the waves). The phase of the normal stress is $\frac{5}{6}\pi$ in advance: that is, the maxima occur one-twelfth of a wavelength forward from the troughs. These results, particularly that for the phase of τ_s, can be interpreted to indicate a kind of 'sheltering' on the leeward slopes of the waves; but this will be made much clearer by an example which is to be considered as part of § 8. At least it can be said that, despite the rather artificial character of this linear-profile model, these phase relationships seem perfectly in keeping with intuition about the general nature of wind forces on waves (we recall the useful remarks by Lamb (1932, p. 630) concerning what is to be expected in this matter).

† This formula was also obtained by Dr Longuet-Higgins in his work cited in the previous footnote.

6. A simple profile approximating a laminar boundary layer

As a further simple example, we consider a velocity profile characterized by a region $0 \leqslant \eta \leqslant \delta$ (region (i)) in which U is given by

$$U = U_\infty \sin K\eta \qquad (K = \pi/2\delta), \tag{6.1}$$

and beyond which (in region (ii)) U remains constant at the value U_∞ (see figure 4(*b*)). This profile is a fairly close approximation to the laminar boundary layer along a plane, if we take $\delta = 4{\cdot}8XR_X^{-\frac{1}{2}}$, X being the distance from the start of the boundary layer and R_X the Reynolds number based on this distance (cf.

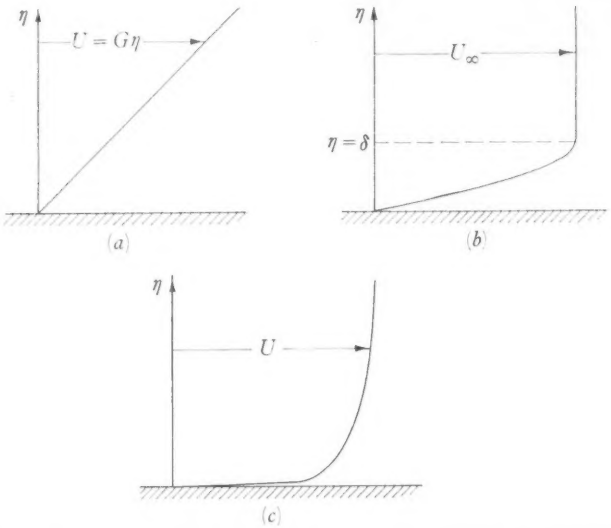

FIGURE 4. Types of velocity profile considered: (*a*) linear profile; (*b*) laminar boundary-layer profile approximated by a quarter-period sinusoid; (*c*) turbulent boundary-layer profile.

Lamb 1932, p. 686). With this value of δ, the important parameter $U'(0) = KU_\infty$ is the same as for the exact boundary-layer profile (see, for instance, Schlichting 1955, chapter VII); and it is clear that the small differences between the present profile and the exact one would scarcely affect our analysis. This profile is specially worth considering for the case $c = 0$, since the differential equation (3.3) for ϕ can be solved exactly.

When (5.1) is substituted, equation (3.3) becomes, with $c = 0$,

$$\phi'' + (K^2 - k^2)\phi = 0, \tag{6.2}$$

whose general solution may be expressed

$$\phi = U_\infty(A \sin l\eta + B \cos l\eta), \tag{6.3}$$

where $l = \sqrt{(K^2 - k^2)}$. It also appears from (3.3) that the form of the inviscid solution in region (ii) is simply $\phi = \text{const.} \times e^{-k\eta}$. Therefore, to make ϕ and ϕ'

continuous at $\eta = \delta$, the solution (6.3) must satisfy the condition $\phi'(\delta) = -k\phi(\delta)$. Hence, putting $\theta = l\delta = \frac{1}{2}\pi\sqrt{\{1-(k/K)^2\}}$, we get

$$\frac{A\cos\theta - B\sin\theta}{A\sin\theta + B\cos\theta} = -\frac{k}{l}, \tag{6.4}$$

which gives on rearrangement

$$\frac{A}{B} = \frac{1-(k/l)\cot\theta}{\cot\theta + (k/l)}. \tag{6.5}$$

For use in the boundary condition (4.8), we have $\phi(0) = BU_\infty$, $\phi'(0) = lAU_\infty$ and $U'(0) = KU_\infty$. Thus, if (6.5) is used to eliminate A, (3.7) leads to

$$B\left\{\frac{l - k\cot\theta}{\cot\theta + (k/l)} + 1{\cdot}288\, e^{\frac{1}{6}\pi i}\, m\right\} = -K. \tag{6.6}$$

This relation determines B, and hence A is known through (6.5).

To find the pressure at the boundary, we may use the formula (3.12), putting $\epsilon = 0$ as we can do if the minute pressure variation across the wall layer is to be neglected. This gives

$$P_s = U'(0)\,\phi(0) = KBU_\infty^2 = -\frac{K^2U_\infty^2}{l}\left\{\frac{1-(k/l)\cot\theta}{\cot\theta + (k/l)} + 1{\cdot}288\, e^{\frac{1}{6}\pi i}\frac{m}{l}\right\}^{-1}. \tag{6.7}$$

Following from (2.12), an approximation to the shearing stress on the boundary is provided by

$$T_s = R^{-1}f''(0) = -R^{-1}\{f''(0)/f(0)\}\,\phi(0). \tag{6.8}$$

Hence, using (4.7) and (6.6), and noting that in the present example

$$m = [kKRU_\infty]^{\frac{1}{3}},$$

we find that

$$T_s = 1{\cdot}372\, e^{\frac{1}{3}\pi i}\frac{K^2kU_\infty^2}{lm}\left\{\frac{1-(k/l)\cot\theta}{\cot\theta + (k/l)} + 1{\cdot}288\, e^{\frac{1}{6}\pi i}\frac{m}{l}\right\}^{-1}. \tag{6.9}$$

These expressions for the stresses are too complicated for easy interpretation; but considerable simplification is possible if the boundary-layer thickness δ is taken to be small compared with the wavelength, so that $k\delta$ and hence k/K are small—though still $k\delta \gg R^{-1}$. We need to assume that the wall friction layer still occupies only a small part of the boundary layer; and we also assume that $\Delta = km/K^2$ is small. The checking of these two assumptions will be left until the next section, where a general type of long-wavelength approximation is to be developed. If terms which are $O(k\delta)^2$ are neglected, we have $l \doteqdot K$, $\cot\theta \doteqdot 0$; and (6.7) and (6.9) give approximately

$$P_s = -kU_\infty^2(1 - 1{\cdot}288\, e^{\frac{1}{6}\pi i}\Delta), \tag{6.10}$$

$$T_s = 1{\cdot}372\, e^{\frac{1}{3}\pi i}\, U_\infty^2 k^2/m. \tag{6.11}$$

The error in (6.10) is $O(\Delta^2)$ and that in (6.11) is $O(\Delta)$, the latter estimate being quite adequate since $T_s \ll P_s$.

These results provide the following explicit expressions for the stresses on the wavy boundary $y = a\cos kx$:

$$\begin{aligned} p_s/U_\infty^2 &= -ka\{\cos k\xi - 1{\cdot}288\Delta\cos(k\xi + \tfrac{1}{6}\pi)\} \\ &= -ka\{[1 - 1{\cdot}115\Delta]\cos k\xi + 0{\cdot}644\Delta\sin k\xi\}; \end{aligned} \tag{6.12}$$

$$\tau_s/U_\infty^2 = 1{\cdot}372ka\alpha\cos(k\xi + \tfrac{1}{3}\pi i), \tag{6.13}$$

where $\alpha = k/m$ as in § 5, this quantity being small by assumption (ii) of (2.18). Note that $\sigma_s = p_s$ to the present order of approximation.

In common with the results found for the previous example, both stresses have distributions suggestive of a 'sheltering' action: that is, their minima occur on the leeward slopes of the waves. The pressure sheltering coefficient according to the usual definition (Jeffreys 1924, 1925; Ursell 1956) is in fact $s = 0{\cdot}644\Delta$.

7. Boundary-layer profiles in general

We shall now investigate some approximate methods applicable generally to velocity profiles of boundary-layer type. We particularly wish, with turbulent boundary layers in mind, to be able to deal with comparatively diffuse profiles of the general form indicated in figure 4(*c*). Further, it is now time to complete some calculations for the surface stresses in the interesting case where $c > 0$ so that there is a critical point away from the boundary in a region where the profile is curved. To account for the viscous solution $f(\eta)$, the method applied previously is still useful; but it remains to find a suitable approximation to the solution $\phi(\eta)$ of the 'inviscid' equation (3.3). This equation cannot be solved exactly in terms of known functions except in the two simple cases considered previously—and perhaps in one or two other cases of no interest here. If a high degree of accuracy were required, resort would have to be made to numerical solutions computed for particular profiles—as has been done in various studies of hydrodynamic stability (see, for instance, Lin (1945, Part 3) for calculations relating to parabolic and Blasius profiles). It is more instructive, however, to use the approximate expression derived as follows, which is unrestricted to any particular form of U. Although this is essentially a small-k approximation, thus applying most accurately to thin boundary layers, it probably gives a reasonably good account of the properties of ϕ even for fairly diffuse profiles.

We first observe that over a range excluding any critical point an approximation to the solution of (3.3) for small k is

$$\phi = A(U-c)\,e^{-k\eta}, \tag{7.1}$$

which evidently satisfies (3.3) accurately wherever $U''/k^2(U-c)$ is either very small or very large compared with unity. (It appears, rather remarkably, that this approximation was first noted both by Lighthill (1957, § 6) and by Miles (1957, § 5) in papers dealing with entirely different topics but appearing at the same time in the same journal.) Let us for a moment consider the exceptional case where $c < 0$: that is, the wave travels in the direction opposite to the flow. There is now no critical point, and (7.1) is a uniformly valid approximation over the whole of a flow of boundary-layer type. In the region far from the boundary where U tends to a constant value, ϕ tends to const. $\times\, e^{-k\eta}$ as it should do; whereas in the region near the boundary over which U varies rapidly, $\phi \doteqdot$ const. $\times\,(U-c)$ which satisfies (3.3) approximately for small k. Further, if the arbitrary constant A is put equal to -1, the boundary condition (3.7) is satisfied very nearly provided only that the usual conditions $U'(0) \gg kc$ and $U'(0) \gg \beta$ hold; and also (3.5) gives $f = 0$. Hence, (2.4) and (2.5) reduce to $\psi(\xi,\eta) = \psi_0(\eta)$ and $v = 0$, $u = U(\eta) - c$. The ξ-lines are thus *streamlines* according to this approximation.

The latter result incidentally has considerable interest as evidence supporting the method of linearization set out in § 2. For it shows that, at least in the absence of a critical point, a fair approximation to the actual flow pattern is already obtained simply by 'bending' the primary profile to follow the waves by use of the system of curvilinear co-ordinates. There can therefore be no further doubt about the smallness of the periodic perturbation introduced on the left-hand side of (2.4) to represent the difference between the 'bent' profile and the actual flow.

While serving best for $c < 0$, this approximation also has a somewhat limited usefulness in the case $c = 0$, provided $U''(0) = 0$ so that ϕ does not exhibit singular behaviour at the critical point on the boundary. The wall friction-layer is effectively absent in this approximation, and so the surface shearing stress is indeterminate. According to (3.9), however, an approximation to the pressure at the wave surface is given by

$$P_s = -k^2 \int_0^\infty U^2 e^{-k\eta}\, d\eta. \tag{7.2}$$

Thus the pressure is in exact anti-phase with the wave elevation, no sheltering being indicated.

To deal adequately with the case of a rigid boundary, and to make any progress at all with the case where there is a critical point inside the fluid, an improvement on (7.1) is obviously needed. A method of developing successive uniformly valid approximations to the solution of (3.3) for small k was given by Lighthill (1957, § 6). He applied the method under the restriction that $U - c$ (equivalent to his V) does not vanish anywhere; but it still formally yields results in the absence of this restriction; and certain questions of indeterminacy which then arise can be answered by other considerations (see below). A second approximation to the solution of (3.3) is found by Lighthill's method to be

$$\phi = A(U-c)\, e^{-k\eta}\left[1 + k\int_\eta^\infty \left\{\left(\frac{U_\infty - c}{U-c}\right)^2 - 1\right\} d\eta\right], \tag{7.3}$$

where U_∞ is the constant value approached by U as $\eta \to \infty$. The error in this is proportional to k^2. Details of the derivation may be omitted, as it is easily verified that (7.3) satisfies (3.3) to the order of approximation in question.

This approximate expression for ϕ seems quite adequate for our present purpose. Although the integral in (7.3) is indeterminate for $\eta < \eta_c$ (i.e. $U < c$), we shall see that a simple adjustment indicated by the theory of the full Orr–Sommerfeld equation is sufficient to remove the ambiguity, and so make (7.3) give a correct account of ϕ either side of the critical point. It can be shown that the extra terms present in higher approximations (the next one was given by Lighthill) do not affect the behaviour at the critical point in any vital way.

It is noteworthy that (7.3) reduces as follows in the case of very thin boundary layers: i.e. where the boundary-layer thickness δ is very small compared with k^{-1} and we have $U = U_\infty$ for $\eta \geqslant \delta$. If terms which are $O(k\delta)^2$ are neglected, (7.3) gives, for $\eta < \delta$,

$$\phi = A(U-c)\left[1 + k(U_\infty - c)^2 \int_\eta^\delta \frac{d\eta}{(U-c)^2}\right]. \tag{7.4}$$

This expression is seen to be the sum of two functions of η which each satisfy the equation $(U-c)\phi''-U''\phi=0$ (i.e. equation (3.3) with the term in k^2 omitted); and also (6.4) satisfies the boundary condition which, as demonstrated in § 6, is to be applied at the edge of the boundary layer, i.e. $\phi'(\delta)=-k\phi(\delta)$. It may be recognized that the two functions comprise the leading terms in the well-known Heisenberg expansion (see Lin 1955, p. 34), which expresses the solution of (3.3) in powers of k^2 and has had important applications to stability theory. Unlike (6.3), an approximation taking a few terms of the Heisenberg expansion is not uniformly valid over the whole range $0 \leqslant \eta < \infty$, and would be unsuitable for the application we intend to make to fairly diffuse boundary-layer profiles.

The case of a rigid solid boundary

In our first application of (7.3), let us take $c=0$ and assume no primary pressure gradient so that $U''(0)=0$. For clarity in what follows, it seems worth while to rewrite (7.3) with $c=0$:

$$\phi = AU\,e^{-k\eta}\left[1+k\int_\eta^\infty\left\{\frac{U_\infty^2}{U^2}-1\right\}d\eta\right]. \tag{7.5}$$

The integral in (6.5) diverges without bound for $\eta\to 0$ (i.e. $U\to\eta U'(0)\to 0$); but its product with U converges to a finite limit. Thus, we easily find that

$$\phi(0) = AkU_\infty^2/U'(0). \tag{7.6}$$

It is also easy to show that $\phi'(0)$ is expressible in the form

$$\phi'(0) = AU'(0)\{1+\chi\}, \tag{7.7}$$

where

$$\chi = \int_0^\infty\left\{1-\frac{U'}{U'(0)}\right\}\left\{\frac{U_\infty^2}{U^2}-1\right\}d(k\eta)-\frac{2kU_\infty}{U'(0)}. \tag{7.8}$$

The integral which χ denotes is clearly convergent to a finite limit if $U''(0)=0$, as is assumed; for then $\{U'(0)-U'(\eta)\}\to O(\eta^2)$ as $\eta\to 0$, and so the integrand remains finite at $\eta=0$. If $U''(0)$ were not zero, a logarithmic singularity would arise, as one expects since $\eta=0$ would in this case be a singular point of the differential equation (3.3). To deal with the case of non-zero pressure gradient, the 'modified inviscid' solutions studied by Tollmien (1929) would be required: these satisfy (3.3) away from the critical point, but in its immediate neighbourhood become approximate solutions of the full Orr–Sommerfeld equation. However, we shall not attempt to cover this case.

If the ratio $kU_\infty/U'(0)$ is specified (or $k\delta$), the quantity in (7.7) depends only on the shape of the velocity profile. For example, we find that $\chi=-k\delta=-\frac{1}{2}\pi kU_\infty/U'(0)$ for the sinusoidal profile considered in § 6. Again, for the exact laminar boundary layer along a plane, a numerical integration using Howarth's figures (Schlichting 1955, p. 107) gives $\chi=-1{\cdot}75kU_\infty/U'(0)$. To estimate χ for turbulent boundary-layer profiles is more difficult, since the greatest contribution to the integral (7.8) comes from the region near the boundary —yet outside the viscous sublayer—where the shape of the profile is least accurately known. However, it is still clear that $\chi=O(k\delta^*)$, say, where δ^* is roughly speaking the width of the region over which most of the variation of

U occurs. This may be considerably less than $O(k\delta)$, where δ is the 'overall' boundary-layer thickness; because, for a turbulent profile, U is not much different from U_∞ over most of its width, and so the respective contribution to (7.8) is small. It is inappropriate to go into this matter any further; for we shall regard χ as a small quantity anyway, and presently see that it may be neglected entirely in forming results which suffice as a first approximation.

If we also take $\Delta = kmU_\infty^2/[U'(0)]^2$ to be small, the substitution of (7.6) and (7.7) in the boundary condition (4.8) gives approximately

$$A = -1\{1-\chi-1{\cdot}288\,e^{\frac{1}{6}\pi i}\Delta\}. \tag{7.9}$$

Hence, if this is put into (7.5) and the integral in (7.5) is combined with the definition (7.8) of χ, the result can be written

$$\phi = -\frac{kU_\infty^2}{U'(0)} - U\,e^{-k\eta}\left[1-1{\cdot}288\,e^{\frac{1}{6}\pi i}\Delta - k\int_0^\eta \left\{1-\frac{U'}{U'(0)}\right\}\left\{\frac{U_\infty^2}{U^2}-1\right\}d\eta + \frac{kU}{U'(0)}\right]. \tag{7.10}$$

To find the pressure at the boundary, the integral formula (3.9) is clearly the most appropriate at present, since it is not unduly sensitive to errors in our expression for ϕ. (Note that the alternative formula (3.12) would give a very poor approximation here: it was used without disadvantage in the previous example (§ 6) only because ϕ was known exactly there.) In evaluating (3.9), there is justification for omitting some of the terms in (7.10). As the most important simplification, the integral in (7.10) can be neglected: since the fixed limit in this integral is zero (not ∞ as in (7.5)), its effect tends to be cancelled by the exponential factor multiplying it; and its omission is well justified if $k\delta^*$ is fairly small. Further, two terms which are $O(kU_\infty/U'(0))$ times the leading terms can be neglected, with obvious justification if a turbulent boundary layer is in question, and also if $k\delta$ is small in the case of a laminar boundary layer. Accordingly, we obtain the approximation

$$P_s = -k^2(1-1{\cdot}288\,e^{\frac{1}{6}\pi i}\Delta)\int_0^\infty U^2\,e^{-k\eta}\,d\eta. \tag{7.11}$$

The shearing stress can be found in exactly the same way as in § 6. The result to a first approximation is

$$T_s = 1{\cdot}372\,e^{\frac{1}{6}\pi i}\,U_\infty^2\,k\alpha, \tag{7.12}$$

which is the same as (6.11) except that here no specific profile is implied and we have $\alpha = k/m = k^{\frac{2}{3}}R^{-\frac{1}{3}}[U'(0)]^{-\frac{1}{3}}$.

These results probably give reasonable estimates of P_s and T_s even for profiles which are fairly diffuse measured against a wavelength; but clearly they are most accurate when $k\delta$ is small. A survey of the various approximations which have been introduced shows (7.11) and (7.12) to become *exact* as $k\delta \to 0$, provided $m\delta$ still remains small, i.e. provided the assumption that the wall layer takes up only a small part of the boundary layer remains valid for thin boundary layers. This assumption, together with the one that Δ is small, will be examined presently. Note that when $k\delta$ is very small, $U = U_\infty$ over most of the range of integration of the integral in (7.11); and so this equation reduces approximately to (6.10). For

very thin boundary layers, therefore, we have that the magnitude *and phase* of both the surface pressure and shearing stress become independent of the profile shape.

We observe from (7.11) that the amplitudes of the component of p_s in phase with the wave elevation and of the component in phase with the slope are respectively given, as fractions of U_∞^2, by

$$a\mathscr{R}\{P_s\}/U_\infty^2 = -ka(1-1{\cdot}115\Delta)\,I, \tag{7.13}$$

$$a\mathscr{I}\{P_s\}/U_\infty^2 = 0{\cdot}644ka\Delta I = kas, \tag{7.14}$$

where

$$I = \int_0^\infty (U/U_\infty)^2\, e^{-k\eta}\, d(k\eta). \tag{7.15}$$

In (7.14), s is the sheltering coefficient as usually defined. The integral I is easily computed for particular velocity profiles, its value being insensitive to fine details of the profile such as the rather uncertain region near the wall for a turbulent boundary layer.

Consider, for instance, the case where the $\frac{1}{7}$-power law of velocity distribution is a suitable approximation: here the profile is given by $U/U_\infty = (\eta/\delta)^{\frac{1}{7}}$ over most of the region $0 \leqslant \eta \leqslant \delta$, but is rounded off to make the slope continuous at $\eta = \delta$, and is joined smoothly to the straight line $U = \eta U'(0)$ in the viscous sublayer next to the boundary (we recall this is not to be confused with our 'wall layer', which needs to be rather thinner than the sublayer for the present calculations to apply—see § 8). The latter details scarcely affect I, to which therefore a good approximation is

$$I = (k\delta)^{-\frac{2}{7}} \int_0^{k\delta} z^{\frac{2}{7}} e^{-z}\, dz + \int_{k\delta}^\infty e^{-z}\, dz.$$

The first integral may be expressed in terms of the incomplete gamma function. Successive integration by parts gives the following asymptotic expansion for large $k\delta$:

$$I = \frac{\Gamma(\frac{9}{7})}{(k\delta)^{\frac{2}{7}}} - e^{-k\delta}\left\{\frac{2}{7k\delta} - \frac{10}{49(k\delta)^2} + \ldots\right\}. \tag{7.16}$$

It may also be of interest to calculate I for the 'universal' logarithmic law of velocity distribution for turbulent flow over a smooth plane (Schlichting 1955, p. 406). This may be expressed

$$U/U_* = 2{\cdot}5 \log (9U_* R\eta), \tag{7.17}$$

where U_* is Prandtl's friction velocity defined by $U_*^2 = \tau_0 = R^{-1}U'(0)$: also $U_*^2/U_\infty^2 = c_f$, the usual 'local coefficient of skin friction'. Hence, (7.15) gives

$$I = 6{\cdot}3c_f \int_0^\infty [\log (9U_* R\eta)]^2\, e^{-k\eta}\, d(k\eta).$$

This integral is identifiable with one of the Laplace transforms in the tables edited by Erdélyi (1954, § 4.6, no. 13). We find that

$$I = 6{\cdot}3c_f\{\tfrac{1}{6}\pi^2 + [\log (\gamma k/9U_* R)]^2\}, \tag{7.18}$$

where $\gamma = e^C$, $C \doteqdot 0{\cdot}5772$ being Euler's constant.

A comparison with Motzfeld's experiments

The measurements by Motzfeld (1937) of the pressure distribution over a rigid wavy surface placed in a wind tunnel were mentioned in § 1. For his first model the wave amplitude and length were 0·75 and 30 cm, so that $ka = 2\pi a/\lambda = 0{\cdot}157$; and the observed pressure distribution was very nearly sinusoidal, with its maximum slightly in advance of the wave trough, as predicted by the theory. We shall now compare his measurements of the in-phase pressure amplitude and sheltering coefficient with values given by the preceding formulae. Remembering that Motzfeld's wave-train was only three wavelengths long (a feature criticized adversely by Ursell (1956)) and that there was a considerable pressure gradient along the tunnel, it will be seen that the agreement is as good as one could reasonably expect.

Motzfeld estimated values of the skin-friction coefficient c_f by fitting the universal logarithmic curve to the observed velocity profile in the wind tunnel. At the Reynolds number of the tests on his first wave model, he found $c_f = 0{\cdot}00173$. Now it is easily shown that Δ is equivalent to $c_f^{-\frac{5}{8}} R_\lambda^{-\frac{1}{8}}$, where R_λ is the Reynolds number based on U_∞ and wavelength (i.e. $R_\lambda = U_\infty \lambda/\nu$ if U_∞ and λ express *dimensional* quantities). If U_∞ is identified with the maximum air velocity (at the middle of the tunnel), we have $R_\lambda = 330{,}000$, and so obtain $\Delta = 0{\cdot}0021$.

The presence of the opposite wall of the tunnel evidently had an insignificant effect on conditions at the wave surface. This is shown by Motzfeld's measurements of the velocity profile at different positions over a wavelength: it is also indicated by the fact that $k\eta = 4{\cdot}2$ at the opposite wall, so that $e^{-k\eta}$ was quite small there. To find I, the most satisfactory course is to make a numerical integration based on the measured profile. This gives $I = 0{\cdot}71$. (We remark that $k \times$ (*half the tunnel height*) is rather too large for the formulae (7.16) and (7.18) to be reliable; and in fact they considerably overestimate I.)

Hence, we estimate the right-hand side of (7.13) to be $-0{\cdot}11$. The corresponding experimental result is $-0{\cdot}10$. Our estimate of the sheltering coefficient is $s = 0{\cdot}010$; whereas the experimental value is 0·034 (note Motzfeld's c_d, values of which are given in his table 1, is equivalent to $(ka)^2 s$). The discrepancy between these values of s may well be attributable to the experimental difficulties of measuring the very small pressure component in phase with the wave slope: the amplitude of this component was only a few percent of the amplitude of the total distribution.

Concluding remarks on the analysis for a rigid boundary

It remains to check the general assumption of small Δ and also the assumption that $m\delta$ remains small for limitingly thin boundary layers. We shall incidentally consider how our formulae for the surface stresses reduce when the Reynolds number is made infinite.

It is suitable just here to relax the scheme of using dimensionless variables and assign dimensions appropriately to all symbols. The only change of notation required by this is to replace R by ν^{-1} everywhere: thus, for instance, we now

have $m = [kU'(0)/\nu]^{\frac{1}{3}}$, which has the dimension of (length)$^{-1}$. The parameters Δ and $m\delta$ to be considered are, of course, still dimensionless.

Consider first a laminar boundary layer, formed in the absence of pressure gradient, at a distance X from its starting point. To comply with the basic assumption that variations in the primary profile are negligible over a wavelength, X must be fairly large in comparison with the wavelength λ: that is, kX must be large compared with unity. This requirement tends to conflict with one that $k\delta$ should be small; but evidently both can be satisfied if the Reynolds number R_X defined below is sufficiently large. The familiar Blasius formula gives $U'(0) = 0{\cdot}332\nu^{-\frac{1}{2}}X^{-\frac{1}{2}}U_\infty^{\frac{3}{2}}$; and a fair estimate of the boundary-layer thickness is $\delta = 6\nu^{\frac{1}{2}}X^{\frac{1}{2}}U_\infty^{-\frac{1}{2}}$. Hence, there easily follows

$$m\delta = 4{\cdot}2(kX)^{\frac{1}{2}}, \tag{7.19}$$

and

$$\Delta = kmU_\infty^2/[U'(0)]^2 = 6{\cdot}3(kX)^{\frac{4}{3}}R_X^{-\frac{1}{2}}, \tag{7.20}$$

where $R_X = U_\infty X/\nu$. It is also found that

$$\alpha = 0{\cdot}230\Delta/(kX)^{\frac{2}{3}}. \tag{7.21}$$

Equation (7.19) shows that $m\delta \gg 1$ as required; and (7.20) shows that, with X fixed, Δ becomes small when R_X is made sufficiently large (e.g. by increasing the velocity U_∞ in the main stream). Clearly, the justification for assuming Δ small is not in this example as readily forthcoming as one might wish; but we remark that anyway it would be no great trouble to calculate expressions for the stresses without restriction on Δ if this were thought worth while.

By means of (7.21) a clear comparison can be made between the magnitudes of the pressure component in phase with the wave slope and of the shear-stress component in phase with the wave elevation. This comparison has interest in the following way. Suppose the wave to be travelling forward *slowly*, so that although $c > 0$ the present calculations still apply approximately, i.e. we have the second special case considered in § 4. Then each of these stress components does a proportional amount of work on the wave, the respective rates of energy transfer being the same when the stresses have the same magnitude (cf. Lamb 1932, § 350). According to (7.12) and (7.14), the ratio of the shear-stress component to the pressure component is $O(\alpha/\Delta)$, which is seen from (7.21) to be very small and—rather surprisingly—independent of Reynolds number.

In studies of viscous fluid motion there is always interest in what happens in the limit as the Reynolds number is made to tend uniformly to infinity. It is well known that the limiting character of the motion may differ from that according to the theory of inviscid fluids. The present approximations evidently improve with increasing R_X, provided X is fixed; and there is no doubt about their remaining valid as $R_X \to \infty$. In this limit we get $\Delta = \alpha = 0$, and the boundary-layer thickness shrinks to zero, so that (7.11) and (7.12) give $p_s = -kaU_\infty^2 \cos k\xi$ and $\tau_s = 0$. This expression for the pressure is that given by ideal-fluid theory applied to the (Kelvin–Helmholtz) model of a uniform primary flow extending right down to the boundary.

Next consider a turbulent boundary layer with a velocity distribution approximated by the $\frac{1}{7}$-power law. For this form of boundary layer, Schlichting (1955,

p. 433) gave $\delta = 0{\cdot}37XR_X^{-\frac{1}{5}}$ and $U'(0) = 0{\cdot}0296\nu^{-1}U^2R_X^{-\frac{1}{5}}$. These formulae lead to

$$m\delta = 0{\cdot}12(kX)^{\frac{1}{3}}R_X^{\frac{2}{7}}, \tag{7.22}$$

$$\Delta = 350(kX)^{\frac{4}{3}}R_X^{-1}, \tag{7.23}$$

and

$$\alpha = 0{\cdot}0092\Delta(kX)^{-\frac{2}{3}}R_X^{\frac{2}{7}}. \tag{7.24}$$

We recall that the $\frac{1}{7}$-power law is valid in the range $5 \times 10^5 < R_X < 10^7$. With such values of R_X, (7.22) shows the condition $m\delta \gg 1$ to be very amply satisfied; and (7.23) shows we may have quite large values of kX while still having $\Delta \ll 1$. The two requirements are far more readily met than in the previous case. Equation (7.24) indicates that the ratio α/Δ is again small; hence the action of pressure is again more effective than that of shearing stress in supplying energy to a slowly moving wave. The results in the limit as $R_X \to \infty$ are the same as before.

Waves progressing with a fair speed in the direction of flow

We now turn to the case where there is a critical point $U = c$ at some significant distance $\eta = \eta_c$ from the boundary. The first task is to decide the correct interpretation of (7.3) for $\eta < \eta_c$: this expression is at present ambiguous owing to the singularity of the integrand at $\eta = \eta_c$. The difficulty is common to any uniformly valid approximation to the solution of (3.3), and can only be resolved by matching ϕ to the appropriate solutions of the full Orr–Sommerfeld equation which, unlike the inviscid solution, remain valid through the vicinity of the critical point. (This recalls our remarks following equation (3.3).) As this matter has been very fully examined by Lin (1955, chapter 8) and others in the context of stability theory, there is no need to go into it in any detail here. The relevant conclusion is that (7.3) becomes a physically correct approximation on either side of a narrow region surrounding the critical point if, for $\eta < \eta_c$, the path of integration is indented below the real axis under the singularity. The thickness of the 'friction layer' around the critical point is $O(kRU_c')^{-\frac{1}{3}}$ and so may be assumed to be very small. The derivatives of (7.3) cease to be valid approximations in this region. Note, however, that the approximation to $\phi(\eta)$ itself is valid *everywhere*, as (7.3) remains finite at $\eta = \eta_c$: thus it is clearly quite safe to use (7.3) in the integral expression (3.9) for the pressure.

The contribution to the integral in (7.3) from an infinitesimal indentation under the singularity is readily found by the calculus of residues. This contribution will be seen presently to play a crucial part in determining the pressure component in phase with the wave slope; and this result is obviously closely related to the matters discussed at the end of § 3, where we recalled the theory of Miles (1957) showing that a quasi-sheltering action can arise from the effects of a critical point. This is the principal effect due to the integral part of our expression for ϕ, which is otherwise of secondary importance. It appears, therefore, that the usefulness of the present approximation can be greatly improved by the slight modification as follows, which makes (7.3) give an accurate result at the critical point.

We first remark that although the integral in (7.3) is to be regarded as a second-order term for most values of η, it becomes dominant near the critical point. For

$\eta = \eta_c$ exactly, the integral is infinite; but, as was noted in connexion with (7.6) and also two paragraphs ago, the whole expression gives the finite value

$$\phi_c = Ak(U_\infty - c)^2 e^{-k\eta_c}/U'_c. \tag{7.25}$$

Here we write $\phi_c \equiv \phi(\eta_c)$ and $U'_c \equiv U'(\eta_c)$. Now, this will be shown later to be a rather poor approximation to ϕ_c if A is determined by the boundary conditions. A better approximation can be found quite easily by other means, as will be done later; and so a useful course is to rewrite (7.3) in the form

$$\phi = (U-c)\,e^{-k\eta}\left[A + \frac{\phi_c U'_c e^{k\eta_c}}{(U_\infty - c)^2}\int_\eta^\infty \left\{\left(\frac{U_\infty - c}{U-c}\right)^2 - 1\right\} d\eta\right], \tag{7.26}$$

which gives $\phi \to \phi_c$ for $\eta \to \eta_c$, the value of ϕ_c being left undetermined for the present. This expression keeps the same status as (7.3) as a second-order approximation in terms of k, since (7.25) is accurate to a first approximation in k.

A more explicit form of (7.26) for $\eta < \eta_c$ readily follows when the substitution $U - c = U'_c(\eta - \eta_c) + \frac{1}{2}U''_c(\eta - \eta_c)^2 + O(\eta - \eta_c)^3$ is made in the integrand. The singularity is circuited by a small semicircle under the real axis; and hence we are led to the expression

$$\phi = (U-c)\,e^{-k\eta}\left[A - i\pi\phi_c e^{k\eta_c}\frac{U''_c}{U'^2_c} + \frac{\phi_c U'_c e^{k\eta_c}}{(U_\infty - c)^2}\mathscr{P}\int_\eta^\infty \left\{\left(\frac{U_\infty - c}{U-c}\right)^2 - 1\right\}\right], \tag{7.27}$$

where $\mathscr{P}$ indicates the principal value of the integral. For $\eta > \eta_c$, this expression is of course to be replaced by (7.26).

The difference between (7.26) and (7.27) is clearly going to make P_s a complex quantity when ϕ is substituted in the formula (3.9). However, we must also anticipate the possibility of quasi-sheltering as a consequence of the exact 'viscous' boundary condition on ϕ, which includes the complex quantity $f'(0)/f(0)$. But, recalling § 4, we expect the latter effect to be significant only if the ratio $mc/U'(0)$ is fairly small and the critical point lies very close to the boundary. Nevertheless, this case definitely seems relevant to turbulent flows, for which the critical point may lie even inside the viscous sublayer for quite large values of the fraction c/U_∞. (It is of interest to note that a conservative estimate of the thickness of the sublayer is indicated by $U/U_* = 5$, U_* being Prandtl's friction velocity. Thus, the fraction of U_∞ attained at the edge of the sublayer is $5U_*/U_\infty = 5c_f^{\frac{1}{2}}$. With the typical value $c_f = 0{\cdot}0025$, this fraction is $\frac{1}{4}$.)

From (7.27) we obtain

$$\phi(0) = -c(A - \Omega), \tag{7.28}$$

where

$$\Omega = i\pi\phi_c e^{k\eta_c}\frac{U''_c}{U'^2_c} - \frac{\phi_c U'_c e^{k\eta_c}}{(U_\infty - c)^2}\mathscr{P}\int_0^\infty \left\{\left(\frac{U_\infty - c}{U-c}\right)^2 - 1\right\} d\eta. \tag{7.29}$$

In what follows we take the magnitude of Ω to be reasonably small compared with unity, which implies (as in our treatment of χ earlier) that one wavelength reasonably well covers the region of the profile where most of the variation of U occurs. (Perhaps a fair estimate of the order of magnitude of Ω would be $k \times$ (*momentum thickness of boundary layer*).) Equation (7.27) also leads to

$$\phi'(0) = U'(0)\{A - \Omega\} + \phi_c U'_c e^{k\eta_c}/c, \tag{7.30}$$

where some terms of the order of $kc\Omega$ have been dropped, being negligibly small.

These expressions satisfy the boundary condition (4.12) to a first approximation if $A = -1+\Omega$. To obtain a second approximation, we write $A = -1+\Omega+\epsilon$ and, neglecting squares and products of Ω and ϵ, we obtain from (4.12)

$$\epsilon = -\frac{\phi_c U_c' e^{k\eta_c}}{c^2\left\{\dfrac{f'(0)}{f(0)}+\dfrac{U'(0)}{c}\right\}}, \tag{7.31}$$

which may also be written

$$\epsilon = \frac{\alpha\phi_c U_c' e^{k\eta_c}}{c^2\left\{\dfrac{1}{D(-z_0)}-\dfrac{1}{z_0}\right\}}, \tag{7.32}$$

where we have introduced the Tietjens function D and the notation $\alpha = k/m$, $z_0 = mc/U'(0)$. It should be noted that the approximation to A thus obtained remains valid even when c is so small that the critical point is brought down to the linear region of the profile very close to the boundary; for, though the integral in (7.29) is then $O\{kU^2/U'(0)\,c\}$ and so becomes infinite for $c \to 0$, this order of magnitude is still small if the critical point is not so extremely close to the boundary as to lie well inside the wall friction-layer, i.e. $m\eta_c$ is not $\ll 1$. In fact, for $m\eta_c = 1$, this quantity is equivalent to Δ, which was shown earlier to be small. The quantity ϵ is also of this order when $m\eta_c = O(1)$.

Hence, eliminating A from (7.26) and (7.27), we obtain

$$\phi = (U-c)\,e^{-k\eta}\left[-1+\epsilon+\langle i\pi\phi_c e^{k\eta_c} U_c''/U_c'^2\rangle - \frac{\phi_c U_c' e^{k\eta_c}}{(U_\infty-c)^2}\,\mathscr{P}\int_0^\eta\left\{\left(\frac{U_\infty-c}{U-c}\right)^2-1\right\}d\eta\right], \tag{7.33}$$

where the quantity indicated by $\langle\ \rangle$ is to be put equal to zero for $\eta < \eta_c$. This result is now used in (3.9) to find the pressure at the wave surface. To estimate the pressure component in phase with the wave, it seems justifiable to neglect the small quantity ϵ and the integral in (7.33) (the second simplification may be justified in the same way as the corresponding step made when proceeding from (7.10)). Thus, as an approximation likely to be good enough for most practical applications, the amplitude of this component can be expressed

$$a\mathscr{R}\{P_s\} = -k^2 a\int_0^\infty (U-c)^2\,e^{-k\eta}\,d\eta. \tag{7.34}$$

The calculation of the component in phase with the wave slope is more interesting. Writing its amplitude as $(U_\infty-c)^2\,kas$ and assuming ϕ_c to be real, we deduce from (7.33) and (3.9) that $s = s_1+s_2$ where

$$s_1 = \frac{\pi\phi_c k\,e^{k\eta_c}\,U_c''}{(U_\infty-c)^2\,U_c'^2}\int_{\eta_c}^\infty (U-c)^2\,e^{-k\eta}\,d\eta, \tag{7.35}$$

$$s_2 = \mathscr{I}\left\{\left(\frac{1}{D(-z_0)}-\frac{1}{z_0}\right)^{-1}\right\}\left[\frac{\phi_c\alpha U_c' e^{k\eta_c}}{c^2(U_\infty-c)^2}\right]\int_0^\infty (U-c)^2\,e^{-k\eta}\,d\eta. \tag{7.36}$$

An estimate of ϕ_c is now needed, together with a check that it is real. By integrating (3.3) under the condition $\phi \to 0$ for $\eta \to \infty$, it can be shown (cf. Miles 1957, p. 193) that

$$U_c' \phi_c = k^2 \int_{\eta_c}^{\infty} (U - c)\, \phi \, d\eta. \tag{7.37}$$

(This relationship is exact; and it has in fact already been noted implicitly in the paragraph containing equation (3.12).) A sufficiently accurate approximation to ϕ_c is obtained by taking the leading term of (7.33) and using it for ϕ on the right-hand side of (7.37); thus (7.37) gives

$$\phi_c = -\frac{k^2}{U_c'} \int_{\eta_c}^{\infty} (U - c)^2 e^{-k\eta} \, d\eta, \tag{7.38}$$

which shows ϕ_c to be real in this approximation. This is clearly a much better estimate than the value $-k(U_\infty - c)^2 e^{k\eta_c}/U_c'$ given by (7.25) with $A \doteqdot -1$; but the two become the same for very thin boundary layers. It may be remarked that the accuracy of our treatment of the case $c = 0$ could have been somewhat improved by taking a similar estimate for $\phi(0)$ instead of (7.6); but this scarcely seemed worth while. The only changes in the results for that case are readily seen to be as follows: Δ is to be multiplied by the integral I (e.g. in the formula (7.14) for the sheltering coefficient); and the expression (7.12) for the shearing stress is also to be multiplied by I.

The component sheltering coefficients can now be expressed in reasonably neat forms. Some simplification is allowable if the critical point is assumed to be considerably less than a wavelength away from the boundary, so that $e^{k\eta_c} \doteqdot 1$. This assumption is, of course, consistent with the overall scheme of approximation, provided we exclude the unusual case where c is very nearly equal to U_∞. Hence, there finally are obtained

$$s_1 = -k\pi (U_\infty - c)^2 \frac{U_c''}{U_c'^3} J^2, \tag{7.39}$$

$$s_2 = -\mathscr{I}\left\{\left(\frac{1}{D(-z_0)} - \frac{1}{z_0}\right)\right\} \alpha \left(\frac{U_\infty}{c} - 1\right)^2 J^2, \tag{7.40}$$

where

$$J = \int_{\eta_c}^{\infty} \left(\frac{U - c}{U_\infty - c}\right)^2 e^{-k\eta} \, k \, d\eta.$$

The separation of s into these two components is interesting since it illustrates two physically distinct 'modes' of sheltering. First, s_1 represents an effect due entirely to the critical point, and is independent of Reynolds number; however, we emphasize that s_1 is decidedly a real-fluid property, since the singular behaviour of ϕ at the critical point—upon which s_1 crucially depends—remains ambiguous unless the effect of viscosity there is considered. Equation (7.39) clearly corresponds to (3.16), and is also equivalent to the expression for the sheltering coefficient derived by Miles (1957, equation (5.2)) on the basis of an inviscid-fluid model, the ambiguities necessarily entailed by the presence of a critical point being resolved in the same way as here (see p. 192 of his paper). Note that s_1 would usually be positive since U_c'' would usually be negative.

On the other hand, s_2 essentially depends on the action of viscosity at the boundary; and, recalling the result found in § 5, we may expect that s_2 will not be positive unless z_0 is fairly small. If z_0 is large enough for the asymptotic formula (4.14) to apply, then (7.40) gives very approximately

$$s_2 = \left(\frac{k}{2Rc}\right)^{\frac{1}{2}} \left(\frac{U_\infty}{c} - 1\right)^2 J^2 = -\pi^{\frac{1}{2}} R_w^{-\frac{1}{2}} \left(\frac{U_\infty}{c} - 1\right)^2 J^2, \tag{7.41}$$

where R_w is the 'wave Reynolds number' expressible as $c\lambda/\nu$ if c and λ denote the dimensional wave velocity and length. Thus, the effect of friction at the wave surface is to decrease the overall sheltering coefficient s for waves travelling with a fair speed compared with U_∞; however, the magnitude of s_2 is quite small since, to be consistent with other features of the physical model, R_w is large. For instance, s_2 is scarcely significant in comparison with the values of s_1 calculated by Miles (1957) for some practical examples of wind blowing over sea waves.

Incidentally, while asymptotic formulae for large z_0 are being considered, we may suitably write down an approximate expression for the shearing stress on the boundary. This is easily found by use of the formula (4.14) in conjunction with (2.12), writing $T_s = R^{-1}f''(0) = R^{-1}\{f''(0)/f(0)\}\{c - \phi(0)\}$, where the last step follows (3.5) and we have $c - \phi(0) = \epsilon c$ from (7.33). The result is

$$T_s = e^{\frac{3}{4}\pi i} k(U_\infty - c)^2 (k/Rc)^{\frac{1}{2}} J. \tag{7.42}$$

This shows the shearing stress to be of the same order of magnitude as the 's_2' part of the pressure in phase with the wave slope. The maximum shearing stress occurs one-eighth of a wavelength downstream from the wave trough.

We return to the discussion of the sheltering coefficient, passing now to the case where z_0 is fairly small. The critical point will now lie very close to the boundary so that s_1 will be practically zero, both because U_c'' has become extremely small and because $U_c' = U'(0)$ is large. As mentioned before, this case is exemplified by a critical point in the viscous sublayer of a turbulent boundary layer, c being less than, say, $\frac{1}{3}U_\infty$. If we put $D(-z_0) = D_r + iD_i$ and use the definition $z_0 = mc/U'(0)$, equation (7.40) may be arranged to give

$$s_2 = -\left\{\frac{D_i}{(D_r - z_0)^2 + D_i^2}\right\} \left\{\frac{km(U_\infty - c)^2}{[U'(0)]^2}\right\} J^2. \tag{7.43}$$

This yields a positive value of s_2 only when $D_i < 0$, that is when $z_0 < 2{\cdot}3$, this result being the same as found in § 5 for a linear velocity profile. Values of the quantity in the first curled bracket are tabulated as a function of z_0 in table 1, having been calculated from values of D_r and D_i given by Holstein (1950). The table shows this quantity to be largest when z_0 is slightly less than 1, that is, when the critical point is at a distance slightly less than m^{-1} from the boundary. Note that (7.42) remains valid when $c \to 0$; for then $J \to I$ (equation (7.15)), and (7.42) reduces to $s_1 = 0{\cdot}644\Delta I^2$ in agreement with (7.14) in its *modified* form (I replaced by I^2) suggested a few paragraphs ago.

Remembering the significance of the sheltering coefficient with regard to energy transfer between the flow and the wave-train, it is interesting to compare the various circumstances as the wave speed increases from very small values and the

critical point moves away from the wave surface. First, s is positive and s_1 is negligible; but it becomes negative when η_c increases beyond the small distance $2{\cdot}3m^{-1}$. A negative value of s implies an energy source within the waves in order to maintain c a real constant: without an energy supply the waves would presumably be damped by the action of the flow under these conditions. Eventually s becomes positive again due to the component s_1 outweighing s_2. For a logarithmic profile, Miles (1957) showed that s_1 is a maximum according to a formula like (7.39) when $k\eta_c = 0{\cdot}017$, which means when $\eta_c = 0{\cdot}0027\lambda$. When η_c increases much beyond this value, s_1 decreases very rapidly; and it is possible that s may take a small negative value due to s_2 again outweighing s_1. Finally, we note that if c is slightly negative, so that the wave moves against the flow, the theory indicates that s is still positive; but the direction of energy transfer reverses with the sign of c, so that in this case the waves tend to be damped by the flow.

z_0	G	z_0	G
0	$-0{\cdot}644$	2·5	$+0{\cdot}089$
0·5	$-1{\cdot}601$	3·0	0·183
1·0	$-1{\cdot}458$	3·5	0·155
1·5	$-0{\cdot}960$	4·0	0·088
2·0	$-0{\cdot}206$	4·5	0·038

TABLE 1. The function $G(z_0) = D_i/\{(D_r - z_0)^2 + D_i^2\}$.

For a limitingly thin boundary layer and also $R \to \infty$, it is seen that T_s, s_1 and s_2 all tend to zero (s_1 because it is $O(k\delta)$). In the limit the only stress on the wave is the in-phase pressure given by (7.34): this becomes $-ka(U_\infty - c)^2$, which is the value according to the Kelvin–Helmholtz theory.

8. Conclusion

Validity of the approximate viscous solution

Properties of the function $f(\eta)$ have been a vital consideration in many parts of this study; and, as remarked near the beginning of § 4 where the approximation to $f(\eta)$ was introduced, there is a need to examine rather carefully the assumptions forming the basis of this approximation. Several other remarks bearing on this matter have already been made; and indeed enough probably has been said here and there to cover the main points concerned. However, to round off the discussion, it seems desirable to review the assumptions in question, and in particular examine the somewhat doubtful case of turbulent boundary-layer profiles with large rates of shear near the wave surface.

We recall that $f(\eta)$ is a solution of (3.1) which, since it diminishes very rapidly with increasing η, is approximately a solution of (4.1). The accuracy of the approximate equation (4.1) requires that (i) $\alpha = k/m$ is small, and (ii) the 'linear' region of the velocity profile, over which $U = \eta U'(0)$ approximately, covers the region where the magnitude of $f(\eta)$ is still significant in comparison with its value on the boundary. The latter region is $O(m^{-1})$ in width. In § 5 where a wholly linear profile was considered, condition (i) was seen very clearly to be the only one on

which the approximation to $f(\eta)$ depended. This condition would be very well satisfied for most physical applications where the Reynolds number is fairly large. It implies that the wavelength greatly exceeds the width of the friction layer, and so holds for all but extremely short waves. We may note, however, that a physical example for which α were $O(1)$ or greater could be treated very successfully by use of the linear-profile model of § 5, the exact expression (5.3) for $f(\eta)$ being kept intact. This is so because the disturbance would then be confined entirely to the region of the friction layer, so that the effects of profile curvature would very likely be negligible.

Condition (ii) need not be interpreted very stringently. For instance, if the profile starts to curve appreciably even before η gets much beyond m^{-1}, only the 'tail end' of $f(\eta)$ is affected by the curvature; and presumably the approximation based on the linear profile is still reasonably good. The assumption of (ii) will now be tested with regard to laminar and turbulent boundary-layer profiles. It will be convenient to revert to the dimensional form of notation used in the third subsection of § 7.

In a laminar boundary layer along a plane (i.e. the Blasius profile), the velocity gradient becomes 10 % less than $U'(0)$ at a distance $\eta_{10} = 1{\cdot}54XR_X^{-\frac{1}{2}}$. The size of $m\eta_{10}$ may be regarded as an indication of the validity of the assumption under consideration. We have $m = [kU'(0)/\nu]^{\frac{1}{3}}$ and $U'(0) = 0{\cdot}332U_\infty^2\nu^{-1}R_X^{-\frac{1}{2}}$, and hence obtain

$$m\eta_{10} = 2{\cdot}2(kX)^{\frac{1}{3}}. \tag{8.1}$$

This is quite large if the wavelength is a small fraction of X, as it must be to satisfy the assumption of approximately parallel flow. Clearly, condition (ii) is amply satisfied in applications of the theory to laminar boundary layers.

The usual estimate of the thickness of the viscous sublayer in a turbulent boundary layer is $5\nu/U_*$ (e.g. Schlichting 1955, p. 407). The velocity profile is almost exactly linear where η has less than this value, but its divergence from the straight line $\eta U'(0)$ is not very marked until η takes considerably larger values (this is best seen by plotting the numerous available experimental measurements of $U(\eta)$ against a linear scale of η, instead of the usual logarithmic scale). For the present purpose, the value $\eta = 10\nu/U_*$ is still a fairly conservative estimate of the limit within which the viscous solution should become small. A suitable criterion as required is therefore that $10m\nu/U_*$ should be at least about unity, and of course preferably larger. Since $U'(0) = U_*^2/\nu = c_f U_\infty^2/\nu$, this criterion can be expressed

$$\left.\begin{aligned} 10(k\nu/U_*)^{\frac{1}{3}} &> \sim 1, \\ \text{or} \qquad 18{\cdot}5c_f^{-\frac{1}{6}}(\lambda U_\infty/\nu)^{-\frac{1}{3}} &> \sim 1. \end{aligned}\right\} \tag{8.2}$$

With Motzfeld's experimental values $U_\infty\lambda/\nu = 330{,}000$ and $c_f = 0{\cdot}00173$ quoted in § 7, the left-hand side of (8.2) is 0·77. Thus, the approximation is probably still reasonably accurate, although this would appear to be a marginal case. However, the value of U_* in the experiments (about 80 cm/sec) was somewhat exceptionally large. A value $U_* = 10$ cm/sec, for instance, is typical of a light to moderate wind over water, the flow being 'aerodynamically smooth'. With this value of U_* and the typical value for air $\nu = 0{\cdot}17$ cm^2/sec, the left-hand side of (8.2) is unity for $\lambda = 107$ cm. It could therefore be expected that the approximate viscous solution would be quite reliable for waves less than about a metre in length.

A generalization by Fourier's theorem

We reconsider (5.6) and (5.9), which express the normal and tangential stresses p_s and τ_s on a solid or slowly moving wave bounding a uniform shear flow. The simple yet somewhat unusual form of these results makes it attractive to generalize them, by Fourier's theorem, so as to apply when the boundary is an arbitrary perturbation from a plane. This will provide a particular clear illustration of the idea, which has been frequently mentioned, that a type of sheltering action occurs even according to linearized theory when the stresses bear certain phase relations to the wave. Only the first-order terms in (5.6) and (5.9) will be retained, since the terms having α as a factor can be regarded as of secondary importance.

It then follows that if the deformation in the boundary is non-periodic and given by

$$y = \zeta(x) = \frac{1}{\pi}\int_0^\infty \{g_1(k)\cos kx + g_2(k)\sin kx\}\,dk, \tag{8.3}$$

where, according to Fourier's theorem,

$$g_1(k) = \int_{-\infty}^{\infty} \zeta(x)\cos kx\,dx, \quad g_2(k) = \int_{-\infty}^{\infty} \zeta(x)\sin kx\,dx, \tag{8.4}$$

then the stresses are

$$p_s = -\frac{A}{\pi}\int_0^\infty \{g_1(k)\cos(kx-\tfrac{1}{6}\pi) + g_2(k)\sin(kx-\tfrac{1}{6}\pi)\}\,k^{-\frac{1}{3}}\,dk, \tag{8.5}$$

and

$$\tau_s = \frac{B}{\pi}\int_0^\infty \{g_1(k)\cos(kx+\tfrac{1}{6}\pi) + g_2(k)\sin(kx+\tfrac{1}{6}\pi)\}\,k^{\frac{1}{3}}\,dk, \tag{8.6}$$

where $A = 0{\cdot}776R^{-\frac{1}{3}}G^{\frac{5}{3}}$ and $B = 1{\cdot}065R^{-\frac{2}{3}}G^{\frac{4}{3}}$.

Consider, for example, the case where the boundary profile is the single-humped curve

$$y = \frac{ab^2}{x^2+b^2}. \tag{8.7}$$

One finds without difficulty that $g_1(k) = \pi ab\,e^{-kb}$ and $g_2(k) = 0$. Hence, (8.5) and (8.6) give

$$\begin{aligned} p_s &= -Aab\int_0^\infty e^{-kb}\cos(kx-\tfrac{1}{6}\pi)\,k^{-\frac{1}{3}}\,dk \\ &= -Aab\Gamma(\tfrac{2}{3})\,(x^2+b^2)^{-\frac{1}{3}}\cos\left(\tfrac{2}{3}\tan^{-1}\frac{x}{b} - \tfrac{1}{6}\pi\right); \end{aligned} \tag{8.8}$$

$$\begin{aligned} \tau_s &= Bab\int_0^\infty e^{-kb}\cos(kx+\tfrac{1}{6}\pi)\,k^{\frac{1}{3}}\,dk \\ &= \tfrac{1}{3}Bab\Gamma(\tfrac{1}{3})\,(x^2+b^2)^{-\frac{2}{3}}\cos\left(\tfrac{4}{3}\tan^{-1}\frac{x}{b} + \tfrac{1}{6}\pi\right). \end{aligned} \tag{8.9}$$

To illustrate how the stresses are distributed over the boundary profile, figure 5 shows graphs of the functions $\frac{1}{2}(x^2+1)^{-1}$, $(x^2+1)^{-\frac{1}{3}}\cos(\frac{2}{3}\tan^{-1}x - \frac{1}{6}\pi)$, and $(x^2+1)^{-\frac{2}{3}}\cos(\frac{4}{3}\tan^{-1}x + \frac{1}{6}\pi)$. The interpretation to be given the three curves is perfectly clear in the light of (8.7), (8.8) and (8.9). The figure shows the pressure to be everywhere negative (note that $-p_s$ is represented), being greatest in

magnitude slightly on the leeward side of the boundary hump. The shearing stress changes sign and becomes negative farther on the leeward side, indicating a tendency towards a reversal of the flow some way downstream. These features have the same general character as if the flow separated on the downstream side, thus causing sheltering in the usually understood sense. Of course, the present flow does not separate: the point being emphasized is that an infinitesimal disturbance can produce effects similar to those due to separation.

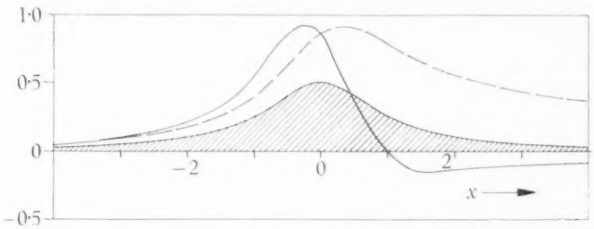

FIGURE 5. Graphs of the stresses on a solid hump due to uniform shearing flow in the x-direction. The curve shaded underneath represents the boundary profile. The other full-line curve represents the shearing stress; and the dashed line represents the (negative) pressure. The vertical scale is arbitrary.

Applications of formulae for the surface stresses

Aside from the intrinsic interest they may have, the various formulae that have been developed for the stresses on the wavy boundary offer the possibility of usefulness in problems concerning wave generation by the action of a flow. For instance, they might be applied to the study of two-dimensional flutter waves on a membrane. The present theory has been restricted to real values of the wave velocity c; but this is relevant to conditions of 'neutral stability' under which a simple-wave disturbance in a system is propagated unchanged, the factors tending respectively to damp or amplify the wave being exactly balanced. The determination of neutral conditions is usually the first aim of stability investigations.

Although the principle of the method whereby the stress formulae would be applied is perhaps fairly obvious, it seems worth outlining explicitly. Suppose wave formation is expected to occur in a certain deformable body whose interface with the fluid is a plane; and suppose the physical properties of the undisturbed flow are specified, including the velocity profile. The method assumes the interface to be perturbed by a simple wave, of infinitesimal amplitude a and *arbitrary* wave-number k and velocity c, which by appeal to the principle of Fourier synthesis covers every physically possible form of infinitesimal disturbance. Now, the present formulae provide estimates of the periodic stresses, proportional to a and depending on k and c, which the flow exerts against the wave. Hence, complete dynamical boundary conditions can be formulated which, together with a kinematical condition expressible in terms of k and c, determine the motion of the body. The action of the flow is thus regarded as an influence analogous to, say, surface tension—which for a given deformation produces an easily calculable normal force. The solution of the separate dynamical problem for the body would

in general lead to a relation between k and c, with various physical properties such as viscosity or stiffness of the body involved as parameters (in effect, the connexion between k and c would emerge as a condition of 'self-consistency' of the dynamical system: if c is allowed to be complex, waves with any k and c_r are of course possible; but for a given k only certain discrete values of c_r, if any, are consistent with $c_i = 0$). This relation would define the class of neutral waves; and from the result there would probably be little difficulty in deciding the combinations of physical parameters for which instability may occur (cf. Feldman (1957), where stability conditions involving a large number of parameters are discussed).

When the second medium is another fluid, strictly speaking another property of the wave interface enters the stress formulae, namely β (equation (2.9)) which relates to the slipping of particles in the surface relative to their positions on the undisturbed plane. However, several reasons have been given why β may be negligible; and it would seem that the effect of β would be quite unimportant in most problems concerning a gas-liquid interface, i.e. the stresses are the same as on a similar wave moving over a flexible solid. Also, one may obviously expect the stresses to become approximately the same as on a fixed solid when c is sufficiently small; but a more precise criterion for this has been seen to be that $mc/U'(0)$ should be $O(1)$ or less.

An alternative approach to problems of wave formation in a two-phase system is to set out mathematics at once embracing the whole model, yet likely to be of such complexity as to lose sight of physical reasoning. In contrast, the 'divided attack' suggested here has the advantage that a helpful stocktaking from a physical viewpoint can be made at the intermediate stage. For instance, it can be seen whether or not the surface stresses supply energy to the wave, which action is of course necessary for the survival of a neutral wave when the second medium is dissipative. Further, the relative importance of the normal and shearing stresses can be well understood with reference to energy considerations; and a qualitative assessment of the conditions most likely to promote waves may be possible even without a detailed study of the mechanics of the second medium. Again, the normal stress component in phase with the wave can be neatly interpreted as an accession (if the stress is positive) or decrement to the inertia of the second medium (we recall that Kelvin–Helmholtz instability is due solely to the inertial effects of the upper fluid).

We emphasize, however, that energy arguments serve best to provide only some additional physical insight into problems of wave formation, and are preferably not to be relied upon alone for the deduction of stability conditions. Energy methods are well known to be unreliable in the classical problems of hydrodynamic stability (Lin 1955, § 4.5; Schlichting 1955, p. 313). Solution of the linearized dynamical equations is a better course, being concerned with quantities of the first rather than second order in the wave amplitude. If the question is wave generation by the action of flow on a mobile boundary, the way is open to the latter approach when, as provided here, the interfacial stresses are completely known.

REFERENCES

ERDÉLYI, A. (ED.) 1954 *Tables of Integral Transforms*, Vol. 1. New York: McGraw-Hill.

FELDMAN, S. 1957 *J. Fluid Mech.* **2**, 343.

GOLDSTEIN, S. (ED.) 1938 *Modern Developments in Fluid Dynamics.* Oxford University Press.

HOLSTEIN, H. 1950 *Z. angew. Math. Mech.* **30**, 25.

JEFFREYS, H. 1924 *Proc. Roy. Soc.* A, **108**, 189.

JEFFREYS, H. 1925 *Proc. Roy. Soc.* A, **110**, 241.

KNUTH, E. H. 1954 *Jet Propulsion*, **24**, 359.

LAMB, H. 1932 *Hydrodynamics*, 6th ed. Cambridge University Press.

LIGHTHILL, M. J. 1953 *Proc. Roy. Soc.* A, **217**, 478.

LIGHTHILL, M. J. 1957 *J. Fluid Mech.* **3**, 113.

LIN, C. C. 1945 *Quart. Appl. Math.* **3**, Part 1, p. 117; Part 2, p. 218; Part 3, p. 277.

LIN, C. C. 1955 *The Theory of Hydrodynamic Stability.* Cambridge University Press.

LOCK, R. C. 1954 *Proc. Camb. Phil. Soc.* **50**, 105.

MILES, J. W. 1957 *J. Fluid Mech.* **3**, 185.

MOTZFELD, H. 1937 *Z. angew. Math. Mech.* **17**, 193.

PHILLIPS, O. M. 1957 *J. Fluid Mech.* **2**, 417.

QUICK, A. W. & SCHRÖDER, K. 1944 Wartime report summarized by W. Mangler in *Ministry of Aircraft Production Rep. and Trans.*, no. 1003, §2 (1948).

SCHLICHTING, H. 1955 *Boundary Layer Theory.* London: Pergamon.

STANTON, T. E., MARSHALL, D. & HOUGHTON, R. 1932 *Proc. Roy. Soc.* A, **137**, 283.

TOLLMIEN, W. 1929 *Nachr. Ges. Wiss. Göttingen*, **1**, 21; English translation in *Nat. Adv. Comm. Aero., Wash., Mem.* no. 609.

URSELL, F. 1956 Wave generation by wind, article in *Surveys in Mechanics* (Ed. Batchelor and Davies). Cambridge University Press.

WUEST, W. 1949 *Z. angew. Math. Mech.* **29**, 239.

ZONDEK, B. & THOMAS, L. H. 1953 *Phys. Rev.* **90**, 738.

Torsional oscillations of a plane in a viscous fluid

By S. ROSENBLAT

Department of Applied Mathematics, University of Liverpool

(Received 15 December 1958)

On the assumption that the rotational oscillations of a rigid plane are small, boundary-layer type solutions of the Navier–Stokes equations are attempted by an expansion of the velocity components in power series of the amplitude. First- and third-order approximations to the transverse velocity are obtained, from which a correction to the moment on a disk of finite radius is found.

The first non-vanishing approximation to the radial-axial flow (a second-order term) is seen to have a steady component and a component with frequency twice that of the plate. The former component appears to persist outside the boundary layer, and at large distances from the plate to have the character of an irrotational stagnation flow. A re-examination not involving the series approximation reveals that although steady radial flow does exist outside the boundary layer, it is a viscous flow and is confined within a secondary layer. The ratio of the thicknesses of the two layers is found to be inversely proportional to the amplitude of the oscillations. These results indicate that a second-order flow in a region where the first-order flow field vanishes should not be accepted without further discussion.

1. Introduction

The problem of small rotational oscillations of a body of revolution has received considerable attention (see, for example, Kestin & Persen 1954), since it relates to a well-known method of measuring the coefficient of viscosity. Prior to the work of Carrier & di Prima (1956), however, virtually all investigations used Stokes's slow-motion equations, in which the flow was assumed to be entirely circumferential. Consequently, errors arising from the presence of radial flow were neglected.

Carrier & di Prima were principally concerned with evaluating the correction to the torque on a sphere when a second approximation is taken. In the course of the calculations a radial flow was derived but was not discussed in any detail. Commencing with the Navier–Stokes equations in spherical polar co-ordinates, these authors expanded the velocity components in powers of the amplitude of oscillation, and solved the resulting differential equations. The method led to very complicated expressions which were eventually reduced to a practical form by assuming small viscosity.

On the other hand, an early application of the boundary layer equations to time-periodic flows was undertaken by Schlichting (1932), who examined the small two-dimensional oscillations of a cylinder in a stationary fluid. Using a

similar small-amplitude expansion, Schlichting found a first-order fluctuating shear layer close to the body. The second approximation, however, yielded a steady secondary flow which did not vanish at large distances from the cylinder and whose magnitude was independent of the viscosity. This effect was ascribed to Reynolds stresses set up in the fluid by the oscillatory motion.

The primary aim of the present paper is to investigate the secondary flows which arise when an infinite plane lamina performs small torsional oscillations in a fluid otherwise at rest. Since for a plane the terms neglected in the boundary-layer approximation vanish identically, the Navier–Stokes equations may be used to derive solutions of the boundary-layer type. If λ is the frequency of the oscillations, then $1/\lambda$ is a typical time, and the boundary-layer thickness will clearly be of order $\sqrt{(\nu/\lambda)}$, where ν is the kinematic viscosity.

Expansion of the velocity components in powers of ϵ, the amplitude of the oscillation, leads to two sets of linear partial differential equations, with simple boundary conditions. The first-order solution is simply the well-known unsteady shear layer for the transverse velocity.

The second-order solution reveals a secondary radial-axial flow composed of a steady term and a term of frequency 2λ. It appears that, as in Schlichting's solution, the steady radial component persists outside the boundary layer. Its form at large distances from the plate is found to be that of an irrotational stagnation flow.

Further considerations result in a correction to the transverse velocity, of third order and containing terms of frequency λ and 3λ. It is found that if $|M|$ is the amplitude of the first-order torque on a disk of radius a, then inclusion of third-order effects leads to a torque of amplitude $|M|\,(1-0{\cdot}101\epsilon^2)$. This contrasts with $|M|\,(1+0{\cdot}015\epsilon^2)$ for the torque on a sphere obtained by Carrier & Di Prima (1956).

A re-examination of the steady radial flow is then undertaken. It is indicated that this flow is set up within the boundary layer by the action of centrifugal force, compared with which the convective inertia terms are neglected in the series approximation. However, outside the boundary layer the centrifugal term becomes vanishingly small, while (axially) inward convection is effective in preventing outward diffusion of vorticity beyond a certain distance. Thus the power series in ϵ ceases to converge outside the boundary layer, and for a correct representation of the flow here the convective terms must be included in the equation of motion.

A solution of the appropriate equation is then obtained, first by an approximate Pohlhausen-type method, and subsequently by numerical means. These solutions show that radial flow, although existing outside the boundary layer, is viscous and is confined within a secondary layer whose thickness is order ϵ^{-1} times that of the shear layer. Outside this secondary layer there is merely a constant axial inflow, as demanded from continuity considerations. Thus we conclude that the irrotational flow, derived from the series approximation and qualitatively similar to that obtained in the two-dimensional case by Schlichting (1932), does not in fact occur.

2. Method of solution

Suppose the plane $z = 0$ to represent a lamina of infinite extent, and the space $z > 0$ to be occupied by an incompressible viscous fluid of density ρ and kinematic viscosity ν. Let (r, ϕ, z) be a set of cylindrical polar co-ordinates, fixed in space, and let the lamina perform torsional oscillations about the axis $r = 0$, the fluid being otherwise at rest. If the amplitude of angular displacement is ϵ, and the frequency of oscillation is λ, then the plate has angular velocity $\omega \cos \lambda t$, or, in complex notation, $\omega e^{i\lambda t}$, where $\omega = \epsilon\lambda$.

Let u, v and w denote respectively the radial, transverse and axial components of velocity, and p the fluid pressure. Then the appropriate Navier–Stokes equations of motion are

$$\frac{\partial u}{\partial t} + u\frac{\partial u}{\partial r} + w\frac{\partial u}{\partial z} - \frac{v^2}{r} = -\frac{1}{\rho}\frac{\partial p}{\partial r} + \nu\left[\frac{\partial^2 u}{\partial r^2} + \frac{\partial}{\partial r}\left(\frac{u}{r}\right) + \frac{\partial^2 u}{\partial z^2}\right], \tag{1}$$

$$\frac{\partial v}{\partial t} + u\frac{\partial v}{\partial r} + w\frac{\partial v}{\partial z} + \frac{uv}{r} = \nu\left[\frac{\partial^2 v}{\partial r^2} + \frac{\partial}{\partial r}\left(\frac{v}{r}\right) + \frac{\partial^2 v}{\partial z^2}\right], \tag{2}$$

$$\frac{\partial w}{\partial t} + u\frac{\partial w}{\partial r} + w\frac{\partial w}{\partial z} = -\frac{1}{\rho}\frac{\partial p}{\partial z} + \nu\left[\frac{\partial^2 w}{\partial r^2} + \frac{1}{r}\frac{\partial w}{\partial r} + \frac{\partial^2 w}{\partial z^2}\right], \tag{3}$$

while the equation of continuity is

$$\frac{\partial u}{\partial r} + \frac{u}{r} + \frac{\partial w}{\partial z} = 0. \tag{4}$$

Since radial symmetry obtains, all derivatives with respect to ϕ are omitted. The relevant boundary conditions of the problem are

$$\left.\begin{aligned} u = 0, \quad v = r\omega e^{i\lambda t}, \quad w = 0 \quad \text{at} \quad z = 0, \\ u \to 0, \quad v \to 0 \quad \text{as} \quad z \to \infty. \end{aligned}\right\} \tag{5}$$

We now attempt a solution of the system (1)–(5) in the form

$$\left.\begin{aligned} u = r\omega F'(\eta, \tau), \quad v = r\omega G(\eta, \tau), \quad w = -2\omega\sqrt{(2\nu/\lambda)}\, F(\eta, \tau), \\ p = p(z, t), \quad z = \sqrt{(2\nu/\lambda)}\,\eta, \quad t = \tau/\lambda, \end{aligned}\right\} \tag{6}$$

where the accent denotes differentiation with respect to η. The continuity equation is satisfied, equations (1) and (2) reduce to the dimensionless forms

$$\frac{\partial F'}{\partial \tau} + \epsilon[F'^2 - G^2 - 2FF''] = \tfrac{1}{2}F''', \tag{7}$$

$$\frac{\partial G}{\partial \tau} + 2\epsilon[F'G - FG'] = \tfrac{1}{2}G'', \tag{8}$$

respectively, and the boundary conditions become

$$F = F' = 0, \quad G = e^{i\tau} \quad \text{at} \quad \eta = 0; \qquad F' \to 0, \quad G \to 0 \quad \text{as} \quad \eta \to \infty. \tag{9}$$

The velocity components u, v and w are now completely determined from (7)–(9), whereupon the pressure can be obtained from (3).

It is next assumed that a solution can be found by expanding F and G in ascending powers of the parameter ϵ. On substituting the series

$$F(\eta,\tau) = F_0(\eta,\tau)+\epsilon F_1(\eta,\tau)+\epsilon^2 F_2(\eta,\tau)+\ldots \tag{10}$$

and

$$G(\eta,\tau) = G_0(\eta,\tau)+\epsilon G_1(\eta,\tau)+\epsilon^2 G_2(\eta,\tau)+\ldots \tag{11}$$

into (7) and (8), and equating coefficients of like powers of ϵ, we obtain the following systems of linear partial differential equations:

$$\frac{\partial F_0'}{\partial \tau} = \tfrac{1}{2}F_0''', \tag{12a}$$

$$\frac{\partial F_1'}{\partial \tau} + F_0'^2 - G_0^2 - 2F_0F_0'' = \tfrac{1}{2}F_1''', \tag{12b}$$

$$\frac{\partial F_2'}{\partial \tau} + 2[F_0'F_1' - G_0G_1 - F_0F_1'' - F_0''F_1] = \tfrac{1}{2}F_2''', \quad \text{etc.}, \tag{12c}$$

$$\frac{\partial G_0}{\partial \tau} = \tfrac{1}{2}G_0'', \tag{13a}$$

$$\frac{\partial G_1}{\partial \tau} + 2[F_0'G_0 - F_0G_0'] = \tfrac{1}{2}G_1'', \tag{13b}$$

$$\frac{\partial G_2}{\partial \tau} + 2[F_0'G_1 + F_1'G_0 - F_0G_1' - F_1G_0'] = \tfrac{1}{2}G_2'', \quad \text{etc.}, \tag{13c}$$

with boundary conditions

$$F_N = F_N' = 0 \quad \text{at} \quad \eta = 0; \qquad F_N' \to 0 \quad \text{as} \quad \eta \to \infty, \quad N = 0, 1, 2 \ldots, \tag{14}$$

$$G_0 = e^{i\tau}, \quad G_{N+1} = 0 \quad \text{at} \quad \eta = 0; \qquad G_N \to 0 \quad \text{as} \quad \eta \to \infty, \quad N = 0, 1, 2 \ldots. \tag{15}$$

It is clear that the first approximations (12*a*) and (13*a*) are equivalent to neglecting $u(\partial u/\partial r)$, $w(\partial u/\partial z)$, v^2/r compared with $\partial u/\partial t$ in (1), and $u(\partial v/\partial r)$, $w(\partial v/\partial z)$, uv/r compared with $\partial v/\partial t$ in (2). Such an approach was employed by Schlichting (1932), and at this stage it appears to be valid here provided the amplitude ϵ is sufficiently small.

3. First approximation to the transverse velocity

The solution of equation (12*a*) satisfying the boundary conditions (14) is obviously

$$F_0(\eta,\tau) \equiv 0. \tag{16}$$

On the other hand, (13*a*) has the solution

$$G_0(\eta,\tau) = e^{i\tau}e^{-(1+i)\eta},$$

which, in real notation, is

$$G_0(\eta,\tau) = e^{-\eta}\cos(\tau-\eta). \tag{17}$$

This is the well-known shear-wave solution for a flat plate oscillating in its own plane in a fluid at rest. Thus its properties have been fully discussed and need not be considered further here. The continuous curves in figure 2 illustrate the function

$$e^{-\eta}\cos(\tau-\eta) - \cos\tau,$$

which is merely $G_0(\eta,\tau)$ taken relative to the oscillating plate.

Since $F_0 = 0$, the first-order solution of the system (1)–(5) is a transverse velocity given by

$$v = r\omega\, e^{-\sqrt{(\lambda/2\nu)}\,z}\cos(\lambda t - \sqrt{(\lambda/2\nu)}\,z), \tag{18}$$

and no radial or axial velocity. The transverse shearing stress is defined to be

$$\tau_t = \rho\nu\left(\frac{\partial v}{\partial z}\right)_{z=0}, \tag{19}$$

so that the first approximation is, from (18),

$$\tau_t = -\rho r\omega\sqrt{(\nu\lambda)}\cos(\lambda t + \tfrac{1}{4}\pi). \tag{20}$$

This shearing stress is seen to have a phase lead of $\frac{1}{4}\pi$ over the oscillations of the plate.

Although we are dealing with a plane of infinite extent, the results obtained above may be applied to a circular disk of radius a provided edge effects can be neglected. This seems to be justified if a is large compared with the thickness of the boundary layer. In this case the frictional torque (for the two sides of the disk) is

$$M = -4\pi\int_0^a r^2\tau_t\,dr. \tag{21}$$

Hence, using (20), the first approximation to the moment is

$$M = \pi c_1^4\rho\epsilon\sqrt{(\nu\lambda^3)}\cos(\lambda t + \tfrac{1}{4}\pi). \tag{22}$$

These results are well known.

4. Radial and axial velocities

Since $F_0 = 0$, the first non-vanishing approximations to the radial and axial velocities are obtainable from the second-order solution F_1 of equation (12b). Substituting from (17) into (12b), we have

$$\frac{\partial F_1'}{\partial\tau} - \tfrac{1}{2}e^{-2\eta}[1 + e^{2i\tau}e^{-2i\eta}] = \tfrac{1}{2}F_1''', \tag{23}$$

with boundary conditions

$$F_1(0) = 0, \quad F_1'(0) = 0, \quad F_1'(\infty) = 0. \tag{24}$$

The form of (23) invites a substitution

$$F_1(\eta,\tau) = f(\eta) + h(\eta)\,e^{2i\tau}, \tag{25}$$

and this leads to the two equations

$$2ih' - \tfrac{1}{2}e^{-2(1+i)\eta} = \tfrac{1}{2}h''', \tag{26a}$$

$$-e^{-2\eta} = \tfrac{1}{2}f''', \tag{26b}$$

with $\qquad f(0) = f'(0) = h(0) = h'(0) = 0; \quad f'(\infty) = h'(\infty) = 0.$

The solution of (26a) is readily seen to be

$$h = A + Be^{-\sqrt{2}(1+i)\eta} + Ce^{\sqrt{2}(1+i)\eta} - \frac{1+i}{16}e^{-2(1+i)\eta},$$

where A, B and C are integration constants. Application of the boundary conditions immediately leads to

$$A = \frac{1+i}{16}(1-\sqrt{2}), \quad B = \frac{1+i}{8\sqrt{2}}, \quad C = 0;$$

whereupon we have

$$h = \frac{1+i}{16}[1-\sqrt{2}+\sqrt{2}\,e^{-\sqrt{2}(1+i)\eta}-e^{-2(1+i)\eta}], \tag{27a}$$

and

$$h' = -\frac{i}{4}[e^{-\sqrt{2}(1+i)\eta}-e^{-2(1+i)\eta}]. \tag{27b}$$

Equation (26*b*) has the solution

$$f = A+B\eta+C\eta^2+\tfrac{1}{8}e^{-2\eta}.$$

The requirements $f(0) = 0$ and $f'(0) = 0$ yield $A = -\frac{1}{8}$, $B = \frac{1}{4}$, while in order that f' should remain finite as $\eta \to \infty$ it is necessary that $C = 0$. These values give

$$f = -\tfrac{1}{8}[1-2\eta-e^{-2\eta}], \tag{28a}$$

and

$$f' = \tfrac{1}{4}[1-e^{-2\eta}], \tag{28b}$$

which, however, does not satisfy $f'(\eta) \to 0$ as $\eta \to \infty$. The significance of this result will be discussed subsequently.

Reverting to real notation, we have from (25), (27) and (28)

$$F_1(\eta,\tau) = -\tfrac{1}{8}(1-2\eta-e^{-2\eta})-\tfrac{1}{16}\{(2-\sqrt{2})\cos(2\tau+\tfrac{1}{4}\pi) - 2\,e^{-\sqrt{2}\eta}\cos(2\tau-\sqrt{2}\eta+\tfrac{1}{4}\pi)+\sqrt{2}\,e^{-2\eta}\cos(2\tau-2\eta+\tfrac{1}{4}\pi)\}, \tag{29}$$

and

$$F_1'(\eta,\tau) = \tfrac{1}{4}(1-e^{-2\eta})+\tfrac{1}{4}\{e^{-\sqrt{2}\eta}\sin(2\tau-\sqrt{2}\eta)-e^{-2\eta}\sin(2\tau-2\eta)\}. \tag{30}$$

Equations (29) and (30) show that the radial and axial velocities are each composed of a steady term and an unsteady term of frequency twice that of the torsional oscillations. Indeed, this was to be anticipated on physical grounds. For a fluid particle adjacent to the wall and distance r from the axis experiences a centrifugal force $\rho r\Omega^2$ per unit volume, where Ω is the angular velocity. Since $\Omega = \omega\cos\lambda t$, the centrifugal force is $\rho r\omega^2\cos^2\lambda t = \frac{1}{2}\rho r\omega^2(1+\cos 2\lambda t)$, having the two components mentioned.

We may therefore divide the radial and axial velocities u and w each into a steady part, denoted respectively by u_s and w_s, and a fluctuating part u_f, w_f. From equations (6), (29) and (30), these are given by

$$u_s = \frac{r\omega\epsilon}{4}\{1-e^{-\sqrt{(2\lambda/\nu)}z}\}, \tag{31}$$

$$w_s = \frac{\omega\epsilon}{4}\sqrt{\left(\frac{2\nu}{\lambda}\right)}\{1-\sqrt{(2\lambda/\nu)}\,z-e^{-\sqrt{(2\lambda/\nu)}z}\}, \tag{32}$$

$$u_f = \frac{r\omega\epsilon}{4}\{e^{-\sqrt{(\lambda/\nu)}z}\sin(2\tau-\sqrt{(\lambda/\nu)}\,z)-e^{-\sqrt{(2\lambda/\nu)}z}\sin(2\tau-\sqrt{(2\lambda/\nu)}\,z)\}, \tag{33}$$

$$w_f = \frac{\omega\epsilon}{8}\sqrt{\left(\frac{2\nu}{\lambda}\right)}\{(2-\sqrt{2})\cos(2\tau+\tfrac{1}{4}\pi)-2\,e^{-\sqrt{(\lambda/\nu)}z}\cos(2\tau-\sqrt{(\lambda/\nu)}\,z+\tfrac{1}{4}\pi) + \sqrt{2}\,e^{-\sqrt{(2\lambda/\nu)}z}\cos(2\tau-\sqrt{(2\lambda/\nu)}\,z+\tfrac{1}{4}\pi)\}. \tag{34}$$

Relative to the oscillations of the plate, the unsteady radial velocity u_f is seen to have a phase lag which tends to $\frac{1}{2}\pi$ at the plate. Moreover u_f decreases exponentially with distance from the wall, the rate of diminution depending on the factor $\sqrt{(\nu/\lambda)}$, which is the order of thickess of the boundary layer. That is, the fluctuating radial component becomes negligible outside the boundary layer.

This is shown in figure 1, which illustrates the variation of the non-dimensionalized velocity $4u_f/r\omega\epsilon$ with $\eta = \sqrt{(\lambda/2\nu)}\,z$ at selected times.

The unsteady axial term w_f has a phase lead of $\frac{1}{4}\pi$ over the transverse velocity. Outside the boundary layer, continuity demands that some unsteady axial velocity should persist, and in fact, for large z,

$$w_f \sim \frac{\omega\epsilon}{8}\sqrt{\left(\frac{2\nu}{\lambda}\right)}\,(2-\sqrt{2})\cos(2\tau+\tfrac{1}{4}\pi),$$

which is quite small for small viscosity.

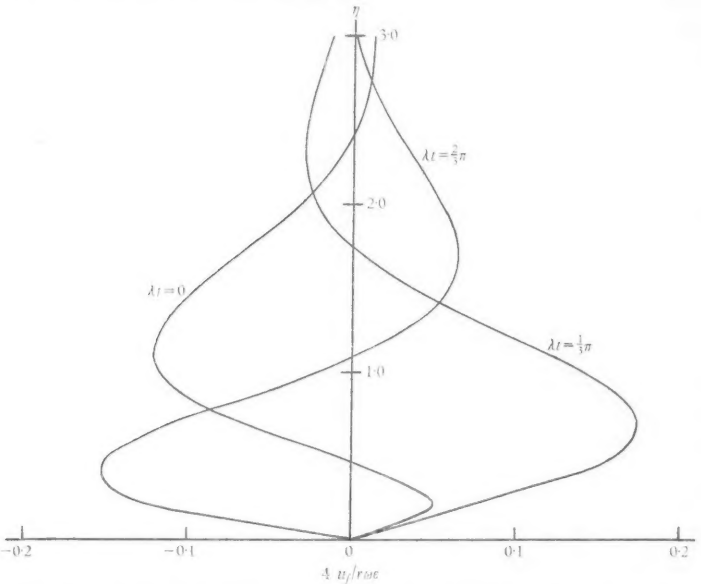

FIGURE 1. Variation of $4u_f/r\omega\epsilon$ with $\eta = (\lambda/2\nu)\,z$ at times (i) $\lambda t = 0$, (ii) $\lambda t = \frac{1}{3}\pi$, (iii) $\lambda t = \frac{2}{3}\pi$.

The centrifugal and shearing forces at the plate give rise to steady components of radial and axial velocity. The radial velocity u_s, as seen from equation (31), consists of two terms, one of which decreases exponentially with z, and so vanishes outside the boundary layer, whereas the other is independent of distance from the plate. Thus for large z,

$$u_s \sim \frac{r\omega\epsilon}{4}. \tag{35}$$

Consequently, it would appear that, unlike the fluctuating component, a steady radial flow persists outside the boundary layer. Furthermore, this flow has the important feature that its magnitude is independent of the value of the kinematic viscosity.

Correspondingly, the asymptotic axial flow outside the boundary layer is, from (32),

$$w_s \sim \frac{\omega\epsilon}{4}\sqrt{\left(\frac{2\nu}{\lambda}\right)}\left\{1-\sqrt{\left(\frac{2\lambda}{\nu}\right)}\,z\right\}. \tag{36}$$

Here the first term represents the axial velocity required by continuity to balance the radial flow within the boundary layer, while the second term, independent of viscosity, balances the asymptotic radial flow outside the boundary layer.

The form of equations (31) and (32) permits the definition of a stream function for the steady radial-axial flow, namely

$$\psi = \frac{r^2\omega\epsilon}{4}\sqrt{\left(\frac{\nu}{2\lambda}\right)}\left[\sqrt{\left(\frac{2\lambda}{\nu}\right)}z - 1 + e^{-\sqrt{(2\lambda/\nu)}z}\right]$$

such that

$$u_s = \frac{1}{r}\frac{\partial\psi}{\partial z}, \quad w_s = -\frac{1}{r}\frac{\partial\psi}{\partial r},$$

satisfying continuity requirements. At large distances from the plate we have that

$$\psi \sim \frac{r^2\omega\epsilon}{4}\left\{z - \sqrt{\left(\frac{\nu}{2\lambda}\right)}\right\}, \tag{37}$$

which is the stream function of an axially symmetrical stagnation flow against an imaginary wall distant $z = \sqrt{(\nu/2\lambda)}$ from the plate. Thus we have achieved the apparent result that torsional oscillations of the plate induce a steady potential flow which is such that the smaller the viscosity the closer its streamlines approach the plate. We re-examine this result in § 6.

As a matter of interest we calculate an approximate expression for the pressure gradient normal to the disk. From equations (3) and (6), we find

$$-\frac{1}{\rho\omega\lambda}\sqrt{\left(\frac{\lambda}{2\nu}\right)}\frac{\partial p}{\partial z} = -2\frac{\partial F}{\partial\tau} + 4\epsilon FF' + F''$$
$$\doteq \epsilon\left[F_1'' - 2\frac{\partial F_1'}{\partial\tau}\right],$$

to first order in ϵ. Substituting from (29) and (30), we obtain eventually

$$-\frac{1}{\rho\omega\lambda}\sqrt{\left(\frac{\lambda}{2\nu}\right)}\frac{\partial p}{\partial z} = \frac{\epsilon}{4}[2\,e^{-\sqrt{(2\lambda/\nu)}z} + \sqrt{2}\,e^{-\sqrt{(2\lambda/\nu)}z}\sin(2\lambda t - \sqrt{(2\lambda/\nu)}z + \tfrac{1}{4}\pi)$$
$$-(2-\sqrt{2})\sin(2\lambda t + \tfrac{1}{4}\pi)]. \tag{38}$$

The contribution from the potential-type flow is of order ϵ^2, and so has been neglected here.

Finally, we calculate the radial shearing stress at the plate,

$$\tau_r = \rho\nu\left(\frac{\partial u}{\partial z}\right)_{z=0}.$$

Substituting for u from (31) and (33), we find

$$\tau_r = \frac{\rho r\omega\epsilon}{4}\sqrt{\left(\frac{2\lambda}{\nu}\right)}[1 + (\sqrt{2}-1)\sin(2\lambda t + \tfrac{1}{4}\pi)]. \tag{39}$$

5. Third approximation to the transverse velocity

Since $F_0 = 0$, equation (13*b*) becomes

$$\frac{\partial G_1}{\partial\tau} = \tfrac{1}{2}G_1'',$$

of which the solution satisfying $G_1(0) = 0$, $G_1(\infty) = 0$ is clearly

$$G_1(\eta, \tau) = 0.$$

(It can moreover easily be demonstrated that

$$F_{2N}(\eta,\tau)=0, \quad G_{2N+1}(\eta,\tau)=0, \quad N=0,1,2\ldots.)$$

Thus the second approximation to the transverse velocity is zero, and the third approximation is given from $G_2(\eta,\tau)$, which satisfies the equation

$$\frac{\partial G_2}{\partial \tau}+2[F_1'G_0-F_1G_0']=\tfrac{1}{2}G_2'', \tag{40}$$

with boundary conditions $G_2(0)=0$, $G_2\to 0$ as $\eta\to\infty$. From equations (17), (29) and (30) we find that, in complex notation,

$$\begin{aligned}F_1'G_0-F_1G_0' = \tfrac{1}{4}e^{i\tau}\Big\{&\tfrac{1}{2}(1-i)\,e^{-(1+i)\eta}+(1+i)\,\eta\,e^{-(1+i)\eta}-(\tfrac{3}{4}-i)\,e^{-(3+i)\eta}\\&-\tfrac{1}{4}(\sqrt{2}-1)\,e^{-(1-i)\eta}+\left(\frac{\sqrt{2}}{4}-\frac{i}{2}\right)e^{-[\sqrt{2}+1+i(\sqrt{2}-1)]\eta}\Big\}\\&+\frac{i}{16}e^{3i\tau}\{e^{-3(1+i)\eta}-(2-\sqrt{2})\,e^{-(\sqrt{2}+1)(1+i)\eta}-(\sqrt{2}-1)\,e^{-(1+i)\eta}\}.\end{aligned} \tag{41}$$

The form of (41) suggests that a solution of equation (40) could be

$$G_2(\eta,\tau)=\chi(\eta)\,e^{i\tau}+\zeta(\eta)\,e^{3i\tau}, \tag{42}$$

and on substituting (41) and (42) into (40), we obtain the pair of linear differential equations

$$\begin{aligned}\chi''-2i\chi = &\tfrac{1}{2}(1-i)\,e^{-(1+i)\eta}+(1+i)\,\eta\,e^{-(1+i)\eta}-(\tfrac{3}{4}-i)\,e^{-(3+i)\eta}\\&-\tfrac{1}{4}(\sqrt{2}-1)\,e^{-(1-i)\eta}+\left(\frac{\sqrt{2}}{4}-\frac{i}{2}\right)e^{-[\sqrt{2}+1+i(\sqrt{2}-1)]\eta},\end{aligned} \tag{43a}$$

$$\zeta''-6i\zeta=\frac{i}{4}[e^{-3(1+i)\eta}-(2-\sqrt{2})\,e^{-(\sqrt{2}+1)(1+i)\eta}-(\sqrt{2}-1)\,e^{-(1+i)\eta}], \tag{43b}$$

with boundary conditions

$$\chi(0)=\zeta(0)=\chi(\infty)=\zeta(\infty)=0.$$

The real and imaginary parts of the solutions χ, ζ of (43a) and (43b) are found to be

$$\begin{aligned}\mathscr{R}\{\chi\} = &-\cos\eta\{[\tfrac{3}{80}+\tfrac{1}{8}\eta+\tfrac{1}{4}\eta^2]\,e^{-\eta}+\tfrac{1}{40}e^{-3\eta}\}+\sin\eta\left\{\left[\frac{15\sqrt{2}-21}{80}+\frac{3}{8}\eta\right]e^{-\eta}+\frac{11}{80}e^{-3\eta}\right\}\\&+\tfrac{1}{16}e^{-(\sqrt{2}+1)\eta}[\cos(\sqrt{2}-1)\,\eta-\sqrt{2}\sin(\sqrt{2}-1)\,\eta],\end{aligned} \tag{44a}$$

$$\begin{aligned}\mathscr{I}\{\chi\} = &\cos\eta\left\{\left[\frac{5\sqrt{2}-11}{80}+\frac{3}{8}\eta\right]e^{-\eta}+\frac{11}{80}e^{-3\eta}\right\}+\sin\eta\{[\tfrac{3}{80}+\tfrac{1}{8}\eta+\tfrac{1}{4}\eta^2]\,e^{-\eta}+\tfrac{1}{40}e^{-3\eta}\}\\&-\tfrac{1}{16}e^{-(\sqrt{2}+1)\eta}[\sqrt{2}\cos(\sqrt{2}-1)\,\eta+\sin(\sqrt{2}-1)\,\eta],\end{aligned} \tag{44b}$$

$$\begin{aligned}\mathscr{R}\{\zeta\} = &\tfrac{1}{48}\{-e^{-\sqrt{3}\eta}\cos\sqrt{3}\eta+e^{-3\eta}\cos 3\eta-3(\sqrt{2}-1)\\&\times[e^{-(\sqrt{2}+1)\eta}\cos(\sqrt{2}+1)\,\eta-e^{-\eta}\cos\eta]\},\end{aligned} \tag{44c}$$

$$\begin{aligned}\mathscr{I}\{\zeta\} = &\tfrac{1}{48}\{e^{-\sqrt{3}\eta}\sin\sqrt{3}\eta-e^{-3\eta}\sin 3\eta+3(\sqrt{2}-1)\\&\times[e^{-(\sqrt{2}+1)\eta}\sin(\sqrt{2}+1)\,\eta-e^{-\eta}\sin\eta]\}.\end{aligned} \tag{44d}$$

From equation (42) we have that, in real notation,

$$G_2 = \mathscr{R}\{\chi\}\cos\tau - \mathscr{I}\{\chi\}\sin\tau + \mathscr{R}\{\zeta\}\cos 3\tau - \mathscr{I}\{\zeta\}\sin 3\tau, \tag{45}$$

so that to third order the transverse velocity is

$$v = r\omega(G_0 + \epsilon^2 G_2), \tag{46}$$

with G_0 and G_2 given respectively by (17) and (46). Figure 2 illustrates the dimensionless transverse velocity relative to a set of axes fixed in the plate. The continuous curves represent, for selected times, the function $G_0 - \cos\tau$, while the broken curves represent

$$G_0 + \epsilon^2 G_2 - \cos\tau$$

for the case $\epsilon = \frac{1}{2}$. The vertical straight lines are the values of $\cos\tau$ at the relevant times. It is seen that the difference between the first and third approximations is quite small close to the plate and rather larger at moderate distances (inside the boundary layer).

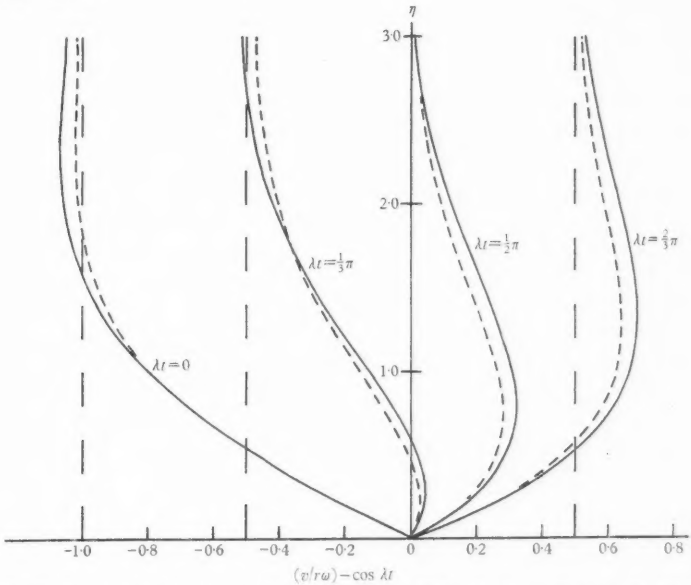

FIGURE 2. Variation of $(v/r\omega) - \cos\lambda t$ with $\eta = \sqrt{(\lambda/2\nu)}\, z$ at times (i) $\lambda t = 0$, (ii) $\lambda t = \frac{1}{3}\pi$, (iii) $\lambda t = \frac{1}{2}\pi$, (iv) $\lambda t = \frac{2}{3}\pi$: ———— first approximation; — — — — second approximation.

Using (44)–(46), we now find for the fluctuating shearing stress at the wall

$$\tau_l = \rho\nu\left(\frac{\partial v}{\partial z}\right)_{z=0} = \rho\nu r\omega\sqrt{\left(\frac{\lambda}{2\nu}\right)}$$
$$\times\{\sin\tau(1 - 0{\cdot}262\epsilon^2) - 0{\cdot}012\epsilon^2\sin 3\tau - \cos\tau(1 + 0{\cdot}060\epsilon^2) + 0{\cdot}012\epsilon^2\cos 3\tau\}. \tag{47}$$

Hence by (21) the moment on a disk of radius a is, to a third approximation,

$$M' = \frac{\pi a^4\rho\epsilon}{\sqrt{2}}\sqrt{(\nu\lambda^3)}$$
$$\times\{\cos\tau(1 + 0{\cdot}060\epsilon^2) - 0{\cdot}012\epsilon^2\cos 3\tau - \sin\tau(1 - 0{\cdot}262\epsilon^2) + 0{\cdot}012\epsilon^2\sin 3\tau\}. \tag{48}$$

From this equation and (22), we find for the magnitude of the fluctuating torque

$$|M'| = |M|\{1 - 0{\cdot}101\epsilon^2\}. \tag{49}$$

As a matter of interest it can easily be verified that the result (49) remains unaltered if the terms in $\cos 3\tau$, $\sin 3\tau$ are omitted from the preceding formulae. This means that, to third order, the third harmonic terms only have an effect on the phase of the fluctuating torque.

We see that the third approximation to the transverse velocity necessitates a negative correction to the moment of $0{\cdot}101\epsilon^2|M|$; that is, a decrease of about $2{\cdot}5\,\%$ when $\epsilon = \frac{1}{2}$ and $0{\cdot}6\,\%$ when $\epsilon = \frac{1}{4}$. These values may be contrasted with those obtained, by a somewhat different procedure, by Carrier & Di Prima (1956) for a torsionally oscillating sphere. Their result, translated into our notation, was

$$|M'| = |M|\{1 + 0{\cdot}015\epsilon^2\},$$

yielding an increase of about $0{\cdot}4\,\%$ when $\epsilon = \frac{1}{2}$ and $0{\cdot}1\,\%$ when $\epsilon = \frac{1}{4}$. Thus it would seem that for a disk the increment to the torque is about 7 times as great as for a sphere and of opposite sign.

Finally, it should be noted that the results (47)–(49) have value only if equations (29) and (30) constitute a good approximation to the second-order radial-axial flow close to the plate. It is indicated in §6 that this is the case, even though they are a bad approximation at larger distances.

6. The steady radial flow

At this stage a discussion of the results obtained so far is worth-while. As demonstrated in figure 2, the value of the transverse velocity is not greatly altered when the third approximation is taken in place of the first; and, as expected, the third approximation vanishes outside the boundary layer, even though its evaluation involves the non-vanishing radial-axial terms. Hence, there is no reason to doubt the validity of the series expansion (11), and therefore we assume in the subsequent calculations that the transverse velocity is given, to a good approximation, by

$$v = r\omega\, e^{-\sqrt{(\lambda/2\nu)}\,z} \cos\{\lambda t - \sqrt{(\lambda/2\nu)}\,z\}. \tag{18 *bis*}$$

Moreover, we assume that equations (33) and (34) adequately represent the unsteady radial and axial velocities, and do not consider them further here. To establish this would of course necessitate quite complicated calculations.

On the other hand, the unexpected form of the steady radial-axial component suggests that in this case a further investigation is warranted. Assuming that u/r is independent of r, and that there is no radial pressure gradient, the steady radial and axial velocities may be taken to be governed by the equations

$$u_s \frac{\partial u_s}{\partial r} + w_s \frac{\partial u_s}{\partial z} - \frac{\overline{v}^2}{r} = \nu \frac{\partial^2 u_s}{\partial z^2} \tag{50}$$

and

$$\frac{\partial u_s}{\partial r} + \frac{u_s}{r} + \frac{\partial w_s}{\partial z} = 0, \tag{51}$$

where $\bar{v}$ is the root-mean-square value of the transverse velocity (18); that is,

$$\bar{v} = \frac{r\omega}{\sqrt{2}} e^{-\sqrt{(\lambda/2\nu)}\, z}. \tag{52}$$

The boundary conditions to be satisfied are

$$u_s = w_s = 0 \quad \text{at} \quad z = 0; \qquad u_s \to 0 \quad \text{as} \quad z \to \infty. \tag{53}$$

On the assumption that the series (10) for u_s, w_s is valid, the first approximation to u_s is given from the equation

$$\nu \frac{\partial^2 u_s}{\partial z^2} = -\frac{\bar{v}^2}{r}, \tag{54}$$

whose solution is (31). At large distances from the plate $\bar{v}$ is vanishingly small and consequently the asymptotic equation for u_s is

$$\nu \frac{\partial^2 u_s}{\partial z^2} = 0. \tag{55}$$

This explains why the radial flow at large distances is independent of viscosity; and the solution of (55) is equation (35).

This solution, however, is acceptable only if the convective inertia terms $u_s(\partial u_s/\partial r)$, $w_s(\partial u_s/\partial z)$ can be neglected for all z, and it is clear on physical grounds that this cannot be the case. The vorticity created at the plate has imparted to it a radial velocity component as a result of centrifugal action. This vorticity diffuses away from the plate and beyond the boundary layer. But, as the edge of the layer is approached, the transverse velocity becomes vanishingly small, so that radial motion is no longer maintained by centrifugal force and can persist only because of the diffusion of vorticity to large distances. At the same time the convection of the fluid by itself, hitherto negligible, will be principally axial—towards the plate—as it has to balance the fluid forced radially out by centrifugal action. It must therefore be anticipated that instead of persisting at large z, diffusion of vorticity, and consequently steady radial flow, will be limited to within a finite distance of the plate—a distance determined by the counteraction of outward diffusion and inward convection.

Applying these considerations to the equation of motion (50) we see that the inertia terms $u_s(\partial u_s/\partial r)$, $w_s(\partial u_s/\partial z)$ are negligible compared with the centrifugal term $\bar{v}^2/r$ only in the region where the latter is non-vanishing, that is, within the boundary layer. Elsewhere the inertia forces are at least comparable with the centrifugal force, and so outside the boundary layer a correct estimation of the flow must take account of them. Alternatively, this means that the series expansion (10) in powers of ϵ yields valid approximations inside the boundary layer only.

(An interesting parallel to these results is afforded by the well-known Oseen's equations for flow past an obstacle at low Reynolds numbers. In this case it appears that close to the obstacle inertia forces are negligible and Stokes' equations provide a good approximation. But at large distances these inertia forces, though still very small, are now of similar magnitude to the viscous forces. Thus Stokes' equations are no longer satisfactory and Oseen's equations are required for a reasonable approximation to the flow field.)

We now seek a solution of equations (50)–(53) which does not involve the approximation arising from the series (10). On writing

$$u_s = r\omega\epsilon f'(\eta), \quad w_s = -2\omega\epsilon\sqrt{\left(\frac{2\nu}{\lambda}\right)}f(\eta), \quad z = \sqrt{\left(\frac{2\nu}{\lambda}\right)}\eta, \tag{56}$$

equation (50) becomes

$$\epsilon^2(f'^2 - 2ff'') - \tfrac{1}{2}e^{-2\eta} = \tfrac{1}{2}f'''. \tag{57}$$

The steady radial flow will, by the foregoing argument, be confined within some secondary layer whose thickness, however, may be large compared with that of the primary layer discussed so far. By use of a Pohlhausen-type method, an approximate solution may be obtained which gives an estimate of the thickness of this secondary layer.

We suppose that the flow takes place within a distance d of the plate. Then we seek a solution of the integral of equation (57) over the range 0 to d, with the assumption that conditions at ∞ are satisfied at $\eta = d$. The relevant boundary conditions will then be

$$\text{at } \eta = 0: \quad f = 0, \quad f' = 0, \quad f''' = -1,$$
$$\text{at } \eta = d: \quad f' = f'' = f''' = \ldots = 0,$$

while integration of (57) now gives

$$3\epsilon^2\int_0^d f'^2\,d\eta - \tfrac{1}{4} = -\tfrac{1}{2}f''(0). \tag{58}$$

A solution of (58) may take the form

$$f' = -\tfrac{1}{4}\{e^{-2\eta} - e^{-\eta/d}\}. \tag{59}$$

This gives $f' = 0$ at $\eta = 0$; moreover, assuming that $d \gg 1$, that is, that the secondary layer is considerably thicker than the primary layer, we have

$$f'''(0) = -1 + O(d^{-2}),$$

which nearly satisfies the condition on $f'''(0)$. When $\eta \ll 1$, $e^{-\eta/d} \doteqdot 1$, so that (59) behaves like the function f' of equation (28b) close to the plate.

Substitution from (59) into (58) leads to

$$\frac{3\epsilon^2}{2}\left(\frac{1}{4} - \frac{2d}{2d+1} + \frac{d}{2}\right) = \frac{1}{d} \tag{60}$$

as the equation determining d. It may be noticed that if the terms on the left-hand side of (60), which represent the convection, are neglected, we obtain $d = \infty$, as expected. As it stands, however, equation (60) yields

$$d \doteqdot \frac{1{\cdot}155}{\epsilon} + 0{\cdot}250 \tag{61}$$

for the order of thickness of the secondary layer. Equation (61) shows that if d_1 is the thickness when $\epsilon = \frac{1}{4}$, and d_2 that when $\epsilon = \frac{1}{2}$, then

$$\frac{d_1}{d_2} \doteqdot 1{\cdot}90. \tag{62}$$

Thus we have that provided ϵ is sufficiently small, steady radial flow takes place within a layer of thickness $O(\epsilon^{-1})$ times that of the primary layer.

In other words, the order of thickness of the secondary layer is

$$\epsilon^{-1}\sqrt{(\nu/\lambda)} = \sqrt{(\nu/\omega\epsilon)},$$

and this could have been estimated from first principles. For steady flow occurs in a region where inertia forces are comparable in magnitude with viscous forces, that is, where $u_s(\partial u_s/\partial r) \sim \nu(\partial^2 u_s/\partial z^2)$. Since $u_s \sim r\omega\epsilon$, and taking $z \sim \delta$, the layer thickness, we find $r\omega^2\epsilon^2 \sim \nu(r\omega\epsilon/\delta^2)$, which gives $\delta \sim \sqrt{(\nu/\omega\epsilon)}$.

Outside the secondary layer there is merely a constant axial inflow whose value is obtained from integration of (59). We find that

$$f(\infty) = \tfrac{1}{4}(d - \tfrac{1}{2}),$$

which leads to

$$f \doteqdot 1{\cdot}09 \quad \text{when} \quad \epsilon = \tfrac{1}{4}, \qquad f \doteqdot 0{\cdot}52 \quad \text{when} \quad \epsilon \doteqdot \tfrac{1}{2}. \tag{63}$$

From equation (56) we now have

$$w_s(\infty) = O(\epsilon\sqrt{(\nu\lambda)}),$$

technically a first-order effect. But this is explained by the continuity equation which requires that $\partial w_s/\partial z \sim u_s/r$, i.e. that $w_s \sim \delta$, $\omega\epsilon \sim \epsilon\sqrt{(\nu\lambda)}$.

Of course, equation (59) is no more than a rough approximation to the solution of (57), useful in obtaining an estimate of d. In order to deduce a correct representation of the functions f and f', it is necessary to resort to numerical solutions of equation (57). Such solutions were calculated with the aid of the Mercury Automatic Computer at the University of Manchester, for the two values $\epsilon = \frac{1}{4}$ and $\epsilon = \frac{1}{2}$.

These solutions yielded the following results. Taking $f' \leqslant 0{\cdot}01$ as a measure of the layer within which radial flow is confined, it was found that

$$\text{for } \epsilon = \tfrac{1}{4}, \quad f' = 0{\cdot}01 \quad \text{when} \quad \eta = d_1 = 13{\cdot}16;$$
$$\text{for } \epsilon = \tfrac{1}{2}, \quad f' = 0{\cdot}01 \quad \text{when} \quad \eta = d_2 = 7{\cdot}24.$$

These give

$$\frac{d_1}{d_2} \doteqdot 1{\cdot}82,$$

in close agreement with (62). This tends to confirm our conclusion that steady flow occurs within a layer whose order of thickness is $\epsilon^{-1}\sqrt{(2\nu/\lambda)}$. Again, it was found that for large η, f tends asymptotically to 0·99 when $\epsilon = \frac{1}{4}$, and to 0·50 when $\epsilon = \frac{1}{2}$. These values for the inflow also agree with the approximate values (63).

The steady components of radial and axial velocity are illustrated in figures 3 and 4, respectively. In figure 3, the curve designated (I) represents the solution f' given by equation (28*b*) which is independent of ϵ and becomes irrotational for large η. The curves (II) and (III) are the function f' obtained from the numerical solution of (57) for $\epsilon = \frac{1}{4}$ and $\epsilon = \frac{1}{2}$, respectively. A similar notation is used for the curves of f in figure 4.

It is immediately clear that well within the primary layer, say for $\eta < \frac{1}{2}$, the values of f' and f derived from the power series expansion are very close to those obtained from the numerical solution. This means that, as indicated earlier, very close to the plate the dominant factor in determining the radial flow is the centrifugal force, and neglect of convection is justified.

On the other hand, for $\eta > \frac{1}{2}$ the curves begin to diverge, taking the forms illustrated. The radial velocity given by the numerical solution tends to zero instead of a finite value, thus satisfying the required boundary condition, at infinity. Similarly, the axial velocity tends asymptotically to a constant inflow in place of a linear function of distance from the plate. The divergence between the potential-flow solution and the secondary-layer solution decreases with ϵ, which is to be anticipated from an inspection of (57).

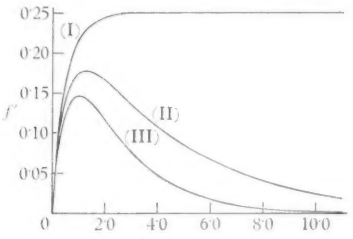

FIGURE 3

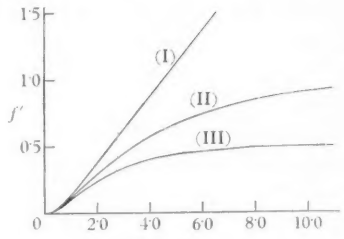

FIGURE 4

FIGURE 3. The steady radial flow. Variation of $f' = u_s/r\omega\epsilon$ with $\eta = \sqrt{(\lambda/2\nu)}z$. (I) f' from series expansion; (II) f' from numerical solution, $\epsilon = \frac{1}{4}$; (III) f' from numerical solution, $\epsilon = \frac{1}{2}$.

FIGURE 4. The steady axial flow. Variation of $f = -w_s/2\omega\epsilon\sqrt{(\lambda/2\nu)}$ with $\eta = \sqrt{(\lambda/2\nu)}z$. (I) f from series expansion; (II) f from numerical solution, $\epsilon = \frac{1}{4}$; (III) f from numerical solution, $\epsilon = \frac{1}{2}$.

Thus we conclude that a true representation of the induced steady radial-axial flow can only be obtained by including the convective inertia terms. These terms, although small, play a decisive role in determining the character of the flow at large distances from the plate.

It is noteworthy that our solution is consistent with the well-known Karman rotating-disk solution for steady flow. In the latter it is found that radial flow is confined within the boundary layer of the transverse velocity. Here also, inward axial flow prevents outward diffusion of vorticity beyond the layer, whose thickness is of order $\sqrt{(\nu/\omega)}$, ω being the steady angular velocity of the disk.

In conclusion it must be remarked that, with the new values of f' and f, the third approximation to the transverse velocity will be altered. But since there has been little variation in the values of f' and f close to the plate, it is unlikely that the transverse velocity will suffer much change except possibly towards the edge of the layer, where it in any case tends to zero. Consequently, we expect the third-order values of shearing stress and moment derived in § 5 to be valid.

REFERENCES

CARRIER, G. F. & DI PRIMA, R. C. 1956 *J. Appl. Mech.* **23**, 601.

KESTIN, J. & PERSEN, L. N. 1954 *Brown University Rep.* no. AF-891/2.

SCHLICHTING, H. 1932 *Phys. Z.* **33**, 327.

SCHLICHTING, H. 1955 *Boundary Layer Theory.* Pergamon: London.

Measurements of intermittency of turbulent motion in a boundary layer

By V. A. SANDBORN

Lewis Research Center, National Aeronautics and Space Administration, Cleveland, Ohio

(Received 22 December 1958)

Previous observations of turbulent motion at large wave-numbers have revealed the existence of an uneven distribution of turbulent energy. The spotty distribution of the turbulent motion at high wave-numbers is here studied experimentally for the turbulent boundary layer. The high wave-number intermittency is observed at all locations through and along the boundary layer from near transition to near separation.

The flatness factors for the longitudinal turbulent component at different wave-numbers are measured to give a quantitative value for the intermittency at particular wave-numbers. Upstream of the separation region the flatness factors are found to depend on wave-number and longitudinal distance, but not on the distance from the wall. It appears that the intermittency develops in the transition region and does not diminish very rapidly with distance downstream. Near separation the flatness factors change radically in distribution near the wall, and are there no longer independent of distance from the wall.

Introduction

Turbulence is one of the least understood branches of fluid dynamics. There is still need for a physically consistent model to describe the fluctuations and without such a model there is little hope of solving theoretically the equations of motion. From both the theoretical and experimental point of view a more detailed knowledge of the structure of the turbulent fluctuations is necessary before an adequate model can be constructed.

The foregoing is not meant to imply that nothing is understood of turbulence. A great deal is indeed known of some of the general features of the turbulent fluctuations. In particular, a very detailed study, both theoretical and experimental, may be found in the literature for homogeneous turbulence. Batchelor (1953) has summarized the present state of knowledge of this particular type of idealized turbulence. The state of understanding in turbulent shear flows is by no means as advanced as the theory of homogeneous turbulence, but certain progress is being made (Townsend, 1956; Klebanoff, 1955). However, none of the theoretical or experimental work is devoted at any length to the detailed study of the structure of the turbulent fluctuations. For the most part, knowledge of turbulence is based on the gross effects and not on an understanding of the mechanism.

The observation of the turbulence mechanism in a boundary layer, or for that matter in any turbulent flow, is very difficult. Direct visual observations in a smoke tunnel or a water channel have been somewhat successful (Hama, Long & Hegarty, 1956; Weske, 1957; Kline, 1957), and as the visualization technique and understanding of the phenomena improve, these observations will shed much light on the flow structure. The hot wire has proved a valuable tool in statistical studies of turbulent flows; however, it is quite difficult to visualize the physical picture of turbulence from a hot-wire trace. For a study of the small-scale, high-frequency motion of turbulence, present flow-visualization techniques are inadequate, and the hot wire must be used.

The present paper presents some experimental observations with a hot-wire anemometer that appear to be of interest in the understanding of the turbulent mechanism, particularly the small-scale high-wave-number features. By electronically examining isolated frequency components of the over-all turbulent signal in the turbulent boundary layer, a lump or intermittent character is observed at the high frequencies. Measurements of the flatness factor of the frequency components were made to give an indication of the extent of the intermittency over the complete frequency spectrum. The physical picture of what is being observed is certainly inadequate; however, the measurements are presented at this time with the hope that they may contribute to the over-all picture of the turbulent structure.

Measurement procedure

Test facility

The data reported herein were taken along the test wall (3 in. above the centre line) of the NACA Lewis laboratory 6- by 60-inch boundary-layer channel described by Sandborn (1953). A diagram of the channels is shown in figure 1. The test wall of the channel is a flat Masonite plate 12 ft. long. The opposite wall is constructed of flexible porous bronze. Suction through the porous wall prevents its boundary layer from interfering with the layer on the test wall. Removable sections are also provided so that the distance between the channel inlet contraction and the test wall can be varied. The widths of the channel between test wall and porous wall for the present test condition are listed in table 1. Sketches of the probes used to survey the boundary layer are shown in figure 2.

Electronic equipment

The constant-temperature hot-wire-anemometer equipment is that described in detail by Laurence & Landes (1952). Details of further modifications to the equipment and the method of evaluating the turbulent fluctuations from hot-wire signals are given by Sandborn & Slogar (1955*a*). A 0·0002-inch-diameter by 0·040-inch-long tungsten wire was used for the present measurements. A commercially available true root-mean-square vacuum-tube voltmeter was used for direct measurement of the hot-wire output. The over-all accuracy of the constant-temperature-anemometer system is compared with the conventional constant-current system by Sandborn (1955). It was found that the two systems are equivalent for shear-flow measurements.

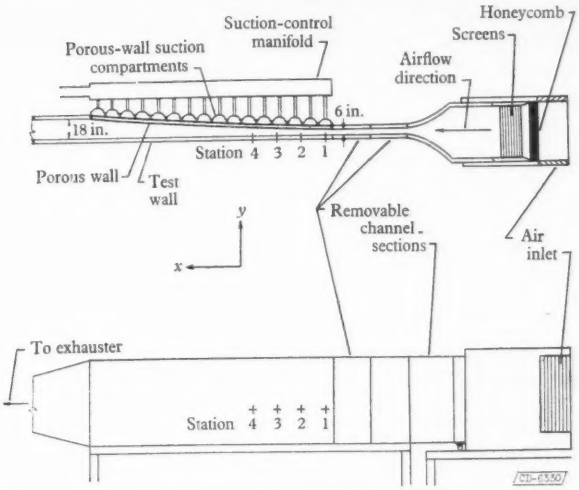

FIGURE 1. Diagram of 6- by 60-inch subsonic boundary-layer channel.

Station	Distance from contraction (in.)	Channel width (in.)	Pressure gradient, lb./sq.ft. / ft.	Boundary-layer thickness (in.)
	0	6·00	—	—
	10	↓		
	20			
	30			
	40			
Start of channel expansion	44	6·00	—	—
1	49·13	6·05	0·0016	0·9
	50	6·05		
	60	6·2		
2	65·63	6·3	0·0256	1·0
	70	6·4		
	80	7·0		
3	83·25	7·3	0·0294	2·0
	90	7·7		
	100	8·6		
4	100·75	8·7	0·0160	3·3
	110	9·5		
	120	10·3		
5	121·38	10·4	0·0112	5·2
	130	11·2		
	140	12·2		

[Channel height, 60 in.]

TABLE 1. Channel geometry

Commercially available variable electronic filters were used to analyse the contribution to the turbulence signal from various frequency bands. Typical band shapes at various frequencies are shown in figure 3.

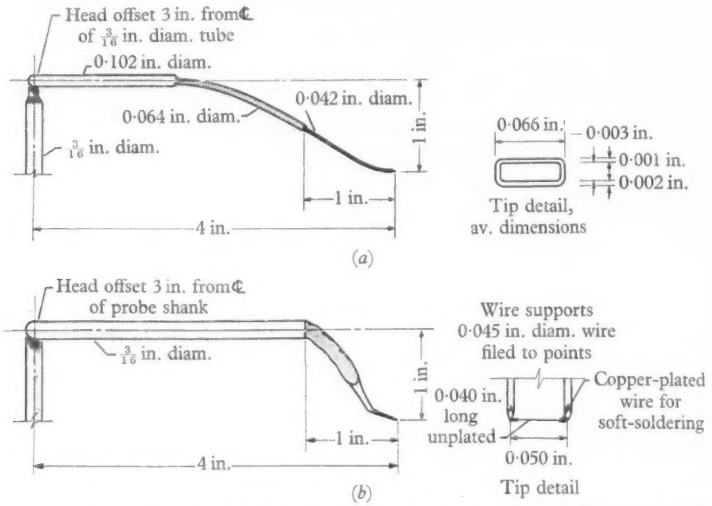

FIGURE 2. Survey probe details. (*a*) Total-pressure probe. (*b*) Hot-wire probe.

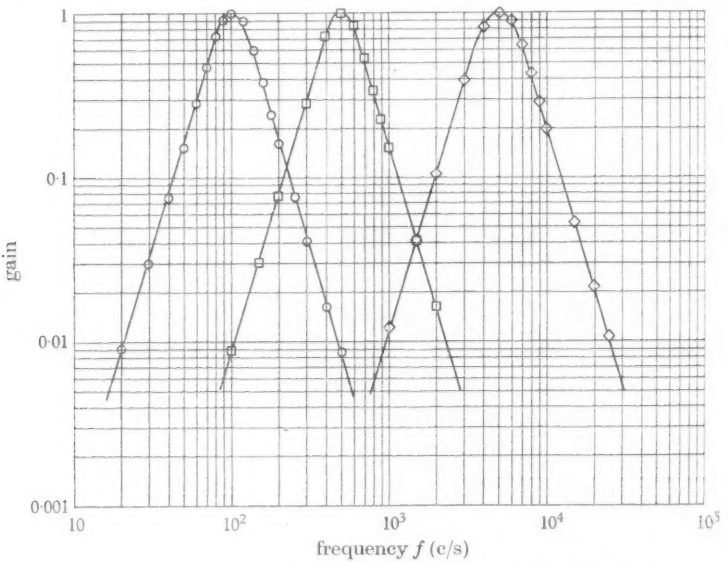

FIGURE 3. Typical bands obtained from band pass filters.

A Philbrick multiplier was employed to obtain the fourth power of the turbulence signal necessary for determining the flatness factor or intermitteney. The unit consists of two multipliers, such that the instantaneous squared signal is fed into both sides of the second multiplier. The output of the second multiplier

is read directly with a direct-current vacuum-tube voltmeter. A calibration of the multipliers is shown in figure 4. For the turbulence signals encountered in the present analysis it was necessary to operate the multipliers at very low output levels. The low levels are required in order that the very large intermittent bursts of turbulence do not saturate the multipliers. A typical calibration for the low voltage levels made in connexion with evaluating one day's data is shown as an insert on figure 4. The drift of the multiplier is indicated by the two calibrations taken 7 hr apart, as noted on the insert.

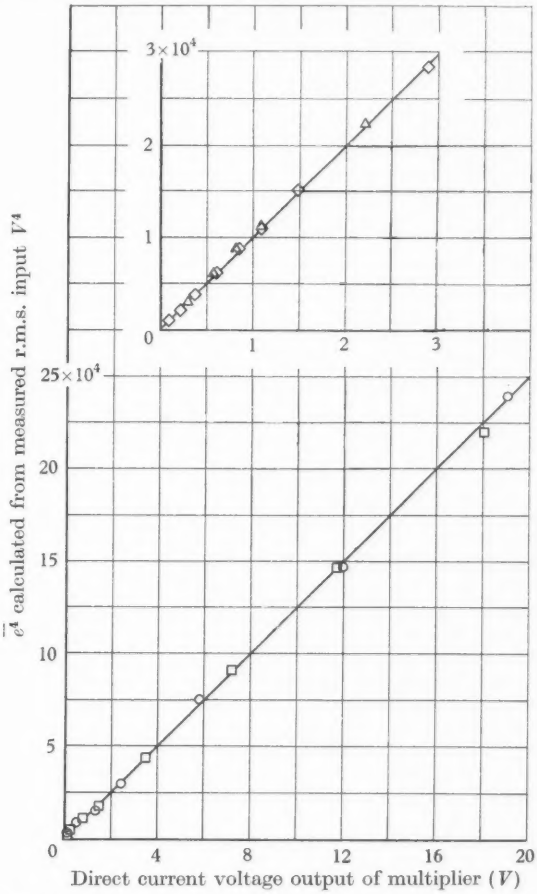

FIGURE 4. Calibration of Philbrick multipliers for obtaining fourth power of hot-wire signal. Typical low-voltage-level calibration: ◇, sine-wave calibration; △, repeat calibration 7 hr apart; ○, sine-wave; □, triangular wave.

With the exception of the values of turbulent intensities, which were obtained from direct readings, all the measurements presented were first recorded on magnetic tape and then analysed from the tape. The tape recorder was accurate for frequencies from 30 to greater than 10,000 c/s (± 2 db from 30 to 15,000 c/s). For the very low frequencies a pen recorder was used to trace the fluctuations.

Results

Intermittency and flatness factor

To study the small-scale features of the turbulent motion with a hot wire, the large-scale, low-frequency components are removed by using an electronic filter. The wave form displayed on an oscillograph screen after the low frequencies are removed is quite different from what is expected. Instead of being uniformly distributed in time (or space) as it flows past the wire, the small-scale turbulence appears to be contained in quite sharply defined lumps or bursts. The lump character of the turbulence is shown in figure 5. For these particular traces, two electronic filters were employed, so that the traces shown are within a narrow frequency band around the frequency noted (figure 5). The traces are for a very low Reynolds number flow, $1{\cdot}9 \times 10^5$ per foot at station 1 (since they can then be more clearly photographed), and may not be the truest representation of the phenomenon at higher Reynolds numbers. Also, the traces shown were arbitrarily selected; thus, the number of lumps implied from the figures may not be exactly representative. (Note that the time basis for each trace does not correspond to any other trace.) The particular y-distances shown in figure 5 were chosen to demonstrate the existence of these bursts throughout the layer and should not be compared for stations 1 and 4.

This uneven distribution of turbulent energy is not characteristic of the usual picture of turbulence. However, there is evidence to suggest that it is quite universal for turbulent flow in general. Batchelor & Townsend (1949) indicate evidence of the same type of intermittency for measurements in isotropic turbulence and for turbulence in the wake of a cylinder.

The lump character of the turbulent motion corresponds to a measurable 'intermittency' in the output signal. Batchelor (1953, p. 184) assigns a value γ as the fraction of time a given signal is turbulent. Thus, γ is termed the intermittency factor. For $\gamma = 0$ the flow is laminar, and for $\gamma = 1$ the flow is turbulent all the time. The original definition of the intermittency factor was given by Townsend (1948). Electronically, it is possible to obtain a measure of γ directly from the hot-wire signal, as was done by Klebanoff (1955); however, such a circuit was not immediately available for evaluating the present data. A second indirect method was employed to determine the degree of intermittency in the present study. Instead of counting the bursts directly, the flatness factor, $\overline{u^4}/(\overline{u^2})^2$, of the hot-wire signals was measured. The flatness factor is an approximate indication of the intermittency. Since the flatness factor may be written as

$$\frac{\overline{u^4}}{(\overline{u^2})^2} = \frac{\int_{-\infty}^{\infty} u^4 P(u)\,du}{\left[\int_{-\infty}^{\infty} u^2 P(u)\,du\right]^2}, \tag{1}$$

where $P(u)$ is the probability of a fluctuation velocity of magnitude u in a band du, it may be seen that $\overline{u^4}/(\overline{u^2})^2$ represents a measure of the extent of the skirts of the probability density curve, since the fourth power weights the large values of u heavily. A burst or large-amplitude-type intermittent signal will affect the

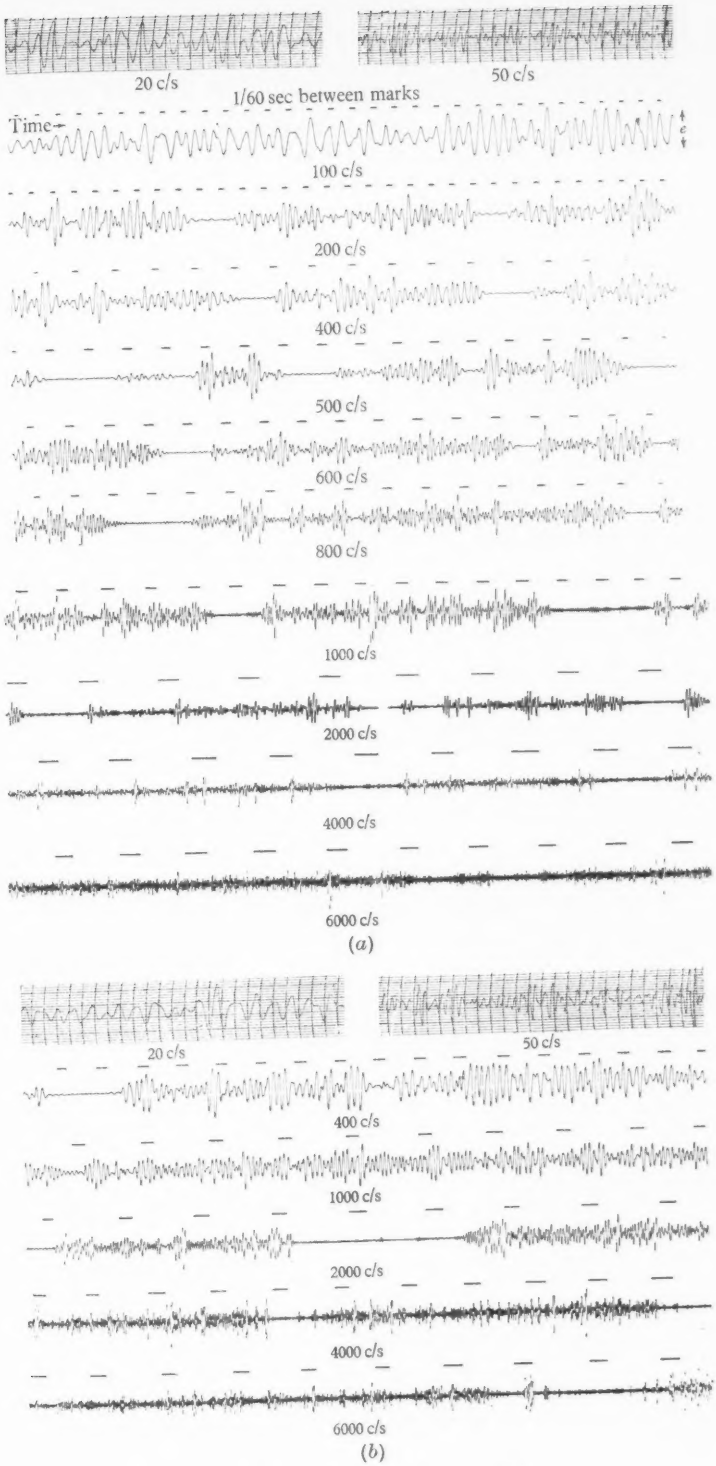

FIGURE 5. For legend see p. 229

skirts of the probability curve greatly; thus, a relation between flatness factor and intermittency is suggested. Batchelor (1953, p. 184) demonstrates that the flatness factor and the intermittency factor may be related for an idealized model of the probability curve. The case considered by Batchelor (a distribution in which the central peak is of infinite height, but encloses a finite area $1-\gamma$), leads to the relation

$$\text{flatness factor} = \frac{3}{\gamma} = \frac{\overline{u^4}}{(\overline{u^2})^2}. \tag{2}$$

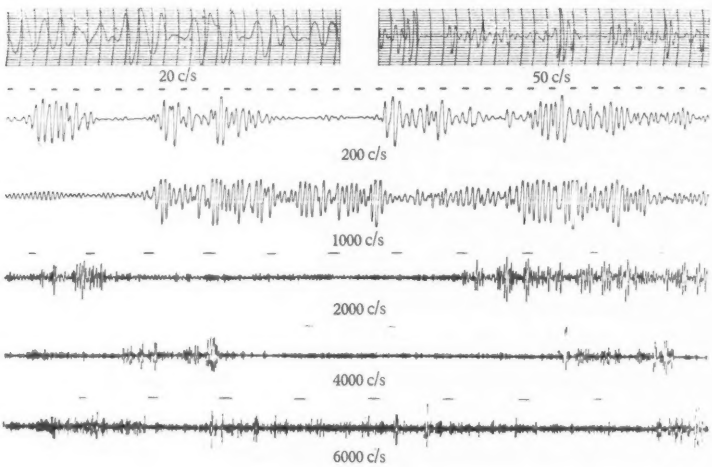

(*c*)

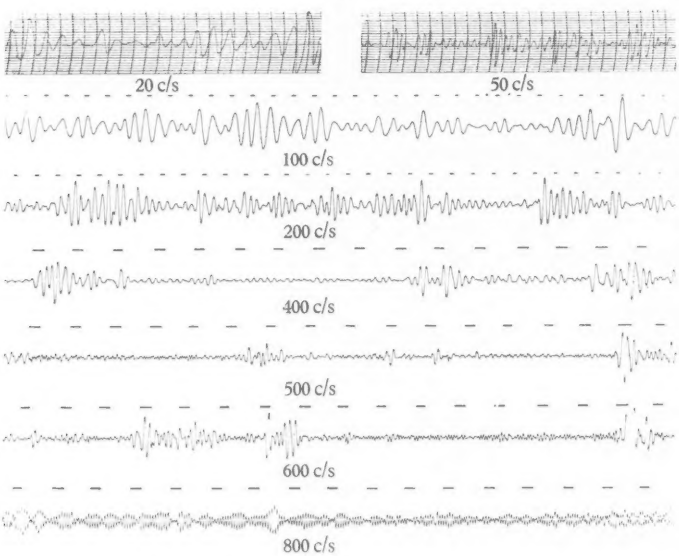

(*d*)

FIGURE 5. For legend see p. 229.

This relation comes from the Gaussian distribution values of $\overline{u^4}/(\overline{u^2})^2 = 3$ and $\gamma = 1$. Klebanoff (1955) demonstrated that equation (2) gives reasonable values for the intermittency factor in a boundary layer where the distributions are other than Gaussian.

First observations of the bursts in the high-frequency range were made at the time the measurements by Sandborn & Braun (1956) were carried out. A preliminary set of flatness factors was measured at that time with a simple squaring

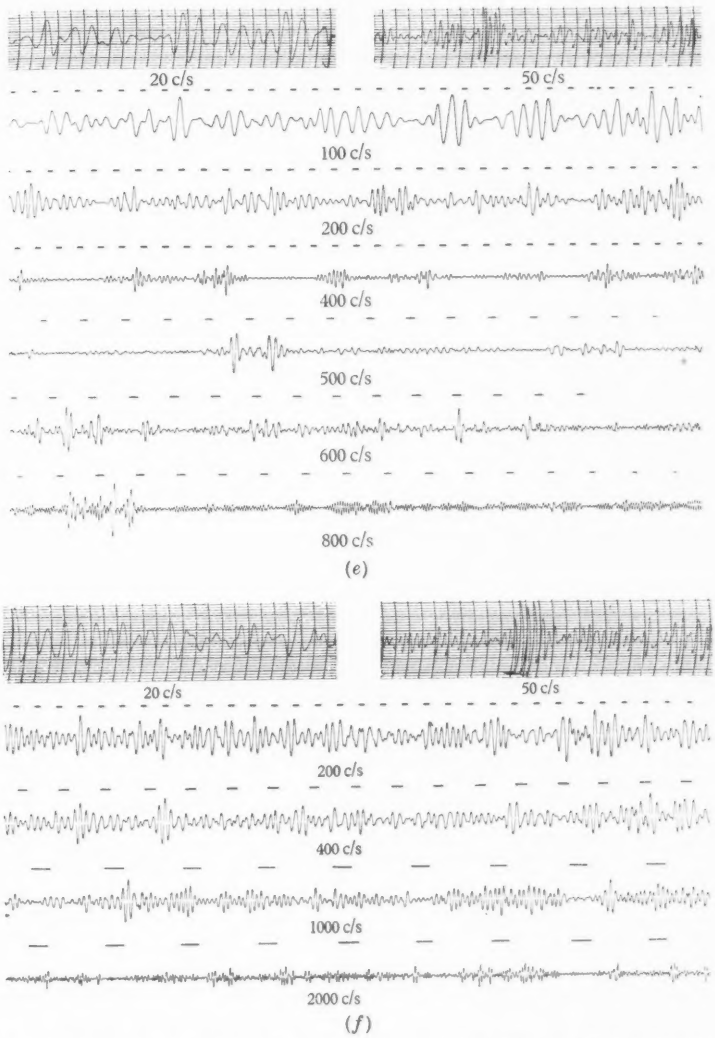

FIGURE 5. Distribution of turbulent fluctuations at various frequencies (amplitude varied between traces). (*a*) Station 1, $y = 0{\cdot}005$ in. (*b*) Station 1, $y = 0{\cdot}100$ in. (*c*) Station 1, $y = 0{\cdot}400$ in. (*d*) Station 4, $y = 0{\cdot}005$ in. (*e*) Station 4, $y = 0{\cdot}010$ in. (*f*) Station 4, $y = 1{\cdot}00$ in.

circuit (similar to one described by Townsend (1947)) and a true r.m.s. voltmeter. The data from these preliminary measurements are shown in figure 6. Only one high-pass filter was employed in the recording of these data. The results confirmed the use of flatness factor to explore the quantitative nature of the bursts, and a more elaborate study was therefore undertaken and is reported in the following sections. The preliminary measurements are included here since they

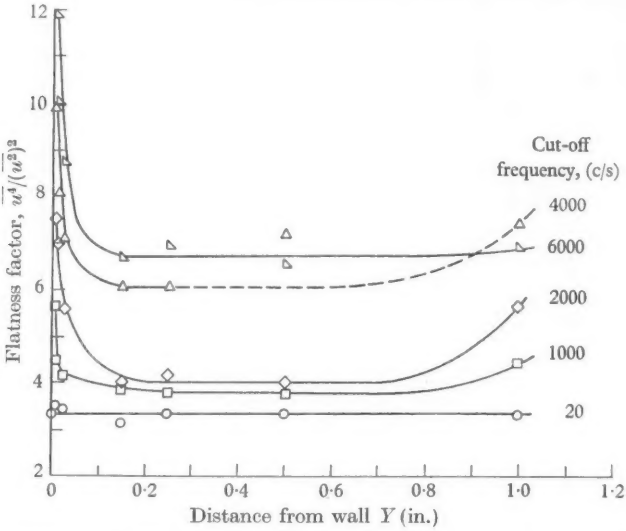

FIGURE 6. Variation of flatness factor with distance from wall and filter cut-off frequency. Data for flow conditions and station 1 of Sandborn & Slogar (1955*b*). ($U_1 = 48{\cdot}6$ ft./s., $\partial p/\partial x \approx 0{\cdot}01$ lb./sq.ft./ft., temp. = 74° F.; $p_{\text{bar}} = 29{\cdot}60$ in. Hg.)

are for the rather extensively surveyed flow. (The flow conditions corresponding to figures 6 and 7 must be obtained from Sandborn & Braun (1956) and Sandborn & Slogar (1955*b*), since channel dimensions and flow velocity were changed for the present measurements.) Figure 6 suggests that the sharp rise in flatness factor near the wall might be due in part to the presence of the solid boundary. (Note that the data do not extend out to the intermittent outer edge of the layer, $\delta \approx 1{\cdot}8$ in.) However, if the effect of local mean velocity, U, is removed by employing wave number $2\pi f/U$ instead of frequency, f, the flatness factor appears to be nearly independent of distance from the wall (figure 7). (The data beyond 6000 c/s, noted in figure 7 by solid points, departed markedly from the universal curve, but it was thought that the noise level of the electronic circuits caused the deviation.)

Measurements

To obtain a more graphic picture of the intermittency, it was necessary to reduce the flow velocity. The lower velocities in turn lower the frequencies at which the intermittency occurs and thus make it possible to obtain clearer photographs of the phenomenon. Figure 5 shows oscillograph traces for a flow

with a Reynolds number per foot of $1{\cdot}9 \times 10^5$ at station 1 (see table 1). This flow is such that station 1 is just at the end of the transition region, with a very slight amount of bursts observable in the over-all turbulent traces. The flow pressure distribution and boundary-layer development for this Reynolds number are summarized in figure 8. The mean and fluctuating velocity distributions are shown in figures 9 and 10 for stations 1 to 4. The fluctuating velocities are plotted as a ratio of both the local mean velocity U, and the freestream mean velocity U_1. No corrections were made for the high intensities of turbulence encountered.

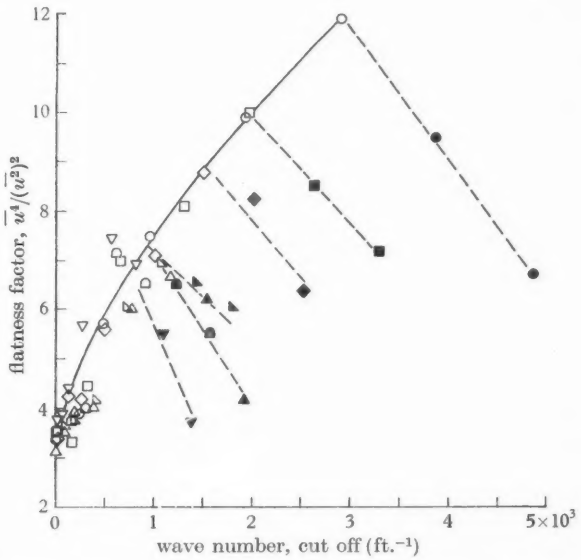

FIGURE 7. Flatness factor at different wave numbers. Data for flow conditions and station 1 of Sandborn & Slogar (1955*b*). ($U_1 = 48{\cdot}6$ ft./s., $\partial p/\partial x \approx 0{\cdot}01$ lb./sq.ft./ft., temp. = 74° F.; $p_{\text{bar}} = 29{\cdot}60$ in. Hg.)

	Distance from wall, Y (in.)	Local mean velocity, U (ft./s.)		Distance from wall, Y (in.)	Local mean velocity, U, (ft./s.)
○	0·005	13	◺	0·250	35
□	0·010	19	⬠	0·500	40
◇	0·025	25	▽	1·00	46
△	0·150	33			

Solid symbols for 8000 and 10,000 c/s.

For the very low velocities encountered near the wall there is a question as to how accurately a total-head probe can measure the pressure. Attempts to correct the readings using the correction curve given by Homann (1936) are shown on the mean velocity plots. Comparison of the indicated velocities obtained with a hot wire suggests that a very large error exists in the total-head-probe data near the wall at stations 3 and 4. The values obtained with the hot wire are plotted in figures 9(*b*) to (*d*) and were used in the calculation of wave-

number in the analysis. Actually, even the hot-wire measurements may indicate too great a velocity in the region near the wall, since molecular conduction between the wire and the wall causes an excess of heat transfer; however, for the 0·0002-inch-diameter wire this error is small.

The flow conditions are not exactly identical for each station. The complete set of mean velocity profiles and the hot-wire measurements for stations 1 and 4 were recorded during one tunnel run, while the hot-wire surveys at stations 2 and 3 were recorded during another run. A check between the hot-wire data for mean velocity and the total-pressure data at stations 2 and 3 shows a slight

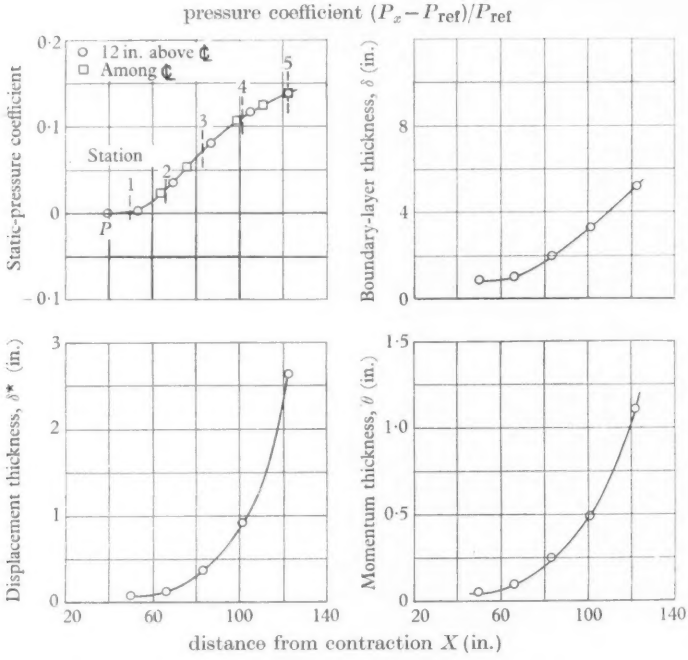

FIGURE 8. Parameters specifying boundary-layer flow.
(P_{ref} = 5·42 lb./sq.ft. below atmospheric.)

discrepancy (figures 9*b* and *c*). However, this variation of flow conditions was believed to be too small to affect the flatness-factor measurements. Since the two runs were made within the same 8-hour period, the temperature was nearly constant at 76° F. and the barometric pressure was 29·24 in. of mercury.

The measured values of flatness factor for stations 1 to 4 are plotted in figure 11. Except for the intermittency of the outer edge of the layer, the flatness factors at stations 1 to 3 (figures 11*a* to *c*) are apparently dependent only on wave-number, as found in the earlier preliminary measurements (figure 7). Station 4 (figures 11*d* and *e*), which is near separation, exhibits a very different distribution of flatness factor near the wall, although the outer region of the layer of station 4 again suggests a distribution of intermittency dependent only

on wave-number. (Note that the outer region of the layer is the region away from the wall where only the turbulent transport properties are important. The outer edge of the layer is the region where the flatness factor of the over-all turbulence signal becomes greater than 3. The two regions will overlap. The outer-edge intermittency will not be discussed in the present paper; however, some distributions of flatness factor with wave-number for the outer-edge region are noted by the dashed curves on the wave-number plots.)

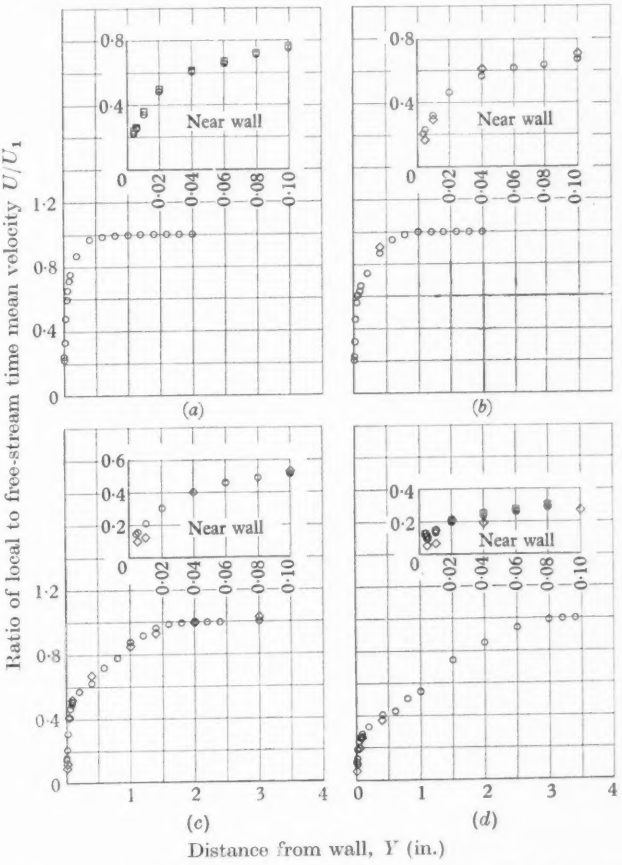

FIGURE 9. Mean velocity distributions. (*a*) Station 1, $U_1 = 32{\cdot}2$ ft./s. (*b*) Station 2, $U_1 = 30{\cdot}2$ ft./s. ○, actual measurement; □, corrected for probe Reynolds number effect; ◇, hot-wire measurement. (*c*) Station 3, $U_1 = 26{\cdot}6$ ft./s. (*d*) Station 4, $U_1 = 23{\cdot}3$ ft./s.

Before proceeding with a general discussion of the observations, a reservation is in order. The hot wire has a finite length (0·040 in.) and does not give a point measurement; therefore, the trace observed and analysed is an integral of the turbulence over the wire length. The turbulence must be a size such that only one burst can on the average strike the wire at a time. If two or more independent bursts can pass over the wire at nearly the same time they would tend

to decrease the apparent intermittency. The wire length should also be small compared to the wavelength of the particular frequency being observed if the burst is due to single eddies (or waves). The wire length (0·040 in.) corresponds to a wave-number of 1900 ft.$^{-1}$, which is near the point where most of the flatness factor measurements start to decrease. If, however, the bursts are composed of several eddies or oscillations (as might be implied from figure 5) then the wire length need only be small compared to the over-all size of the burst.

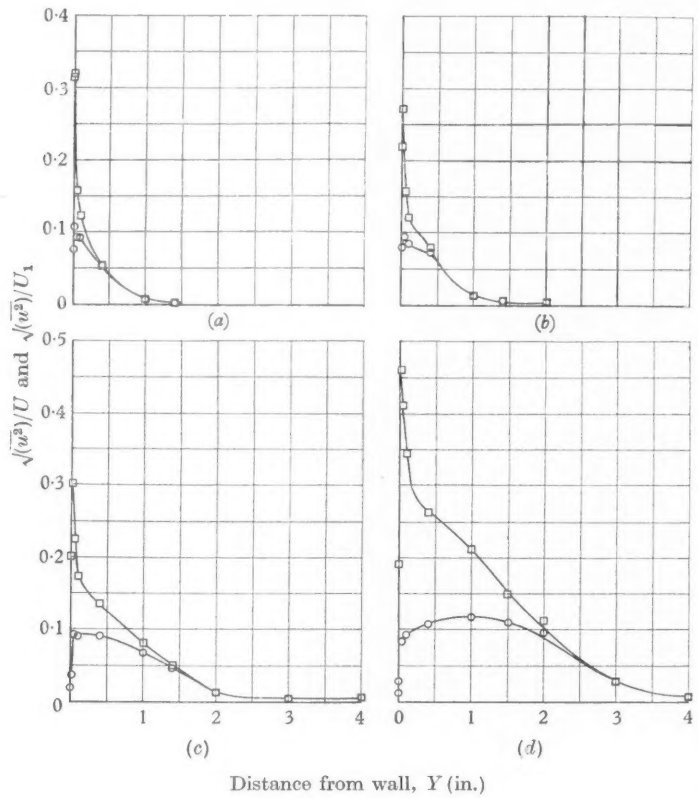

FIGURE 10. Turbulent velocity distributions. (*a*) Turbulent velocity, station 1. (*b*) Turbulent velocity, station 2: □, $\sqrt{(\overline{u^2})}/U_1$; ○, $\sqrt{(\overline{u^2})}/U$. (*c*) Turbulent velocity, station 3. (*d*) Turbulent velocity, station 4.

Discussion

An understanding of the present observations of the small-scale motion is far from complete. Little theoretical information is available for this high-wave-number region, even for isotropic turbulence. Batchelor devotes the last section of his monograph to a discussion of 'the small-scale properties of the motion'. His remarks concerning the small-scale motion will be utilized in discussing the results presented herein.

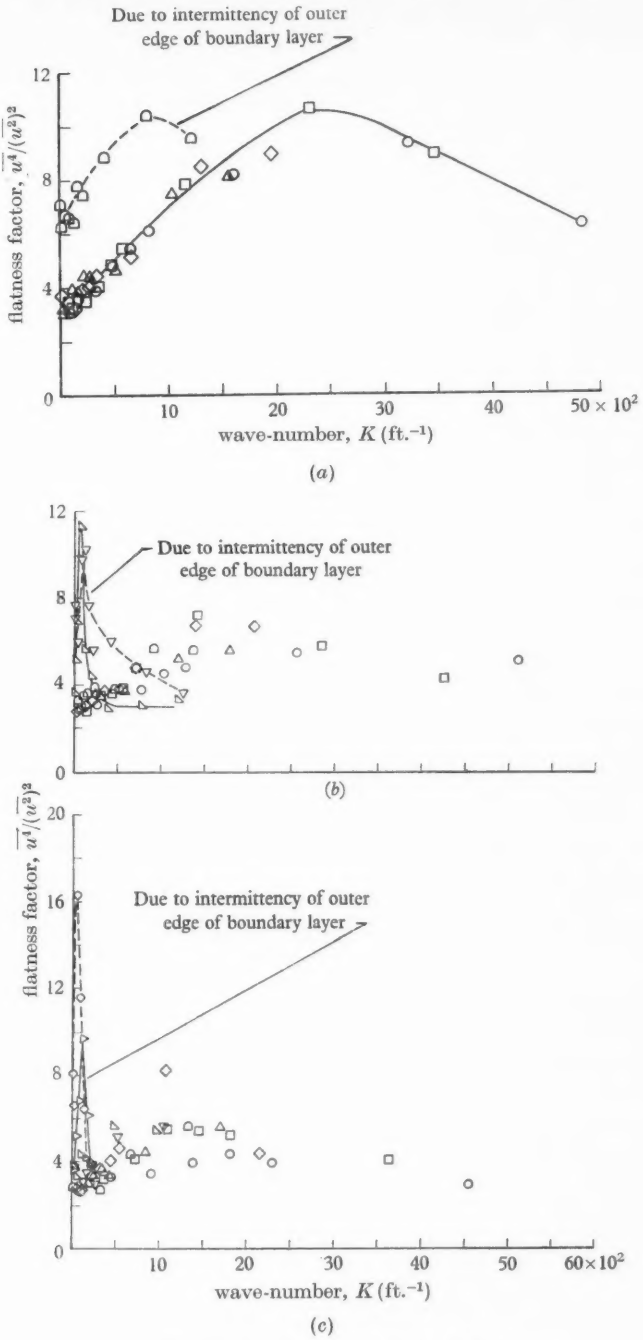
Due to intermittency of outer edge of boundary layer
flatness factor, $\overline{u^4}/(\overline{u^2})^2$
wave-number, K (ft.$^{-1}$)
(a)
Due to intermittency of outer edge of boundary layer
(b)
flatness factor, $\overline{u^3}/(\overline{u^2})^2$
Due to intermittency of outer edge of boundary layer
wave-number, K (ft.$^{-1}$)
(c)

FIGURE 11. For legend see p. 236.

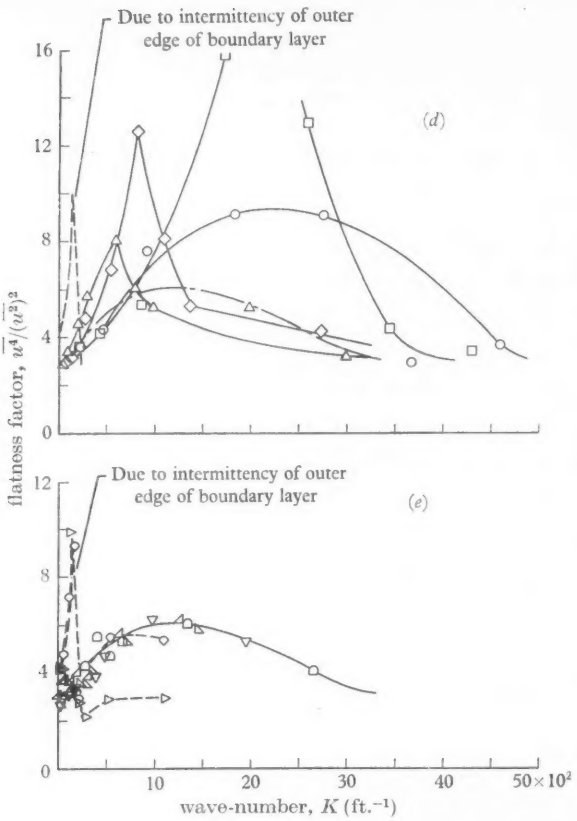

FIGURE 11. Flatness factor at various wave-numbers. (*a*) Station 1. *y*-distance (in.): ○, 0·005; □, 0·010; ◇, 0·040; △, 0·100; ▢, 0·400. (*b*) Station 2. (*c*) Station 3. *y*-distance (in.): ○, 0·005; □, 0·010; ◇, 0·040; △, 0·100; ▢, 0·400; ▽, 1·00; ◺, 1·40; ▷, 2·00; ♢, 4.00. (*d*) Station 4, very near wall. (*e*) Station 4, outer region of layer. *y*-distance (in.): ○, 0·005; □, 0·010; ◇, 0·40; △, 0·100; ▢, 0·400; ▽, 1·00; ◺, 1·50; ◿, 2·00; ♢, 3·00; ▷, 4·00.

It appears logical to assume that the present observations are directly related to the increase in flatness factor with successively higher velocity derivatives reported by Batchelor & Townsend (1949). However, since Batchelor & Townsend employed successively higher velocity derivatives to indicate the character of the turbulence at high frequencies, while the present measurements employ frequency bands, it is impractical to make a direct comparison of measurements. The orders of magnitude of the flatness factors reported by Batchelor and Townsend are the same as found for stations 2, 3, and the outer region of station 4 (figures 11*b*, *c* and *e*).

The uniformity of the intermittency with distance from the wall, observed at station 1 (figures 7 and 11*a*), appears to require that the intermittency has developed at some distance upstream. The high values of flatness factor observed at station 1, as compared with the values at stations 2 and 3, also indicate that

the intermittency may have started upstream of station 1 and is decreasing somewhat with flow distance. Since station 1 is only slightly downstream of the region of transition from laminar to turbulent flow, it is to be expected that this intermittency must originate within the transition region; but the mechanism is not understood. Bursts or intermittency in the over-all hot-wire signals have been observed in the transition region by Schubauer & Klebanoff (1956), but no information is available on the intermittency at high frequencies in this region. Since it is still not clear what causes the transition bursts to appear in the laminar flow, there is no clear picture of the chain of events that will lead to the observed intermittency at high frequency.

There is limited evidence, both theoretically and experimentally, to suggest how intermittency may arise. The general ideas of the effects of inertia forces would seem to suggest that intermittency is possible. Batchelor (1953, p. 186) cites several examples to show that the non-linear inertia forces give rise to regions of strong isolated vortices; and, since it is also known that turbulent energy is transported from one part of wave-number space to another by inertia forces (Batchelor, 1953, p. 84), it is not hard to see that regions of intermittency might exist. Further measurements must be made in the transition region before it is possible to trace the exact development of the intermittency.

Stations 2 and 3, as well as the outer region of station 4 (figures 11*b*, *c* and *e*), suggest a somewhat constant value of flatness factor with wave-number. The decrease in magnitude of the flatness factors over that of station 1 indicates a trend toward homogeneity. It has been suggested that the tendency to homogeneity with motion downstream is due partly to the shearing action in the boundary layer drawing out turbulent spots. Since the magnitudes of flatness factor are similar to those reported by Batchelor & Townsend (1949) one may suggest that the turbulence for stations 2, 3 and outer 4 is quite similar to the free turbulence flow. There is, of course, the possibility that the scale size of the turbulence is decreasing; thus, the finite wire length would make it appear that the flatness factor has decreased at these stations. While the increase in flatness factor at low wave-numbers is similar for all stations, the peaks in the curves appear to be reached at a lower wave-number the farther downstream the station is located. There is always a question in regard to what the peak and downward slope in these curves of flatness factor mean. It is possible that the electronic noise of the instrument, which will have a flatness factor near 3, may actually be causing the decrease. Again, how accurately the instruments can be read when the signal becomes very intermittent may also influence the measured values of intermittency.

Near the wall at station 4 a completely different type of intermittency is apparently encountered (figure 11*d*). While there is some question as to the accuracy of determining the mean velocity near the wall, it does not appear that the wave-numbers could ever be corrected in a consistent way to give one curve. These distributions suggest a production of intermittency is in progress. This flow at station 4 is near separation; however, there is reason to believe that the profile is not in the separation region as yet ($\delta^*/\theta < 2$). Visual observations of oscillograph traces downstream of station 4 in the separation region suggest

very much the same patterns as seen at station 4, except that the frequencies are lower and the over-all signal has an intermittency also.

Several observations from the present set of data can be qualitatively related to flow observations made in a water table by Kline (1957). Water-table observations, explored with dyes, show that the turbulent boundary layer separates first in a highly irregular, intermittent manner. The outbreak of bursts such as shown in figure 11 (*d*) is certainly suggestive of an approach to an intermittent separation. Injection of smoke into the present boundary layer near separation also suggests that an intermittent separation is occurring downstream of station 4.

In a very recent water-channel study, Kline & Runstadler (1958) were able to observe the flow visually in the region of the boundary layer very near the wall. By injecting dye into the layer very near the wall, they observed 'islands of hesitation' very near the wall at all locations in the boundary layer from transition to separation. The islands appear as stretched filaments of dye in the direction of flow, which move downstream slower than the surrounding fluid. With each island a longitudinal vortex appears to be generated. (There is a striking similarity between the observations in the water channel and the rather idealized model of an unstable viscous sublayer proposed sometime ago by Einstein & Li (1955). This instability near the wall is of interest here in that it suggests a possible source of the high-frequency intermittency.) The present data have been examined for evidence of such islands. However, Kline has pointed out that the islands are very small and may be obscured by the hot-wire length.

If these islands exist near the wall it was thought that their presence might be indicated by bursts in the over-all (all frequencies) hot-wire signal. However, only at station 4 was there evidence of a rise in the value of flatness factor (of the over-all signal measured from the magnetic tape) in the region where the islands might be expected. The over-all flatness factor for station 4 is shown in figure 12. The points at the outer intermittent edge of the layer are not faired in, since the data are too meagre to define the curve. (The higher values of flatness factor appearing in the over-all signal at $y = 0{\cdot}005$ and $0{\cdot}010$ in. on figure 12 correspond to the y values of the circles and squares on figure 11 (*d*).) For the other stations (1, 2 and 3), although not shown, the measurements suggest, if anything, a trend toward a periodic signal, since the flatness factors are less than 3 (for a sine wave $\overline{u^4}/(\overline{u^2})^2 = 1{\cdot}5$, for a triangular wave $\overline{u^4}/(\overline{u^2})^2 = 1{\cdot}8$). Thus, from the intermittency measurements, any indication of islands near the wall is limited to the region approaching separation.

A second observation appears to have some connexion with the concept of islands of hesitation. The over-all signals being monitored on an oscillograph indicated a rather pronounced trend toward skewness at the wall as the flow continued toward separation. A rough idea of this skewness can be obtained by considering the pen recorder traces for $y = 0{\cdot}005$ at station 4 shown in figure 13, where the skewness is associated with the large-amplitude sharp peaks in one direction on the trace and the low-amplitude broad peaks in the other direction. (Unfortunately, the loss of low-frequency response for the tape recorder depresses the skewness, so the pen recorder gives a somewhat more graphic

picture in this case.) The suggestion of a predominant direction for the fluctuation would be compatible with the idea of islands of hesitation. It will, of course, be of value to pursue the study of this skewness further.

While the observations made in a water table may suggest possible ways in which the high frequencies become intermittent, it is evident that a direct chain of events is yet to be defined. There is a suggestion from the data that the intermittency phenomenon is associated with transition and separation rather than

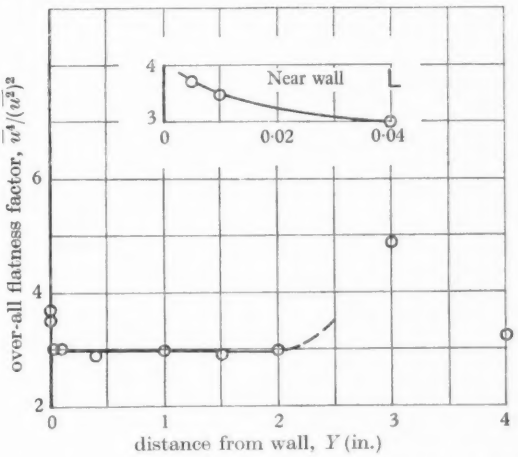

FIGURE 12. Flatness factor distribution for over-all signal at station 4.

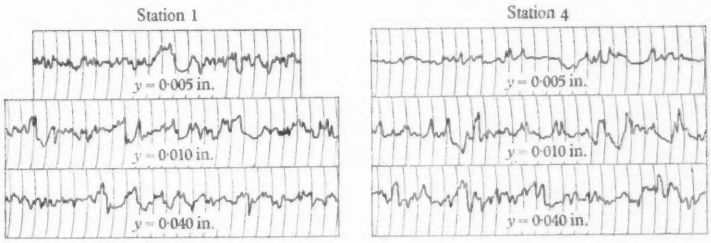

FIGURE 13. Low-frequency part of over-all turbulent fluctuations.

with the turbulent layer far from either region. The intermittency at stations 2 and 3 appears to be more a consequence of something that has happened upstream rather than something developing at the particular point of measurement. Thus, one may conclude that if islands exist at stations 2 and 3 they are too small to affect the observations.

The present measurements are still somewhat crude, partly because of a lack of appreciation of the mechanism causing the intermittency. The data would appear in fact to add another complication, that of spatial inhomogeneity, to an already too complex problem. There are, however, some rather encouraging results to be found in the data. In particular, the existence of a fairly uniform flatness factor with wave-number independent of distance from the wall indicates

the extent to which the turbulence is mixed throughout the boundary layer. This assumes that the bursts are generated locally and not at all y-distances in the boundary layer. The uniformity further suggests that the effects of the inertia terms, which will vary in the boundary layer, on the bursts are not pronounced.

It was first suspected that intermittent separation could be traced directly to the intermittency observed after transition; however, the measurements at station 4 suggest that a second mechanism enters as separation is approached. The second mechanism could well be the islands of hesitation suggested from Kline's observations.

REFERENCES

Batchelor, G. K. 1953 *The Theory of Homogeneous Turbulence.* Cambridge University Press.

Batchelor, G. K. & Townsend, A. A. 1949 The nature of turbulent motion at large wave-numbers. *Proc. Roy. Soc.* A, **199**, 238.

Einstein, H. A. & Li, H. 1955 Shear transmission from a turbulent flow to its viscous boundary sub-layer, ch. xiii. *Heat Transfer and Fluid Mech. Inst.*

Hama, F. R., Long, J. D. & Hegarty, J. C. 1956 On transition from laminar to turbulent flow. *Tech. Note BN*-81, *TN*-56-381. Inst. Fluid Dynamics and Appl. Math., Univ. Maryland. (Contract *AF*-18(600)-1014.)

Homann, F. 1936 Einfluss grosser Zähigkeit bei Strömung um Zylinder. *Forsch. IngWes.*, Bd. 7, Heft 1.

Klebanoff, P. S. 1955 Characteristics of turbulence in a boundary layer with zero pressure gradient. *NACA Rep.* 1247 (supersedes *NACA TN* 3178).

Kline, S. J. 1957 Some new conceptions on the mechanism of stall in turbulent boundary layers. *J. Aero. Sci.* **24**, no. 6.

Kline, S. J. & Runstadler, P. W. 1958 Some preliminary results of visual studies on the flow model of the wall layers of the turbulent boundary layer. *Rep. MD*-3 Dep. Mech. Eng., Standford Univ. (Contract *AF* 49(638)-295.)

Laurence, J. C. & Landes, L. G. 1952 Auxiliary equipment and techniques for adapting the constant-temperature hot-wire anemometer to specific problems in air-flow measurements. *NACA TN* 2843.

Sandborn, V. A. 1953 Preliminary experimental investigation of low-speed turbulent boundary layers in adverse pressure gradients. *NACA TN* 3031.

Sandborn, V. A. 1955 Experimental evaluation of momentum terms in turbulent pipe flow. *NACA TN* 3266.

Sandborn, V. A. & Slogar, R. J. 1955*a* Study of the momentum distribution of turbulent boundary layers in adverse pressure gradients. *NACA TN* 3264.

Sandborn, V. A. & Slogar, R. J. 1955*b* Longitudinal turbulent spectrum survey of boundary layers in adverse pressure gradients. *NACA TN* 3453.

Sandborn, V. A. & Braun, W. H. 1956 Turbulent shear spectra and local isotropy in the low-speed boundary layer. *NACA TN* 3761.

Schubauer, G. B. & Klebanoff, P. S. 1956 Contributions on the mechanics of boundary-layer transition. *NACA Rep.* 1289 (supersedes *NACA TN* 3489).

Townsend, A. A. 1947 The measurement of double and triple correlation derivatives in isotropic turbulence. *Proc. Camb. Phil. Soc.* **43**, 560.

Townsend, A. A. 1948 Local isotropy in the turbulent wake of a cylinder. *Austr. J. Sci. Res.* **1**, 161.

Townsend, A. A. 1956 *The Structure of Turbulent Shear Flow.* Cambridge University Press.

Weske, J. R. 1957 Experimental study of detail phenomena of transition in boundary layers. *Tech. Note BN*-91, *TN*-57-62. Inst. Fluid Dynamics and Appl. Math., Univ. Maryland (Contract *AF*-18(600)-893).

An analysis of the vortex street generated in a viscous fluid

By JOHN W. SCHAEFER* AND SALAMON ESKINAZI
Syracuse University, Syracuse, New York

(Received 26 December 1958)

An analytic solution for the velocity field of a vortex street generated in a viscous fluid is developed. A method is presented for the determination of the true transverse spacing of vortices. Experimental geometry and velocity data, obtained by hot-wire techniques, are presented.

The experimental results verified the validity of the analytic solution. The vortices of a real viscous vortex street were found to resemble very closely the exponential solution of the Navier–Stokes equations for an isolated axisymmetric rectilinear vortex. Three basic regions of vortex street behaviour were apparent at each Reynolds number investigated—a 'formation region' in which the vortex street is developed and large dissipation of vorticity occurs, a 'stable region' in which the vortices display a stable periodic laminar regularity, and an 'unstable region' in which the street disappears and turbulence develops. Geometry and velocities were determined.

1. Introduction

The periodicity in wakes in the form of discrete vortices at an intermediate range of Reynolds number ($R = U_0 d/\nu$, where U_0 is the free-stream velocity, d the cylinder diameter and ν kinematic viscosity) has been recognized for many years. In the lower portion of this range, $40 < R < 125$, there exists an ordered and stable wake—a vortex system commonly referred to as the Kármán vortex street.

Academic and practical interest in the vortex street phenomenon has resulted in many theoretical and experimental investigations of the vortex system generated behind a two-dimensional bluff obstacle. This available literature concerning viscous vortex streets may best be summarized as descriptive but incomplete analytically. As pointed out by Rosenhead (1953), a quantitative theoretical treatment which will consolidate the facts already available is needed.

The purpose of this investigation is the development of an analytic solution for the velocity field of a viscous vortex street and the accurate determination of street geometry. An experimental analysis was performed to support and verify the analytic results.

Most of the experimental results on this subject were obtained through photographs of the streak-lines developed by colour dyes or suspensions in the fluid.

* Now at Lewis Research Center, National Aeronautics and Space Administration, Cleveland, Ohio.

In most instances careful precautions were taken to photograph a steady flow by moving the camera with the fluid. Since vortices move at a relative velocity to the free stream, the apparent centres of the vortices as observed in the photograph are then centres of zero relative velocity and not the centres of maximum vorticity. Hooker (1936) used this argument to show the reasons for great discrepancies in the measurements of street geometry. Tyler (1930) applied the hot-wire technique for measurements of velocity in the Kármán street. Since then this technique has become very productive for measurements of velocity and geometry of the vortex street. The results presented here have been obtained with the hot-wire technique.

2. Analytic considerations

The solution of the Navier–Stokes equations for a viscous vortex system is not available in its general form. It is the interest of this investigation to rely on a mathematical description of a viscous vortex street based on linearizing methods which allow superposition of solutions. The basic solution of the Navier–Stokes equations for an isolated rectilinear viscous vortex growing in time due to viscosity will be considered as the elemental vortex in the superposition method.

The isolated viscous vortex

The Navier–Stokes equations in vorticity form for a two-dimensional flow field in the (x, y)-plane is

$$\frac{D\zeta}{Dt} = \nu\left(\frac{\partial^2\zeta}{\partial x^2} + \frac{\partial^2\zeta}{\partial y^2}\right), \tag{1}$$

where ζ is the vorticity and ν is the kinematic viscosity. In the case of isolated rectilinear vortices, equation (1) reduces to

$$\frac{\partial\zeta}{\partial t} = \nu\left(\frac{\partial^2\zeta}{\partial r^2} + \frac{1}{r}\frac{\partial\zeta}{\partial r}\right), \tag{2}$$

where r is the radial distance from the axis of rotation. Therefore, for an isolated rectilinear vortex initially of strength $\Gamma_0/2\pi$ concentrated along the axis of rotation, the vorticity at a time t and any position r is given by

$$\zeta = \frac{\Gamma_0}{4\pi\nu t}\exp\left(-\frac{r^2}{4\nu t}\right). \tag{3}$$

The circulation around a circle of radius r is

$$\Gamma = \int_0^{2\pi} v_\theta r\, d\theta = \int_0^{2\pi}\int_0^r \zeta r\, d\theta\, dr = \Gamma_0\left[1 - \exp\left(-\frac{r^2}{4\nu t}\right)\right], \tag{4}$$

where θ is the polar angle; and therefore the circumferential velocity of the vortex is

$$v_\theta = \frac{\Gamma}{2\pi r} = \frac{\Gamma_0}{2\pi r}\left[1 - \exp\left(-\frac{r^2}{4\nu t}\right)\right]. \tag{5}$$

For vanishing viscosity and time, or for large r, the solution reduces to that for a potential vortex. Equation (5) is plotted in figure 2.

The potential vortex street

The co-ordinates appropriate to the following theory, as shown in figure 1, are explained below. The co-ordinate x is the distance downstream from the tripping cylinder to the point in the flow field $P(x, y)$ under study. The co-ordinate s is the distance in the x-direction from the nearest vortex to the left of P to the

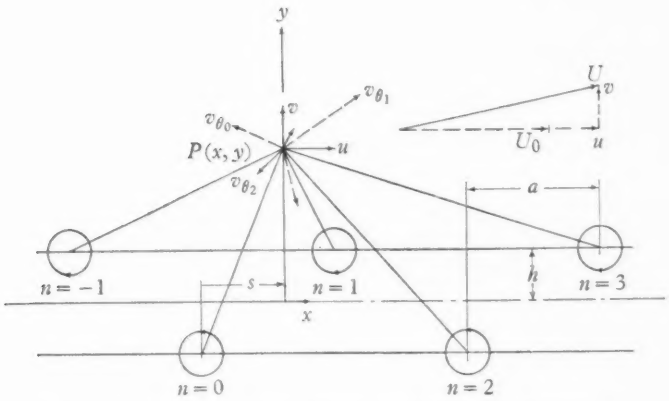

FIGURE 1. Idealized vortex street; geometry and co-ordinates.

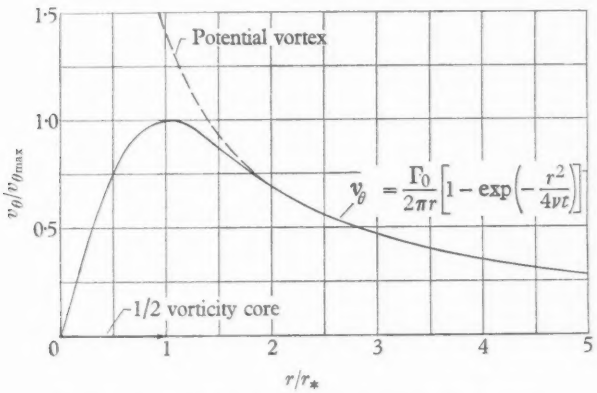

FIGURE 2. Peripheral velocity of an isolated vortex.

point P. This vortex, to the left of P, is considered the reference vortex $n = 0$. The indice n represents any other vortex a distance na in the x-direction away from the reference vortex. Negative n indicates a vortex to the left of P; positive n to the right of P. Therefore, the term $(x - s + na)$ is the distance from the tripping cylinder to any vortex. Similarly, $(x - s + na)/2af$ is the time in the life of any vortex from its generation at the tripping cylinder, f being the frequency of vortex shedding. The equations developed below are therefore valid for $-\infty < y < \infty$ and for half a cycle, i.e. $0 < s < a$.

In this co-ordinate representation, the velocity components for an idealized potential Kármán street of an infinite extent are given by the following summations:

$$\left.\begin{aligned} u &= \frac{\Gamma}{2\pi}\sum_{\pm n=0}^{\infty}(-1)^{|n|}\frac{y-(-1)^{|n|}h}{[|n|\,a\mp s]^2+[y-(-1)^{|n|}h]^2}, \\ v &= \frac{\Gamma}{2\pi}\sum_{\pm n=0}^{\infty}\pm(-1)^{|n|}\frac{|n|\,a\mp s}{[|n|\,a\mp s]^2+[y-(-1)^{|n|}h]^2}. \end{aligned}\right\} \tag{6}$$

Here h is the transverse distance from the street centreline to the path of the vortex centres. Each term in the summation is of the type

$$u=\frac{\Gamma}{2\pi}\frac{y'}{r^2} \quad \text{and} \quad v=\frac{\Gamma}{2\pi}\frac{x'}{r^2},$$

where x', y' and r are co-ordinates from the axis of an isolated vortex. Equations (6) may be altered to represent the solution for a finite, variable-geometry vortex street. This is accomplished by limiting the number of terms of the summation and replacing h and a by h_n and a_n where h_n and a_n are functions of the vortex position.

The viscous vortex street

Hooker (1936) presented an analysis in which only the vortex nearest the point of interest was considered viscous. Since the peripheral velocity outside the vorticity core varies as $1/r$, a viscous vortex behaves essentially as a potential vortex outside the core. Therefore, vortices far from the point of interest may be considered as potential vortices. This method, therefore, suggests essentially a potential street of vortices with a single viscous vortex described by equation (5) replacing the potential vortex nearest the point of interest.

A more general solution for a finite, viscous, variable-geometry vortex street was developed from equations (6). After incorporating the decay term of each vortex as given by equation (5) and the variable geometry h_n (a is a constant with distance downstream at a given Reynolds number as determined experimentally) the velocity components are

$$\left.\begin{aligned} u &= \frac{\Gamma_0}{2\pi}\sum_{\pm n=0}^{k}\left[\left\{(-1)^{|n|}\frac{y-(-1)^{|n|}h_n}{[|n|\,a\mp s]^2+[y-(-1)^{|n|}h_n]^2}\right\}\right. \\ &\qquad \left.\times\left\{1-\exp\left(-\frac{[|n|\,a\mp s]^2+[y-(-1)^{|n|}h_n]^2}{4\nu[(x-s+na)/2af]}\right)\right\}\right], \\ v &= \frac{\Gamma_0}{2\pi}\sum_{\pm n=0}^{k}\left[\left\{\pm(-1)^{|n|}\frac{|n|\,a\mp s}{[|n|\,a\mp s]^2+[y-(-1)^{|n|}h_n]^2}\right\}\right. \\ &\qquad \left.\times\left\{1-\exp\left(-\frac{[|n|\,a\mp s]^2+[y-(-1)^{|n|}h_n]^2}{4\nu[(x-s+na)/2af]}\right)\right\}\right]. \end{aligned}\right\} \tag{7}$$

For a finite street, the limit of summation k is not necessarily the same for positive and negative n.

Equations (7) reduce to Hooker's solution if $k=\infty$, $h_n=$ const., and $n=0$ in the decay term only.

Because of an absence of *a priori* knowledge of Γ_0, equations (7) are more useful in the following dimensionless form, for which the diameter d of the tripping cylinder is used as reference length:

$$\left.\begin{aligned} q_x &= \sum_{\pm n=0}^{k}\left[\left\{(-1)^{|n|}\frac{\dfrac{y}{d}-(-1)^{|n|}\dfrac{h_n}{d}}{\left[|n|\dfrac{a}{d}\mp\dfrac{s}{d}\right]^2+\left[\dfrac{y}{d}-(-1)^{|n|}\dfrac{h_n}{d}\right]^2}\right\}\times\left\{1-\exp\left(-\frac{\left[|n|\dfrac{a}{d}\mp\dfrac{s}{d}\right]^2+\left[\dfrac{y}{d}-(-1)^{|n|}\dfrac{h_n}{d}\right]^2}{4\nu\left[\dfrac{(x-s+na)/d}{2(a/d)fd^2}\right]}\right)\right\}\right], \\ q_y &= \sum_{\pm n=0}^{k}\left[\left\{\pm(-1)^{|n|}\frac{|n|\dfrac{a}{d}\mp\dfrac{s}{d}}{\left[|n|\dfrac{a}{d}\mp\dfrac{s}{d}\right]^2+\left[\dfrac{y}{d}-(-1)^{|n|}\dfrac{h_n}{d}\right]^2}\right\}\times\left\{1-\exp\left(-\frac{\left[|n|\dfrac{a}{d}\mp\dfrac{s}{d}\right]^2+\left[\dfrac{y}{d}-(-1)^{|n|}\dfrac{h_n}{d}\right]^2}{4\nu\left[\dfrac{(x-s+na)/d}{2(a/d)fd^2}\right]}\right)\right\}\right], \end{aligned}\right\} \tag{8}$$

where $q_x = 2\pi u d/\Gamma_0$ and $q_y = 2\pi v d/\Gamma_0$.

This viscous vortex street solution was obtained from the superposition of the solutions of equation (2) for the velocity distribution of isolated axisymmetric viscous vortices. The correlation of analytic and experimental results indicates that equation (5) represents very closely the peripheral velocity of a vortex in a viscous vortex street. This fact justifies the assumed axial symmetry of the vortices. The results of Timme (1957) also substantiate this conclusion. Therefore, superposition affords a very close approximation of the actual flow conditions of a viscous vortex street. At downstream positions very close to the generating cylinder, the results of this theory are in relatively poorer agreement with the actual conditions because of the immediate proximity of the cylinder and because of the rolling-up process of the vortex sheet into fully-developed vortices.

The method of analysis is represented in figures 1 and 3.

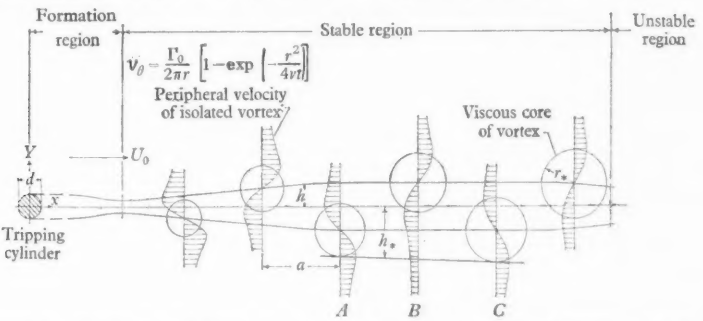

FIGURE 3. Vortex street configuration at $R = 62$, velocity and geometry to scale.

3. Method of evaluation of the velocity field

The determination of the vortex street velocities, as given by equations (8), requires an accurate knowledge of the basic geometric parameters including the extent of the street. These parameters have been determined experimentally and analytically.

The longitudinal spacing was determined experimentally, as will be described in § 4. In the fully developed stable vortex street, this spacing was found to be constant with x for a given Reynolds number. The periodicity was determined from the velocity fluctuation oscillogram and was also found to be constant with x for the fully developed street at a given Reynolds number. The initial time in the life of a vortex was assumed to be at $x = 0$, the axis of the tripping cylinder. Therefore, as indicated in the velocity equations, the life of the vortex n is $t = (x - s + na)/2af$.

In a viscous vortex, the vorticity is concentrated in a finite circular core which grows with time according to equation (3). The outer boundary of the core is defined as $r = r_*$, this value of r being where the velocity is a maximum as shown in figure 2. This value as determined by differentiation of equation (5) is given by

$$\frac{r_*^2}{4\nu t} = 1{\cdot}26.$$

The dimensionless core radius r_*/d, which grows with time, is given by

$$\frac{r_*}{d} = \sqrt{\left(5{\cdot}04\frac{\nu t}{d^2}\right)}. \tag{9}$$

A preliminary analysis indicated that the maximum velocity fluctuation does not occur along the path of vortex centres as some experimenters have asserted. An analysis based on the configuration of a general vortex street, as in figure 3, demonstrated that the maximum velocity fluctuation occurs in the immediate neighbourhood of the core edge farthest from the street centreline. As shown in figure 3, let h_* be that distance from the street centreline, and let us visualize a hot wire at some point along the path of h_*. When vortices A and C pass the hot-wire location, they will induce their maximum peripheral velocity on the hot wire. However, when vortex B is directly above the hot wire, it will induce a weaker velocity in the opposite direction. By varying the position of the hot wire from h_* to any y, it can be observed from figure 3 that the magnitude of fluctuation within a cycle will decrease when the hot wire is moved in either direction. Then the y-location of the maximum induced velocity variation is in the neighbourhood of h_*. This fact was verified in the analysis. The position of maximum fluctuating velocity is easily determined experimentally, and since it occurs very near the outer edge of the vortex core, the dimensionless path of vortex centres h/d is therefore given by

$$\frac{h}{d} = \frac{h_*}{d} - \frac{r_*}{d}. \tag{10}$$

The value of the viscosity required for the determination of r_*/d, in equation (9), was taken as the molecular viscosity since the wake may be described as in

a state of laminar oscillation. Also Timme (1957) has shown that in the Reynolds number range for which a stable vortex street exists, the molecular viscosity determines the decay process.

Upon determination of the geometry, time and extent of the vortex street, the numerical solution for the velocity field relative to the free-stream velocity was determined from equations (7) and (8). Since the initial circulation Γ_0 is an unknown parameter, the velocity field was computed in terms of the dimensionless velocity q_x and q_y. The solutions describe the dimensionless velocity

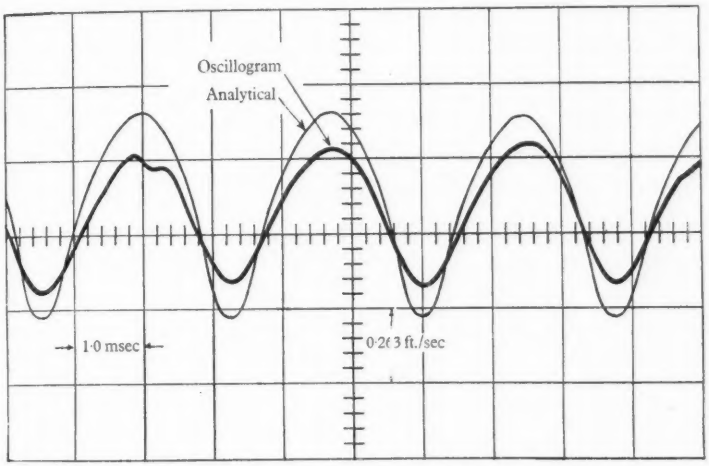

FIGURE 4. Velocity fluctuation at $R = 62$, $x/d = 10$, $y/d = 0$.

distribution of a vortex street generated behind a cylinder moving with a velocity of Q_0 in a still fluid. If a dimensionless free-stream velocity of Q_0 is superposed on the above solutions, the flow of a fluid about a stationary cylinder is achieved. Therefore, the dimensionless total velocity vector is

$$\mathbf{Q} = \mathbf{Q}_0 + \mathbf{q}, \tag{11}$$

where $\mathbf{q} = \mathbf{i}q_x + \mathbf{j}q_y$ and $\mathbf{Q}_0 = 2\pi\mathbf{i}U_0 d/\Gamma_0$. Since Γ_0 is unknown, the analytic solution was matched to the experimental results at a point in the flow field in order to determine Q_0. The match point was taken at $x/d = 10$, $y/d = 0$ for a Reynolds number of 62, the only Reynolds number at which the analysis was performed. The dimensionless free-stream velocity was determined by satisfying the relation $Q_T/Q_0 = U_T/U_0$ at the match point (Q_T and U_T denote time averages of Q and U). The time average of $\mathbf{q}$ from equation (11) was also matched at that point using (8). Q_0 was determined from the known terms Q_T/Q_0 and $Q_T - Q_0$.

At any desired point in the flow field $P(x, y)$, the velocity was determined from equation (11) by substitution of the results of equations (8) for varying s and the determined value of Q_0. A plot of the velocity over a cycle gave Q_T at the point, and also the root-mean-square value $\tilde{q}'_T$ and peak-to-peak value $\hat{q}'_T$ of the fluctuating component of velocity q'. A comparison of analytic and experimental results is presented in figures 4 to 12 and table 1.

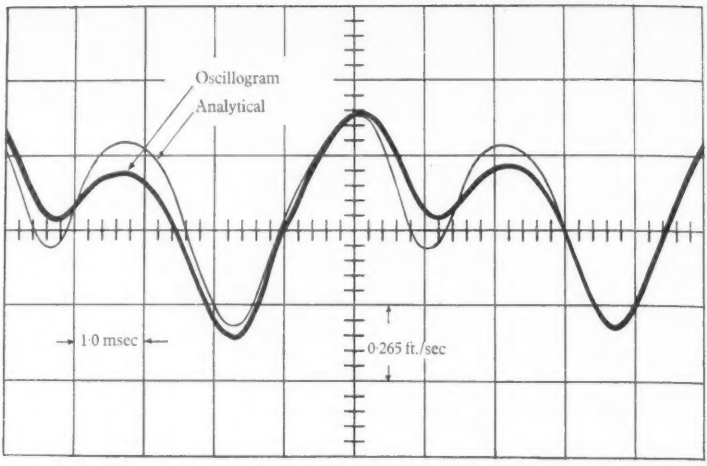

FIGURE 5. Velocity fluctuation at $R = 62$, $x/d = 10$, $y/d = 0{\cdot}429$.

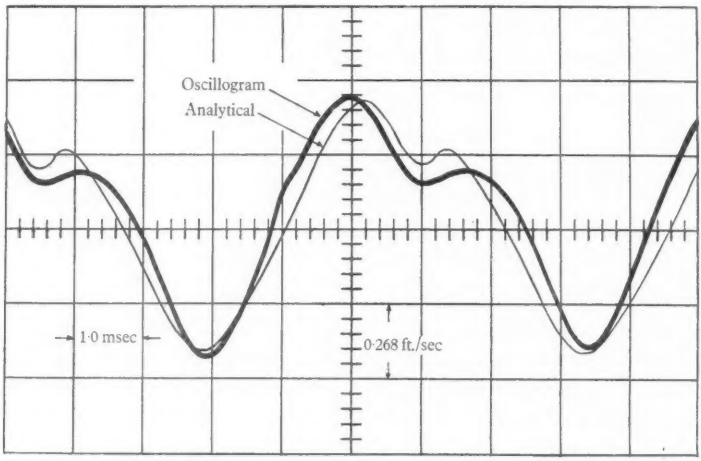

FIGURE 6. Velocity fluctuation at $R = 62$, $x/d = 10$, $y/d = 0{\cdot}857$.

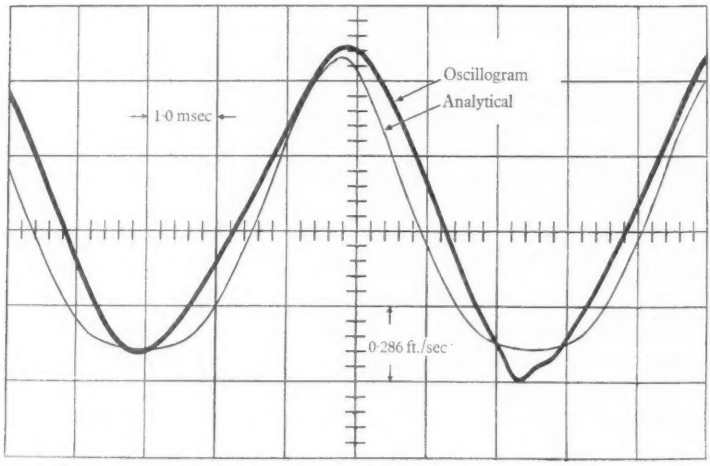

FIGURE 7. Velocity fluctuation at $R = 62$, $x/d = 10$, $y/d \doteq 1{\cdot}714$.

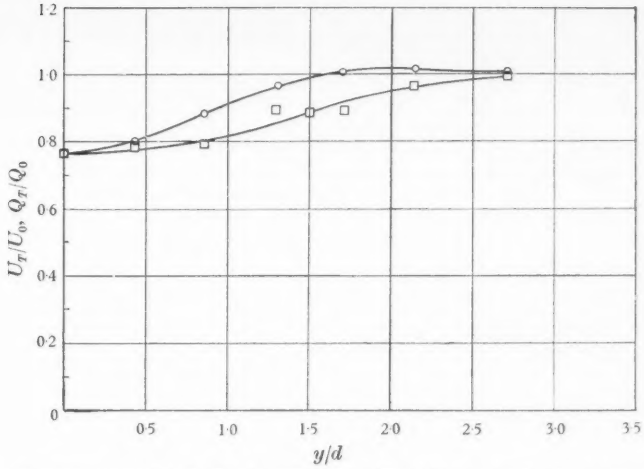

FIGURE 8. Time average total velocity, $R = 62$, $x/d = 10$. ○, Analytic; □, experimental.

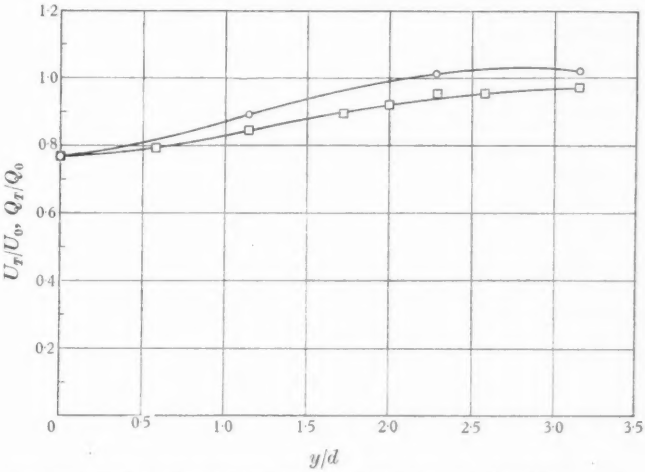

FIGURE 9. Time average total velocity, $R = 62$, $x/d = 20$. ○, Analytic; □, experimental.

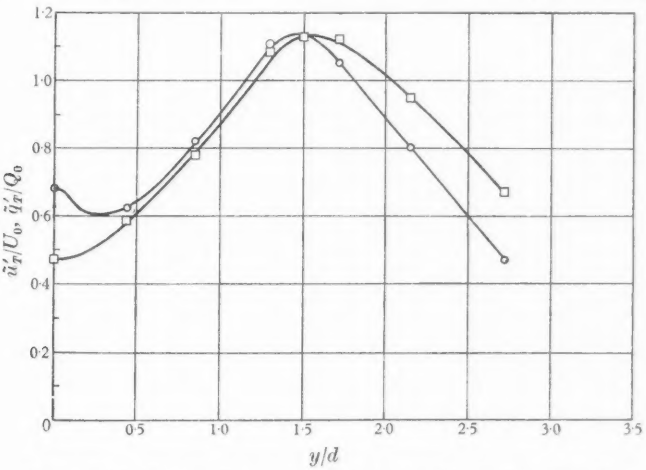

FIGURE 10. Root-mean-square of velocity fluctuation, $R = 62$, $x/d = 10$. ○, Analytic; □, experimental.

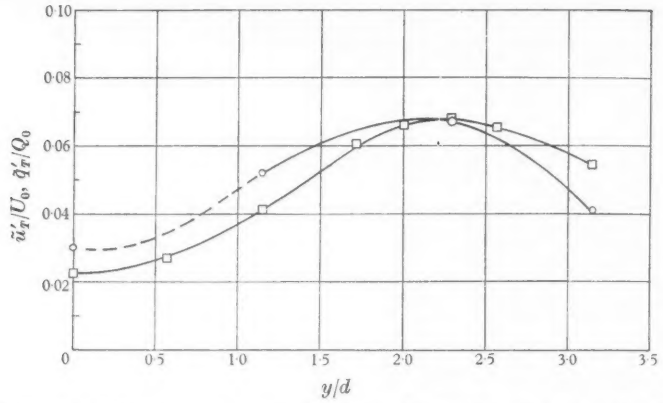

FIGURE 11. Root-mean-square of velocity fluctuation, $R = 62$, $x/d = 20$. ○, Analytic; □, experimental.

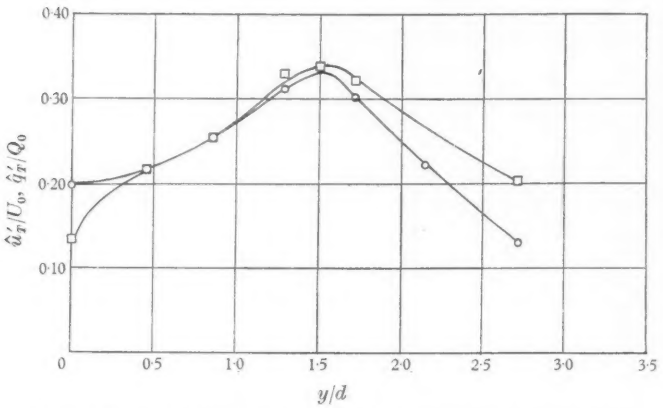

FIGURE 12. Peak-to-peak velocity fluctuation, $R = 62$, $x/d = 10$. ○, Analytic; □, experimental.

x/d	y/d	U_T/U_0	Q_T/Q_0	$\tilde{u}'_T/U_0$	$\tilde{q}'_T/Q_0$	$\hat{u}'_T/U_0$	$\hat{q}'_T/Q_0$
10	0	0·762	0·762	0·047	0·068	0·132	0·198
	0·429	0·782	0·799	0·059	0·062	0·216	0·216
	0·857	0·793	0·886	0·078	0·082	0·253	0·254
	1·286	0·892	0·968	0·109	0·110	0·331	0·312
	1·714	0·892	1·006	0·112	0·105	0·323	0·302
	2·143	0·964	1·018	0·095	0·080	0·279	0·222
	2·714	0·997	1·014	0·067	0·047	0·202	0·130
20	0	0·760	0·772	0·022	0·030	—	—
	1·143	0·843	0·891	0·041	0·052	—	—
	2·286	0·951	1·010	0·068	0·067	—	—
	3·143	0·971	1·021	0·054	0·041	—	—

TABLE 1. Comparison of analytic and experimental velocities, $R = 62$

4. Experimental procedures

A hot-wire anemometer was used for all velocity and geometry measurements because of its high sensitivity, reliability and its convenience in determining the desired results. The constant-current hot-wire set, built at Syracuse University, was similar to the set used by Eskinazi & Yeh (1956).

The vortex street system was generated in a circular low-turbulence wind tunnel of diameter 18 in. with a continuously variable flow velocity from 0 to 20 ft./sec. A tripping cylinder of circular cross-section generated the vortex street. The cylinder was mounted in a traversing mechanism for variation of longitudinal distance from the hot wire. The cylinders used were 0·035 and 0·080 in. piano wire; all data presented here were obtained with the 0·035 in. diameter tripping cylinder.

Vortices are shed from a tripping cylinder at a definite shedding frequency depending on Reynolds number; this frequency is preserved throughout the stable region of a street. Therefore, the cyclic variation of velocity at a fixed point is very stable and consistent for moderate Reynolds numbers. The hot wire, positioned at a fixed point $P(x, y)$, recorded the cyclic variation in time or s. The hot wire was positioned parallel to the axis of rotation of the vortices; therefore, the velocity vector was at all times on a plane perpendicular to the axis of the hot wire. The hot wire therefore responded to the total velocity vector.

The mean voltage across the hot wire determined the temporal mean velocity. The cyclic voltage fluctuation from the hot wire was compensated for the heat capacity lag. The magnitude and wave forms of the velocity fluctuations were determined respectively from a root-mean-square voltmeter and a dual channel oscilloscope. Since the street periodicity was never in excess of 800 c/s, an electrical filter with flat response to 1000 c/s was used to eliminate amplifier noise in the measured signals.

The spacing h_* was determined from the plots of the root-mean-square fluctuating velocity (a plot of peak-to-peak fluctuating velocity yields the same h_*). The spacing h_* is essential in determining the path of vortex centres as outlined previously. This spacing should not be confused with h, the transverse spacing of the path of vortex centres.

The longitudinal spacing a was determined with a special hot-wire system. Two hot wires were fixed at a known longitudinal distance apart. The longitudinal spacing was computed from the phase angle between the two fluctuating hot-wire signals and the known distance between the hot wires.

The hot-wire material was tungsten of 0·00015 in. diameter. The central sensing portion was of approximately $\frac{1}{16}$ in. length; the ends were copper plated for soldering to the probe needle points.

A sensitive alcohol micromanometer was used for pressure measurements. The free-stream velocity head was sensed by a total pressure probe in the flow and a static pressure tap at the wall. The mouth of the total pressure probe was of a high aspect ratio rectangular cross-section to eliminate the necessity of corrections due to viscous effects at low velocities.

5. Results and discussion

Comparison of analytic and experimental velocity

A comparison of analytic and experimental results was performed at $x/d = 10$ and 20 and $R = 62$ for all comparable velocity variables. The analytic velocity fluctuation wave forms are plotted to scale on the experimental oscillograms in figures 4 to 7. Comparison of time average total velocities U_T/U_0 and Q_T/Q_0 are presented in figures 8 and 9, root-mean-square velocity fluctuation $\tilde{u}'_T/U_0$ and $\tilde{q}'_T/Q_0$ in figures 10 and 11 and peak-to-peak velocity fluctuation $\hat{u}'_T/U_0$ and $\hat{q}'_T/Q_0$ in figure 12.

The analytic results demonstrate favourable agreement with the actual experimental flow conditions. The favourable comparison allows the following conclusions:

(1) The vortices of the real vortex street behave approximately according to equations (4) and (5).

(2) The vortex street analysis of equations (7) is a good approximation of actual conditions.

(3) The radius of the vortex core is closely determined by equation (9), and the outer edge of the core is very nearly coincident with the position of maximum velocity fluctuation.

(4) The transverse spacing of vortices is closely determined by equation (10).

(5) The assumed origin of time, $x = 0$, is justified.

The greatest discrepancy in the comparison of results is in the time average total velocity. This discrepancy appears to be primarily due to experimental error in measurement of U_T/U_0. The analysis below supports this observation. The carrier velocity of vortices in the street U_V may be determined experimentally in two ways:

$$U_V = 2fa, \tag{12}$$

and

$$U_V = U_T + |(\mathbf{u}' + \mathbf{v}')|_{s=0}. \tag{13}$$

The result of equation (12) for $R = 62$ is $U_V/U_0 = 0{\cdot}92$. Based on the position of the vortex centre in the analytic wave form, the experimental value from equation (13) is $U_V/U_0 = 0{\cdot}85$ approximately. Since the values of a and f substituted in equation (12) correlate well with those of other experimenters, the value $U_V/U_0 = 0{\cdot}92$ is reasonably accurate. Experimental results for U_T therefore appear to be lower than the true value. This discrepancy was estimated to be partially due to the non-linear effect of large velocity fluctuation on the measured time average total velocity U_T. It is also interesting to note that the largest discrepancy occurs in the region of largest velocity fluctuation. From the analysis shown in figure 19, the vortex carrier velocity is given by $Q_V/Q_0 = 0{\cdot}91$, which is in good agreement with equation (12).

Circulation

The dimensionless free-stream velocity determined from the match of analytic and experimental results is $Q_0 = 2{\cdot}565$. Therefore, from the definition of Q_0, the total circulation of a vortex in the fully developed state is

$$\Gamma_0 = 2\pi d U_0/Q_0 = 0{\cdot}0261 \text{ ft.}^2/\text{sec}.$$

From boundary-layer theory, the rate K at which vorticity in the form of vortex sheets is generated at the tripping cylinder is given by

$$K = \frac{d\Gamma}{dt} = \frac{d}{dt}\iint_A \zeta dx dy = \Lambda U_0^2,$$

where Λ is defined as

$$\Lambda = \frac{1}{U_0^2}\frac{d}{dt}\iint_A \zeta dx dy,$$

and U_0 is the free-stream velocity just outside the boundary layer (see Birkhoff & Zarantonello 1957). In the case when $v = 0$,

$$\Lambda = \frac{1}{U_0^2}\int u\frac{\partial u}{\partial y}dy.$$

For a laminar parabolic boundary layer, $\Lambda = 0{\cdot}5$. Assuming that vorticity is conserved in the rolling-up to form vortices, the rate of generation of vorticity may be written also as

$$K = \Gamma_0 f.$$

Substituting the experimental conditions and the circulation of this investigation, we get $\Lambda = 0{\cdot}343$ and therefore

$$\Gamma_0 = \frac{0{\cdot}343U_0^2}{f}.$$

The result of this investigation based on the fully developed street gives a smaller value of Λ than that analytically predicted by the laminar parabolic boundary-layer theory. It is therefore apparent that vorticity is partly lost in the rolling-up to form fully developed vortices. As presented by Birkhoff (1953), an empirical analysis by Prandtl substantiates this finding. Prandtl determined that the initial vorticity decreases to about half where the first vortex centres appear.

Solving for Λ from the experimental results of Timme (1957) at a Reynolds number of 200 (moving cylinder in still water), we find $\Lambda = 0{\cdot}46$. The discrepancy in Λ is attributed to the difference in vorticity dissipation in the two experiments. It is also of interest to note that, as determined by Roshko (1953), $R = 200$ is in a Reynolds number range ($150 < R < 300$) in which considerable experimental scatter occurs due to instability of the wake.

Geometry

The longitudinal spacing a of the stable vortex street is constant at a given Reynolds number as shown in figure 13 for four Reynolds numbers. This fact has been well substantiated by other investigations, i.e. Taneda (1955), Goldstein (1943) and Roshko (1953). The variation of longitudinal spacing with Reynolds number is presented in figure 14. The results of Taneda (1955), for experiments in water for a large range of Reynolds numbers, agree very well with the results of this investigation. Taneda's results are also plotted, together with the results of this investigation and that of Timme. The results of the empirical analysis developed below are also presented.

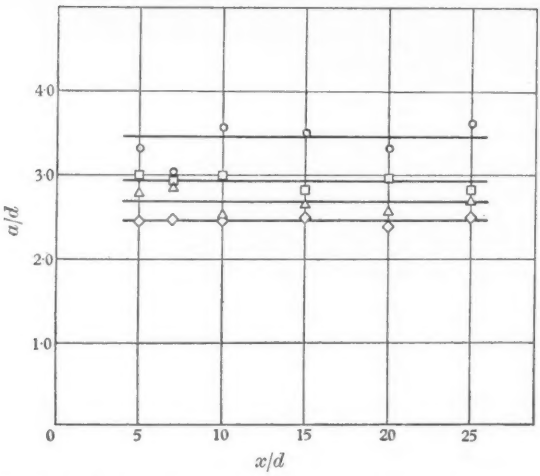

FIGURE 13. Longitudinal spacing versus distance downstream. ○, $R = 59$; □, $R = 75$; △, $R = 98$; ◇, $R = 122$.

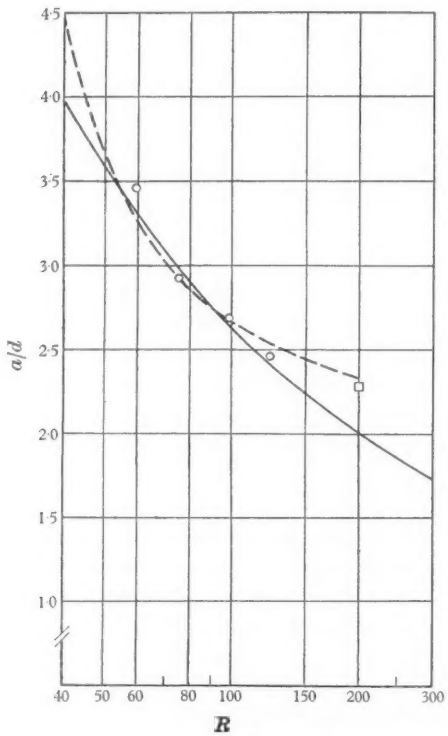

FIGURE 14. Summary of longitudinal spacing results. —, Taneda, experimental; – – –, equation (14); □, Timme; ○, Schaefer and Eskinazi.

An interesting empirical result may be derived from the determined longitudinal spacing. From equation (12) for the carrier velocity of vortices,

$$\frac{a}{d} = \frac{U_V}{2fd}.$$

If $U_V = C_V U_0$, where C_V is assumed tentatively to be independent of Reynolds number, then

$$\frac{a}{d} = \frac{C_V U_0}{2fd} = \frac{C_V}{2S} = \frac{C_V R}{2F},$$

where S is the Strouhal number fd/U_0 and F the dimensionless frequency fd^2/ν. The empirical results of Kovasznay (1949) and Roshko (1953), valid for $40 < R < 150$, also agree with the results of this investigation; they found $S = 0{\cdot}212(1 - 21{\cdot}2R^{-1})$, which is the same as $F = 0{\cdot}212R - 4{\cdot}5$, and the substitution of this into the above equation gives

$$\frac{a}{d} = \frac{C_V R}{0{\cdot}424R - 9{\cdot}0}. \tag{14}$$

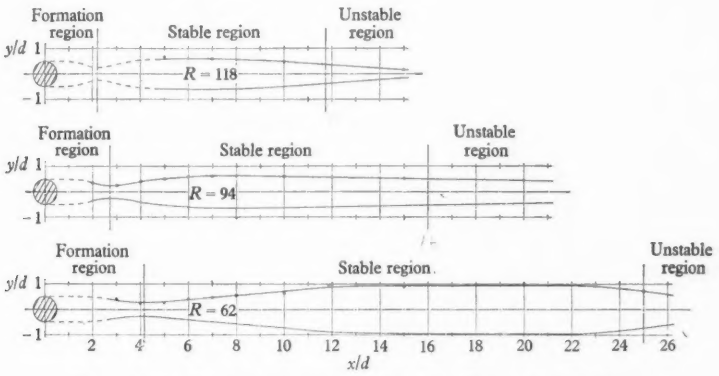

FIGURE 15. Transverse spacing for three Reynolds numbers.

With the determined value of C_V, equation (14) is plotted in figure 14 as a function of Reynolds number. The good agreement of experimental results and equation (14) indicates that U_V/U_0 is dependent of R and that its value is close to 0·90 in the stable range of the street.

The variation of transverse spacing with distance downstream for three Reynolds numbers is shown in figure 15. A tabulation of all transverse spacing parameters h_*/d, r_*/d, and h/d is presented in table 2. As seen in figure 15, the path of vortex centres exhibits similar variation at all Reynolds numbers investigated. A necking-down in h/d is apparent at a short distance from the tripping cylinder; this is followed by an increase to a maximum value; h/d then decreases at large distances from the tripping cylinder. Goldstein (1943) postulates a similar downstream variation, and states that upon formation of the vortex street the distance between rows increases until a position of transitional stability is reached at which time there is no further increase; the increase in core radius

then becomes the dominating factor and the stable system tends to close up and disappear.

At each Reynolds number (figure 15), the x/d distance at which the minimum spread of the path of centres occurs near the tripping cylinder is nearly coincident with the position of maximum downstream velocity fluctuation. This position is defined as the start of the fully developed street. The region between the tripping cylinder and this minimum point is therefore referred to as the 'formation region'.

Reynolds number	x/d	h_*/d	r_*/d	h/d	h/a
62	3	0·91	0·51	0·40	0·12
	4	0·83	0·59	0·24	0·07
	5	0·91	0·65	0·26	0·08
	6	1·14	0·72	0·42	0·13
	7	1·26	0·78	0·48	0·15
	8	1·40	0·83	0·57	0·18
	10	1·57	0·93	0·64	0·20
	12	2·00	1·01	0·99	0·30
	15	2·03	1·12	0·91	0·28
	20	2·31	1·31	1·00	0·31
	25	2·17	1·46	0·71	0·22
94	2	0·71	0·36	0·35	0·13
	3	0·70	0·44	0·26	0·10
	4	0·91	0·51	0·40	0·15
	5	1·09	0·57	0·52	0·19
	6	1·22	0·63	0·59	0·22
	7	1·31	0·68	0·63	0·23
	8	1·37	0·72	0·65	0·24
	10	1·41	0·81	0·60	0·22
	12	1·46	0·88	0·58	0·22
	15	1·51	0·98	0·53	0·20
	20	1·59	1·14	0·45	0·18
118	5	1·17	0·50	0·67	0·27
	7	1·20	0·60	0·60	0·24
	10	1·21	0·71	0·50	0·20
	15	1·03	0·87	0·16	0·06

TABLE 2. Transverse spacing parameters and spacing ratio

At large distances behind the tripping cylinder the vortex street exhibits an unstable behaviour. This instability becomes apparent approximately at the downstream position where the vorticity core extends to the path of centres of the opposite row; i.e. $h/d = r_*/2d$. The region in which $h/d < r_*/2d$ is therefore termed the 'unstable region'. The region of the stable vortex street, between the 'formation region' and 'unstable region' is referred to as the 'stable region'.

The regions are shown in figure 15. The start of the stable region is governed approximately by the empirical relation

$$R\left(\frac{x}{d}\right)_f \doteqdot 260,$$

where $(x/d)_f$ is the distance downstream at which the stable region begins. The end of the stable region is governed approximately by the relation

$$R\left(\frac{x}{d}\right)_s \doteqdot 1500,$$

where $(x/d)_s$ is the distance downstream at which the stable region ends.

The formation region is characterized by the development of the stable vortex street and dissipation of vorticity as previously mentioned. Kovasznay (1949) observed the existence of the formation region in his investigation. He states that in the formation of a vortex street vortices are not shed directly from the tripping cylinder but develop some distance downstream as an instability in the laminar wake.

The unstable region is characterized by irregular behaviour and the eventual transition to turbulence. Taneda (1955) observed two possible phenomena in this region, one a transition to turbulence and the other the eventual formation of a vortex street of large scale. Goldstein (1943) mentions only the former characteristic.

A number of other experimenters have attempted to measure transverse spacing. Tyler (1930), in his hot-wire experiments, assumed the incorrect relation $h/d = h_*/d$. Photographic techniques have been applied by other experimenters in which the point of zero velocity was assumed to be the vortex centre. Hooker (1936) pointed out that this assumption was incorrect; the point of maximum vorticity which is the vortex centre is not coincident with the point of zero velocity. This fact is apparent from figure 19. Timme's experimental and analytic results also substantiate this fact.

The variation of the spacing ratio h/a as defined in this investigation, with distance downstream at a given Reynolds number is proportional to h, since the longitudinal spacing is a constant. The maximum spacing ratios are approximately equal to the value predicted by Kármán (1912), $h/a = 0{\cdot}281$, in his idealized analysis. From the plots of h/d and a/d, it was found that $(h/a)_{\max} = 0{\cdot}28$ at $R = 62$ and $(h/a)_{\max} = 0{\cdot}24$ at $R = 94$ and 118. The experimental values are tabulated in table 2. Other experimenters have observed large values up to 0·525; it is believed that these large values are due to the previously mentioned incorrect methods of determining the transverse spacing.

Velocity

The variation of the time average of total velocity U_T/U_0 with distance from the vortex street centreline is presented in figure 16 for a number of downstream positions. The transverse variation of velocity deficiency $U_{T_{\max}} - U_T$ is compared with an exponential decay as shown in figure 17. The normalized variables are the local velocity deficiency divided by the maximum velocity deficiency, and $b_{\frac{1}{2}} = 1$ where $\Delta U_T/\Delta U_{T_{\max}} = 0{\cdot}5$.

The variation of fluctuating velocity $\tilde{u}'_T/U_0$ with distance from the street centreline is presented in figure 18 for a number of downstream positions and a Reynolds number of 62. The position in y/d of the maximum peak-to-peak velocity fluctuation is essentially coincident with the position of maximum root-mean-square of velocity fluctuation in all cases.

The velocity fluctuation wave forms at $x/d = 10$ are presented at various transverse locations in figures 4 to 10. Some low-amplitude wave forms exhibit a small 'pip' on the signal—this is hot-wire bridge noise and is not instability

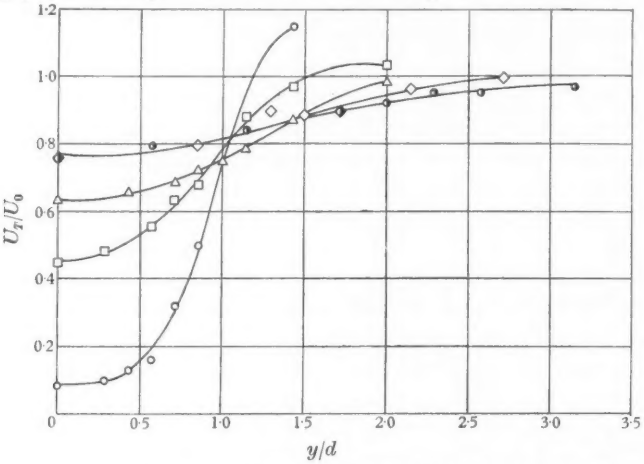

FIGURE 16. Experimental time average total velocity, $R = 62$. ○, $x/d = 2$; □, $x/d = 4$; △, $x/d = 6$; ◇, $x/d = 10$; ◑, $x/d = 20$.

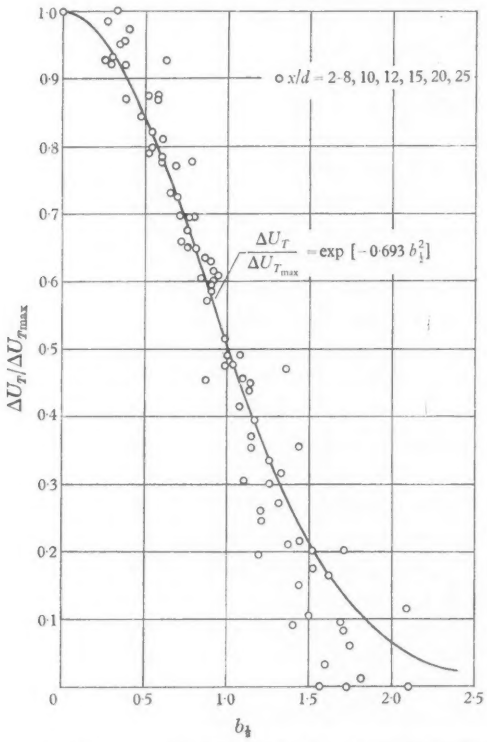

FIGURE 17. Exponential character of total velocity, $R = 62$.

in the vortex street. The wave forms at $y/d = 0$ exhibit a frequency double that of the shedding frequency because of the equal influence of the symmetrically staggered rows.

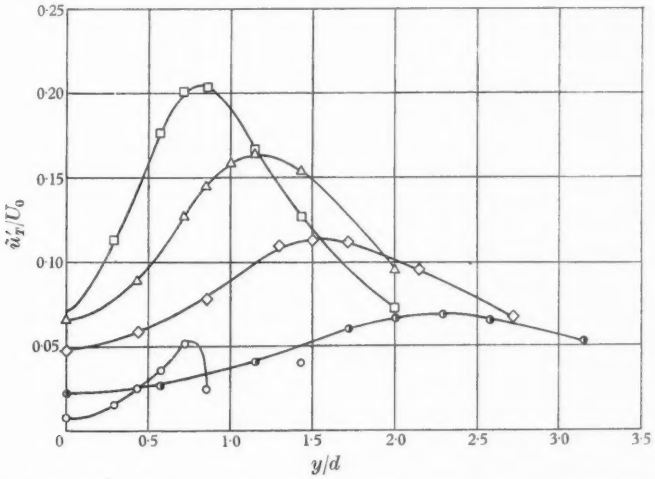

FIGURE 18. Experimental root-mean-square of velocity fluctuation, $R = 62$. ○, $x/d = 2$; □, $x/d = 4$; △, $x/d = 6$; ◇, $x/d = 10$; ◑, $x/d = 20$.

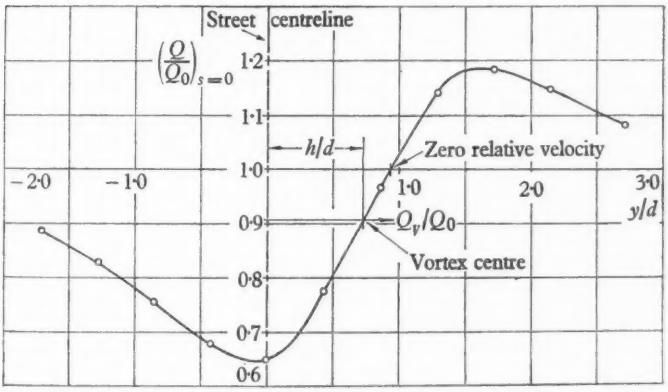

FIGURE 19. Analytic transverse velocity variation through a vortex, $R = 62$, $x/d = 10$.

No quantitative analysis of vortex street velocity at Reynolds numbers higher than 122 was undertaken in this investigation. However, a number of observations are of interest. Above a Reynolds number of approximately 125, occasional irregular behaviour was apparent at all downstream locations. The rate of occurrence and randomness of these disturbances increased with increasing Reynolds number. A low frequency 'whip' of the whole vortex street at large distances downstream was also apparent. The amplitude of the whip increased with increasing Reynolds number.

6. Conclusions

The vortex street generated behind a circular obstacle is essentially composed of vortices which behave according to the solution for an isolated viscous vortex, equations (4) and (5), as presented in figure 2. The velocity at any point in the stable vortex street wake relative to free stream is the summation of the velocity contributions at the point from all vortices.

The vortex street phenomenon in the Reynolds number range $50 < R < 125$ may be divided into three distinct areas of behaviour, the 'formation', 'stable' and 'unstable' regions as shown in figure 15. The formation region is the region immediately behind the tripping cylinder in which the vortex street develops and a dissipation of vorticity occurs. The stable region is the region of the fully developed stable vortex street in which the vortices display a periodic laminar regularity. The unstable region is the region far downstream which exhibits irregular behaviour and the eventual transition to turbulence. Above a Reynolds number of approximately 125, a completely stable vortex street is not apparent.

The transverse spacing is accurately determined by equation (10).

A large velocity deficiency, a backflow, exists directly behind the tripping cylinder. The amplitude of velocity fluctuation at the start of the stable region may be as great as 75 % of the average velocity.

REFERENCES

Birkhoff, G. 1953 Formation of vortex streets. *J. Appl. Phys.* **24**, 98–103.

Birkhoff, G. & Zarantonello, E. H. 1957 *Jets, Wakes, and Cavities*, pp. 283, 284. New York: Academic Press.

Eskinazi, S. & Yeh, H. 1956 An investigation on fully developed turbulent flows in a curved channel. *J. Aero. Sci.* **23**, 23–35.

Goldstein, S. 1943 *Modern Developments in Fluid Dynamics*, vol. II, pp. 553–71. Oxford University Press.

Hooker, S. G. 1936 On the action of viscosity in increasing the spacing ratio of a vortex street. *Proc. Roy. Soc.* A, **154**, 67–89.

von Kármán, T. & Rubach, H. 1912 Über den Mechanismus des Flussigkeits- und Luftwiderstandes. *Phys. Z.* **13**, 49–59.

Kovasznay, L. S. G. 1949 Hot-wire investigation of the wake behind cylinders at low Reynolds numbers. *Proc. Roy. Soc.* A, **198**, 175–90.

Lamb, H. 1945 *Hydrodynamics*, 6th ed., p. 578. Dover Publications.

Milne-Thomson, L. M. 1955 *Theoretical Hydrodynamics*, pp. 541, 542, 360. London: Macmillan Co.

Rosenhead, L. 1953 Vortex systems in wakes. *Advanc. Appl. Mech.* vol. III, pp. 185–95. New York: Academic Press.

Roshko, A. 1953 On the development of turbulent wakes from vortex streets. *NACA TN* 2913.

Schlichting, H. 1955 *Boundary Layer Theory*. New York: McGraw-Hill.

Taneda, S. 1952 Studies on wake vortices (II), experimental investigation of the wake behind cylinders and plates at low Reynolds numbers. *Res. Inst. Appl. Mech.*, Vol. I, pp. 29–40.

Timme, A. 1957 Über Die Geschwindigkeitsverteilung in Wirbeln. *Ingen. Archiv*, Bd XXV, pp. 205–25.

Tyler, E. 1930 A hot-wire method for measurement of the distribution of vortices behind obstacles. *Phil. Mag.* (7), **9**, 1113–30.

The analysis of temperature fluctuations by pulse-counting techniques

By A. A. TOWNSEND
Emmanuel College, Cambridge

(Received 15 January 1959)

To determine experimentally the mean value of a randomly fluctuating quantity, it may be necessary to measure the average value over a considerable interval of time. This problem arose in a recent study of the temperature fluctuations over a heated horizontal plate, and a system was used that depended on the counting of electrical pulses generated at a rate proportional to the quantity being measured. The advantage of this technique is that mean values may be measured over time intervals of almost unlimited length with little added difficulty for the experimenter. Circuits are described which measure: (*a*) the mean square of a fluctuating quantity and of its time-derivative, (*b*) the statistical distribution of the fluctuations, (*c*) the mean frequency of the fluctuation assuming a particular value, and (*d*) the mean product of two fluctuating quantities. Over the range of use, the stability and linearity of the calibrations is better than 1 %, more than sufficient for work on natural convection. In its present form, the equipment responds uniformly to all frequencies below 100 c/s, but it would not be difficult to extend this range of response to higher frequencies.

1. Introduction

It has been recognized since the time of Reynolds that the fluctuations occurring in turbulent flow are so irregular that no significance can be attached to individual measurements and that theoretical and experimental investigations must be made in terms of mean values (or statistical expectations) of a small group of functions of the fluctuations. The particular functions chosen do not form a complete statistical specification as their choice is dictated by reasons of theoretical or experimental convenience, but it is usual to hope that they specify the most significant aspects of the flow. Most laboratory work concerns turbulent flows that are statistically stationary in time and then the mean values are obtainable, in principle, as time-averages over periods sufficiently long compared with the time-scale of the fluctuations. In practice, the effective duration of the averaging process depends on the technique of measurement and one adequate for measuring the rapid fluctuations in a wind-tunnel (e.g. use of a continuously reading instrument with a response-time of about 5 sec) may be nearly useless for the much slower fluctuations occurring in the atmosphere or in systems of natural convection. With these and similar flows, it may be necessary to average over periods of 10 min or more, which requires that either the measuring equipment or the experimenter must 'remember' all the fluctua-

tions over this time. An obvious technique is to record the fluctuations on magnetic tape or on photographic paper and to analyse them later, but recording is an unnecessary complication of laboratory work unless there is a special advantage in having a time record, e.g. the possibility of determining the auto-correlation function. A more convenient method is to generate electrical pulses at a rate proportional to the quantity whose mean value is required and, by counting the total number of pulses emitted during a suitably long interval of time, to obtain an approximation to the mean value.

This paper describes a group of pulse-counting techniques that were developed for a recent study of the temperature fluctuations over a heated horizontal plane (Townsend 1959). With the appropriate combinations of the electrical circuits, it was possible to measure mean values, mean squares and statistical distributions of either the temperature, the temperature gradient or the time rate-of-change of temperature. The actual analysing equipment is loosely based on a system built and used by Thomas (1956) for measuring the auto-correlation function of the temperature fluctuations by observing the rate of coincidences between two frequency-modulated trains of pulses, and the availability of this equipment and knowledge of its qualities and defects were of considerable assistance in the development of the present system. Similar methods have been used in studies of turbulence, by Corrsin & Kistler (1954) and by others, but, to my knowledge, they have not been used to measure the group of quantities that are commonly measured with the hot-wire anemometer and its associated equipment.

2. The resistance thermometer

The fluctuations of temperature are detected as changes in resistance of a short length of platinum wire, 1–2 mm long and 2·5 μ in diameter, which forms one arm of a Wheatstone bridge. The bridge is supplied with alternating current

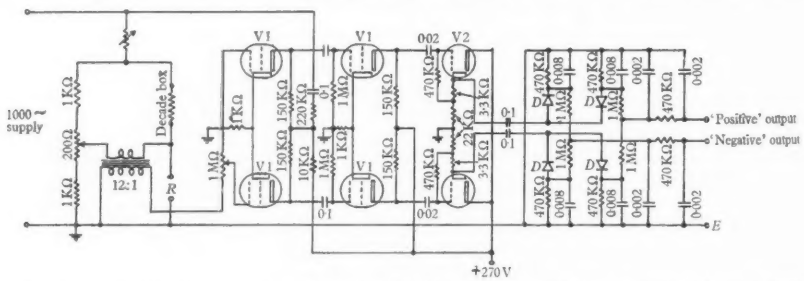

FIGURE 1. Circuit diagram of Wheatstone bridge and amplifier for use with resistance thermometer. (V1 type EF37, V2 type ECC35; *D*, crystal rectifier; *R*, thermometer element.)

at 1000 c/s and the output is amplified and converted by a phase-sensitive rectifier to an output directly proportional to the resistance unbalance of the bridge (figure 1). The output is balanced with respect to earth, that is, there are two output leads whose potentials differ by an amount proportional to the bridge unbalance but have a sum equal to ground potential. They will be distinguished

by calling them the 'positive' output and the 'negative' output, the 'positive' output being the one which has a positive potential when the resistance of the thermometer element exceeds the balance resistance. After passing through the necessary filter circuits to reduce the alternating-current ripple to a negligible amount, the electrical output responds to resistance changes with a lag of about 2 msec. This is sufficiently rapid for measurements of natural convection, although it would not be difficult to improve the speed of response by using alternating current of higher frequency.

3. Measurement of mean values

The production of pulses at a rate proportional to the resistance unbalance of the Wheatstone bridge is conveniently achieved by a modification of a familiar time-base circuit (figure 2). The condenser C is charged by the anode current of a pentode which is connected so that this current is very nearly proportional to

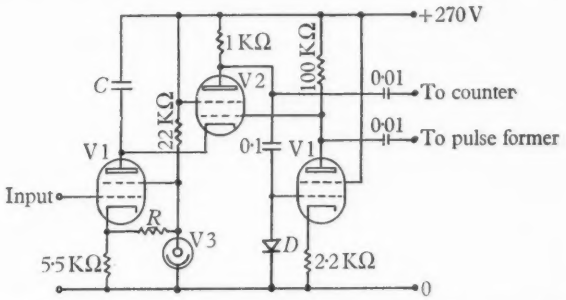

FIGURE 2. Circuit diagram of primary pulse generator. (V 1 type CV 138, V 2 type CV 416; D, crystal rectifier.) The adjustment of C and R is described in the text. Approximately, $C = 0{\cdot}05\,\mu$F, $R = 250\,$KΩ.

the potential of the control grid if this potential is positive and zero if it is negative. When the charge on the condenser reaches a critical value, the trigger circuit is excited and discharges the condenser. If the discharge process is instantaneous, the trigger circuit emits an electrical pulse whenever the total charge transmitted by the charging pentode has increased by a definite amount, that is, whenever the time-integral of the *positive* values of the input has increased by a fixed amount. The total number of pulses emitted is so proportional to the time-integral of the positive values of the input over the time of observation.* If one such circuit is used with each side of the output of the thermometer system (the 'positive' and 'negative' outputs mentioned in the previous section), the difference between the total numbers of 'positive' and 'negative' pulses is proportional to the time integral of the output and so to the average out-of-balance of the Wheatstone bridge over the time of counting. Obviously this requires nearly identical performance of the two pulse circuits, and this is secured

* In use, the total number of pulses recorded is always so large that the unregarded 'fractions' at the beginning and end of the counting periods are a negligible part of the total.

by adjustment of the resistances R and the condensers C (figure 2). The resistances are adjusted until the pulse rate is proportional to input and then one condenser is adjusted to make the constants of proportionality the same in the two circuits.

4. Measurement of mean squares and mean products

The measurement of the mean square of a fluctuating input depends on constructing from each pulse emitted by the primary pulse circuits a pulse of square wave-form and standard duration (approximately 1 msec). These pulses are

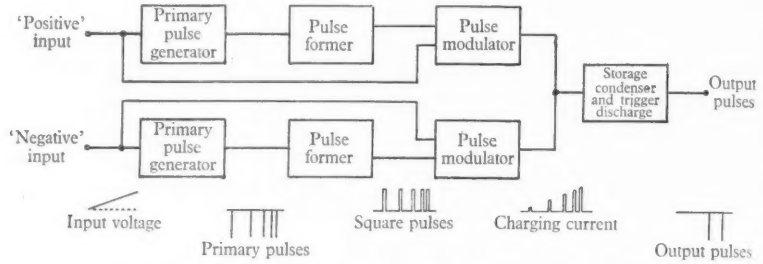

FIGURE 3. Block diagram of circuit for measuring mean squares, showing wave-forms in the 'positive' channel for the indicated 'positive' input.

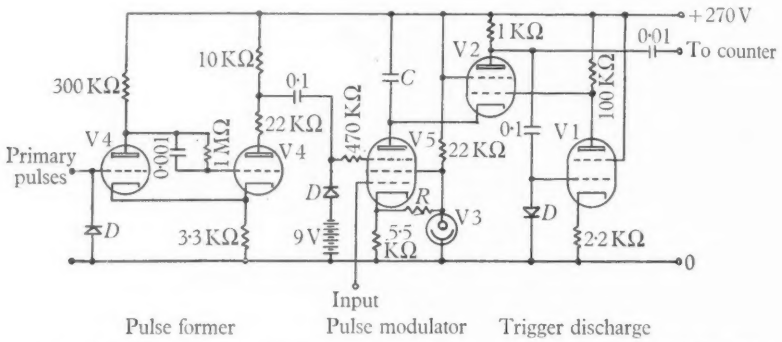

FIGURE 4. Details of circuit for measuring mean squares. (V1 type CV138, V2 type CV416, V3 type CV287, V4 type CV858, V5 type CV2209.) N.B. The condenser C is also charged by modulated pulses transmitted by a 'negative' channel not shown here.

used to switch on for their duration a current proportional to the input that produced them, and these modulated pulses of current charge a condenser which, like the condenser in the primary pulse circuit, is discharged when its potential reaches a critical value. The distinction between 'positive' and 'negative' inputs and the corresponding pulses makes necessary a duplication of the pulse-forming and pulse-modulation circuits but the modulated pulses of current from both channels are used to charge the same condenser, as is shown in the block diagram (figure 3). Details of the circuits are shown in figure 4. A simple way of looking at the working of this arrangement is to say that the storage condenser is receiving pulses of current whose recurrence frequency and

intensity are both proportional to the input and to infer that the number of discharges in a time interval is proportional to the average square of the input. This view makes it appear that the equipment will not measure accurately the mean square of an input that varies appreciably in a time comparable with the interval between successive primary pulses. That this is not correct may be seen from the following argument. The probability that (say) the 'positive' channel should produce a primary pulse in a short time-interval is proportional to the input at that time, and a primary pulse, when it occurs, leads to the storage condenser receiving a charge proportional to the time integral of the input over a subsequent time, τ, equal to the duration of the 'square' pulse. Consequently, the expected charge received by the condenser in unit time is proportional to

$$\overline{e(t)\int_t^{t+\tau} e(t')\,dt'} = \int_0^\tau R(\theta)\,d\theta, \tag{4.1}$$

where $R(\theta) = \overline{e(t)\,e(t+\theta)}$ is the covariance between values of the input, separated in time by an interval θ. If τ is small compared with the time-scale of the fluctuations, the expected charge per unit time and so the expected pulse-rate are proportional to $\overline{e^2(t)}$, the mean square of the input. This condition is usually satisfied.

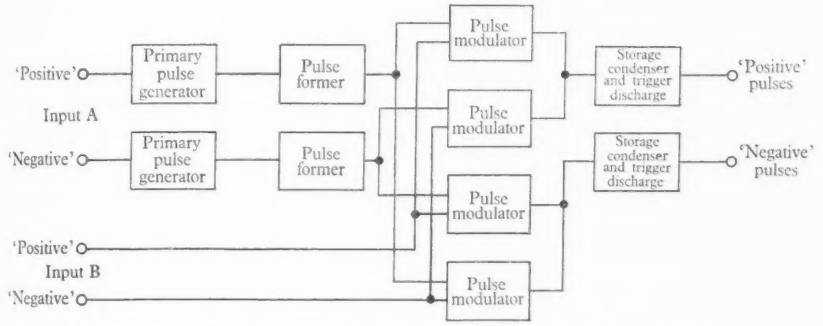

FIGURE 5. Block diagram of circuit for measuring mean products.

It is necessary that the performances of the two channels be the same if the system is to work in the manner described. This requires that the durations of the pulses from each pulse-forming circuit should be the same and that the heights of the modulated pulses should be the same for the same inputs. The first requirement is satisfied by adjustment of the coupling condenser in the pulse-forming circuit, and the second by using a common cathode resistance for the two pulse modulators and by approximate matching of the valves.

This method of measuring the mean square of a fluctuating signal is easily adapted for the measurement of the mean product of two fluctuating signals. For this, it is necessary to use two storage condensers, one receiving current pulses at a mean rate proportional to the mean of the positive values of the product and the other at a mean rate proportional to the mean of the negative values. The whole arrangement is shown as a block diagram in figure 5.

5. Performance and errors

The actual performance of these circuits departs from the ideal in several respects. In the first place, the variation of charging current of the storage condenser with input voltage is not linear for inputs less than 2 V and this leads to counting rates slightly above the 'ideal' values. Secondly, the trigger circuits do not work if the charging currents are too small, and the emission of pulses ceases completely if the input is less than 0·5 V. Thirdly, the circuit is insensitive and ignores input fluctuations during periods of condenser discharge. The first two defects concern the response at low inputs and low counting rates, and their consequences are negligible if the input fluctuations cover a sufficient range. The insensitivity during the time of condenser discharge reduces high counting rates in the ratio $(1+nt_d)^{-1}$ (where n is the 'ideal' counting rate and t_d is the discharge time). Since t_d is roughly 0·05 msec, this is a negligible reduction, even at the counting rate for the maximum input (nearly 300 sec^{-1}). These defects are also present in the operation of the squaring and multiplying circuits but have even less effect on the measurements obtained.

The ability of the squaring and multiplying circuits to respond to high-frequency components (that is, to include their contribution in the counting rate) depends mostly on the duration of the 'square' pulses, as is shown by equation (4.1). For a pulse duration of 1 msec, the response at 250 c/s is 65 % of the low-frequency response, and is 93 % at 100 c/s.

Other errors may arise from instability of the necessary adjustments and changes in the sensitivity of the various elements of the system. In the design, efforts have been made to relate the performance of the various circuits to values of resistances rather than to valve characteristics, and the long-term stability is surprisingly good with overall calibrations repeating from one day to another within $\frac{1}{2}$ %. It perhaps should be pointed out here that the influence of these variations on the actual measurements is reduced very considerably by the use of 'positive' and 'negative' channels. If only one channel were used, it would be necessary to restrict the input to positive values and then the mean square of the fluctuation from the mean would be obtained as the difference of two counting rates of similar magnitude. For example, if the fluctuations are normally distributed, the standard deviation may not exceed 0·4 of the mean if negative excursions are to be sufficiently improbable and the ratio of the mean square to the square of the mean will lie between 1 and 1·16. As the mean-square deviation from the mean is computed from the difference between an observed counting-rate proportional to the mean square and a calculated counting-rate proportional to the square of the mean, the instrumental uncertainty in this difference will be about ten times greater than the uncertainty in the basic calibrations. Using a second channel for negative excursions of the input allows adjustment of the input so that the square of the mean is small compared with the mean square, and then the uncertainty in the measurement of the mean-square fluctuation is of the same order of magnitude as the uncertainty of the calibration.

In use, the pulses emitted by the two primary pulse circuits and by the 'squaring' circuit are counted simultaneously, and the total numbers recorded

in a measured time-interval are used to calculate the average and the average square of the fluctuation from an arbitrary but known zero, taken over the same time-interval. The probable deviations of these averages from the true mean

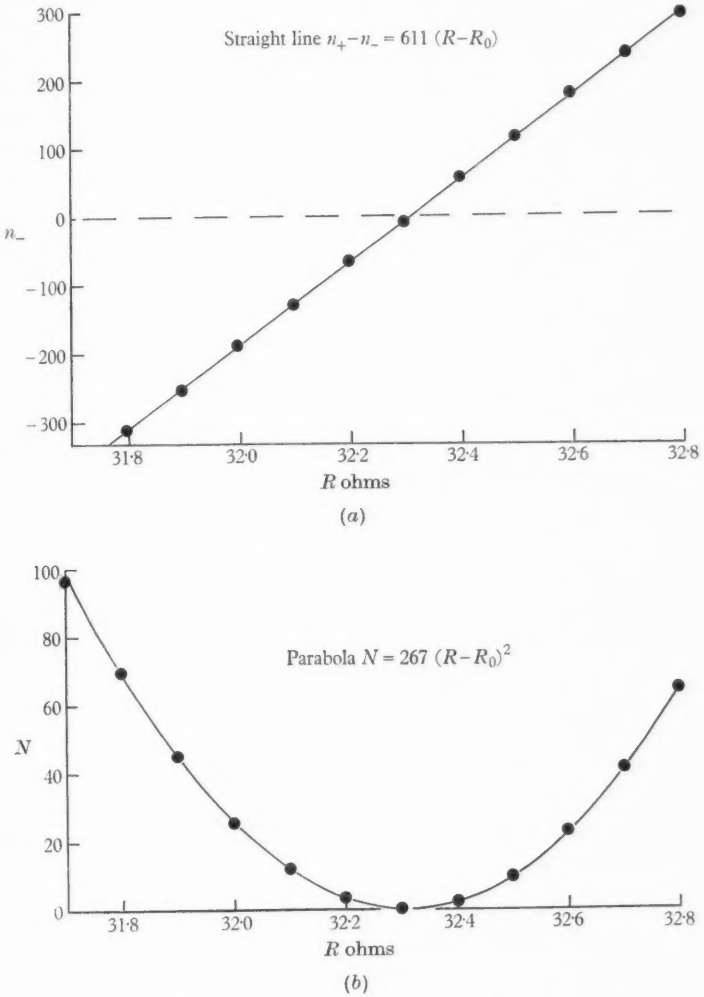

FIGURE 6. Typical calibration curves. (n_+, n_- are the pulse rates in the 'positive' and 'negative' channels, N is the pulse rate from the 'squaring' circuit, and R is the resistance in ohms of the thermometer element.)

values depend on the ratios of the time-scales of the fluctuations to the period of counting, but this statistical uncertainty is exactly what would arise if a time-lapse record of the same duration were analysed. In effect, the electrical system carries out the numerical analysis as the information arrives, rather than later.

6. Measurement of the distribution of fluctuations

The mean square of the fluctuation from the mean is a convenient but incomplete measure of the fluctuations, and useful information is often obtainable from the statistical distribution of the fluctuation amplitudes. This may be measured with the circuit shown in figure 7. In this, a square-wave of large amplitude and recurrence frequency 50 c/s is applied to the suppressor grids of five similar pentodes and switches the anode currents on and off at the same frequency. The magnitude of each anode current is determined by the potential

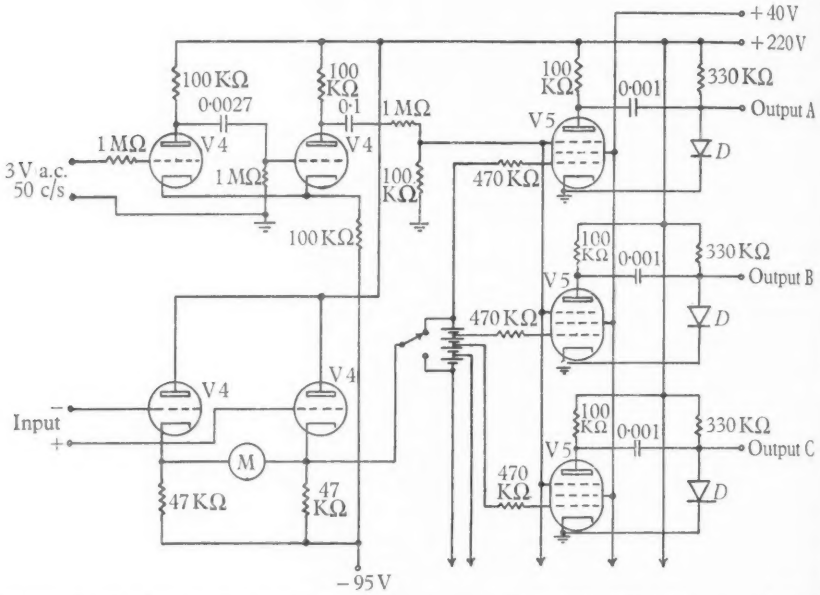

FIGURE 7. Details of circuit for the measurement of statistical distributions of input fluctuations. (V 4 type CV 858, V 5 type CV 2209; *D*, crystal rectifier. N.B. Only three of the five pentodes are shown. The voltmeter *M* gives a visual indication of the slower fluctuations.)

of the control grid, and only if this potential exceeds a critical value is the variation of anode current (caused by the switching) sufficient to transmit through the diode discriminator pulses of sufficient strength to work a dekatron counter. By means of a cathode follower, each grid potential is linearly related to the input and each pentode begins to transmit countable pulses when the input potential exceeds a critical value. By the use of bias cells, the five critical values are separated by intervals of approximately 1·5 V, and a switching system (only partially shown in figure 7) allows the five critical potentials to be changed together so that a range of critical potentials from $-10{\cdot}5$ V to $+10{\cdot}5$ V is available. Pulses are transmitted by each pentode during the time that the input potential exceeds the critical value, and the total number counted is proportional to the fraction of the time of observation that the input exceeded the critical value,

which is an approximation to the probability that a fluctuation should exceed this value. Five such probabilities can be measured simultaneously and twenty can be measured in four successive runs without alteration of the thermometer bridge.

Naturally, the transmission of countable pulses does not begin suddenly at the critical potential and there is a transition range, due in part to residual ripple at 1000 c/s. The change from zero to maximum counting-rate occurs over a range of input potential that is about 10 % of the spacing between successive critical potentials (figure 8), but this resolution is ample for the analysis of ordinary distributions.

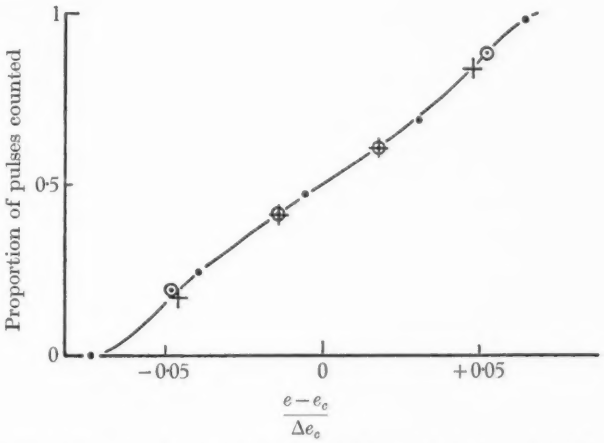

FIGURE 8. Resolution curve for the statistical analyser. (e_c is the potential at which half the pulses are counted, and Δe_c is the difference between successive values of e_c.)

7. Measurement of the time-derivative of a fluctuation

It is of interest to study the rate of change of fluctuations and this may be done in two ways. The first and more comprehensive method is to construct from the thermometer output an electric signal proportional to the time-rate-of-change of the output and to analyse this signal with the circuits described above. This has been done with a standard circuit (Townsend 1947) modified to work accurately at very low frequencies (figure 9). The relation between input and output is

$$\text{Output} = \tau_0 \frac{d}{dt}(\text{input}), \tag{7.1}$$

where

$$\tau_0 = \frac{\alpha\mu}{\mu+1} C_2 \frac{R_2 R_3}{R_1},$$

and μ is the amplification factor of the pentodes, connected as triodes,

α is the fraction of the total cathode current reaching the anode,

and the circuit components have been selected so that

$$2C_1R_1 = C_2(R_2+R_3). \tag{7.2}$$

In the actual circuit, the characteristic time, τ_0, was calculated to be 0·0309 sec, using the measured valve characteristics and component values.

The second method is very simple to use and depends on measuring the frequency with which the fluctuation from the mean changes sign from negative to positive. This frequency is

$$N_0 = \frac{1}{2\pi}\left[\overline{\left(\frac{de}{dt}\right)^2}\Big/\overline{e^2}\right]^{\frac{1}{2}} \tag{7.3}$$

if the fluctuations and their rates-of-change are statistically independent and normally distributed (Rice 1945). A simple circuit that produces a pulse whenever

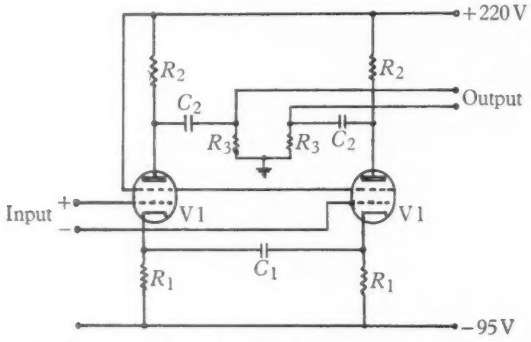

FIGURE 9. Circuit for differentiation with respect to time. (V 1 type CV 138, actual values $R_1 = 9{\cdot}8 \times 10^4\,\Omega$, $R_2 = 9{\cdot}9 \times 10^4\,\Omega$, $R_3 = 1{\cdot}00 \times 10^6\,\Omega$, $C_1 = 0{\cdot}220\,\mu$F, $C_2 = 0{\cdot}0396\,\mu$F.)

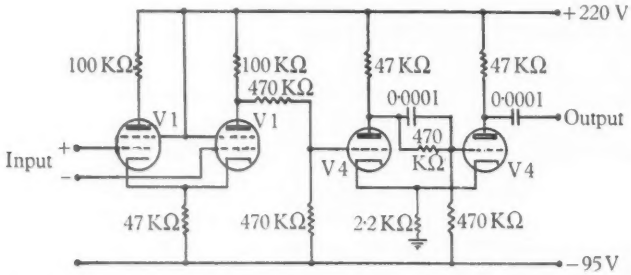

FIGURE 10. Circuit for counting zero crossings. (V 1 type CV 138, V 4 type CV 858.)

the input passes through a critical value is shown in figure 10. It consists of a directly-coupled amplifier whose output controls a Schmitt trigger circuit whose current distribution changes discontinuously at a critical grid voltage (Farley 1955, p. 58). Neglecting a small amount of 'backlash', the right-hand triode conducts whenever the input is less than the critical value and is non-conducting when it exceeds this value. Consequently, the small condenser connected to its anode transmits a positive pulse as the input increases through the critical value and a negative pulse as it decreases through the value. The purpose of the amplifier is to reduce the effective backlash to a negligible amount. Owing to the difficulty of interpreting the results if the statistical distributions are not normal, this method is less useful than the first for the study of fluctuations of unknown characteristics, but its simplicity makes it a valuable addition to the whole system of measurement.

8. Calibration and pulse-counting

The pulses originating in the various circuits are counted with a five-channel, scale-of-1000, electrical counter, using three stages of dekatrons and a mechanical counter. The various calibrations were made by substituting for the resistance-thermometer element a decade resistance box, covering the range, 10–110 Ω, in steps of 0·01 Ω, and observing the counting rates.

REFERENCES

Corrsin, S. & Kistler, A. L. 1954 *Tech. Note, Nat. Adv. Comm. Aero., Wash.*, no. 3133.

Farley, F. J. M. 1955 *Elements of Pulse Circuits.* Methuen: London.

Rice, S. O. 1944 *Bell System Tech. J.* **23**, 282.

Thomas, D. B. 1956 Ph.D. dissertation: University of Cambridge.

Townsend, A. A. 1959 *J. Fluid Mech.* **5**, 209.

Reverse flow and supersonic interference

By JOSEPH H. CLARKE
Division of Engineering, Brown University, Providence, Rhode Island

(Received 19 January 1959)

First, from a volumetric formulation of the momentum theorem of linearized theory, a general analytic proof is presented of the invariance of the drag of an arbitrary spatial distribution of horseshoe vortices and sources under reversal of the undisturbed flow. By consideration of the interference drag of two such singularity distributions, a reverse-flow relation for steady subsonic or supersonic flow is then obtained. This relation, a generalization of the Ursell–Ward theorem, may be applied to configurations with bodies whose surfaces are not quasi-cylindrical and whose surface pressures are quadratically related to the perturbation velocity.

The relation is used to discuss several interfering two-body arrangements in supersonic flow. It is shown that, in certain cases, the drag and lift may be determined without knowledge of the interference flow field associated with the arbitrarily prescribed body geometry. The simplicity of the results permits the formulation of optimum problems. The invariance of the drag under flow reversal with unchanged geometry is also established.

Introduction

The development of the reverse-flow or reciprocity relations of linear small-disturbance theory was initiated by the discovery of the invariance of the pressure drag of symmetric non-lifting wings in supersonic flow with respect to reversal of the flow direction (von Kármán 1947). The subject was treated independently on a considerably more general basis at about the same time by Hayes (1947). The theoretical and practical ramifications of subsequent contributions are extensive and need not be recounted here. This research, however, has resulted in two principal theorems which are of interest in the present paper.

In connexion with the first, there is considered lineal, planar, or spatial distributions of horseshoe vortices and sources, singularities sufficient† to produce the same effect in the stream as any body or arrangement of bodies.‡ It is shown

† When the vorticity appearing in the general solution for the perturbation field is distributed over a cylindrical reference surface or a volume, it may be re-expressed as horseshoe vorticity.

‡ In this paper, the word body refers to any obstacle to which perturbation flow theory is applicable. By fusiform body is meant a body of fuselage or projectile shape. A slender body is a fusiform body whose section by meridional or transverse planes exhibits the degree of regularity required in the theory of Ward (1949). A quasi-cylindrical body is one whose boundary conditions and surface pressures may, within the approximation, be discussed on a cylindrical reference surface, with generators parallel to the undisturbed stream, which is near the actual surface (e.g. a pair of wing panels supported by an infinite body whose shape differs but slightly from a circular cylinder with finite diameter).

that the drag of any distribution of these two singularities is unchanged if, in the undisturbed stream, the sign of the velocity vector is changed without change in Mach number or density (Hayes 1947). The sign of the singularity strengths may be reversed with the flow. Hayes' theorem does not deal explicitly with the geometry of the system represented which is, in general, different in the reverse flow. The theorem has been discussed for planar wings in connexion with the development of conditions for minimum drag in the combined flow field (Jones 1951) and for more general arrangements of bodies in the same connexion (Jones 1956). The proofs are based on physical arguments concerning the interference between two discrete singularities in forward and reverse flow, and involve the superposition of the pressure and cross-flow induced by each in a reference plane containing the two singularities; the arguments do not deal explicitly with cases where the bodies are not quasi-cylindrical or the pressure is not linearly related to the perturbation velocity.

The second theorem mentioned is the Ursell–Ward theorem, which contains virtually all of the other theorems developed thus far for steady flow as special cases (Ursell & Ward 1950; Heaslet & Spreiter 1953). This is an identity involving surface integrals related to the drag integral, and connecting a forward flow past a quasi-cylindrical body (or bodies) to the reverse flow past another such body which has the same reference surface; the linear pressure relationship pertains. The theorem can be used to relate the flow past a body with specified geometry or pressure distribution to the reverse flow past a body whose geometry or pressure distribution may be independently specified. The two bodies may therefore be identical. As is evident in the formulation used in the present paper, this theorem contains the first theorem as a special case, but only for the quasi-cylindrical bodies to which it may be applied.

Starting from a volumetric formulation of the momentum theorem, this paper presents, as a preliminary, a general analytic proof of Hayes' theorem which clarifies aspects of the physical derivation discussed above. There is then obtained a reverse-flow theorem for steady subsonic or supersonic flow which is related to the Ursell–Ward theorem, but which may be applied as well to arrangements containing bodies whose surfaces are not quasi-cylindrical and whose surface pressures are not linearly related to the perturbation velocity. Whereas such bodies need not be identical in forward and reverse flow, they must be related in a manner to be discussed; this geometric restriction is concomitant with the relaxation of the two aforesaid restrictions. The relation is a generalization, in the sense just indicated, of the Ursell–Ward theorem, and it is possible to obtain the surface representation of the results presented with a similar derivation. However, the relation is more generally formulated with use of the equality, in forward and reverse flow, of the interference drags of two spatial singularity distributions, the first associated with the bodies in forward flow and the second with the bodies in reverse flow. The underlying unity of the two theorems just discussed is therefore established, and a view consistent with the extensive interference literature is maintained. The present relation contains, in fact, the two theorems as special cases.

In the second portion of the paper, the reverse-flow relation is used to discuss

the drag and lift of several interfering two-body arrangements in supersonic flow. The arrangements considered not only serve to exhibit some implications of the theorem, but are of theoretical and practical interest in themselves. The applicability of the relation is, however, by no means restricted to these specific configurations.

Considerable attention has recently been devoted to the problem of achieving favourable interference in arrangements of bodies in a moderate supersonic flow, and in some cases optimum problems have been posed in very general terms. Reference is made to the methods of Jones (1956), Lomax (1955), Lomax & Heaslet (1956*a*) and E. W. Graham, Lagerstrom, Licher & Beane (1957). Frequently, problems are set such that the orientations and singularity distributions of bodies in the arrangement are sought which reduce or minimize the drag of the system, subject to restraints on lift, volume, etc. (M. E. Graham 1955; Licher 1955; Lomax & Heaslet 1956*b*; Friedman & Cohen 1954). When the bodies interfere, each induces a cross-flow on the other surfaces, resulting in a distortion of the isolated boundaries associated with the singularities of each. The geometry of the arrangement is usually discussed only in general terms.

When an optimum, or otherwise suitable, geometry is arrived at by such methods, it is necessary in practice to determine the flow field, and particularly the drag and lift, produced by these boundaries for other values of incidence and Mach number. In any case, when the geometry of an arrangement is prescribed, cancellation of the mutual cross-flow by introduction of an interference flow is required. As illustrated by the wing-fuselage interference problem (see Lawrence & Flax 1954), the labour in determining the interference flow defined by this classical indirect formulation is great. Depending on how the problem is posed, favourable shapes might remain to be sought subsequent to the calculation.

In the present paper, the reverse-flow relation is first used to establish the invariance of the drag of the two-body arrangements under flow reversal with unchanged geometry. It is then shown that it is possible, for supersonic flow, to determine the drag and lift of certain of these interfering body arrangements, whose geometry is arbitrarily prescribed, with no knowledge of the interference flow field. The forces are constructed from the solution for the flow field of each body when it appears isolated in forward flow and in reverse flow. The determination is possible when the interference flow produced on each body does not influence the other; when this restriction is not satisfied, an incomplete knowledge of the interference flow suffices for the determination of the aerodynamic forces. The method uses the reverse flow theorem to relate the force appearing when the two bodies interfere without mutual distortion in forward flow to the force appearing when the same bodies interfere with mutual distortion in the hypothetical reverse flow. The relations obtained are of sufficient simplicity to permit formulation of optimum problems. The method lends itself to application to other related arrangements.

The aerodynamic force

Consider the steady, homentropic flow of a compressible gas past an arrangement of bodies whose inclinations are small with respect to the remote uniform stream with velocity

$$\mathbf{U} = U\mathbf{i}, \tag{1}$$

where $U > 0$ in forward flow and $U < 0$ in reverse flow, $\mathbf{i}$ is a unit vector in the positive direction of the cartesian co-ordinate x, and $\mathbf{j}$ and $\mathbf{k}$ are similarly defined for the cartesian co-ordinates y and z. If the fluid velocity $\mathbf{q}$ is written

$$\mathbf{q} = \mathbf{U} + \mathbf{V}, \tag{2}$$

then the perturbation velocity

$$\mathbf{V} = u\mathbf{i} + v\mathbf{j} + w\mathbf{k} \tag{3}$$

is governed by the equation

$$\nabla . \mathbf{W} = 0 \tag{4}$$

together with the definitions

$$\mathbf{W} = \Phi . \mathbf{V}, \quad \Phi = \begin{bmatrix} -B^2 & 0 & 0 \\ 0 & 1 & 0 \\ 0 & 0 & 1 \end{bmatrix}, \tag{5}$$

where $B^2 = M^2 - 1$, M being the Mach number of the undisturbed stream. Further,

$$\nabla \times \mathbf{V} = 0 \tag{6}$$

exterior to any regions of trailing vorticity.

The aerodynamic force on the bodies may be evaluated through use of the momentum theorem. If equation (2) and the continuity equation are used therein, and the pressure p and density ρ are then eliminated by means of the approximate relations

$$(p - p_0)/\rho_0 = -\mathbf{U} . \mathbf{V} - \tfrac{1}{2}\mathbf{V} . \mathbf{W} \tag{7}$$

and

$$\rho/\rho_0 = 1 - (M^2/U^2)\, \mathbf{U} . \mathbf{V}, \tag{8}$$

where the subscript 0 denotes conditions in the undisturbed stream, the momentum theorem appears in the form (Ward 1955*a*)

$$\mathbf{F} = \rho_0 \mathbf{U} \times \oint_S \mathbf{n} \times \mathbf{V} dS + \rho_0 \oint_S (\tfrac{1}{2}\mathbf{V} . \mathbf{W}\mathbf{n} - \mathbf{V}\mathbf{W} . \mathbf{n})\, dS. \tag{9}$$

Here S is any surface with outward unit normal $\mathbf{n}$ which completely encloses the bodies, and $\mathbf{F}$ is the total aerodynamic force on the bodies, provided that the total source strength enclosed by S is zero. The first term evidently gives a force perpendicular to the undisturbed stream.

Equation (9) is correct within the quasi-cylinder approximation

$$t \ll 1, \tag{10}$$

t being the appropriate thickness ratio, or the slender body approximation

$$t^2 \log t \ll 1, \tag{11}$$

but, depending on the choice of S, may contain terms of higher order than required. A lower approximation to (7) and (8), and therefore to (9), is often used

for slender bodies which is, in fact, slightly too low if the bodies are closed. It is assumed that (9) is also adequate for arbitrary fusiform bodies, the approximation being (Lighthill 1945, 1954)

$$u \ll 1, \tag{12}$$

and for arbitrary body arrangements. The condition (12) is about equivalent to (11) but may fall at least to (10) locally, as at shoulders. Within approximations (10), (11) or (12), the boundary condition on the surfaces A of the bodies

$$(\mathbf{U}+\mathbf{V}).\mathbf{n} = 0 \tag{13}$$

may be written

$$(\mathbf{U}+\mathbf{W}).\mathbf{n} = 0, \tag{14}$$

essentially because $\mathbf{V}$ and $\mathbf{W}$ differ only in their x-components and the x-component of $\mathbf{n}$ is small. The momentum flux given by (9) vanishes within the approximation of (14) to (13) when S is chosen as A. If the drag D is defined as the component of $\mathbf{F}$ in the direction of flow, if edge forces are neglected and S is taken as A, and if use is made of (14), then (9) gives for the drag

$$D = \frac{U}{|U|}\mathbf{F}.\mathbf{i} = \frac{U}{|U|}\rho_0 \oint_A (\mathbf{U}.\mathbf{V}+\tfrac{1}{2}\mathbf{V}.\mathbf{W})\,\mathbf{n}.\mathbf{i}\,dS, \tag{15}$$

which is consistent with a surface integration of the pressure given by (7). For quasi-cylinders, however, the approximation to the pressure

$$(p-p_0)/\rho_0 = -\mathbf{U}.\mathbf{V} = -Uu \tag{16}$$

suffices, whereas for slender bodies the relation (Ward 1949)

$$(p-p_0)/\rho_0 = -Uu-\tfrac{1}{2}(v^2+w^2) \tag{17}$$

is required on or near the surface. Equation (17) is still correct for arbitrary fusiform bodies (Lighthill 1945, 1954). The term $-\frac{1}{2}B^2u^2$ in (15) may then always be discarded.

Let the bodies be represented by a spatial distribution of vorticity and sources over the regions T interior to the surfaces A of the bodies (a thickness distribution can temporarily be ascribed to a plate wing). The spatial distribution corresponding to a given body is not generally unique, and this freedom might be used to smooth out any singularities appearing in the intensities of surface or lineal distributions. With the body interiors regarded as part of the fluid domain, the surface integrals in (9) may be transformed to volume integrals. The identity appropriate to the second integral follows from (34) below by discarding subscripts. Equation (9) may then be written (Ward 1955*b*)

$$\mathbf{F} = \rho_0\mathbf{U}\times\int_T \nabla\times\mathbf{V}\,dT + \rho_0\int_T [\mathbf{W}\times(\nabla\times\mathbf{V})-\mathbf{V}\nabla.\mathbf{W}]\,dT. \tag{18}$$

Integration over the volume of each body gives the force on that body. A more direct derivation of (18) leads to difficulties in obtaining the correct approximation to the integrands for slender and other fusiform bodies.

For a spatial distribution of vorticity with intensity $\boldsymbol{\Omega}$ and sources with an intensity f such that the mass flux per unit volume is $\rho_0 f$, the linearized equations for $\mathbf{V}$ which replace (4) and (6) are (Ward 1955*a*)

$$\nabla.\mathbf{W} = f, \tag{19}$$

and

$$\nabla\times\mathbf{V} = \boldsymbol{\Omega}, \tag{20}$$

where f and $\boldsymbol{\Omega}$ are related to the geometry. The conservation in space of vorticity is assured by the relation

$$\nabla . \boldsymbol{\Omega} = 0, \tag{21}$$

which follows from (20). Let the vorticity at each point be resolved according to the expression

$$\boldsymbol{\Omega} = \Omega_x \mathbf{i} + \boldsymbol{\omega}, \tag{22}$$

where $\boldsymbol{\omega}$ is a vector perpendicular to the x-axis which is referred to here as bound vorticity. If the drag is formed from (18), and if (5), (19), (20) and (22) are used, there results after slight rearrangement

$$D = -\rho_0 \frac{U}{|U|} \int_T (\mathbf{i} \times \boldsymbol{\omega} . \mathbf{V} + f \mathbf{i} . \mathbf{V}) \, dT. \tag{23}$$

Comparison with the lateral force in (18), a version of the Kutta–Joukowski relation, shows that the term $\rho_0 \mathbf{U} \times \boldsymbol{\omega}$ is the elemental lateral force perpendicular to the bound vorticity at each point; comparison with (16) shows that $-\rho_0 \mathbf{U} . \mathbf{V}$ is equal to the linear homentropic pressure difference. The first term is then the product of the elemental lateral force and the component of the cross-flow in its direction. The general volumetric representation of drag then yields a result closely resembling, in its two terms, the familiar relations of wing theory for a planar distribution of lift and thickness, respectively. Its significance stems from its applicability to the more restrictive fusiform bodies as well as to quasi-cylinders, so that no distinction between the classes of bodies need be made over T. Thus (23) permits, as for quasi-cylinders, the convenient decomposition of the drag of a distribution of singularities into self-induced drag and various interference drags (E. W. Graham *et al.* 1957). On the other hand, the formulation (15) requires, for bodies which are not quasi-cylindrical, integration of the product of the quadratic pressure and cross-flow over the actual body surfaces produced by the collective effect of all singularities; the drag decomposition mentioned is not possible. Equation (9), with a truncated cylindrical surface S, for example, provides a reference surface and quadratic products permitting drag decomposition for both classes of bodies, but in this formulation each point on the body surfaces A corresponds to a region of S, and vice versa.

The exhibited properties of the momentum theorem have their counterparts in the reverse flow relations to follow.

The perturbation velocity field

A solution to (19) and (20) has been given by Ward (1952*a*,*b*, 1955*a*), the appropriate form of which is

$$\mathbf{V}(\mathbf{r}) = -\frac{1}{2\pi\epsilon} {}^{*}\!\int_d f(\boldsymbol{\rho}) \nabla \frac{1}{R} d\tau - \frac{B^2}{2\pi\epsilon} {}^{*}\!\int_d \boldsymbol{\Omega}(\boldsymbol{\rho}) \times (\mathbf{r} - \boldsymbol{\rho}) \frac{1}{R^3} d\tau, \tag{24}$$

where $\mathbf{r} = x\mathbf{i} + y\mathbf{j} + z\mathbf{k}$, $\boldsymbol{\rho} = \xi\mathbf{i} + \eta\mathbf{j} + \zeta\mathbf{k}$, $R = \sqrt{\{(x-\xi)^2 - B^2[(y-\eta)^2 + (z-\zeta)^2]\}}$, $\epsilon = 1$ for $M > 1$ and $\epsilon = 2$ for $M < 1$, * denotes Hadamard's finite part of an integral, and d denotes the domain of dependence of the point $\mathbf{r}$: the region of the space τ interior to the fore Mach cone from $\mathbf{r}$ in supersonic flow; the entire space

τ in subsonic flow. The second integral is recognized as a compressible generalization of the Biot–Savart law. It may be recast as horseshoe vorticity by constructing elemental trailing vortex pairs and articulating these to the bound vorticity at each point. Then (24) becomes

$$\mathbf{V}(\mathbf{r}) = \frac{-1}{2\pi\epsilon}\,{}^{*}\!\int_d \left\{ f(\boldsymbol{\rho})\,\nabla\frac{1}{R} + B^2\boldsymbol{\omega}(\boldsymbol{\rho})\times(\mathbf{r}-\boldsymbol{\rho})\frac{1}{R^3} + [\boldsymbol{\omega}(\boldsymbol{\rho}).\nabla][\mathbf{i}\times(\mathbf{r}-\boldsymbol{\rho})\,\psi(\mathbf{r},\boldsymbol{\rho})] \right\} d\tau, \tag{25}$$

where

$$\psi(\mathbf{r},\boldsymbol{\rho}) = \frac{1}{[(y-\eta)^2+(z-\zeta)^2]}\left[\frac{U}{|U|}(\epsilon-1)+\frac{(x-\xi)}{R}\right]. \tag{26}$$

The first term in (25) gives the effect of the sources, the second the effect of the bound vorticity, and the third the effect of the trailing vortex pairs.

Equations (24) and (25) are invariant under a reflexion of the x- and y-axes, and therefore hold in reverse as well as forward flow.

Invariance of drag of singularity distribution under flow reversal

It may now be shown that the drag of the distribution of horseshoe vortices and sources over the regions T is unchanged by a reversal of the direction of the undisturbed stream.† Let $U = U_F > 0$, the subscript F referring to forward flow. Substitution of (25) into (23) gives for the drag in forward flow

$$D_F = -\rho_0 \int_T dT\,{}^{*}\!\int_d d\tau[\mathbf{i}\times\boldsymbol{\omega}(\mathbf{r})+f(\mathbf{r})\,\mathbf{i}].\left(\frac{-1}{2\pi\epsilon}\right)\left\{ f(\boldsymbol{\rho})\,\nabla\frac{1}{R} + \frac{B^2}{R^3}\boldsymbol{\omega}(\boldsymbol{\rho})\times(\mathbf{r}-\boldsymbol{\rho}) + [\boldsymbol{\omega}(\boldsymbol{\rho}).\nabla][\mathbf{i}\times(\mathbf{r}-\boldsymbol{\rho})\,\psi_F(\mathbf{r},\boldsymbol{\rho})] \right\}. \tag{27}$$

It is desired to reverse the order of the two volume integrations. Such an operation poses no special problems for subsonic flow, but for supersonic flow the singular integrands can pose difficulties in differentiating or integrating under an integral sign; the difference in approach to this problem distinguishes, in part, the research of Volterra and Hadamard concerning the wave equation. Reference is made to the definitions and approach of Lomax, Heaslet & Fuller (1951) or Heaslet & Lomax (1954). The operation of integration under the finite part sign can in fact be performed, and without the appearance of accretive terms, provided that the two volume integrals are properly iterated. If the co-ordinate net is such that the inner or first integration in each case proceeds along a subsonic curve,‡ and the two remaining integrations proceed along supersonic curves, then the proposed reversal is valid. The limit of the inner integration with respect to T becomes, from the geometry, the domain of influence δ of the point $\boldsymbol{\rho}$. The outer integration with respect to τ extends over all of the regions T. Physically, the drag of the horseshoe vortex and source at $\boldsymbol{\rho}$ is now being computed before summing over like singularities. The finite-part concept and the present preferred order of iteration used in both (23) and (25) together allow the singularities to

† It is understood that M and ρ_0 are unchanged under reversal.

‡ A subsonic curve has the property that each successive point, when the curve is traversed in one of the two possible senses, lies in the domain of influence of the preceding point. When no two points on a curve have this property, the curve is supersonic.

be treated as entities, each possessing a flow field and inducing forces like discrete singularities in incompressible flow. This freedom is implicit in the physical arguments of Hayes and Jones.

By formal expansion of the products and rearrangement, the integrand of (27) can be written

$$-[\mathbf{i}\times\boldsymbol{\omega}(\boldsymbol{\rho})+f(\boldsymbol{\rho})\,\mathbf{i}].\left(\frac{-1}{2\pi\epsilon}\right)\left\{f(\mathbf{r})\,\nabla_G\frac{1}{R}+\frac{B^2}{R^3}\boldsymbol{\omega}(\mathbf{r})\times(\boldsymbol{\rho}-\mathbf{r})+[\boldsymbol{\omega}(\mathbf{r}).\nabla_G][\mathbf{i}\times(\boldsymbol{\rho}-\mathbf{r})\,\psi_R(\boldsymbol{\rho},\mathbf{r})]\right\}, \quad (28)$$

where

$$\nabla_G\equiv\mathbf{i}\frac{\partial}{\partial\xi}+\mathbf{j}\frac{\partial}{\partial\eta}+\mathbf{k}\frac{\partial}{\partial\zeta},$$

and

$$\psi_R(\boldsymbol{\rho},\mathbf{r})=-\psi_F(\mathbf{r},\boldsymbol{\rho})$$

from (26), the subscript R referring to the reverse flow $U_R=-U_F<0$. The first term is recognized from (23) as the expression for the elemental drag in reverse flow; the second is recognized from (25) as the expression for the elemental velocity in reverse flow with the roles of $\mathbf{r}$ and $\boldsymbol{\rho}$ interchanged. This result therefore means that the drag induced on the horseshoe vortex and source at $\mathbf{r}$ by the horseshoe vortex and source at $\boldsymbol{\rho}$ in forward flow, is equal to the drag induced on the horseshoe vortex and source at $\boldsymbol{\rho}$ by the horseshoe vortex and source at $\mathbf{r}$ in reverse flow. Trailing vortex pairs induce no streamwise perturbations and hence do not interfere with sources.

Upon substitution of (28) into (27), written with the reversed order of integration, and comparison with (25), there results

$$D_F=\rho_0\int_T d\tau[\mathbf{i}\times\boldsymbol{\omega}(\boldsymbol{\rho})+f(\boldsymbol{\rho})\,\mathbf{i}].\mathbf{V}_R(\boldsymbol{\rho}), \quad (29)$$

since δ becomes the domain of dependence of the point $\boldsymbol{\rho}$ in the reverse flow U_R. As was just noted from (23), the right member of (29) is the drag of the distribution in reverse flow. Thus

$$D_F=D_R \quad (30)$$

for subsonic or supersonic flow. (The contribution to this result of any wing edge forces can be considered separately with the approach of Ursell & Ward (1950). It is possible to demonstrate that the statement (30) includes any edge forces and therefore holds for the complete pressure drag.)

It is customary to reverse with the flow the signs of $\boldsymbol{\omega}$ (or $\boldsymbol{\Omega}$) and f in order to maintain under reversal the same lateral force (18) and real volumes. This does not change the above conclusions.

The shape of the bodies will, in general, be different in the reverse flow so that A, and therefore T, should be different. This distortion under reversal is not given properly here because the singularities have been attached to the space instead of associated with a fictitious captive fluid simulating the bodies and distorting with them. The effect is evidently of no concern in quasi-cylinder theory, and provided that the boundary conditions and pressure are also discussed on the undistorted surfaces instead of the true surfaces, the effect is also negligible in linear theory for more general bodies. The singularities need not, of course, occupy the entire region interior to each body.

A reverse-flow relation

Consider an arrangement of bodies represented in the forward subsonic or supersonic flow U_F by a distribution of horseshoe vortices $\boldsymbol{\omega}_F$ and sources f_F over the connected or unconnected regions T interior to the bodies, and such that the induced flow field satisfies

$$\mathbf{W}_F.\mathbf{n} = -\mathbf{U}_F.\mathbf{n} \tag{31}$$

on the body surfaces A with outward normal $\mathbf{n}$. Also consider a related arrangement of bodies represented in the reverse flow U_R by a different distribution $\boldsymbol{\omega}_R$ and f_R over the same regions T. Suppose that both distributions now appear together in forward flow and also in reverse flow. Let $D_{F,RF}$ be the interference drag in forward flow induced on the latter distribution by the former; let $D_{R,FR}$ be the interference drag in reverse flow induced on the former distribution by the latter. A slight modification of the argument of the last section gives a property of two distinct, interfering distributions under flow reversal. There appears at once the desired reverse-flow relation connecting the original forward and reverse flows:

$$\begin{aligned} D_{F,RF} &\equiv -\rho_0 \int_T (\mathbf{i}\times\boldsymbol{\omega}_R.\mathbf{V}_F + f_R\mathbf{i}.\mathbf{V}_F)\,dT \\ &= \rho_0 \int_T (\mathbf{i}\times\boldsymbol{\omega}_F.\mathbf{V}_R + f_F\mathbf{i}.\mathbf{V}_R)\,dT \equiv D_{R,FR}. \end{aligned} \tag{32}$$

The preceding relation (30) evidently applies to the special case of (32) where the distributions in forward and reverse flow are the same. With use of (5), (19), (20) and (22), the above may be written

$$\mathbf{U}_F.\int_T [\mathbf{V}_F\nabla.\mathbf{W}_R + \mathbf{V}_R\nabla.\mathbf{W}_F - \mathbf{W}_F\times(\nabla\times\mathbf{V}_R) - \mathbf{W}_R\times(\nabla\times\mathbf{V}_F)]\,dT = 0. \tag{33}$$

In order to discuss boundary conditions and surface pressures, the integration over the regions interior to any or all of the bodies may be transformed to an integral over the corresponding surfaces of A by means of the volume-surface integral identity

$$\begin{aligned} &\int_{T'} [\mathbf{V}_F\nabla.\mathbf{W}_R + \mathbf{V}_R\nabla.\mathbf{W}_F - \mathbf{W}_F\times(\nabla\times\mathbf{V}_R) - \mathbf{W}_R\times(\nabla\times\mathbf{V}_F)]\,dT \\ &\qquad = \oint_{A'} (\mathbf{V}_F\mathbf{W}_R.\mathbf{n} + \mathbf{V}_R\mathbf{W}_F.\mathbf{n} - \mathbf{V}_F.\mathbf{W}_R\mathbf{n})\,dS, \end{aligned} \tag{34}$$

where $\mathbf{n}$ is the outward unit normal to A'. This identity was used by Ursell & Ward (1950; see also Ward 1955*a*), and, when the subscripts simply identify two solutions, it serves for the construction of solutions to the simultaneous equations (19) and (20) as does Green's theorem for the related formulation of the theory in terms of the potential.

Unlike the corresponding transformation for the aerodynamic force, the use of (34) in (33) does not immediately give integrals of the form of (15) except for quasi-cylinders, in which case the last term in (34) is negligible and the Ursell–Ward theorem results at once. The desired mixed pressure-slope products can

be constructed by adding and subtracting terms, however, and the accretive terms will be shown in the next section to vanish; use of (31) and the relations

$$\mathbf{U}_R = -\mathbf{U}_F, \quad \mathbf{V}_F.\mathbf{W}_R = \mathbf{W}_F.\mathbf{V}_R$$

then gives the identity

$$\mathbf{U}_F.\oint_{A'}(\mathbf{V}_F\mathbf{W}_R.\mathbf{n}+\mathbf{V}_R\mathbf{W}_F.\mathbf{n}-\mathbf{V}_F.\mathbf{W}_R\mathbf{n})\,dS = \oint_{A'}[(\mathbf{U}_F.\mathbf{V}_F+\tfrac{1}{2}\mathbf{V}_F.\mathbf{W}_F)\,\mathbf{W}_R.\mathbf{n}$$
$$-(\mathbf{U}_R.\mathbf{V}_R+\tfrac{1}{2}\mathbf{V}_R.\mathbf{W}_R)\,\mathbf{W}_F.\mathbf{n}-\tfrac{1}{2}(\mathbf{V}_F+\mathbf{V}_R).(\mathbf{W}_F\mathbf{W}_R.\mathbf{n}-\mathbf{W}_R\mathbf{W}_F.\mathbf{n})$$
$$+\tfrac{1}{2}\mathbf{W}_F.\mathbf{V}_R(\mathbf{W}_F+\mathbf{W}_R).\mathbf{n}]\,dS. \tag{35}$$

When a body is not a quasi-cylinder, the choice of the surface of the related body in reverse flow is, by definition, limited.

The reverse-flow relation (32) or (33), together with the adjoining identities (34) and (35), can be used to provide information concerning the aerodynamic force on any body or arrangement of bodies to which linearized theory is applicable. Formulation in terms of volume integrals as well as surface integrals proves useful. The required relationships have been formally assembled here; their nature and implications are exhibited in the applications below.

Two-body arrangements in supersonic flow

Discussion

In this section the reverse-flow relation is used in several different ways for the determination of the drag and lift in supersonic flow of the interfering two-body arrangements shown in figure 1. Illustrated in figure 1 (*a*) is a fusiform body

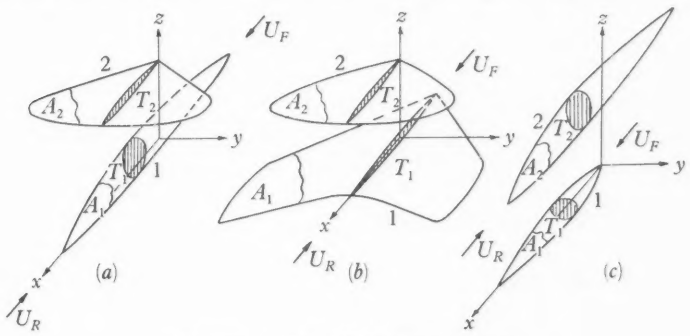

FIGURE 1. Two-body arrangements.

positioned under a wing; figure 1 (*b*) depicts a biplane; figure 1 (*c*) illustrates two fusiform bodies. The perturbation flow field in each case is generated by singularities distributed over the regions T_1 and T_2 interior to the bodies 1 and 2 with areas A_1 and A_2, respectively. The flow field of each isolated body, respectively $\mathbf{V}_1$ and $\mathbf{V}_2$, is assumed known in both forward and reverse flow; the analytical methods required are well known and need not be discussed here.

Most features of the three arrangements appear in a discussion of the first, which exhibits the mixed interfering boundary types: the fusiform body is not

a quasi-cylinder whereas the wing is a plane quasi-cylinder. Linearized theory gives the isolated flow field of the former to the approximation (11) and the latter to the approximation (10). Since the interference does not modify these considerations, the relative magnitudes of the two thickness ratios are taken to be related by

$$t_2 = O[t_1^2 \log t_1], \tag{36}$$

which defines the relative magnitudes of the perturbations. The order of approximation for the arrangement remains as in (11) in terms of t_1. The perturbation velocity satisfies (4), (5) and (6) and may be written

$$\mathbf{V} = \mathbf{V}_1 + \mathbf{V}_2 + \mathbf{V}_1' + \mathbf{V}_2', \tag{37}$$

where $\mathbf{V}_1'$ and $\mathbf{V}_2'$ are the interference flows created on A_1 and A_2, respectively, by the mutual cross-flow. Thus,

$$(\mathbf{V}_1' + \mathbf{V}_2 + \mathbf{V}_2').\mathbf{n} = 0 \quad \text{on } A_1, \tag{38}$$

and

$$(\mathbf{V}_2' + \mathbf{V}_1 + \mathbf{V}_1').\mathbf{n} = 0 \quad \text{on } A_2, \tag{39}$$

because $\mathbf{V}$ and $\mathbf{V}_1$ both satisfy (13) on A_1, and $\mathbf{V}$ and $\mathbf{V}_2$ both satisfy (13) on A_2. $\mathbf{V}_2'$ must also satisfy the Kutta condition

$$\mathbf{V}_2'.\mathbf{k} = \text{finite} \tag{40}$$

on any subsonic trailing edges of A_2. The components of the perturbation velocity associated with the fusiform body are dissimilar in magnitude near its surface and the required quadratic expression (17) for the pressure must be applied to the complete field (37), in general, because of quadratic coupling. On A_2, however, the components of $\mathbf{V}_1$ are all of order $t_1^2 \log t_1$ like the components of $\mathbf{V}_2$ and $\mathbf{V}_2'$. Equation (16) is then sufficient on A_2 or its reference surface.

The problem of the determination of $\mathbf{V}_2'$ is that of the cambered wing. The cancellation of the cross-flow of $\mathbf{V}_2 + \mathbf{V}_2'$ on A_1 with $\mathbf{V}_1'$ could be accomplished with a line of multipoles using the method of von Kármán & Moore (1932). A different approach is possible, however, which provides information required for the application of the reverse-flow relation. Lighthill (1948; see also Ward 1955*a*) has given the solution for the flow past a yawed axisymmetric fusiform body which has a ducted nose of finite diameter and a finite number of discontinuities in slope, but which otherwise fulfils the requirements of slenderness. The discontinuities in u at the surface due to the discontinuous cross-flow at the nose and to the discontinuous slopes are two-dimensional; the associated flow fields subside in a few diameters. It is found that the circumferential flow along the sections by planes $x = \text{const.}$ may be computed with unmodified slender body theory for the purpose of computing the drag from (17). Lighthill (1954) has suggested that a more general fusiform body may be built up from this solution for a finite number of jumps in slope and camber on a slender body by passing to the limit of an infinite number of smoothed discontinuities. The solution for $\mathbf{V}_1$ can be constructed in this way. The same approach would also apply for the determination of the camber-like interference flow $\mathbf{V}_1'$ produced by the wing cross-flow, which will, in general, exhibit discontinuities and vary too rapidly with x to excite an interference potential satisfying the Laplace equation

in the cross-planes. Since the cross-flow is of order $t_1^2 \log t_1$, it is seen from Lighthill's solution that u_1' will be of order $t_1^2 \log t_1$ at discontinuities in cross-flow and $t_1^3 \log t_1$ when the cross-flow varies slowly with x; Lighthill's generalization would then give actual magnitudes of u_1' within this range. Further, the gross order of magnitude of the circumferential flow associated with $\mathbf{V}_1'$ on A_1 is then $t_1^2 \log t_1$ from slender body theory. The gross circumferential flow associated with $\mathbf{V}_1$ must be of order t_1 and, according to these results, may be computed from slender body theory even if the body is not slender. This information is required to discuss the accretive terms in (35).

Remarks concerning the phenomena on the surface A_2 in figure 1 (*a*) apply to both surfaces in figure 1 (*b*). Remarks concerning phenomena on A_1 apply to both surfaces in figure 1 (*c*).

Reversal of flow direction with unchanged geometry

Suppose first that the direction of flow is reversed without changing the geometry or orientation, measured with respect to the invariant co-ordinate system, of each isolated body in the arrangements considered. Interference flows are used in both directions, so that no geometric change due to interference accompanies the reversal. The required singularity distributions are, however, quite different.

Choose $T = T_1 + T_2$, $A = A_1 + A_2$, substitute (34) into (33), and use (35) and (7) in the result, to obtain

$$\oint_{A_1+A_2} [(-p_F/\rho_0)\,\mathbf{W}_R.\mathbf{n} + (p_R/\rho_0)\,\mathbf{W}_F.\mathbf{n} - \tfrac{1}{2}(\mathbf{V}_F+\mathbf{V}_R).(\mathbf{W}_F\mathbf{W}_R.\mathbf{n} - \mathbf{W}_R\mathbf{W}_F.\mathbf{n}) + \tfrac{1}{2}\mathbf{W}_F.\mathbf{V}_R(\mathbf{W}_F+\mathbf{W}_R).\mathbf{n}]\,dS = 0. \quad (41)$$

In the reverse flow

$$\mathbf{W}_R.\mathbf{n} = -\mathbf{U}_R.\mathbf{n} \quad \text{on } A_1 \text{ and } A_2, \quad (42)$$

and from (31)

$$(\mathbf{W}_F+\mathbf{W}_R).\mathbf{n} = 0. \quad (43)$$

Equation (41) becomes

$$\oint_{A_1+A_2} [(p_F/\rho_0)\,\mathbf{U}_R.\mathbf{n} - (p_R/\rho_0)\,\mathbf{U}_F.\mathbf{n} + \tfrac{1}{2}(\mathbf{V}_F+\mathbf{V}_R).(\mathbf{W}_F+\mathbf{W}_R)\,\mathbf{W}_F.\mathbf{n}]\,dS = 0. \quad (44)$$

Introduce on the surface A_1, say, of a fusiform body an orthogonal curvilinear co-ordinate system. At each point on the section of A_1 by planes $x = \text{const.}$, let $\mathbf{i}$ be the unit vector previously defined, $\mathbf{N}$ be the unit outward normal, and $\boldsymbol{\sigma}$ be the unit tangent. The scalar product in the last term of (44) may be written

$$(\mathbf{V}_F+\mathbf{V}_R).(\mathbf{W}_F+\mathbf{W}_R) = -B^2[(\mathbf{V}_F+\mathbf{V}_R).\mathbf{i}]^2 + [(\mathbf{V}_F+\mathbf{V}_R).\mathbf{N}]^2 + [(\mathbf{V}_F+\mathbf{V}_R).\boldsymbol{\sigma}]^2. \quad (45)$$

The first term is of higher order as for the pressure relation (7). In the boundary condition (13), $\mathbf{V}.\mathbf{n}$ may be replaced by $\mathbf{V}.\mathbf{N}$ in linear theory, so that

$$(\mathbf{V}_F+\mathbf{V}_R).\mathbf{N} = 0. \quad (46)$$

With regard to the last term, expand $\mathbf{V}_F$ and $\mathbf{V}_R$ according to (37). For isolated closed slender bodies, the forward and reverse flows differ only in sign. Thus, even for arbitrary fusiform bodies, the circumferential components on A_1 of order t_1 vanish:

$$(\mathbf{V}_{1F}+\mathbf{V}_{1R}).\boldsymbol{\sigma} = 0. \quad (47)$$

The remaining circumferential components are of order $t_1^2 \log t_1$ so that their squares are negligible in (44). Note that no mixed products of order $t_1^3 \log t_1$ appear; terms of this order could not be discarded.

On wing surfaces the last term in (44), as well as the quadratic terms in the pressure relation, are negligible *a priori*. Equation (44) therefore reduces to

$$\oint_{A_1+A_2} p_F \mathbf{n}.\mathbf{i} dS = -\oint_{A_1+A_2} p_R \mathbf{n}.\mathbf{i} dS, \tag{48}$$

or† $$D_F = D_R \tag{49}$$

for the three arrangements.

Evidently, the drag is also invariant under flow reversal with unchanged geometry for the special cases of an isolated, arbitrary, closed fusiform body and an isolated wing. If the former is a slender body, then this result follows independently from (30). For the latter and for other quasi-cylinders as in figure 1 (*b*), the same result follows from the Ursell–Ward theorem, to which bodies it is applicable. The surfaces A may then be taken as both sides of the reference surfaces, the spatial distributions of singularities becoming surface distributions.

Reversal of flow direction with mutual distortion

Suppose next that the direction of flow is reversed without changing the geometry or orientation of each isolated body which appears in the arrangements considered. Now, however, interference flows are used only in the forward stream. In the reverse stream each body induces a cross-flow over the surface of the other, resulting in mutual geometric distortion when the bodies interfere. The reverse flow is completely defined by the geometry of the isolated bodies. The reverse-flow theorem is used to relate the drag in the forward flow of interest to the reverse flow discussed. For reasons already mentioned, it is sufficient to consider the boundary conditions and surface pressures in the reverse flow on the surfaces of the isolated bodies A_1 and A_2 instead of on the true distorted surfaces; use may then be made of (34).

Consider specifically the arrangement in figure 1 (*a*) and choose again $T = T_1 + T_2$, $A = A_1 + A_2$. If (34) is substituted into (33) and use is made of (35), the pressure relations, and the expressions

$$\mathbf{V}_R = \mathbf{V}_{1R} + \mathbf{V}_{2R}, \tag{50}$$

$$(\mathbf{W}_F + \mathbf{W}_{1R}).\mathbf{n} = 0 \quad \text{on } A_1, \tag{51}$$

there results after several cancellations

$$\oint_{A_2} [-(p_F/\rho_0)\mathbf{W}_{2R}.\mathbf{n} + (p_R/\rho_0)\mathbf{W}_F.\mathbf{n} - (p_F/\rho_0)\mathbf{W}_{1R}.\mathbf{n}]\, dS$$
$$+ \oint_{A_1} [-(p_F/\rho_0)\mathbf{W}_{1R}.\mathbf{n} + (p_R/\rho_0)\mathbf{W}_F.\mathbf{n} + \mathbf{U}_F.\mathbf{V}_F\mathbf{W}_{2R}.\mathbf{n}$$
$$+ \tfrac{1}{2}(\mathbf{V}_F + \mathbf{V}_{1R} + \mathbf{V}_{2R}).(\mathbf{W}_F + \mathbf{W}_{1R} + \mathbf{W}_{2R})\mathbf{W}_F.\mathbf{n}]\, dS = 0. \tag{52}$$

† This result must be qualified when wing edge forces are present. With use of tubular surfaces enclosing the singular edges, the result is found to hold for the drag including the contribution thereto of edge forces due to parabolic bluntness but, when the Kutta condition is satisfied in both directions, excluding the contribution thereto of edge forces due to suction.

As above, the scalar product in the last term in (52) may be written

$$(\mathbf{V}_F+\mathbf{V}_{1R}+\mathbf{V}_{2R}).(\mathbf{W}_F+\mathbf{W}_{1R}+\mathbf{W}_{2R}) = -B^2[(\mathbf{V}_F+\mathbf{V}_{1R}+\mathbf{V}_{2R}).\mathbf{i}]^2 + [(\mathbf{V}_F+\mathbf{V}_{1R}+\mathbf{V}_{2R}).\mathbf{N}]^2+[(\mathbf{V}_F+\mathbf{V}_{1R}+\mathbf{V}_{2R}).\boldsymbol{\sigma}]^2. \quad (53)$$

The first term is negligible. In the second term, $(\mathbf{V}_F+\mathbf{V}_{1R}).\mathbf{N} = 0$ and $\mathbf{V}_{2R}.\mathbf{N}$ makes a negligible contribution. In the third term, $\mathbf{V}_F$ is expanded using (37); $(\mathbf{V}_{1F}+\mathbf{V}_{1R}).\boldsymbol{\sigma} = 0$ and the remaining four components are negligible.

In the remainder of (52), use is next made of the boundary conditions satisfied by the several perturbation velocities, and there is obtained†

$$D_F \equiv -\oint_{A_1} p_F\mathbf{n}.\mathbf{i}dS-\oint_{A_2} p_F\mathbf{n}.\mathbf{i}dS = \oint_{A_1} p_R\mathbf{n}.\mathbf{i}dS + \oint_{A_2} p_R\mathbf{n}.\mathbf{i}dS-\oint_{A_1}(-\rho_0\mathbf{U}_F.\mathbf{V}_F)\frac{1}{U_R}\mathbf{V}_{2R}.\mathbf{N}dS-\oint_{A_2} p_F\frac{1}{U_R}\mathbf{V}_{1R}.\mathbf{N}dS. \quad (54)$$

Here $\mathbf{n}$ is the outward unit normal to the undistorted surfaces in forward flow and the pressure p in each integral is as (16) or (17), according to the surface. The drag in forward flow is given by (54) as the drag in reverse flow due to the reverse pressures supported on the undistorted boundaries A_1 and A_2, minus

FIGURE 2. Example in which neither interference flow influences other body.

the drag in forward flow due to the forward pressures supported on the inclined stream surfaces which are induced on each boundary by the cross-flow from the other in reverse flow. Note, however, that the linear pressure relation is to be used in the latter over the surface A_1, instead of the quadratic relation generally appropriate to the nonquasi-cylindrical surface.

Suppose that the interference flow created on each surface in the forward direction does not influence the other surface, as illustrated in figure 2. An example which is appropriate to figure 1 (*b*) of this type of interference is the two-dimensional Busemann biplane or a three-dimensional counterpart. The portion of the surface of each body in the domain of dependence of the other is then not influenced by the interference. Since the domain of dependence of a body in forward flow is its domain of influence in reverse flow, the surface pressures in the last two integrals of (54) depend on only the respective isolated flows over those portions of the surfaces where the reverse cross-flow is different from zero. The drag of the arrangement in forward flow can then be computed from (54) without determining the two interference flow fields. What is required is the flow field of each isolated body in reverse flow and the surface pressure on each isolated forebody in forward flow. When the reflexions are multiple, (54) requires

† The footnote to (49) applies as well to (54). The integrals must be interpreted to include the contribution of any edge parabolic bluntness.

that the interference field be determined only over the portion of each body which appears in the domain of dependence of the other.

Equation (54) and its implications apply as well to the arrangements in figure 1 (*b*) and (*c*). In the latter case, however, the linear pressure relation is to be used in the last integral.

Subject to the edge-force qualification, (49) can be used together with (54) so that the mutual distortion occurs in the flow direction of interest. For example, Friedman & Cohen (1954) have considered two unyawed Sears–Haack bodies of revolution interfering as shown in figure 1 (*c*) in a supersonic flow (regarded here as the reverse flow). They neglected the pressures of the interference flows and took for D_R the first two integrals in the right member of (54). The remaining two integrals can be used to estimate the error. For single reflexions, the surface pressure on each body in forward flow is symmetric about its horizontal plane of symmetry and the normal cross-flow is almost antisymmetric. Therefore, the last two integrals are very small. Expansion of the cross-flow about the body axis and account for the asymmetric surface of integration gives the order of the last two integrals as no larger than $t_1^6 \log t_1$, which is negligible next to the order $t_1^4 \log t_1$ of the leading two.

Use of both volume and surface integrals

The applications of the reverse-flow relation given thus far utilize surface integrals. When, for example, only part of the complete perturbation field is to be considered in one or both flow directions, as on surfaces where superposition is permissible, it is convenient to employ volume integrations for any other bodies which are not quasi-cylinders, in order to use the drag decomposition discussed. Two such applications will now be presented in connexion with the arrangement in figure 1 (*a*).

Choose $T = T_1 + T_2$ in (33) and use (34) in the second volume integral. After comparison of the first with (32), there is obtained

$$\oint_{A_2} (\mathbf{U}_F . \mathbf{V}_F \mathbf{W}_R . \mathbf{n} - \mathbf{U}_R . \mathbf{V}_R \mathbf{W}_F . \mathbf{n}) \, dS + U_F \int_{T_1} (\mathbf{i} \times \boldsymbol{\omega}_R . \mathbf{V}_F + \mathbf{i} \times \boldsymbol{\omega}_F . \mathbf{V}_R + f_R \mathbf{i} . \mathbf{V}_F + f_F \mathbf{i} . \mathbf{V}_R) \, dT = 0. \quad (55)$$

The first application is concerned with a rearrangement of (54). Let

$$\mathbf{V}_F = \mathbf{V}_{1F} + \mathbf{V}'_{1F} + \mathbf{V}_{2F} + \mathbf{V}'_{2F} \quad \text{and} \quad \mathbf{V}_R = \mathbf{V}_{1R}. \quad (56)$$

Equations (56) are substituted in (55) and use is made of the facts that $\boldsymbol{\omega}_{2F}$, $\boldsymbol{\omega}'_{2F}$, $_{2F}$ and f'_{2F} vanish over T_1, and that the interference effects among the singularities distributed over T_1 vanish separately in virtue of (32). Insertion of (16) and (31) in the result gives

$$\oint_{A_2} p_{1R} \mathbf{n} . \mathbf{i} \, dS - \oint_{A_2} p_F \frac{1}{U_R} \mathbf{V}_{1R} . \mathbf{N} \, dS = \rho_0 \int_{T_1} (\mathbf{i} \times \boldsymbol{\omega}_{1R} + f_{1R} \mathbf{i}) . (\mathbf{V}_{2F} + \mathbf{V}'_{2F}) \, dT. \quad (57)$$

Comparison with the right member of (54) shows that (57) re-expresses the sum of the fourth integral plus the contribution of p_{1R} to the second integral as a drag

due to the cross-flow and pressure of $\mathbf{V}_{2F}$ and $\mathbf{V}'_{2F}$ on the known distribution of singularities representing the isolated body in reverse flow. The remaining part of the second integral in the right member of (54) is the drag of the isolated wing in reverse flow. When (57) is used in (54), the flow field of the fusiform body in reverse flow is required only over its surface. But the complete flow field of the isolated wing in both forward and reverse flow is then needed. As has already been discussed, $\mathbf{V}'_{2F}$ vanishes over T_1 for single interference reflexions. The two surface integrals over A_1 in the right member of (54) can also be written as volume integrals over T_1 with the aid of (34).

The second application is concerned with the lift of the arrangement in figure 1 (*a*). The lift in forward flow is that supported by the wing and follows by superposing the pressure due to $\mathbf{V}_{2F}$ and $\mathbf{V}'_{2F}$. The latter interference lift, given by

$$L'_F = 2\int_{\mathscr{A}_2} p'_{2F}\,dS, \tag{58}$$

where $\mathscr{A}_2$ is the lower side of A_2, can be obtained with a technique suggested by one used for isolated wings. Let $\mathbf{V}^*_{2R}$ be the perturbation velocity induced by a flat plate in reverse flow which has an angle of attack α^* and the same plan-form as the actual wing. To obtain this lift, the Kutta condition must be fulfilled by $\mathbf{V}^*_{2R}$ on any subsonic reverse trailing edges to exclude edge force contributions. If the actual wing is without camber and twist, $\mathbf{V}^*_{2R}$ can correspond to the odd part of the actual reverse-flow potential of the isolated wing, and α^* can be the actual angle of attack. Let

$$\mathbf{V}_F = \mathbf{V}_{1F} + \mathbf{V}'_{1F} + \mathbf{V}'_{2F}, \quad \mathbf{V}_R = \mathbf{V}^*_{2R}, \tag{59}$$

and substitute in (55). The vanishing of some vorticity and source terms over T_1 is then noted, the boundary conditions

$$\mathbf{W}_F.\mathbf{n} = 0 \quad \text{on } A_2, \tag{60}$$

and

$$\mathbf{W}_R.\mathbf{n} = \begin{cases} U_R\alpha^* & \text{on lower } A_2, \\ -U_R\alpha^* & \text{on upper } A_2, \end{cases} \tag{61}$$

are utilized, and (16) is inserted. The contributions of p_{1F} and p'_{1F} vanish in the leading term because of (61), p'_{2F} is odd in z, and α^* is constant. The result is seen to be

$$\alpha^* L'_F \equiv 2\alpha^* \int_{\mathscr{A}_2} p'_{2F}\,dS = -\rho_0 \int_{T_1} [\mathbf{i}\times(\boldsymbol{\omega}_{1F}+\boldsymbol{\omega}'_{1F}).V^*_{2R} + (f_{1F}+f'_{1F})\,\mathbf{i}.\mathbf{V}^*_{2R}]\,dT. \tag{62}$$

The interference lift in forward flow is expressed here in terms of an interference drag supported by the forward singularities interior to the interfering body, and due to the cross-flow and streamwise perturbations of the plate wing in reverse flow. For single reflexions, $\boldsymbol{\omega}'_{1F}$ and f'_{1F} vanish in the right member and the interference lift is then determined without knowledge of the interference flows, as before. In fact, the lift can still be determined in this way if $\mathbf{V}'_2$ does influence the fusiform body.

The identity (34) does not transform the volume integrals in the right members of (57) and (62) to surface integrals involving only the mixed pressure-slope

products suggested by the respective integrands unless the cubic terms are suppressed, as for quasi-cylinders; the accretive terms could be evaluated, but, for them to vanish, it is necessary that the effects of the isolated body appear in the final expressions for both flow directions (cf. (45) and (53)). This consequence of the facts that the body pressure relation is non-linear and variations across the body cannot be neglected is otherwise simply illustrated in (57), say, by setting $\boldsymbol{\omega}_{1R} = 0$ and $f_{1R}dT = U_R S'(x)\,dx$ for a line of sources representing a slender body; there results a line integral of the wing-induced linear pressure and body area along its axis. For applications such as the two just given, however, transformation is neither necessary, since boundary conditions are not in question, nor desirable, since the evaluation of surface integrals is generally more troublesome than the evaluation of the line integrals which commonly appear in specific problems.

This research was supported by the United States Air Force through the Air Force Office of Scientific Research, Air Research and Development Command, under Contract no. AF 18(600)–664.

REFERENCES

Friedman, M. D. & Cohen, D. 1954 *Nat. Adv. Comm. Aero., Wash., Tech. Note*, no. 3345.

Graham, M. E. 1955 *Douglas Aircraft Company, Rep.* no. SM-19258.

Graham, E. W., Lagerstrom, P. A., Licher, R. M. & Beane, B. J. 1957 *Nat. Adv. Comm. Aero., Wash., Tech. Mem.* no. 421.

Hayes, W. D. 1947 *North American Aviation, Rep.* no. AL-222.

Heaslet, M. A. & Lomax, H. 1954 *High Speed Aerodynamics and Jet Propulsion.* Vol. vi, Sec. D, p. 122. Princeton University Press.

Heaslet, M. A. & Spreiter, J. R. 1953 *Nat. Adv. Comm. Aero., Wash., Rep.* no. 1119.

Jones, R. T. 1951 *J. Aero. Sci.* **18**, 75.

Jones, R. T. 1956 *Nat. Adv. Comm. Aero., Wash., Tech. Note*, no. 3530.

Kármán, T. von 1947 *J. Aero. Sci.* **14**, 373.

Kármán, T. von & Moore, N. B. 1932 *Trans. Amer. Soc. Mech. Engin.* **54**, 303.

Lawrence, H. R. & Flax, A. H. 1954 *J. Aero. Sci.* **21**, 289.

Licher, R. M. 1955 *Douglas Aircraft Company, Rep.* no. SM-19257.

Lighthill, M. J. 1945 *Rep. Mem. Aero. Res. Counc., Lond.*, no. 2003.

Lighthill, M. J. 1948 *Quart. J. Mech. Appl. Math.* **1**, 90.

Lighthill, M. J. 1954 *High Speed Aerodynamics and Jet Propulsion.* Vol. vi, Sec. E, p. 345. Princeton University Press.

Lomax, H. 1955 *Nat. Adv. Comm. Aero., Wash., Res. Mem.* no. A55A18.

Lomax, H. & Heaslet, M. A. 1956*a* *Nat. Adv. Comm. Aero., Wash., Rep.* no. 1282.

Lomax, H. & Heaslet, M. A. 1956*b* *J. Aero. Sci.* **23**, 1061.

Lomax, H., Heaslet, M. A. & Fuller, F. B. 1951 *Nat. Adv. Comm. Aero., Wash., Rep.* no. 1054.

Ursell, F. & Ward, G. N. 1950 *Quart. J. Mech. Appl. Math.* **3**, 326.

Ward, G. N. 1949 *Quart. J. Mech. Appl. Math.* **2**, 75.

Ward, G. N. 1952*a* *Quart. J. Mech. Appl. Math.* **5**, 432.

Ward, G. N. 1952*b* *Quart. J. Mech. Appl. Math.* **5**, 441.

Ward, G. N. 1955*a* *Linearized Theory of Steady High-Speed Flow.* Cambridge University Press.

Ward, G. N. 1955*b* *The College of Aeronautics, Cranfield.* Report 88.

A theory of electromagnetically driven shock waves

By J. K. WRIGHT AND M. C. BLACK
Atomic Weapons Research Establishment, Foulness, Essex

(Received 5 December 1958)

During the last few years, many experimental devices have been built in which strong shock waves are generated in gases by electromagnetic forces on current-carrying gas particles. The general theory of these devices is discussed, taking external circuit inductance into account. It is shown that a shock wave of constant speed is finally attained. This shock wave is travelling at 90 % of its final speed when the circuit inductance has increased to 3·0 times its initial value.

1. Introduction

In recent years some attention has been directed towards producing strong shock waves in a gas by means of a technique known as electromagnetic driving. The apparatus used may take a variety of forms but the basic principles are very similar. Figure 1 (*a*) shows a simple arrangement as used, for example, by Kolb (1957). A low inductance condenser bank is discharged between two electrodes in a gas. The return path is close to the discharge and the electromagnetic interaction between them drives the current-carrying gas particles away from the return lead with such a force that an intense shock wave is produced.

The electromagnetic forces can be considered in various equivalent ways. One method is to treat the current in the gas as being in the magnetic field due to the current in the return path, but a more convenient approach from our point of view is to look upon the magnetic field H as exerting a pressure $H^2/8\pi$ normal to the field and a tension $H^2/8\pi$ in the direction of the field on the current-carrying gas particles. (Here and throughout this paper the electromagnetic system of units is employed.) In our case the motion is normal to the direction of the field and the hydrodynamics of the gas can therefore be analysed by assuming that the current sheet is forced forwards by a piston exerting a pressure $H^2/8\pi$, and in fact the magnetic field is often said to act as a 'magnetic piston'. Another possible apparatus for generating strong shocks is depicted in figure 1 (*b*). Here the currents in the gas are confined to a cylindrical sheet which is driven inwards under the action of the circumferential magnetic field. At low ambient gas pressures, a stream of high energy particles is driven towards the axis and this is the basis of the various high-speed pinch devices that have been reported by Artsimovich *et al.* (1956), Anderson *et al.* (1957), Bodin & Reynolds (1957), and Hagerman & Mather (1958). At higher gas pressures, collisions occur between the accelerated particles and the relatively stationary particles ahead of them and an imploding shock wave is produced.

It is also possible to produce a cylindrically imploding shock by the electrodeless discharge arrangement shown in figure 1(*c*). When the switch is closed, a current starts to flow in the circuit round the discharge tube. The consequent electric field induced in the gas is greatest at the walls and a current flows in the opposite direction to the primary current. In this case the current paths are

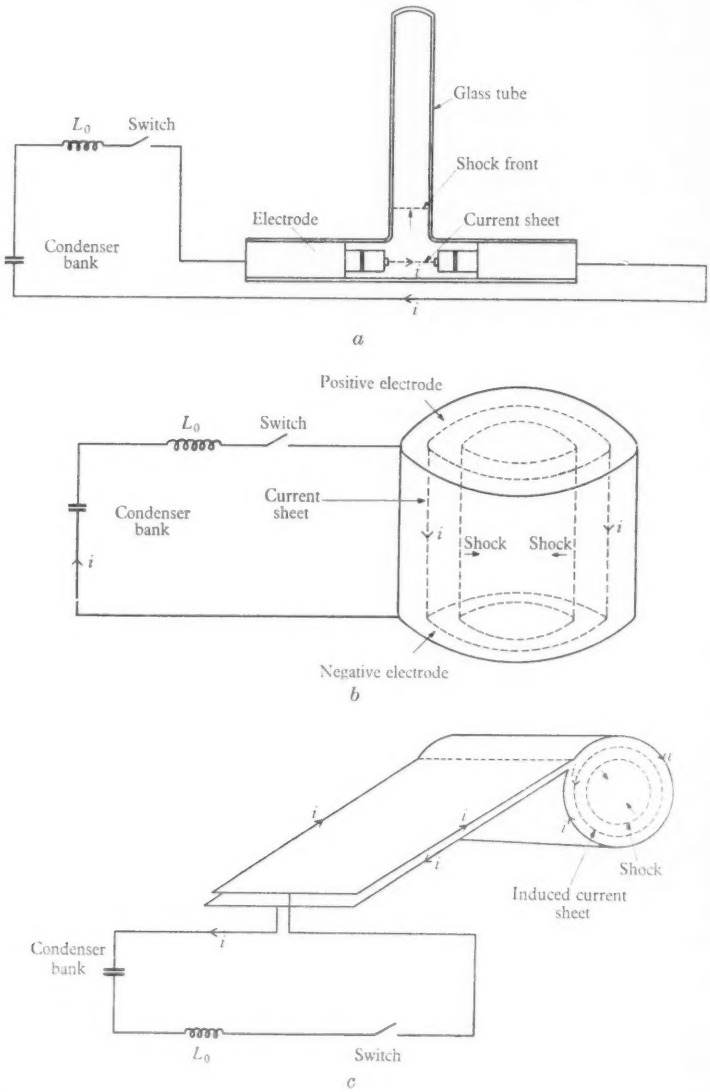

FIGURE 1. Various experimental arrangements for the production of strong shock waves using electromagnetic driving. In each of the arrangements the magnetic field produced by the discharge acts on the current-carrying gas particles which are driven under the action of the Lorentz force.

circumferential and the gas particles are driven inwards by the longitudinal magnetic field. This is the basis of the device reported by Elmore, Little & Quinn (1958).

Although the three practical arrangements differ from each other in their geometrical patterns, when the discharge is first formed the effect of the cylindrical convergence in the cases shown in figures 1 (*b*) and 1 (*c*) is negligible, and we may obtain results applicable to all three devices by analysis of the simple arrangement shown in figure 2. This consists of two parallel plane electrodes of breadth a a distance b apart. When the switch is closed the gas breaks down and currents flow along the path of minimum inductance, i.e. close to the return path. This situation has been analysed by Allen (1957), who assumed that (*a*) the conductivity of the circuit is infinite, (*b*) the thickness of the shock wave is small compared with the dimensions of the discharge chamber, and (*c*) the current rises instantaneously from zero to a finite value and then remains constant.

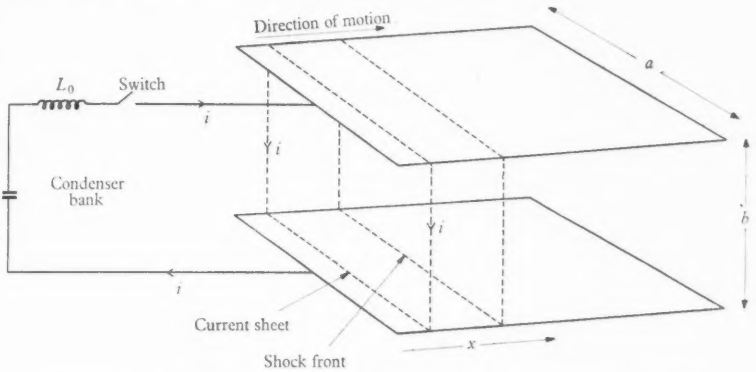

FIGURE 2. A simple one-dimensional model of the electromagnetically driven shock wave apparatus.

In practice there will be a finite time before the steady-state condition (*c*) is attained since the external circuit will have a finite inductance L_0, even initially when the current in the gas chooses the path for which this inductance is a minimum. It is the purpose of this investigation to determine the time taken for the current to build up to its steady value and the effect of the formation time on the structure of the generated shock wave.

In §2 we discuss the equations of motion of the conducting gas and the relevant boundary conditions, putting them in a non-dimensional form convenient for analysis. In §3 we consider the phenomena occurring at a very early stage in the discharge. Here the circuit inductance has risen from L_0 to $L_0 + L$ and we assume L to be negligible compared with L_0. This gives a very convenient similarity solution, which is improved upon in §4 by including L in the equations and using Taylor series expansions. The expansions are applicable, however, only so long as τ, a non-dimensional time, is small. We use this solution as a starting-point for the solution of the whole flow, obtained by the method of characteristics, and this is described in §5. The results are discussed in §6.

2. Basic theory

In our system we have three regions. First of all there is the gas ahead of the shock front which is in its ambient non-ionized condition. There is no magnetic field in this region. Then there is the region of shocked gas where again there is no magnetic field. The boundary conditions between the first and second regions are the normal Rankine–Hugoniot relations for a gas in the absence of a magnetic field. Finally there is the third region where there is no gas but a magnetic field H. There is a current sheet in the gas at the boundary between regions two and three and the boundary conditions equate magnetic pressure in region three with hydrodynamic pressure in region two.

Using Lagrangian co-ordinates, we formulate the equations of motion and boundary conditions of the conducting gas. Let s be the Lagrangian co-ordinate of a particle, and x be the position of that particle at time t. We denote by u, p and ρ the particle speed, pressure, and density at the point (s, t). The gas is initially at rest with density ρ_0.

Equations of motion of the gas

The equations of conservation of mass and momentum are

$$\rho \frac{\partial x}{\partial s} = \rho_0, \tag{2.1}$$

$$\rho \frac{\partial u}{\partial t} = -\frac{\partial p}{\partial x}. \tag{2.2}$$

Using (2.1) and $\dfrac{\partial p}{\partial x} = \dfrac{\partial p}{\partial s} \Big/ \dfrac{\partial x}{\partial s}$ we rewrite (2.2) as

$$\rho_0 \frac{\partial u}{\partial t} = -\frac{\partial p}{\partial s}. \tag{2.3}$$

Once the element of gas with co-ordinate s has been shocked, all further changes at this element are isentropic. This gives a third equation of motion

$$\frac{\partial}{\partial t}(p\rho^{-\gamma}) = 0, \tag{2.4}$$

where for a fully ionized gas, $\gamma = \frac{5}{3}$.

Boundary conditions at the shock

At the shock front we have the boundary conditions

$$x = s, \tag{2.5}$$

and

$$\frac{ds}{dt} = U, \tag{2.6}$$

where U is the velocity of the shock.

We assume that the magnetic pressure is at all times much greater than the ambient pressure so that the Rankine–Hugoniot relations for a singly ionized gas take the simple 'strong shock' form,

$$\rho = 4\rho_0, \tag{2.7}$$

$$u = \tfrac{3}{4}U, \tag{2.8}$$

$$p = \tfrac{4}{3}\rho_0 u^2. \tag{2.9}$$

In these equations, allowance has been made for the partial pressure of the electrons which are supposed to be in thermal equilibrium with the ions, and the ionization and dissociation energies are supposed negligible compared with the thermal energy of the gas.

Boundary conditions at the current sheet

At the current sheet we may equate the magnetic pressure $H^2/8\pi$ outside the gas with the hydrodynamic pressure inside, giving

$$p = \frac{H^2}{8\pi}.$$

H is related to the current i in the discharge, and we may write

$$p = \frac{2\pi i^2}{a^2}. \tag{2.10}$$

When the low impedance current source at a constant potential V_0 is connected to the circuit of negligible resistance and constant inductance L_0, the discharge voltage is given by

$$V = V_0 - L_0 \frac{di}{dt}. \tag{2.11}$$

We also have

$$V = \frac{d}{dt}(Li). \tag{2.12}$$

Equating (2.11) with (2.12), we have

$$L_0 \frac{di}{dt} + \frac{d}{dt}(Li) = V_0,$$

which integrates to

$$(L_0 + L)\, i = V_0 t. \tag{2.13}$$

The inductance of the discharge circuit in the gas, L, is directly proportional to the distance x that the current sheet has travelled, and if the inductance L becomes equal to L_0 at a distance $x = x_0$ we may write $L/L_0 = x/x_0$ and hence equation (2.13) may be written

$$L_0\left(1 + \frac{x}{x_0}\right) i = V_0 t. \tag{2.14}$$

Eliminating i from (2.10) and (2.14), we obtain

$$p\left(1 + \frac{x}{x_0}\right)^2 = \frac{2\pi}{a^2} \frac{V_0^2}{L_0^2} t^2. \tag{2.15}$$

Equation (2.15) gives the boundary condition to be satisfied at the piston, whose Lagrangian co-ordinate is

$$s = 0. \tag{2.16}$$

Since the current takes some time to build up in the discharge, the initial magnetic pressure is very small, but as a consequence of our assumption that the shock pressure is much greater than the ambient pressure, a particle close to the current sheet that has just been shocked will have $\rho = 4\rho_0$ by equation (2.7). Since the pressure increases as the discharge current builds up, this gas particle is

compressed isentropically and its density increases. In the limit, at the current path, we may write

$$s = 0, \quad \rho = \infty. \tag{2.17}$$

We now reduce the equations of motion to a non-dimensional form by the following substitutions:

$$\left.\begin{aligned} \frac{x}{x_0} = \xi, \quad \frac{s}{x_0} = \alpha, \quad \frac{\rho}{\rho_0} = D, \quad \frac{u}{u^*} = v \\ \frac{U}{u^*} = w, \quad \frac{u^* t}{x_0} = \tau, \quad \frac{p}{\rho_0 (u^*)^2} = P, \end{aligned}\right\} \tag{2.18}$$

where

$$(u^*)^4 = \frac{V_0^2}{8\pi\rho_0 b^2}. \tag{2.19}$$

Equations (2.1), (2.3) and (2.4) become

$$D\frac{\partial \xi}{\partial \alpha} = 1, \tag{2.20}$$

$$\frac{\partial v}{\partial \tau} = \frac{\partial P}{\partial \alpha}, \tag{2.21}$$

$$\frac{\partial}{\partial \tau}(PD^{-\gamma}) = 0. \tag{2.22}$$

The boundary conditions at the shock, (2.5) to (2.9), become

$$\left.\begin{aligned} \xi = \alpha, \quad \frac{d\alpha}{d\tau} = w, \\ D = 4, \quad v = \tfrac{3}{4}w, \quad P = \tfrac{4}{3}v^2. \end{aligned}\right\} \tag{2.23}$$

The boundary conditions at the piston, (2.15) to (2.17), become

$$P(1+\xi)^{\gamma} = \tau^2, \quad \alpha = 0, \quad D = \infty. \tag{2.24}$$

3. Similarity solution at early times

In the initial stages we may neglect L compared with L_0. This has the effect of changing the first of the boundary conditions (2.24) at the piston to

$$P = \tau^2. \tag{3.1}$$

We now obtain our equations in terms of a new variable $\eta = \alpha/\tau^2$.

Let

$$P = \tau^2 P_1(\eta), \tag{3.2}$$

$$\xi = \tau^2 \xi_1(\eta), \tag{3.3}$$

$$D = D_1(\eta) \tag{3.4}$$

Equations (2.20) to (2.22) become

$$D_1 \frac{d\xi_1}{d\eta} = 1, \tag{3.5}$$

$$4\eta^2 \frac{d^2\xi_1}{d\eta^2} - 2\eta \frac{d\xi_1}{d\eta} + 2\xi_1 = -\frac{dP_1}{d\eta}, \tag{3.6}$$

$$\frac{d}{d\eta}\left\{\frac{P_1 D_1^{-\gamma}}{\eta}\right\} = 0. \tag{3.7}$$

If the position of the shock is $\eta = \beta$, i.e. $\alpha = \tau^2\beta$, then the speed of the shock is $w = d\alpha/d\tau = 2\tau\beta$, and $v = \frac{3}{4}w = \frac{3}{2}\tau\beta$. Thus the boundary conditions at the shock become

$$\xi_1 = \eta = \beta, \quad D_1 = 4, \quad P_1 = 3\beta^2. \tag{3.8}$$

The boundary conditions at the piston become

$$P_1 = 1, \quad \eta = 0, \quad D_1 = \infty. \tag{3.9}$$

We may integrate (3.7) and use the boundary conditions at the shock, giving

$$P_1 = 3\beta\eta\left(\frac{D_1}{4}\right)^{\gamma}. \tag{3.10}$$

Equations (3.5), (3.6) and (3.10) can be integrated numerically, giving

$$\beta = 0{\cdot}449 \quad \text{and} \quad [\xi_1]_{\eta=0} = -0{\cdot}388.$$

4. Taylor series extension

The solution in §3 is now extended using a Taylor series expansion, thus enabling us to correct for the boundary condition $P(1+\xi)^2 = \tau^2$.

Put

$$\xi = \tau^2\xi_1(1 + A\tau^2), \tag{4.1}$$

$$P = \tau^2 P_1(1 + B\tau^2), \tag{4.2}$$

$$D = D_1(1 + C\tau^2), \tag{4.3}$$

where A, B, and C are functions of η. Terms involving higher orders of τ are negligible for values of $\tau < 0{\cdot}35$.

Equations (2.20) and (2.21) become

$$R - C\frac{d\xi_1}{d\eta} = 0, \tag{4.4}$$

$$4\eta^2\frac{d^2R}{d\eta^2} - 10\eta\frac{dR}{d\eta} + 12R + \frac{dS}{d\eta} = 0, \tag{4.5}$$

where $R = A\xi_1$, $S = BP_1$, and equation (2.22) integrates to

$$PD^{-\gamma} = f(\alpha) \tag{4.6}$$

In our similarity solution we showed that when L is negligible (4.6) becomes

$$f(\alpha) = \frac{3\beta}{4^{\gamma}}\alpha. \tag{4.7}$$

We therefore apply a Taylor series expansion and write (4.6) in the extended case as

$$PD^{-\gamma} = \frac{3\beta}{4^{\gamma}}\alpha(1 + q\alpha), \tag{4.8}$$

where q is a constant and terms of $O(\alpha^3)$ are neglected. Substituting for P and D from (4.2) and (4.3), we obtain

$$S = P_1(\gamma C + q\eta). \tag{4.9}$$

The new shock position is then

$$\alpha_s = \beta\tau^2(1 + E\tau^2). \tag{4.10}$$

At the shock we have

$$\xi_s = \tau^2 \xi\left(\frac{\alpha_s}{\tau^2}\right)(1 + A\tau^2), \tag{4.11}$$

$$P_s = \tau^2 P\left(\frac{\alpha_s}{\tau^2}\right)(1 + B\tau^2), \tag{4.12}$$

$$D_s = D\left(\frac{\alpha_s}{\tau^2}\right)(1 + C\tau^2). \tag{4.13}$$

Equations (4.11) to (4.13) are expanded using (4.10), and our boundary conditions at the shock (2.23) become

$$A = \tfrac{3}{4}E, \quad B = \tfrac{39}{8}E, \quad C = \tfrac{9}{8}E. \tag{4.14}$$

The boundary conditions at the piston (2.24) become

$$S = -2[\xi_1]_{\eta=0}, \quad C = -\tfrac{6}{5}[\xi_1]_{\eta=0}. \tag{4.15}$$

Equations (4.4), (4.5) and (4.9), which are now no longer functions of η alone, can be integrated numerically for a particular value of τ, giving

$$\tau = 0{\cdot}35, \quad E = -0{\cdot}144, \quad \alpha_s = 0{\cdot}054, \quad q = -0{\cdot}981.$$

5. Solution by characteristics

The solution is now completed using the method of characteristics. From (2.20) and (2.21) we obtain the following relations which are used in finite difference form:

$$\delta v - \frac{1}{\sqrt{(\gamma PD)}}\delta P = 0 \quad \text{along} \quad \frac{d\alpha}{d\tau} = -\sqrt{(\gamma PD)}, \tag{5.1}$$

$$\delta v + \frac{1}{\sqrt{(\gamma PD)}}\delta P = 0 \quad \text{along} \quad \frac{d\alpha}{d\tau} = \sqrt{(\gamma PD)}. \tag{5.2}$$

The Taylor series expanded similarity solution may now be used as a starting-point for the numerical integration along the characteristics given by (5.1) and (5.2). This integration was carried out on the A.W.R.E. I.B.M. 704 computor until a shock wave of constant speed was attained.

6. Discussion of results

The position of the shock front and current sheet as a function of time are depicted in figure 3. The curves which are initially parabolic (similarity solution) tend asymptotically to straight lines when the steady state has been attained. Values of the non-dimensional hydrodynamic parameters at the shock front and current sheet are tabulated in table 1. The shock speed w has been calculated as a function of the final steady velocity attained w_f and the result is plotted in figure 4. It will be seen that the shock has achieved 90 % of its final speed after it has travelled a non-dimensional distance 2·5 in a non-dimensional time 3·1. At this time the current sheet has travelled a distance 2·0 units and the total inductance of the system has therefore risen from L_0 to $3{\cdot}0L_0$. We may therefore conclude that the constant current approximation of Allen becomes valid when

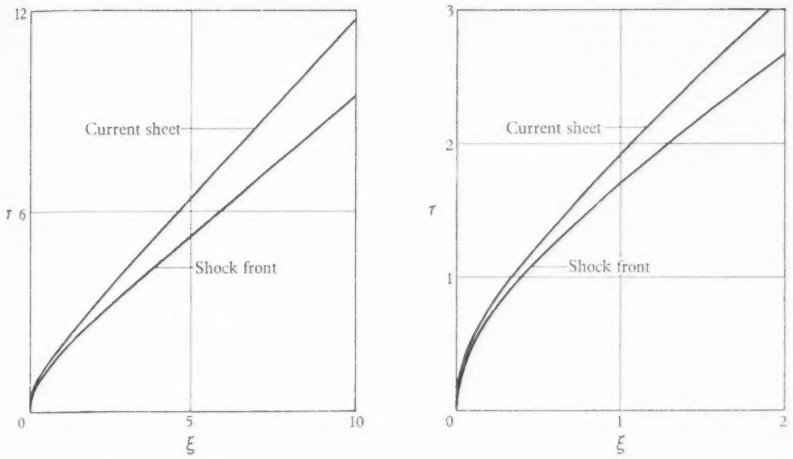

FIGURE 3. Distance–time plot showing the motion of shock front and current sheet. ξ is a non-dimensional distance and τ is a non-dimensional time.

	Piston					Shock				
τ	ξ	P	v	V/V_0	$i/i_{\max}$	ξ	P	v	w	w/w_f
0·05	0·00097	0·00250	0·0384	0·003	0·046	0·00112	0·00151	0·0337	0·0449	0·036
0·10	0·00387	0·00992	0·0767	0·012	0·093	0·00448	0·00601	0·0671	0·0895	0·072
0·15	0·00869	0·0221	0·114	0·025	0·138	0·0101	0·0134	0·0995	0·133	0·107
0·20	0·0154	0·0388	0·152	0·045	0·183	0·0179	0·0236	0·132	0·176	0·142
0·25	0·0240	0·0596	0·188	0·068	0·227	0·0279	0·0364	0·165	0·220	0·177
0·30	0·0343	0·0841	0·225	0·096	0·270	0·0400	0·0515	0·197	0·263	0·212
0·35	0·047	0·112	0·260	0·128	0·311	0·054	0·069	0·227	0·303	0·244
0·40	0·060	0·142	0·295	0·162	0·351	0·070	0·088	0·257	0·343	0·276
0·45	0·076	0·175	0·329	0·199	0·389	0·088	0·110	0·287	0·383	0·309
0·5	0·093	0·209	0·359	0·235	0·426	0·108	0·132	0·315	0·420	0·338
0·6	0·13	0·28	0·42	0·312	0·494	0·15	0·18	0·37	0·49	0·395
0·7	0·18	0·36	0·47	0·389	0·552	0·21	0·23	0·42	0·56	0·451
0·8	0·23	0·43	0·52	0·462	0·605	0·27	0·28	0·46	0·62	0·500
0·9	0·28	0·49	0·56	0·527	0·654	0·33	0·33	0·50	0·67	0·540
1·0	0·34	0·56	0·60	0·588	0·696	0·40	0·39	0·54	0·72	0·580
1·2	0·47	0·67	0·66	0·686	0·762	0·55	0·48	0·60	0·80	0·645
1·4	0·60	0·77	0·72	0·769	0·817	0·72	0·56	0·65	0·87	0·701
1·6	0·75	0·84	0·76	0·826	0·853	0·90	0·64	0·69	0·92	0·741
1·8	0·91	0·89	0·79	0·866	0·878	1·09	0·71	0·73	0·97	0·782
2·0	1·1	0·93	0·81	0·891	0·897	1·3	0·75	0·75	1·00	0·806
2·5	1·5	1·02	0·85	0·940	0·940	1·8	0·85	0·80	1·07	0·862
3·0	1·9	1·06	0·88	0·969	0·958	2·4	0·92	0·83	1·11	0·895
4·0	2·8	1·10	0·90	0·986	0·976	3·5	1·01	0·87	1·16	0·935
5·0	3·7	1·12	0·92	0·995	0·984	4·7	1·06	0·89	1·18	0·951
10·0	8·3	1·15	0·93	1·000	0·998	10·7	1·11	0·91	1·22	0·983

TABLE 1

the inductance of the system has increased to the order of three times its initial value.

When the steady state has been attained, the distance–time relationships for the piston and shock tend to the lines

$$\xi = 0{\cdot}93\tau - 1{\cdot}0, \tag{6.1}$$

and

$$\xi = 1{\cdot}24\tau - 1{\cdot}3, \tag{6.2}$$

corresponding to non-dimensional speeds of 0·93 and 1·24 respectively. Returning to our original physical units, we get final piston and shock speeds given by

$$u = 0{\cdot}416\left(\frac{V_0^2}{\rho_0 b^2}\right)^{\frac{1}{4}}, \quad U = 0{\cdot}554\left(\frac{V_0^2}{\rho_0 b^2}\right)^{\frac{1}{4}}. \tag{6.3}$$

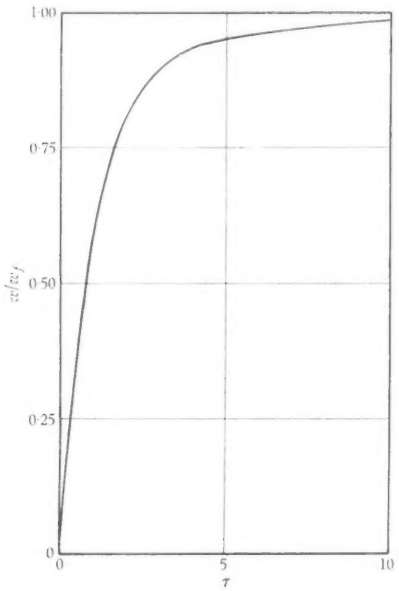

FIGURE 4. Shock speed as a function of time. w/w_f is the shock speed expressed as a ratio of that finally attained, and τ is a non-dimensional time.

The variation of voltage V across the discharge and current i as a function of time can be determined from the boundary conditions at the piston, equations (2.13) and (2.11). We obtain

$$i = \frac{V_0 x_0 \tau}{L_0 u^*(1+\xi)}, \quad V = V_0\left\{\frac{v\tau + \xi + \xi^2}{(1+\xi)^2}\right\}. \tag{6.4}$$

The values of V/V_0 and $i/i_{\max}$ are presented in table 1 and plotted as a function of time in figures 5 and 6.

We now consider the variations of pressure, density, temperature and particle speed in the gas with distance at various values of time. Typical results are presented in figure 7. It will be seen that the density rises rapidly towards the

piston. This is because a particle of gas that is initially close to the origin is compressed to 4 times its initial density by a relatively weak shock. As the current rises in the discharge, the pressure increases and this particle is compressed to a high density. At early stages of the discharge ($\tau = 0{\cdot}1,\ 0{\cdot}35$) the current is rising rapidly and the variation in density extends as far as the shock front, whereas at late stages ($\tau = 10{\cdot}0$) there is a layer of almost constant density behind the shock front before the thin highly compressed layer at the current sheet.

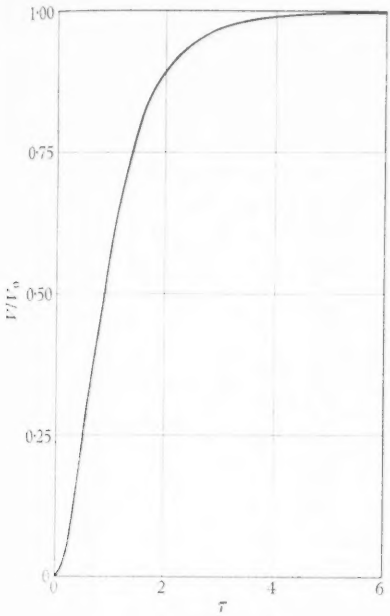

FIGURE 5

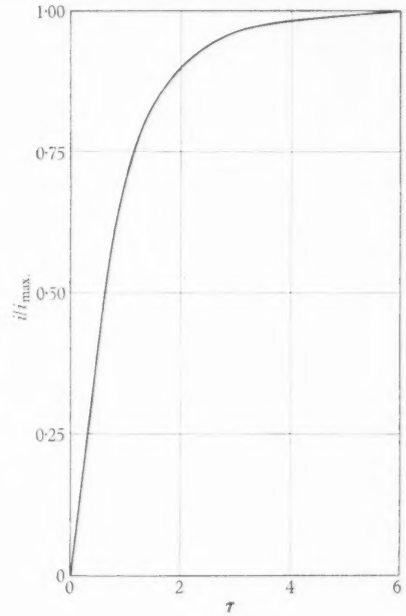

FIGURE 6

FIGURE 5. Voltage across the discharge as a function of time. V/V_0 is the discharge voltage compared with the source voltage, and τ is a non-dimensional time.

FIGURE 6. Discharge current as a function of time. i is the discharge current at non-dimensional time, τ, and i_{max} is the current when the shock has attained a constant speed.

At early stages in the discharge the pressure at the shock front is only 60 % of that at the current sheet. This is because the mass of shocked gas is being accelerated rapidly and there is therefore a large pressure gradient in the gas. As the steady state is gradually attained, the acceleration of the shocked gas falls off and the pressure gradient disappears. Thus, at time $\tau = 10$, the pressure at the shock is 96 % of that at the current sheet.

The variation in temperature in the gas can be easily interpreted since it is proportional to pressure divided by density. At early stages there is a fall in temperature all the way back from the shock front, whereas at late stages we have a region of fairly uniform temperature close to the shock front and a cold slab of gas close to the current sheet. It should be mentioned at this point that all the preceding analysis has assumed that the rate of energy transfer between points

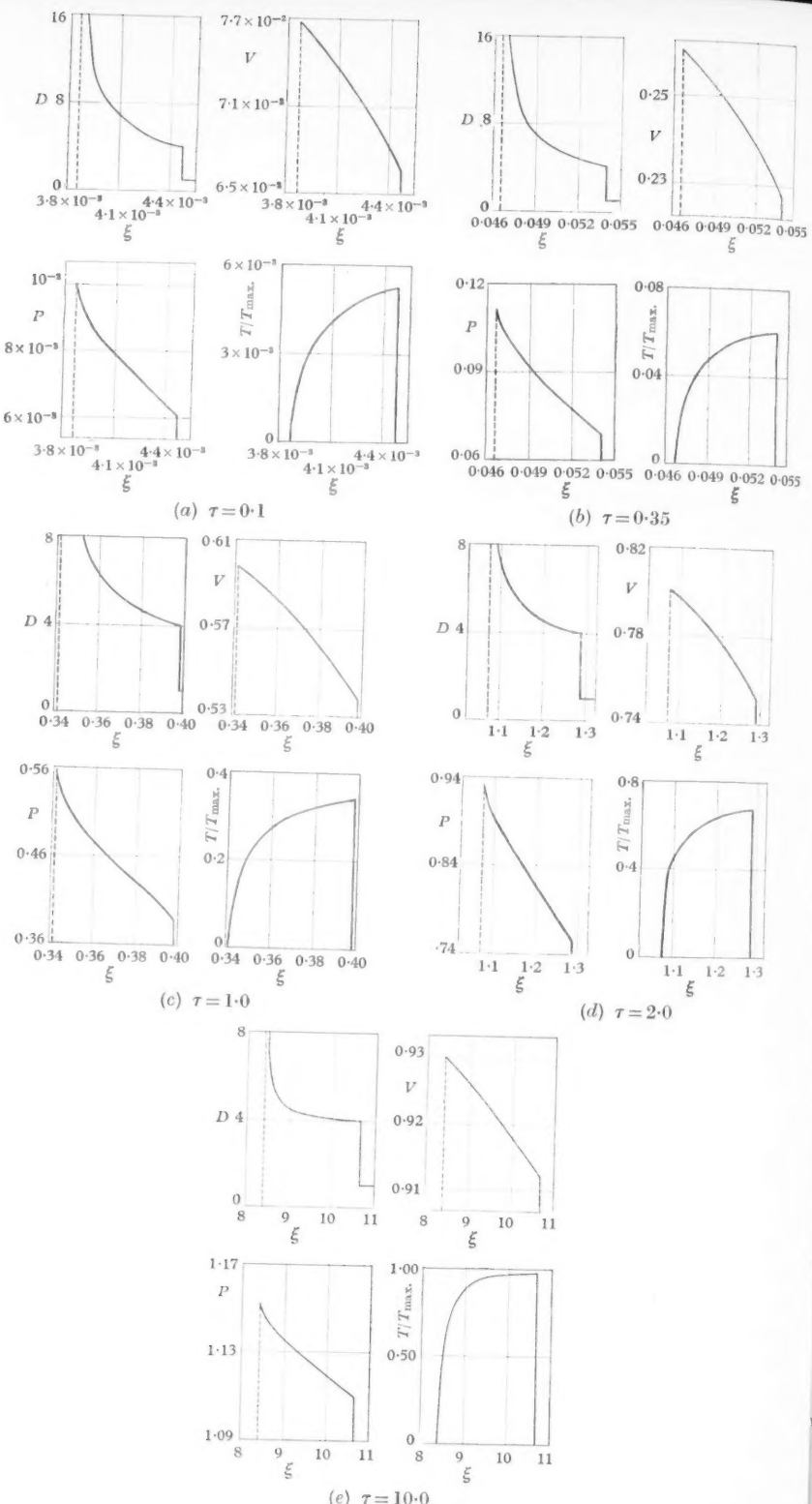

FIGURE 7. Hydrodynamic parameters in the shocked plasma as a function of non-dimensional distance ξ for various values of the non-dimensional time τ.

in the gas by means of thermal conduction is negligible. In practice the thermal conductivity may be very high and, in applying the results of this paper to specific practical cases, it is necessary to satisfy oneself that this basic assumption is valid.

It will be noticed that at all times the particle speed v is remarkably uniform across the gas. This is because at early stages, when the current is rising rapidly, the time taken for sound waves to traverse the gas is very small and local compressions with associated variations in particle speed do not have time to develop.

Finally we return to our initial assumption of a fully ionized and dissociated gas with the ionization and dissociation energies negligible compared with the thermal energy of the gas. In order to completely ionize and dissociate hydrogen, deuterium or tritium, it is necessary to put in 15 eV of energy per atom present. The above assumption is therefore only valid when the thermal energy of the gas is large compared with this energy, i.e. the temperature of the gas must be much greater than $1{\cdot}7 \times 10^5$ °K. Since the similarity solution (§3) gives a shock strength (and therefore temperature) increasing as the square of time, there is a finite time before this condition is attained.

REFERENCES

Allen, J. E. 1957 An elementary theory of the transient pinched discharge. *Proc. Phys. Soc.* B, **70**, 24.

Anderson, D. A., Baker, W. R., Colgate, S., Gilbert, F. C., Ise, J., Pyle, R. V. & White, R. S. 1957 Paper presented at conference on Plasma Physics, Venice.

Artsimovich, L. A., Andrianov, A. M., Bazilevskaya, O. A., Prokhorov, Yu. G. & Filippov, N. V. 1956 *Atomnaya Energiya*, **3**, 76.

Bodin, H. A. B. & Reynolds, J. A. 1957 *Engineering*, **184**, 538.

Elmore, W. C., Little, E. M. & Quinn, W. E. 1958 Neutrons of possible thermonuclear origin. *Phys. Rev. Letters*, **1**, 32.

Hagerman, D. C. & Mather, J. W. 1958 Neutron production in a high power pinch apparatus. *Nature, Lond.*, **181**, 226.

Kolb, A. C. 1957 Production of high energy plasmas by magnetically driven shock waves. *Phys. Rev.* **107**, 345.

The pressure distribution on dihedral wings at supersonic speed

By LU TING
Polytechnic Institute of Brooklyn, Brooklyn, New York

(Received 14 July 1958 and in revised form 2 March 1959)

For wings with supersonic edges and with arbitrary dihedral, twist, camber and thickness distribution, the pressure distribution on the wing exterior to and along the two Mach lines emanating from the vertex of the wing is equal to the corresponding pressure distribution for a planar wing. The problem is to find the pressure distribution inside the two Mach lines. In the present paper, the unknown pressure distribution is approximated by an elementary function of the two surface variables. The (as yet undetermined) constants in the function are then found by the conditions: (i) that the function takes on the corresponding planar values along the two Mach lines, (ii) that it fulfils certain generalized integral relationships (Ting 1959), and (iii) that it satisfies the averaging property of solutions of the wave equation to be developed in this paper. The generalized integral relationship relates the integral of the pressure distribution along the line of intersection of a Mach plane with the wing to the integral along the same line of the prescribed normal velocity. The averaging property relates the pressure distribution along the line of intersection of the surface of the dihedral wing to that on a planar wing.

1. Introduction

The problem of linearized supersonic flow over thin wings with an arbitrary dihedral can be solved if the flow field can be resolved into conical fields (Snow 1948; Germain 1955). On the other hand, if the normal velocity on the wing surface is arbitrary while the dihedral angle is equal to 90°, the problem can be treated by the method of images (Ting 1957).

In general, the problem of supersonic flow over thin wings with supersonic edges, arbitrary dihedral, and with arbitrary twist, camber and thickness distribution, has been solved from a mathematical point of view. However, the numerical evaluation of the solutions is extremely difficult. Moreover, the problem of wings with dihedral is the essence of the interference problem associated with wings and prismatic bodies. Recent studies by Ferri (1955, p. 353), Ferri & Clark (1957), and Ferri, Clarke & Ting (1957) on the effect of body contouring for drag reduction at constant lift have increased the interest in solutions of wing-body interference problems and in the determination of the pressure distribution on dihedral wings.

This paper begins with the derivation of an averaging property of solutions of the wave equation. The integral relationship derived by Ting (1959) as a

generalization of the results of Lagerstrom & Van Dyke (1949), Bleviss (1953), Ferri (1955) and Ferri *et al.* (1957) is then restated and applied to dihedral problems.

When the flow field is homogeneous, as defined in § 4, the procedure for obtaining the approximate pressure distribution on the wing is outlined. Numerical examples are provided for flows whose potentials are homogeneous of order 1 and 2. The former is identical to conical flow, and the corresponding solution is in good agreement with the exact solution of the linearized conical problem.

When the flow field cannot be resolved into a finite number of homogeneous flow fields, a more extended procedure for obtaining the pressure distribution is required; this is outlined and illustrated by an example.

2. Averaging property of solutions of the wave equation

This can be described clearly by referring to the following specific physical problem. For supersonic flow over dihedral wings with prescribed normal velocity on the two planes of the wing, the product of the dihedral angle and the pressure along the line of intersection of the planes is independent of the dihedral angle, and is therefore equal to π times the corresponding pressure distribution for the planar wing.

The mathematical formulation and the proof of this statement are given as follows:

Let ϕ^ν be the solution of the wave equation

$$\phi_{\nu\nu} + \phi_{zz} - \phi_{tt} = 0, \tag{1}$$

which fulfils the initial conditions

$$\phi^\nu = 0 \quad \text{and} \quad \phi^\nu_t = 0 \quad \text{at} \quad t = 0, \tag{2}$$

and satisfies the boundary conditions for the normal derivative of ϕ^ν, namely

$$\phi^\nu_n = g_1(z,t) \tag{3}$$

on the t-z plane where $t > 0$, $z > 0$, and

$$\phi^\nu_n = g_2(z,t) \tag{4}$$

on the s-t plane defined by the parametric equations, $z = s\cos\nu$ and $y = s\sin\nu$, where $s > 0$ and $t > 0$ (cf. figure 1).

The superscript (ν) of ϕ^ν is associated with the angle between the t-z plane and the s-t plane. Then, for different values of ν, the corresponding solutions on the line of intersection of the boundary planes obey the following relationship:

$$\nu\phi^\nu(0,0,t) = \pi\phi^\pi(0,0,t). \tag{5}$$

Equation (5) can be proved by virtue of Green's Theorem (see Ward 1955, p. 55), which states

$$\iint_A^* \phi^\nu(y,z,t)\,\mathbf{Q}\,.\,\mathbf{n}\,dA - \iint_A^* (\mathbf{P}\,.\,\mathbf{n})\,(1/R)\,dA = 0, \tag{6}$$

where (*) means 'the finite part of', and

$$R = [(t_1-t)^2-z^2-y^2]^{\frac{1}{2}},$$

$$\mathbf{P} = \left(\mathbf{j}\frac{\partial}{\partial y}+\mathbf{k}\frac{\partial}{\partial z}-\mathbf{i}\frac{\partial}{\partial t}\right)\phi^\nu,$$

$$\mathbf{Q} = \left(\mathbf{j}\frac{\partial}{\partial y}+\mathbf{k}\frac{\partial}{\partial z}-\mathbf{i}\frac{\partial}{\partial t}\right)(1/R).$$

$\mathbf{i}$, $\mathbf{j}$, $\mathbf{k}$ are the unit vectors along the t, y and z axes respectively, and $\mathbf{n}$ is the unit outward normal vector to the closed surface of integration A. The surface A consists of (see figure 1):

(i) A^*, which is the part of the surface $R = 0$ lying in between the planes $t = 0$, $t = t_1-\delta$ and the boundary planes.

(ii) I, which is the part of the plane $t = 0$, lying inside A^*.

(iii) II, which is the part of the plane $t = t_1-\delta$, lying inside A^*.

(iv) B_1, which is the part of the t-z plane, lying inside A^* and between planes $t = 0$ and $t = t_1-\delta$.

(v) B_2, which is the part of the t-s plane, lying inside A^* and between planes $t = 0$ and $t = t_1-\delta$.

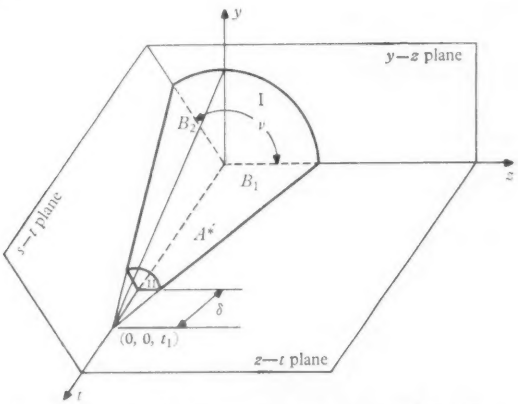

FIGURE 1. Averaging property with boundary data.

As $\delta \to 0$, the finite part of the first integral over II approaches $\nu\phi^\nu(0, 0, t_1)$ and the second integral over II approaches zero and that of both integrals over A^* vanishes (see Ward 1955).

Due to the initial conditions, the boundary conditions, and the vanishing of $\mathbf{Q}.\mathbf{n}$ on the t-z and t-s planes, equation (6) becomes:

$$\nu\phi^\nu(0, 0, t_1) = -\iint_{B_1}\frac{g_1(z, t)\,dz\,dt}{\sqrt{[(t_1-t)^2-z^2]}}-\iint_{B_2}\frac{g_2(s, t)\,ds\,dt}{\sqrt{[(t_1-t)^2-s^2]}}. \tag{7}$$

The terms on the right-hand side of equation (7) are independent of ν, and therefore $\nu\phi^\nu$ is independent of ν and equation (5) is valid.

This property is formulated with homogeneous initial conditions and non-homogeneous boundary conditions. It will be called the averaging property

associated with boundary data in order to differentiate from the averaging property associated with initial data (Ting 1958). The application of the second averaging property can be found in diffraction problems and in the interference problem of a wing and prismatic body.

3. The generalized integral relationship

In this section the requirement for and statement of the generalized integral relationship given by Ting (1959) are restated. As shown in figure 2, a cylindrical surface $y = F(z)$, is placed in a supersonic stream directed along the x-axis, with velocity U and Mach number M. $q_n[x, F(z), z]$ represents the prescribed normal velocity on the cylindrical surface with

$$q_n/U \ll 1 \tag{8}$$

and

$$q_n[x, F(z), z] = 0 \quad \text{for} \quad x < 0. \tag{9}$$

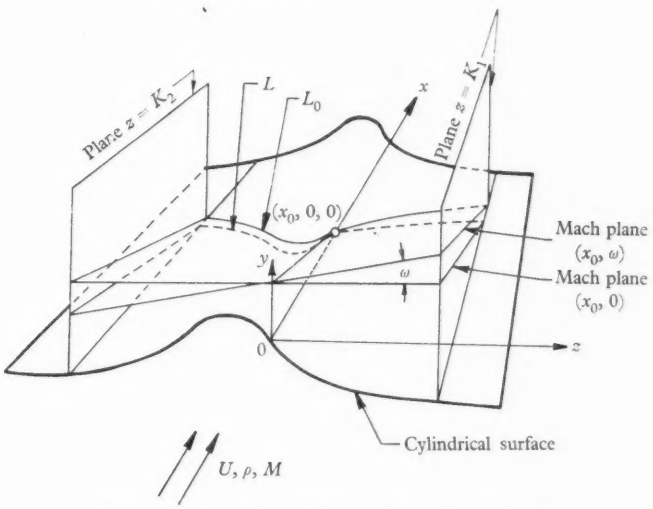

FIGURE 2. The generalized integral relationship.

It will be assumed that $q_n[x, F(z), z]$ is piece-wise continuous and that for any given Mach plane, $x + By = M\beta$, there exist two numbers $K_1(\beta)$ and $K_2(\beta)$ (with $K_1 > K_2$) such that on the Mach plane, the disturbance potential ϕ, due to q_n, is confined inside the region $K_1 > z > K_2$. That is,

$$\phi(x, y, z) = 0$$

for

$$x \leqslant M\beta - By, \quad \infty > z \geqslant K_1(\beta) \quad \text{and} \quad K_2(\beta) \geqslant z > -\infty. \tag{10}$$

The integral of the disturbance pressure along the curve of intersection, L_0, of the cylindrical surface $y = F(z)$ with the Mach plane $x + By = M\beta$ is related to the integral of the prescribed normal velocity $q_n[x, F(z), z]$ as follows:

$$\int_{L_0} p \sin\sigma \, \mathbf{n} \cdot \mathbf{j} \, dL_0 = \frac{\rho U}{B} \int_{L_0} q_n \sin\sigma \, dL_0, \tag{11}$$

where $\mathbf{n}$ is the unit vector normal to the cylindrical surface, $\mathbf{j}$ is the unit vector parallel to y-axis, and σ represents the angle between the x-axis and the tangent to the path of integration.

The integral relationship still holds if the cylindrical surface is rotated about its generatrix, the x-axis, with respect to the co-ordinate axes and the Mach plane. Consequently, if the co-ordinate axes are fixed with respect to the cylindrical surface while the Mach plane is rotated about the x-axis, the integral relationship remains valid and equation (11) becomes

$$\int_L p \sin\sigma \, \mathbf{n}.\boldsymbol{\omega} dL = \frac{\rho U}{B} \int_L q_n \sin\sigma \, dL, \tag{12}$$

where L refers to the line of intersection of the cylindrical surface with the Mach plane defined by

$$x + B(y\cos\omega + z\sin\omega) = M\beta = x_0 \tag{13}$$

and

$$\boldsymbol{\omega} = \mathbf{j}\cos\omega + \mathbf{k}\sin\omega.$$

The Mach plane, which is intercepted by the x-axis at the Mach angle, is specified by two parameters, the x intercept x_0 and the angle of rotation ω. For each value of x_0 and ω, equation (12) gives a linear relationship between the pressure distribution and the normal velocity. It should be noted that for the derivation of the integral relationship the assumption of equation (10) has been made. For the fulfilment of equation (10), there exist certain restrictions on the values of two parameters, x_0 and ω, and a rule for selecting the suitable cylindrical surface.

For dihedral wings with supersonic edges, it is sufficient to discuss only the upper surface for the case where the normal velocity on one of the dihedral planes, $y - z\tan\nu = 0$, vanishes. On the other plane, $y = 0$, the normal velocity $\phi_y = g(x, z > 0)$ is prescribed and vanishes for the region $x < 0$.

To apply the integral relationship, it is clear that the intercept x_0 should not be outside the wing surface. The value of ω should obey the restriction, $\frac{3}{2}\pi - \nu > \omega > -\frac{1}{2}\pi$.

For $\omega > 0$, the wing surface can be chosen as the cylindrical surface and the condition of equation (10) is fulfilled with $K_1 = M\beta/(B\sin\omega)$ and $K_2 = -M\beta/[B(1-\sin\omega)]$.

For $\omega < 0$, the Mach plane will not intercept the positive z-axis. In order to fulfil the condition of equation (10) a modified cylindrical surface should be used. It may be composed of (see figure 3): (1) the portion of the wing surfaces where $z < K'$, (2) the portion of the plane $z = K'$, where $0 < y < K'$, and (3) the portion of the plane $y = K'$, where $z > K'$. Here K' is the z-co-ordinate of the point where the Mach plane intercepts the forward Mach line in the x-z plane issuing from the vertex.

On the portion of the plane $y = K'$, where $z > K'$ and which is ahead of the Mach plane, the flow field is undisturbed; therefore, K' can be chosen as the value for $K_1(\beta)$ in equation (10). The path of integration L with non-zero integrand will then consist of two parts: (1) the segments of straight lines on the surface of the wing inside the domain of influence of the vertex, and (2) the segment of straight line on the plane $z = K'$ which is outside of the domain of influence of the vertex.

On the second segment the pressure distribution and the normal velocity can be obtained from the planar solutions; therefore, the integral relationship along the path L does not involve any unknown function other than the pressure distribution on the wing surface. This is the rule to be observed in selecting the proper cylindrical surface.

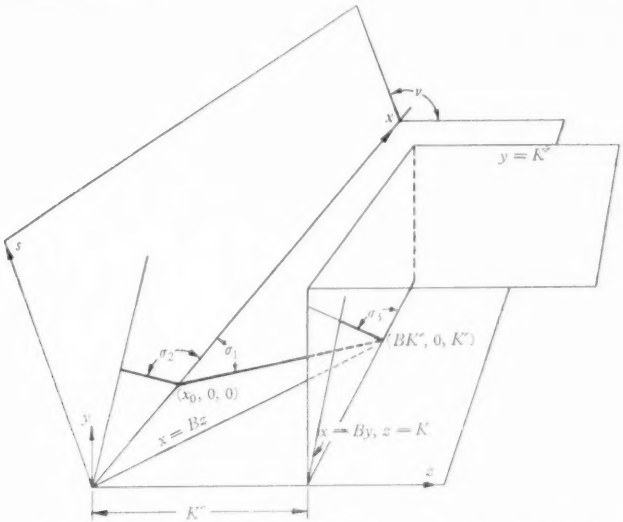

FIGURE 3. Integral relationship for dihedral wings—when the Mach plane does not intercept the positive z-axis.

4. Homogeneous flow

It is sufficient to discuss the case $q_n = 0$ on the dihedral plane $y = z\tan\nu$. On the other plane $y = 0$, the prescribed normal velocity is now expressed as

$$v\,(x > 0, 0, z > 0) = x^m z^n, \tag{14}$$

where m and n are real numbers. The flow field is a homogeneous flow of the $(m+n+1)$th order (see Germain 1955) for which an analytic solution other than the conical solution (homogeneous flow of order 1) is not yet available. However, the method of the present paper can be readily applied regardless of the order.

The pressure distribution on the wing surface inside the domain of influence of the vertex can be expressed in general as

$$\frac{B}{\rho U^2} p_{m,n}(x, 0, z) = x^{m+n} f_1(\eta_1), \tag{15a}$$

and

$$\frac{B}{\rho U^2} p_{m,n}(x, s\sin\nu, s\cos\nu) = x^{m+n} f_2(\eta_2), \tag{15b}$$

where

$$\eta_1 = \frac{Bz}{x} \quad \text{and} \quad \eta_2 = \frac{Bs}{x}.$$

If the functions f_1 and f_2 are approximated by second-order polynomials, i.e.

$$f_j(\eta_j) = a_{0j} + a_{1j}\eta_j + a_{2j}\eta_j^2. \tag{16}$$

there are altogether six unknown constants a_{0j}, a_{1j} and a_{2j}, where $j = 1, 2$. The condition along the Mach lines emanating from the vertex yields the values of $f_1(1)$ and $f_2(1)$, while the averaging property yields $f_1(0)$ and $f_2(0)$. The remaining two linear equations for the six unknowns are furnished by the integral relationship corresponding to two different values of ω. It is evident that the integral relationship is independent of the x-intercept, x_0, of the Mach plane.

For the homogeneous flow of order 1 ($m = n = 0$), the constants are determined for $\nu = 135°$ and the pressure distribution is plotted in figure 4. The deviation from the exact solution of the linearized conical problem is within 10 %.

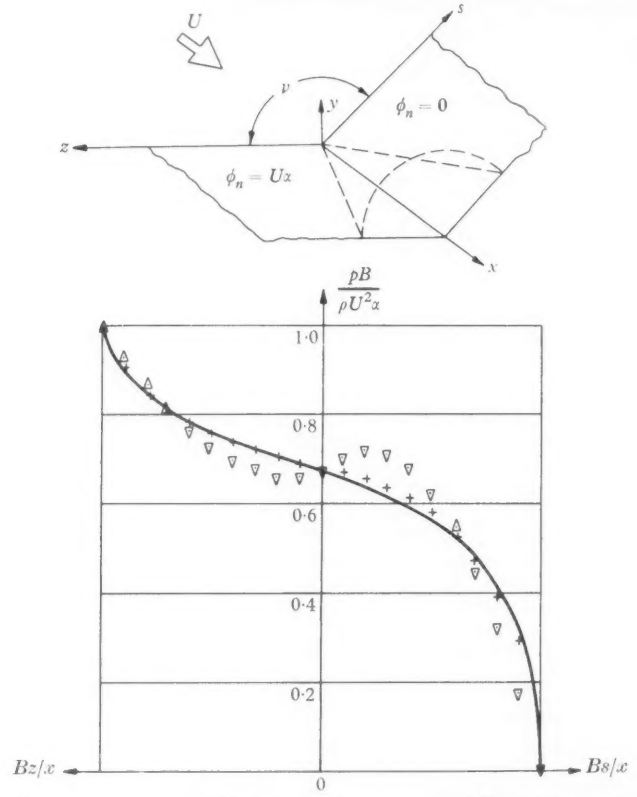

FIGURE 4. Homogeneous flow field of order 1. ——, exact linearized conical solution; +, approximate solution of equation (17); ▽, approximate solution of equation (16).

With the knowledge that the expression for the pressure distribution contains a term like $\sqrt{(1-\eta_j^2)}$ near the Mach lines, it is, therefore, desirable to admit such a term in the approximate expressions of $f_j(\eta_j)$; e.g.

$$f_j(\eta_j) = a_{0j} + a_{1j}\eta_j + b_j\sqrt{(1-\eta_j^2)}. \tag{17}$$

The six unknown constants a_{0j}, a_{1j} and b_j are again determined for the homogeneous solution of order 1, and the corresponding pressure distribution is in good agreement with the exact linearized conical solution (figure 4).

A calculation has been made by Ting (1958) to determine the eight constants when the term $b_j\sqrt{(1-\eta_j^2)}$ is added to the right-hand side of equation (16). The pressure distribution is then in perfect agreement with the exact conical solution.

Figure 5 shows the pressure distribution on the wing for a homogeneous flow of order 2 with $m = 0$ and $n = 1$. The approximate solution in the form of equation (17) differs slightly from that of equation (16).

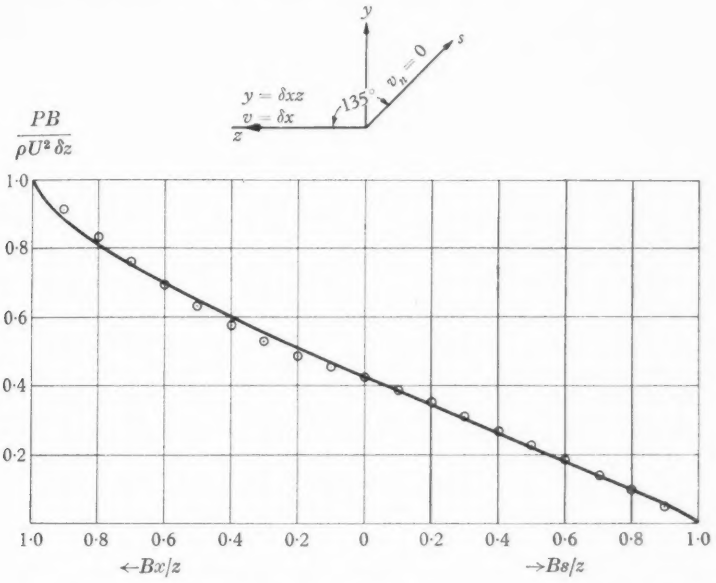

FIGURE 5. Homogeneous flow field of order 2. ——, approximate solution of equation (17); ⊙, approximate solution of equation (16).

5. An example of a non-homogeneous flow field

In principle, the prescribed normal velocity on the wing surface can be expressed as a double power series of x and z. Consequently, the pressure distribution will be

$$p = \sum_m \sum_n a_{mn} p_{m,n}, \tag{18}$$

where $p_{m,n}$ can be obtained by the procedure outlined in the preceding section.

From the engineering point of view, this is not a practical solution if the series of equation (18) does not converge fast enough. For such cases, a different procedure of solution is necessary; this can be best illustrated by an example.

Figure 6 shows a dihedral wing with $\phi_n = 0$ on the plane $y = z\tan\nu$. On the plane $y = 0$, the normal velocity is

$$\phi_y = 0 \quad \text{for} \quad 0 < z < a \quad \text{or} \quad x < 0, \tag{19a}$$

$$\phi_y = \alpha U \quad \text{for} \quad z > a \quad \text{and} \quad x > 0. \tag{19b}$$

This problem is chosen because it exhibits the basic character of diffraction problems and also that of interference problems of wings with prismatic bodies.

For $x < aB$, the disturbance pressure is identical with the planar solution. At $x = aB$, the 'incident disturbance' $p^{(\pi)}$ which originates at the point $x = 0, y = 0, z = a$ reaches the x-axis. For $x > aB$, the incident disturbance is diffracted and/or reflected by the x-s plane ($y = s\sin\nu$, $z = s\cos\nu$). The disturbance due to the corner is confined inside the forward Mach lines $x - Ba = Bz$ in the plane $y = 0$ and $x - Ba = Bs$ in the x-s plane.

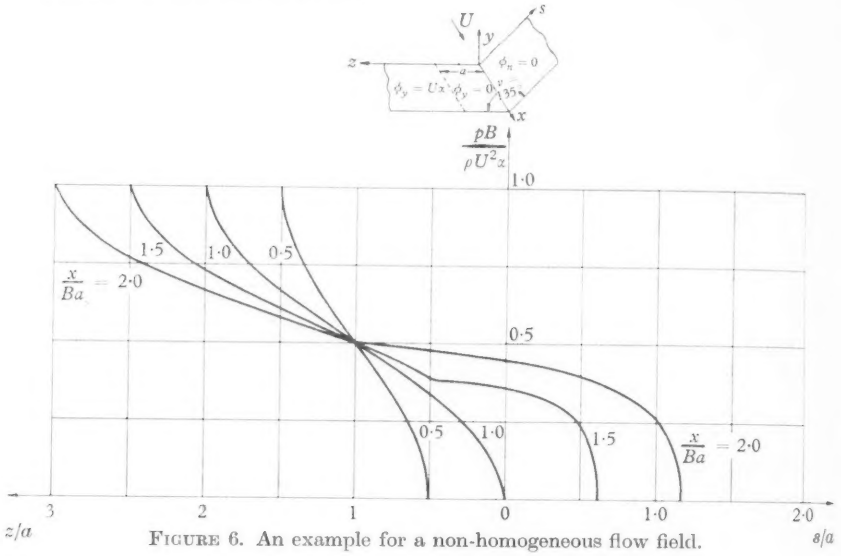

FIGURE 6. An example for a non-homogeneous flow field.

For the case where $\nu < \pi$, the incident disturbance is simply reflected by the x-s plane in the region upstream of the Mach line $x - Ba = Bs$ and behind the hyperbola $x = B\sqrt{(s^2 - 2as\cos\nu + a^2)}$. In this region, the resultant pressure should be $2p^{(\pi)}(x, y = s\sin\nu, z = s\cos\nu)$. The pressure distribution in the domain of disturbance of the corner can be written as

$$p(x, 0, z) = p^{(\pi)}(x, 0, z) + p_1(\bar{x}, z), \tag{20a}$$

$$p(x, s\sin\nu, s\cos\nu) = 2p^{(\pi)}(x, s\sin\nu, s\cos\nu) + p_2(\bar{x}, s), \tag{20b}$$†

where $\bar{x} = x - Ba$, and p_1 and p_2 denote the deviations from the planar pressure distribution.

The conditions for p_1 and p_2 along the Mach lines are

$$p_1(Bz, z) = 0, \tag{21a}$$

and

$$p_2(Bs, s) = 0. \tag{21b}$$

The averaging property yields

$$p_1(\bar{x}, 0) = \left(\frac{\pi}{\nu} - 1\right) p^{(\pi)}(\bar{x} + Ba, 0, 0), \tag{22a}$$

and

$$p_2(\bar{x}, 0) = \left(\frac{\pi}{\nu} - 2\right) p^{(\pi)}(\bar{x} + Ba, 0, 0). \tag{22b}$$

† The term $2p^{(\pi)}$ should be omitted from equation (20*b*) for the case where $\nu > \pi$.

The unknown functions, p_1 and p_2, will be approximated by the following functions of two variables:

$$p_j = [a_{0j} + d_{0j}\eta_j + b_{0j}\sqrt{(1-\eta_j^2)}]\,[\bar{x}/(aB)]^{\frac{1}{2}} + [a_{1j} + d_{1j}\eta_j + b_{1j}\sqrt{(1-\eta_j^2)}]\,[\bar{x}/(aB)]^{\frac{3}{2}}, \tag{23}$$

where $j = 1, 2$, $\eta_1 = Bz/\bar{x}$ and $\eta_2 = Bs/\bar{x}$.

In the approximating functions, a total of twelve unknown constants have been admitted. Eight equations are obtained from equations (21) and (22) for $\bar{x} = 0{\cdot}5Ba$ and Ba, respectively, since in the present problem the length of the chord has been chosen to be $2Ba$. The integral relationship yields four equations corresponding to the Mach planes (x_0, ω) with $x_0 = Ba$, $x_0 = 0{\cdot}5Ba$ and $\omega = 90°$, $\omega = 45°$, respectively, for the case of $\nu = 135°$. The numerical results are shown in figure 6.

p_j is expressed in a series of $[\bar{x}/(aB)]^{\frac{1}{2}}$, $[\bar{x}/(aB)]^{\frac{3}{2}}$, ... in equation (23) due to the fact that $p^{(n)}(\bar{x}+aB, 0, 0)$ can be expressed by a similar series at least for small values of $\bar{x}/(aB)$. However, if a regular power series is employed, the result of the approximation does not differ much from that of equation (23).

For the purpose of improving the approximation, additional terms may be admitted. If terms involving higher powers of $\bar{x}/(aB)$ are added to equation (23), extra values of x_0 should be selected so that there will be additional integral relationships corresponding to the Mach plane (x_0, ω). On the other hand, if additional terms involving η are admitted, the additional equations are obtained by taking more values of ω.

6. Concluding remarks

The averaging property of solutions of the wave equation and the generalized integral relationship are applied to obtain the pressure distribution on dihedral wings if the normal velocity on the dihedral planes is prescribed.

Since the integral relationship gives a linear relationship between the integral of pressure and the integral of normal velocity, it is plausible to apply the integral relationship to solve the problem when the boundary conditions on the dihedral planes are of the mixed type. Consequently, it is feasible to extend the method in the present paper to solve the problem of dihedral wings with subsonic edges.

As a further extension of the work reported here, the problem wherein the boundary is a cylindrical surface may be cited. In this case it is necessary to obtain the pressure distribution based on the integral relationship alone. The feasibility of so obtaining the pressure distribution was demonstrated for the problem of conical flow on dihedral wings by Ting (1958). With the averaging condition replaced by an additional integral relationship, the approximate pressure distribution on the wing surface differs from that of the exact linearized conical solution by 2 %. Attempts are in progress to obtain, from the integral relationship alone, the pressure distribution on a cylindrical surface with its generator parallel to the direction of flow and with a prescribed normal velocity.

This report was supported by the United States Air Force through the Air Force Office of Scientific Research and Development Command, under Contract

AF 18(600)-694, Project no. 1750, under the supervision of Professor Antonio Ferri, to whom the author is indebted for invaluable suggestions. Grateful acknowledgement is due to Professor Paul A. Libby for his interest and helpful discussions.

REFERENCES

Bleviss, Z. O. 1953 *J. Aero. Sci.* **20**, 849.

Ferri, A. 1955 *Proceedings of the Conference on High-Speed Aeronautics, Polytechnic Institute of Brooklyn, New York.*

Ferri, A. & Clarke, J. H. 1957 *J. Aero Sci.* **24**, 1.

Ferri, A., Clarke, J. H. & Ting, L. 1957 *J. Aero. Sci.* **24**, 791.

Germain, P. 1955 *Nat. Adv. Comm. Aero., Wash., Tech. Mem.* no. 1354.

Lagerstrom, P. A. & Van Dyke, M. D. 1949 *Douglas Aircraft Company Rep.* no. SM-13432.

Snow, R. M. 1948 *Quart. Appl. Math.* **5**, 417.

Ting, L. 1957 *J. Aero. Sci.* **24**, 821.

Ting, L. 1958 *Polytechnic Institute of Brooklyn, New York, PIBAL Rep.* no. 397.

Ting, L. 1959 *Quart. Appl. Math.* **16**, 373.

Ward, G. N. 1955 *Linearized Theory of Steady High-Speed Flow.* Cambridge University Press.

REVIEWS

Fluid Mechanics for Engineers. By P. S. Barna. London: Butterworths Scientific Publications. 1957. 371 pp. 57*s*. 6*d*.

To many people who teach elementary fluid mechanics to embryonic engineers, there falls regularly the responsibility of recommending a choice from a long list of textbooks all covering much the same ground. For a lecturer without a book of his own, the choice may be quite difficult. A survey of the booksellers' shelves shows the field to be indeed very full: there are about half a dozen possible winners and a much larger number of outsiders. Because some of these textbooks are very bad, and also because over all the correlation between value and price is not strong, a recommendation to students is an important undertaking.

When assessing any book written 'for engineers', it is necessary to apply a further criterion beyond the general standards desirable in scientific writing. The special requirement is of course that the book should meet the particular needs of engineering students, as distinct from those found by students of physics or applied mathematics approaching the same branch of science. Modern trends in engineering education have made this distinction much less clear than it used to be; but an essential difference must still be recognized. A good introductory textbook on fluid mechanics addressed to engineering students has to cover a wide range of topics necessarily somewhat superficially, emphasizing the utility of theoretical results rather than their rigorous logical justification and in general avoiding all but the simplest mathematical arguments; nevertheless, such a book must give an essentially *correct* account of underlying broad principles, even those which underlie mechanisms whose complete description is an extremely difficult matter—for example, boundary-layer separation and turbulent friction. It does not seem unduly rash to say that among the achievements of modern fluid mechanics there is no important physical result whose fundamental explanation could not be made clear to an intelligent final-year engineering student, provided of course that sufficient expository skill could be mustered. Thus, the scope of elementary engineering texts need never be restricted merely to what is easy mathematically, but depends rather on the ability of authors to extract essentials from the corpus of existing knowledge and present them in simple terms.

In the light of these rather stern generalities, it is pleasant to be able to write that Mr Barna's book is on the whole a fairly satisfactory one: certainly this book is among the better of its kind, and can be regarded as a welcome addition to the list deserving consideration for teaching purposes. Readers sensitive to style will suffer many minor irritations—e.g. equations are often introduced with needlessly clumsy wording—and there are a few blunders; but, after reading the book through, it is recognized that a wide range of material has been presented tersely yet for the most part explicitly. In his preface the author claims: 'Emphasis is laid upon the broad representation of fundamentals,

leaving certain topics not included in the text for the choice of individual teachers.' This is a fair statement as to the character of the book, although the author's second remark does not in fact imply any serious gaps in the coverage. Many worked examples are given to illustrate the theory, and 67 problems are set for the student to work out.

Part I of the book contains ten chapters on topics primarily concerning incompressible fluids, the applications described being well balanced between problems of water flow and low-speed air flow. The short opening chapter outlines hydrostatics quite nicely. Then, unfortunately, at the important stage where the rudiments of fluid dynamics are to be introduced, the standard ebbs far below the good average of the book as a whole. Chapter 2, titled 'perfect fluids in motion', obviously was written without due care. The chapter makes a bad start, a discussion of pathlines and streamlines leaving much to be desired—for instance, no suggestion is made that these are in fact the same in steady flow. After this the usual simple derivation of Bernoulli's equation from Newton's second law is presented; but the author then repeats the common error of interpreting the terms in the equation directly as representing energies (introducing the awkward concept of 'pressure energy'). (Again in the later chapter on compressible flow, the absence of a proper derivation of the energy equation for steady flow seems an unfortunate omission: merely to add the definition of internal energy, $dQ = dE + p\,dv$, to Bernoulli's equation is unconvincing, to say the least.) Another disappointment occurs later in the chapter when momentum considerations are applied to calculate the force exerted by a deflected jet. A page and a half are given to discussing momentum changes of solid bodies, particularly the case of a ball bounced off a wall; and after this one rather expects that the case of a jet will be explained by analogy with a stream of particles, as it can be quite convincingly. But this is not done, the actual explanation being tentative and needlessly feeble for all the space allowed this topic.

To pass on to better things, Chapter 3 is mainly a short account, quite well done, of viscosity and the significance of Reynolds number. It is followed naturally by a chapter on the flow of real fluids in closed conduits. This presents a sensibly balanced mixture of fundamentals and practical data, such as graphs of friction coefficients and a short table of typical roughness lengths for engineering materials.

Chapter 5 deals briefly with steady flows in open channels. Though adequate, this is not one of the better chapters: it runs through the usual material, 'specific energy' and all that, and adds nothing new. An opportunity is missed, for surely the time is ripe for infusing some new ideas into the teaching of this part of hydraulics. It is a pity, for example, that the useful analogies between open-channel flow and one-dimensional compressible gas flow were not exploited. Thus, the Froude number based on local mean velocity and depth is not mentioned explicitly, despite its important role precisely equivalent to that of Mach number.

Then follows a chapter on 'Fluid metering', which gives brief but quite interesting descriptions of orifice meters and other types of flow meter, Pitot tubes, and various manometers. Next, Chapter 7 gives a careful account of

dimensional analysis, explaining formally the details of its technique (e.g. Buckingham's pi theorem), but particularly emphasizing its *purpose* as a tool for the engineer. This chapter is one of the best in the book.

The remaining chapters of Part I are also good. The 52 pages of Chapter 8 give a review of boundary-layer theory whose scope is quite ambitious for a book of this sort. The topics covered include a general description of laminar and turbulent boundary layers, thickness and skin-friction calculations for the laminar boundary over a flat plate, properties of turbulent boundary layers deduced from the $\frac{1}{7}$-power law, separation and form drag, the deduction of the 'law of the wall' from Prandtl's mixing length hypothesis, and the idea of rough or smooth turbulent boundary-layer flows. The author has been fairly skilful in reducing these complex matters to essentials, and this chapter makes an attractive introduction to the subject. As a minor complaint, figure 8.9 is a terrible bungle: about everything possible is wrong with this figure, which fortunately is not an important one. Chapter 9 is a brief but pithy exposition of the elements of wing theory.

In the single chapter on compressible flow comprising Part II, the usual basic topics (e.g. frictionless adiabatic flow in nozzles, flow in uniform ducts with friction, normal shocks, together with a mention of reflected shocks, expansion fans, etc.) are covered fairly adequately; but the chapter could have been greatly improved by added explanation of the fundamental thermodynamic considerations involved. For example, the entropy change across a normal shock is calculated without explaining the meaning of entropy or the significance of its increase through a shock.

The three chapters of Part III give a very readable account of the operation of the main types of rotary pumps and turbines, the emphasis being of course on fundamentals rather than technical detail although there is a reasonable measure of the latter. Rational methods of impeller design, dimensional analysis of machine characteristics, and cavitation are included in the topics discussed. The value of this part of the book is greatly enhanced by a series of excellently reproduced photographs and sectional drawings of machines, just sufficient in number to bring the realities of the subject home to the student without in any way giving the book the character of a technical manual. As an instance of the value of the photographs, the view of a Francis turbine runner on p. 361 conveys in an instant the essential layout and mode of operation of this intricate device, whereas to explain these in words or with simple sketches is very difficult.

The book shows some signs of hasty preparation, particularly of careless proof-reading (e.g. the equation preceding (2.8) looks all right on a cursory glance, but the misprint there could seriously confuse a student); and there are a few bad instances of careless writing. On p. 33, for example, there appears the wholly misleading statement, 'When liquids are in motion, surface tension effects are negligible; they may not be ignored, however, when they are at rest...'. Again, on the previous page, the author writes about the 'modulus of elasticity, E' where the *compression modulus* is implied, although surely he knows that all over the world engineering students learn to associate the symbol E with Young's modulus.

Nevertheless, the overall impression is a favourable one, even allowing for the fact that this book is unduly expensive. It can be recommended for teaching whenever a broad coverage of fundamentals is needed together with a small yet encouraging taste of engineering practice.

T. Brooke Benjamin

A Textbook of Fluid Mechanics. By J. R. D. Francis. London: Edward Arnold (Publishers) Ltd. 1958. 332 pp. 24*s*.

This book is presented, at a price which students should be able to afford, as an attempt to provide a simple yet up-to-date textbook for the earlier years of an engineering degree course.

There is certainly a place for sound but simple books treating fluid mechanics from a broader point of view than the older textbooks of hydraulics and omitting any very detailed treatment of the applications. But an author who embarks on such a book does well to consider carefully his choice both of the subject-matter and of a balance between the teaching of basic principles and the teaching of methods for solving engineering problems. Should the whole of a degree course be covered, or should the more advanced parts of hydraulics, for example, be left to be read elsewhere? Should any attempt be made to deal with high-speed aerodynamics at this stage, or, even briefly, with border-line subjects such as heat transfer or the flow of liquids through permeable media?

The main object ought to be to expound and illustrate the principles of fluid mechanics and to give a clear physical picture of the behaviour of real fluids. The actual range of the book is not so important, except in so far as it may have to cover the requirements of particular examinations. The illustrations of fundamental ideas should of course be drawn from engineering applications whenever possible, so as to be satisfying to a student with his mind on practical matters. Physical principles should be inculcated both overtly and by stealth. If the ideas of dynamical similarity can be driven home a little further in the course of a short chapter on, say, heat transfer, that may be sufficient justification for including such a chapter.

The book under review covers rather more ground than might be expected in view of its declared emphasis on the early part of a degree course. The author begins with two short chapters on hydrostatics. In the course of the introductory chapters on fluid motion which follow, he describes the use of stream function and potential function to describe inviscid two-dimensional incompressible flow. He then deals at some length with Bernoulli's equation and the momentum theorem as applied to a control volume, incompressible flow being assumed. A chapter contributed by Mr G. Jackson provides a substantial introduction to the compressible flow of a perfect gas, including a brief account of the flow about aerofoils at high subsonic and supersonic speeds. Dimensional analysis is treated next, from the point of view of experimental work. The properties of boundary layers are then described. Chapters on the flow in pipes and in open channels follow, and the book ends with chapters on hydraulic machines and some unsteady-flow topics. At the end of each chapter a selection of engineering problems, with solutions, is provided as an exercise for the student.

Mr Francis has made a creditable effort here to give his readers an adequate first statement of principles, and at the same time to engage their interest in fluid mechanics as an engineering subject. His discursive style makes easy reading, and he makes little demand on mathematical ability. He has wisely avoided packing the book with data which can just as well be found in a more specialized treatise. It is therefore all the more regrettable that the book is marred by a lack of precision, and that simplifications made for the sake of easier comprehension are sometimes carried near to the point of confusion.

For instance, the chapter on boundary layers is open to severe criticism on account of many loose statements, particularly ones regarding general concepts such as the development of stresses in turbulent flow; yet if these could be ignored it might be commended as a fairly skilful elementary introduction to the properties of boundary layers and to methods for calculating boundary-layer growth and skin friction. Some of the references to effects of viscosity earlier in the book are also very unsatisfactory. In various places the author uses the words 'eddy' and 'turbulence' in such a way that it is not clear whether he is talking about a turbulent boundary layer, a wholly turbulent flow, or a more or less well-defined separation region. On p. 65 it is stated that 'the tangential force on an aircraft wing produced by the boundary layer produces the drag'.

An example of oversimplification is to be found in the treatment of potential flow. The chapter is headed 'Streamline plotting' and its object is to show how some simple two-dimensional flow patterns can be obtained by graphical or analytical methods. For this purpose the stream function and potential function are defined in a readily understandable way as line integrals normal to and along the streamlines. It is then asserted that 'since the potential function is by definition a property that increases only along the direction of a streamline, and never has a component across it, the equipotential lines are *always* normal to streamlines'. A thoughtful student would be very seriously confused by this, because the given definition of potential—simply as the line integral of velocity along a streamline—of course does not by itself imply that the *only* variations of potential are along the streamline. At the end of the chapter the limitations of the methods described are investigated in an empirical manner. It is stated that 'the theoretical methods, which depend on the property that *streamlines are normal to equipotential lines*, sometimes fail and produce a quite misleading pattern'. The flow of a viscous fluid near a solid boundary and the flow in a forced vortex are shown to be cases in point, but no clear explanation is given of why 'the rules have broken down'. Admittedly, the concept of irrotational motion presents difficulties which are perhaps best avoided in a book of this kind, but these do not justify basing a whole chapter on a misleading definition.

To make matters much worse, however, when the case of the flow about a circular cylinder is quoted as an instructive example, it is stated unequivocally that while viscous effects cause the streamline pattern to be greatly different from that predicted by the potential theory at high Reynolds numbers, they cause little modification of the theoretical pattern at low Reynolds numbers. This is quite inexcusable. A photograph of the Hele-Shaw flow about a circular cylinder, misunderstanding of which can itself give rise to this error, appears as

an illustration. One may speculate whether reproductions of photographs of Hele–Shaw flow in textbooks have done more to help or to hinder the teaching of fluid mechanics.

A summary of the scope and conditions of validity of Bernoulli's equation and the momentum equation as applied to a control surface follows the chapter on compressible gas flow. This may help weaker students to distinguish between the two. It would have been more helpful if Bernoulli's equation and the energy equation for compressible flow had been properly distinguished here instead of being lumped together; it is wrong to say, as on p. 130, that both are essentially derived from Newton's second law. Other statements in this summary could have been made more precise.

Dimensional analysis receives considerable attention, as for example in detailed accounts of its applications to tests on ship and aircraft models and to river model experiments; but elsewhere the author does not make the best use of it. The lift and drag coefficients of aerofoils are introduced in an early chapter as the ratios of the lift and drag to 'hypothetical' lift and drag forces, defined as $\frac{1}{2}\rho V^2 \times$ *an appropriate area*; and the author will not commit himself at this point beyond saying that 'there is considerable evidence that the combination of variables $uA^{\frac{1}{2}}/\nu$ is important in deciding the value of C_{drag} for any shape'. In the chapter on hydraulic machines the readily comprehended non-dimensional coefficients Q/ND^3, gH/n^2D^2, etc., are not introduced until near the end, and the opportunity of forming the specific speed from them is lost.

In the chapter on pipe flow the Chézy and Manning formulae for pipe resistance are quoted before any discussion in terms of the non-dimensional friction coefficient, and so in the reviewer's opinion are given undue prominence. An appendix of typical numerical data includes Bazin's approximate formulae for the Chézy coefficient, surely out of place in this book. In the same appendix values of the loss of head at expansions, contractions, bends and fittings in a pipe are given, without any clear hint of the strong dependence of some of these quantities on upstream conditions, or any clear statement of the Reynolds number range in which the data are applicable.

This is not the really sound elementary textbook which the reviewer would like to see. He is conscious that some of the faults which he has found are not committed consistently throughout the book, and that most of them are not uncommon in textbooks of fluid mechanics, but he considers their complete disappearance long overdue.

E. P. Sutton

Fluid Mechanics (2nd edition). By V. L. Streeter. New York: McGraw-Hill Book Co. 1958. 480 pp. \$7.50 or 58*s*.

The place and scope of the subject of fluid mechanics as part of the fundamental training of engineers is changing substantially. Perhaps inevitably in the early stages of a major development, existing textbooks are adapted to new ideas by the insertion of additional material into a framework which was not designed for it and which is not wholly adequate to bear the changed load. This new edition of a textbook first published in 1951 and now 'enlarged to include

many additional topics' provides some evidence bearing out this reflexion, in spite of the book's many valuable features.

The basic plan of the book is promising: two major divisions, Fundamentals and Applications (consisting of about 270 and 190 pages respectively). That on Fundamentals has chapters on fluid properties, fluid statistics, basic equations (continuity, energy, momentum), viscous effects, dimensional analysis, compressible flow, and two-dimensional irrotational flow. That on Applications has chapters on turbomachinery, flow measurement, closed-conduit flow (steady and unsteady), open-channel flow, and automatic controls and oil hydraulic systems. There are short appendices on elementary calculus, properties of water as a function of temperature up to 212 °F, notation, and the effects of compressibility on aerofoil characteristics. There are also approximately 850 problems (without answers) at the ends of the chapters. It is suggested by the author that the two divisions could appropriately form first and second courses on the subject. In order to make the first course better balanced 'elementary applications are made and illustrated'.

A more detailed study of the way in which the plan is executed raises doubts whether the author has adequately worked out the balance and inter-relation of topics to achieve his declared aim. This is to enable the student 'to recognize the underlying theory and methods of attack that are common to' the broad applications of fluid mechanics. In the Fundamentals division, hydrostatics, together with a brief discussion of the statics of compressible fluids, occupies 60 pages. In comparison only 78 pages are allowed for the dynamics of real fluids with viscous effects, including a good and quite advanced treatment of boundary-layer and mixing-length theory, a discussion of Nikuradse's pipe-friction results, and introductions to the theory of hydrodynamic lubrication and compressible flow in pipes at subsonic velocities. Then 26 pages are given to a compact development of the theory of two-dimensional inviscid incompressible flow, including the definition of circulation and the properties of doublets; but the only example discussed is flow round a cylinder, and no attempt is made to link the theory to experimental observations concerning separation phenomena and velocity and pressure distributions in real fluids.

On the other hand, it is only in the Applications division that one finds discussion of such fundamental phenomena as free vortex motion (p. 272), cavitation (p. 298), and free surface flow at critical depth through or over a constriction (p. 324). And it is surprising to find that the measurement of velocity and static pressure at points in a fluid flow is not discussed until p. 305, and that of turbulent fluctuations until p. 326.

In relation to the aim of the book, the weak feature of the Applications division is that it misses many excellent opportunities to relate empirical results back to fundamentals. Thus in the discussion of the discharge coefficient for a triangular weir (p. 324), it is stated without comment or further reference, 'Experiments show that the coefficient is increased by roughening the upstream side of the weir plate'. It would seem worth commenting on the relation of this result to the character of the boundary layer on the plate. Again, in the discussion of the velocity coefficient for flow through an orifice (p. 311), there is

a good opportunity to introduce the concept of a shear layer, or 'free surface boundary layer'; in this the liquid moves slower than the main body of the jet because it issues from the boundary-layer region on the upstream face of the orifice plate, and in consequence the velocity coefficient is less than unity.

The parts of the book concerned with basic concepts and with incompressible flow conditions in pipes and channels are the best. Each step in the development of the subject is well illustrated with examples. The mathematics is well set out and advanced techniques are avoided; and the emphasis at an early stage of certain topics, such as energy and momentum correction factors and eddy viscosity, helps to provide a firm basis for the more advanced analysis. There are, however, a number of inaccurate statements and loose steps in the argument.

On p. 87 Bernoulli's equation for a frictionless incompressible fluid is correctly derived from momentum considerations, and then without further justification adopted as an *energy* equation. The correct steady flow energy equation is stated on p. 94 and then compared with Bernoulli's equation, but the intervening discussion of 'energy lost' and 'kinetic energy factor' seems misplaced. On p. 138 it is stated that two flows are 'dynamically similar when (*a*) they are geometrically similar, . . . and (*b*) the corresponding streamlines are geometrically similar, or pressure intensities at corresponding points have a constant ratio'. It is unfortunate that neither here nor in the chapter on turbomachinery is the concept of kinematic similarity recognized.

The following passage appears on p. 193, in a discussion of compressible adiabatic flow: 'Flow through a well-insulated (horizontal) pipe is flow with constant energy, as the mechanical energy converted into thermal energy by fluid friction is added to the flow. . . The adiabatic equation does not hold since heat from friction is added.' In the first sentence 'constant energy' is of course being used in a sense different from that where earlier only incompressible flow is considered. Both in the second sentence here and on p. 97, 'reversible adiabatic' must be understood.

The chapter on turbomachinery is fairly traditional. In a book of this kind one would like to have seen the elementary theory of cascades amongst the Fundamentals, and an introductory discussion of its application to turbomachinery here, as well as a discussion of scale effect as a function of Reynolds number.

The final chapter on automatic control and oil hydraulic systems is curiously out of line with the rest of the book. It contains 10 pages on some basic principles of a level control system, with and without a hydraulic amplifier, together with about 20 pages of material drawn largely from the catalogues of makers of high-pressure oil hydraulic equipment. In a book on fluid mechanics a more appropriate use of the space would have been an extended discussion of cavitation and some reference to recent work on such topics as boundary-layer re-attachment and the behaviour of real fluids inside turbomachinery.

Over all the book is lucidly written and maintains the publishers' usual high standards of lay-out, illustrations and book-production. It will be valuable as a reference book for good methods of teaching many topics, for its many worked examples and still more numerous problems, and for its clear presentation of much useful data, well backed by its bibliography. G. S. D. MacLellan

TENTH INTERNATIONAL CONGRESS OF APPLIED MECHANICS

The *Tenth International Congress of Applied Mechanics* will be held in the Congress Building at Stresa (Italy) from *Wednesday*, 31 *August through Wednesday*, 7 *September* 1960.

Apart from a number of invited general lectures the technical sessions of the Congress will be held in two sections, viz.:

SECTION 1: Fluid dynamics (hydrodynamics and aerodynamics).

SECTION 2: Mechanics of solids (rigid body dynamics, vibrations, elasticity, plasticity and theory of structures).

It should be noted that thermodynamics and computational methods as such are not included, although specific applications of computational methods to pertinent problems of one of the two sections mentioned above are acceptable subjects for papers to be read at the Tenth Congress.

Previous Congresses have demonstrated the desirability of an adequate period of time for the presentation and discussion of individual papers. In order to allow a period of 45 minutes for each paper (30 min. for presentation and 15 min. for discussion) a Programme Committee will make a selection from papers submitted for presentation. Abstracts of papers should be submitted *in four copies to the Secretary of the International Committee* (*W. T. Koiter*) *before* 1 *January* 1960. Preferably they should not exceed two type-written pages (doubly-spaced) and in no case should they exceed four pages. In order to facilitate the work of the Programme Committee it is recommended that abstracts be in *two* of the official Congress languages (English, French, German and Italian). Authors are urged to make their abstracts as clear as possible, since selection of papers has to be based upon them. *Decisions of the Programme Committee are final*, and it will be understood that it is impossible to enter into correspondence about them with authors of papers. They will be informed promptly of the decision on each paper.

Day-to-day organization of the Congress is in the hands of the Italian Organizing Committee (President: Prof. G. Colonnetti; Secretary: Dr F. Rolla, Consiglio Nazionale delle Ricerche, Ufficio relazioni internazionali, Piazza delle Scienza 7, Roma). All correspondence (apart from submission of papers) should be addressed to the Italian Organizing Committee. Information on accommodation, also registration forms, will be obtainable from Dr Rolla after 1 September 1959.

The Executive Committee of the International Committee for the Congresses of Applied Mechanics

C. B. BIEZENO, *President*; RICHARD V. SOUTHWELL; W. T. KOITER, *Secretary*; (Prof. Mekelweg 2, Delft, Netherlands).

JOURNAL OF FLUID MECHANICS

Volume 6, Part 2 August 1959

CONTENTS

Shearing flow over a wavy boundary
by T. BROOKE BENJAMIN *page* 161

Torsional oscillations of a plane in a viscous fluid
by S. ROSENBLAT 206

Measurements of intermittency of turbulent motion in a boundary layer
by V. A. SANDBORN 221

An analysis of the vortex street generated in a viscous fluid
by JOHN W. SCHAEFER and SALAMON ESKINAZI 241

The analysis of temperature fluctuations by pulse-counting techniques
by A. A. TOWNSEND 261

Reverse flow and supersonic interference
by JOSEPH H. CLARKE 272

The theory of electromagnetically driven shock waves
by J. K. WRIGHT and M. C. BLACK 289

The pressure distribution on dihedral wings at supersonic speed
by LU TING 302

REVIEWS

Fluid Mechanics for Engineers 313

A Textbook of Fluid Mechanics 316

Fluid Mechanics 318

Printed in Great Britain at the University Press, Cambridge
(Brooke Crutchley, University Printer)